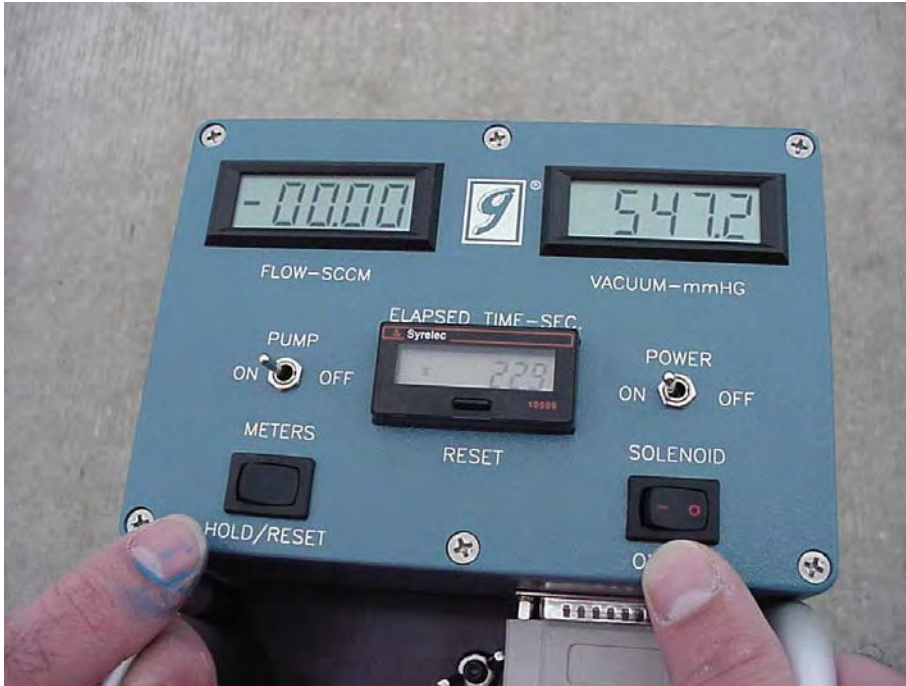


APPENDIX A: PHOTOGRAPHS

General Photographs



Air permeability apparatus control panel.
Photo taken during permeability testing of Site 0, US-23 SB.



MDOT coring rig and technician during coring of Site 0, US-23 SB.



The void from the previous core is filled with a plug (lower right) and mortar while the current core is being taken. Photo taken at Site 1, US-23 SB.



Lower drilling unit used to core the pavement slabs at Site 2, US 23 SB.



A six-inch joint core is extracted after being drilled. Photo taken at Site 2, US-23 SB.



FWD Testing Machine from MDOT. Photo taken at Site 4A, US-23 SB.

SITE 0



Site 0: US-23 Southbound, Section A of MDOT Aggregate Study.
Lower Unit of coring apparatus used to take six-inch core from pavement joint.



Site 0: US-23 Southbound, Section A of MDOT Aggregate Study.
Void left from extraction of six-inch core from the pavement joint.



Site 0: US-23 SB, Section A of MDOT Aggregate Study. Six-inch core extracted from pavement joint. Petrographic analysis will be done on the six-inch core.



Site 0: US-23 SB, Section A of MDOT Aggregate Study. Four-inch core locations. Note the presence of shrinkage cracking in test slab.



Site 0: US-23 SB, Section A of MDOT Aggregate Study.
Permeability testing using the air permeability field apparatus.



Site 0: US-23 SB, Section A of MDOT Aggregate Study.
Coring process for the four-inch core used for permeability and linear traverse testing.



Site 0: US-23 SB, Section A of MDOT Aggregate Study.
Four-inch core used for permeability and linear traverse testing.



Site 0: US-23 SB, Section A of MDOT Aggregate Study. Four-inch core used for compressive strength testing. Note the reinforcing steel in the upper portion of the core.

SITE 1



Site 1: US-23 SB, Section B of MDOT Aggregate Study.
Permeability testing using the air permeability field apparatus.



Site 1: US-23 SB, Section B of MDOT Aggregate Study. Six-inch core extracted from pavement joint. Petrographic analysis will be done on the six-inch core.



Site 1: US-23 SB, Section B of MDOT Aggregate Study.
Four-inch core used for permeability and linear traverse testing.

SITE 2



Site 2: US-23 SB, Section C of MDOT Aggregate Study. Six-inch core extracted from pavement joint. Petrographic analysis will be done on the six-inch core.



Site 2: US-23 SB, Section C of MDOT Aggregate Study. Surface of traveling lane. Note the popouts in the lower right corner.

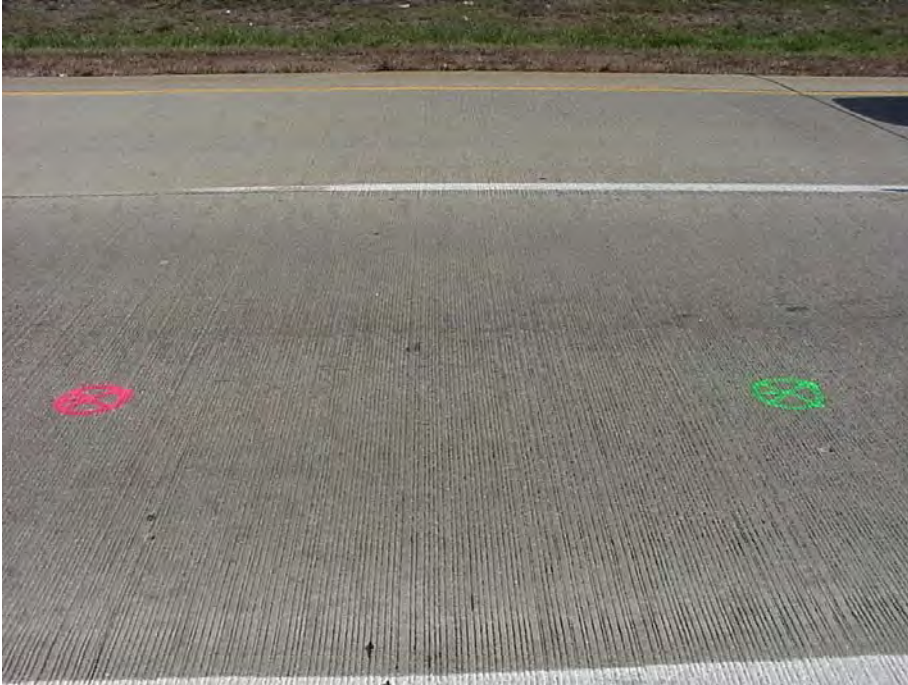


Site 2: US-23 SB, Section C of MDOT Aggregate Study. Surface of outside traveling lane including expansion joint. Note the excellent condition of the joint.



Site 2: US-23 SB, Section C of MDOT Aggregate Study. Four-inch core used for permeability and linear traverse testing.

SITE 3

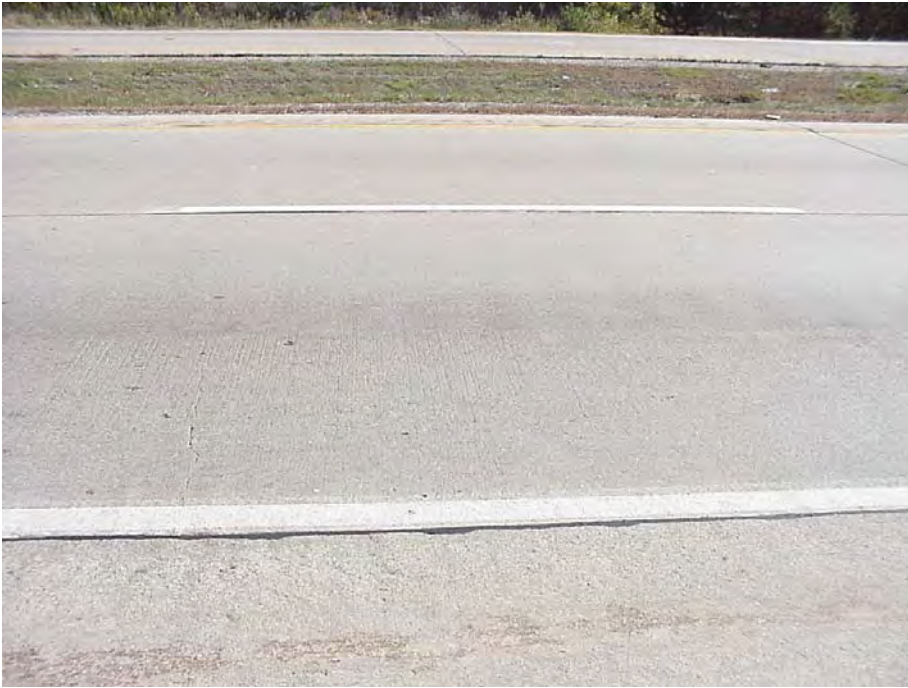


Site 3: US-23 SB, Section D of MDOT Aggregate Study. Surface of traveling lane showing the position of the cores taken to test compressive strength (green), permeability, and air void spacing (pink).



Site 3: US-23 SB, Section D of MDOT Aggregate Study. Surface of traveling lane showing the position of the six-inch cores. Note the shrinkage cracking throughout the site.

SITE 4



Site 4: US-23 SB, Sta 610+56. Surface of traveling lane showing transverse cracking, map cracking, and popouts.



Site 4: US-23 SB, Sta 610+56. Pavement surface and transverse joint. Note the seal of the transverse joint is failing.



Site 4: US-23 SB, Sta 610+56. Surface of traveling lane showing map cracking.

SITE 4A



Site 4A: US-23 SB; Starts @ Sta 176+36. Surface of traveling lane-showing Popouts.



Site 4A: US-23 SB; Starts @ Sta 176+36. Surface of traveling lane showing popouts.

SITE 6



Site 6: I-69 EB, Sta 1534+93. View showing the pavement surface, bituminous shoulder and several concrete patches.



Site 6: I-69 EB, Sta 1534+93. View showing the pavement surface. Note the transverse crack (lower left) and the alligator cracking of the bituminous shoulder.



Site 6: I-69 EB, Sta 1534+93. View showing the pavement surface. Note the transverse crack, concrete patch, and the spalling at the lower right edge of the concrete patch.



Site 6: I-69 EB, Sta 1534+93. View showing the pavement surface. Note the vertical separation between the traveling lane and the bituminous shoulder.



Site 6: I-69 EB, Sta 1534+93. View showing a concrete patch. Note the expansion joint on the right side of the patch and the spalling at the upper right corner.

SITE 14



Site 14: M-81 EB. View showing the pavement surface, gravel shoulder and several joint repair patches.



Site 14: M-81 EB. View showing spalling at the end of a transverse crack.



Site 14: M-81 EB. View showing spalling along a severe transverse crack.



Site 14: M-81 EB. View showing the pavement surface, gravel shoulder, transverse cracks and several joint repair patches.

SITE 19



Site 19: M-53 NB @Station 520. Between 17th and 18th Mile road, view showing the cracking pattern near a transverse joint.



Site 19: M-53 NB @Station 520. Between 17th and 18th Mile road, view showing the cracking pattern near a transverse joint.



Site 19: M-53 NB @Station 520. Between 17th and 18th Mile road, view showing the cracking pattern near a transverse joint.



Site 19: M-53 NB @Station 520. Between 17th and 18th Mile road, view showing the cracking pattern near a transverse joint

SITE 26A



Site 26A: US-10 WB, Sta 137+08. View showing the cracking pattern pavement surface and loose particles.



Site 26A: US-10 WB, Sta 137+08. View showing the popouts, cracking pattern and spalling on the pavement. The spalling has already been patched with asphalt.



Site 26A: US-10 WB, Sta 137+08. View showing the spalling along the longitudinal joint which has been patched by asphalt. Lower right corner shows a view of expansion joint.



Site 26A: US-10 WB, Sta 137+08. View showing the transverse joint completely spalled and patched with asphalt.

SITE 26B



Site 26B: US-10 WB, Sta 137+08. View showing the cracking pattern pavement surface and completely spalled longitudinal joint.



Site 26B: US-10 WB, Sta 137+08. View showing the popouts, cracking pattern and loose particles.



Site 26B: US-10 WB, Sta 137+08. View showing spalling along the longitudinal joint which has been patched by asphalt.



Site 26B: US-10 WB, Sta 137+08. View showing the skewed joint. Also showing spalling at the corners of joint.

SITE 27



Site 27: US-10 WB, Sta 114+00. View showing the cracking pattern on pavement surface with breakup of the pavement.



Site 27: US-10 WB, Sta 114+00. View showing the Popouts, cracking pattern and spalled transverse joint.



Site 27: US-10 WB, Sta 114+00. View showing spalling along the transverse joint and coring locations for petrographic analysis.

SITE 28



Site 28: US-27 SB Starts @ Station 519+07, View showing the cracking pattern along the poorly done asphalt patching.



Site 28: US-27 SB Starts @ Station 519+07, View showing the cracking pattern along the transverse cracking.



Site 28: US-27 SB Starts @ Station 519+07, View showing the cracking pattern near the longitudinal joint.



Site 28: US-27 SB Starts @ Station 519+07, View showing the asphalt patching done on transverse joint.

SITE 29



Site 29: I-275 SB, View showing the cracking pattern pavement with white staining coming out of the cracks. Also showing poorly done asphalt patching.



Site 29: I-275 SB, View showing the cracking pattern and asphalt patching at the transverse joint.



Site 29: I-275 SB, View showing asphalt patching along the transverse joint and also the cracking pattern.



Site 29: I-275 SB, View showing cracking pattern with white exudate coming out of the cracks.



Site 29: I-275 SB, View showing the cracking pattern near the asphalt patching.



Site 29: I-275 SB, View showing the cracking pattern with white exudate coming out of the cracks (right side of the picture).

APPENDIX B: TEST SITE INSPECTION DATA

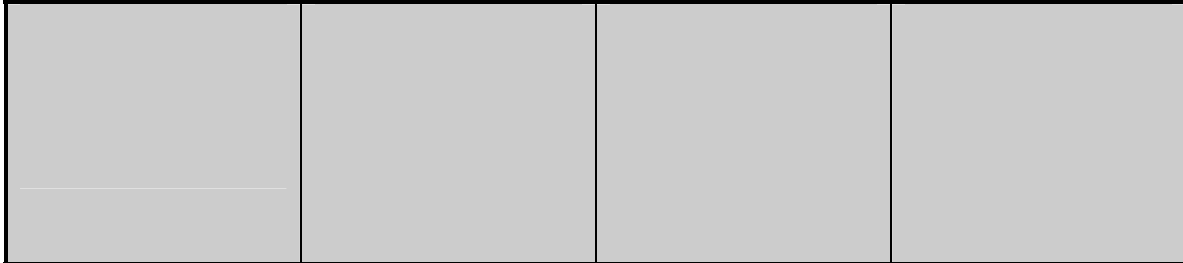
Site 0

DATE: 10/13/1999

SITE #: 0

LOCATION: Route: US-23 SB; Starts @ Sta 432+27; South of MP 6; Section A of MDOT Aggregate Study

JOINT SPACING: 27' (8.2 m), 10' (3.0 m) tied concrete shoulders

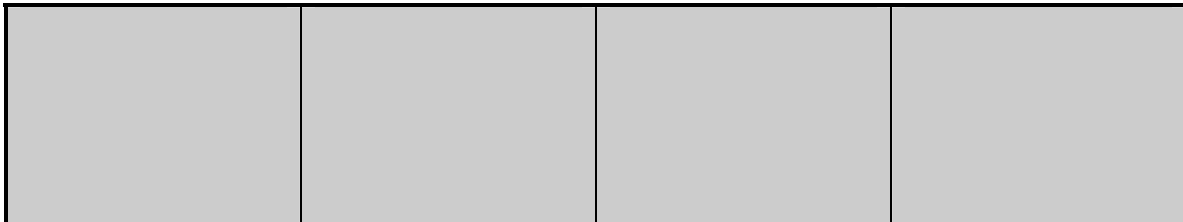


*****SLAB 1*****
TYPICAL MRD SLAB

SLAB 2

SLAB 3

SLAB 4

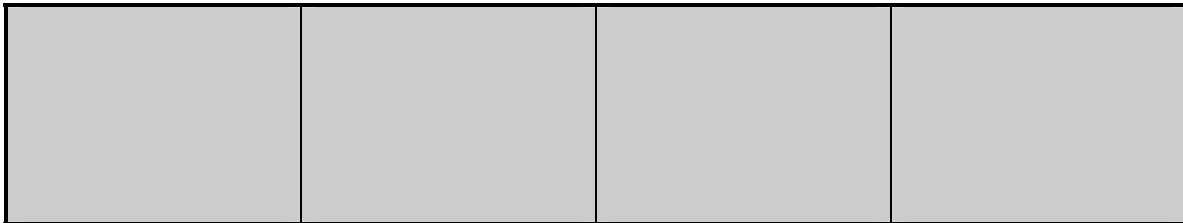


SLAB 5

SLAB 6

SLAB 7

SLAB 8

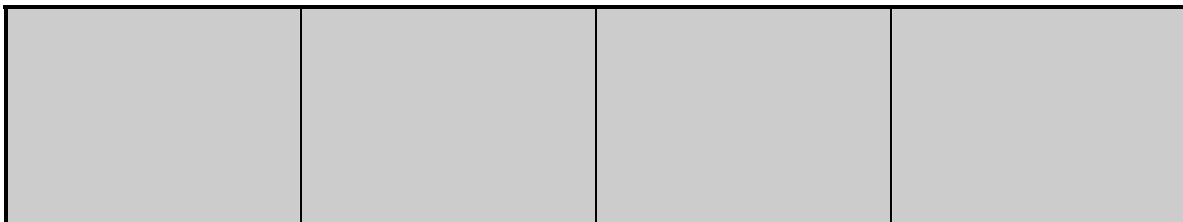


SLAB 9

SLAB 10

SLAB 11

SLAB 12

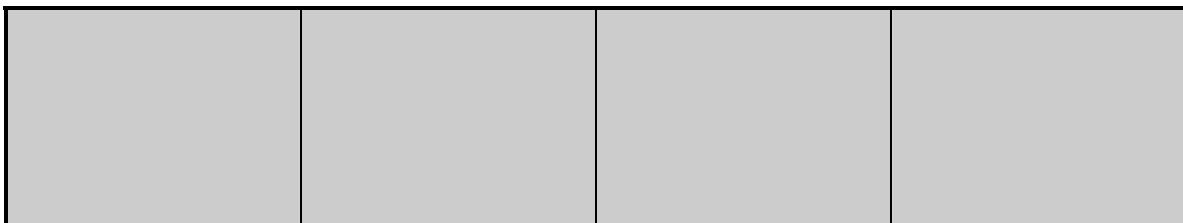


SLAB 13

SLAB 14

SLAB 15

SLAB 16






SLAB 17

SLAB 18

SLAB 19

SLAB 20

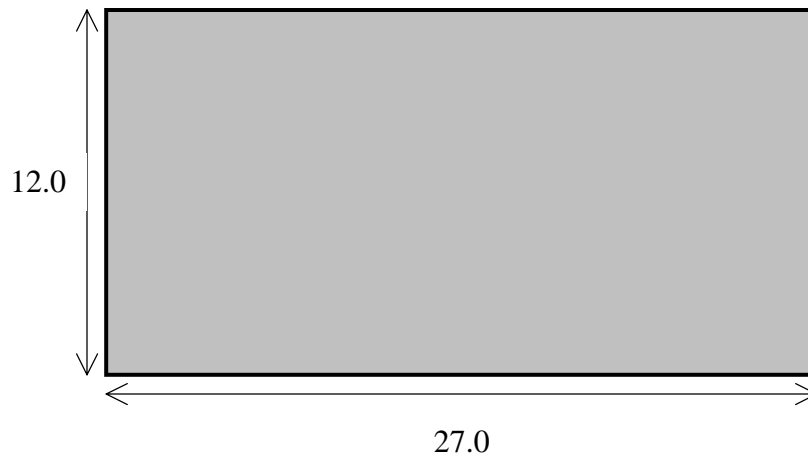
KEY: <i>Transverse Cracking</i>	<i>Patching</i>		1. Spalling	5. High steel
Low 	Full-depth Concrete 		2. D-Cracking	6. Polished agg
Moderate 	Asphalt Patch 		3. Poor sealant	7. Faulting
High •••••	Expansion joint 		4. ASR	8. Long. crack

COMMENTS: Shrinkage cracking every 6-8"; shoulder is different concrete type than mainline pavement (different color)

CRACK SPACINGS:

<u>Slab 1</u>	<u>Slab 2</u>	<u>Slab 3</u>	<u>Slab 4</u>
J ₁ -C ₁ C ₁ -C ₂ C ₂ -C ₃	J ₂ -C ₁ C ₁ -C ₂ C ₂ -C ₃	J ₃ -C ₁ C ₁ -C ₂ C ₂ -C ₃	J ₄ -C ₁ C ₁ -C ₂ C ₂ -C ₃
<u>Slab 5</u>	<u>Slab 6</u>	<u>Slab 7</u>	<u>Slab 8</u>
J ₁ -C ₁ C ₁ -C ₂ C ₂ -C ₃	J ₂ -C ₁ C ₁ -C ₂ C ₂ -C ₃	J ₃ -C ₁ C ₁ -C ₂ C ₂ -C ₃	J ₄ -C ₁ C ₁ -C ₂ C ₂ -C ₃
<u>Slab 9</u>	<u>Slab 10</u>	<u>Slab 11</u>	<u>Slab 12</u>
J ₁ -C ₁ C ₁ -C ₂ C ₂ -C ₃	J ₂ -C ₁ C ₁ -C ₂ C ₂ -C ₃	J ₃ -C ₁ C ₁ -C ₂ C ₂ -C ₃	J ₄ -C ₁ C ₁ -C ₂ C ₂ -C ₃
<u>Slab 13</u>	<u>Slab 14</u>	<u>Slab 15</u>	<u>Slab 16</u>
J ₁ -C ₁ C ₁ -C ₂ C ₂ -C ₃	J ₂ -C ₁ C ₁ -C ₂ C ₂ -C ₃	J ₃ -C ₁ C ₁ -C ₂ C ₂ -C ₃	J ₄ -C ₁ C ₁ -C ₂ C ₂ -C ₃
<u>Slab 17</u>	<u>Slab 18</u>	<u>Slab 19</u>	<u>Slab 20</u>
J ₁ -C ₁ C ₁ -C ₂	J ₂ -C ₁ C ₁ -C ₂	J ₃ -C ₁ C ₁ -C ₂	J ₄ -C ₁ C ₁ -C ₂

TYPICAL MRD SLAB: Slab 1



COMMENTS: Shrinkage cracking typically 6-8" apart and very tight, predominantly transverse; No Popouts.

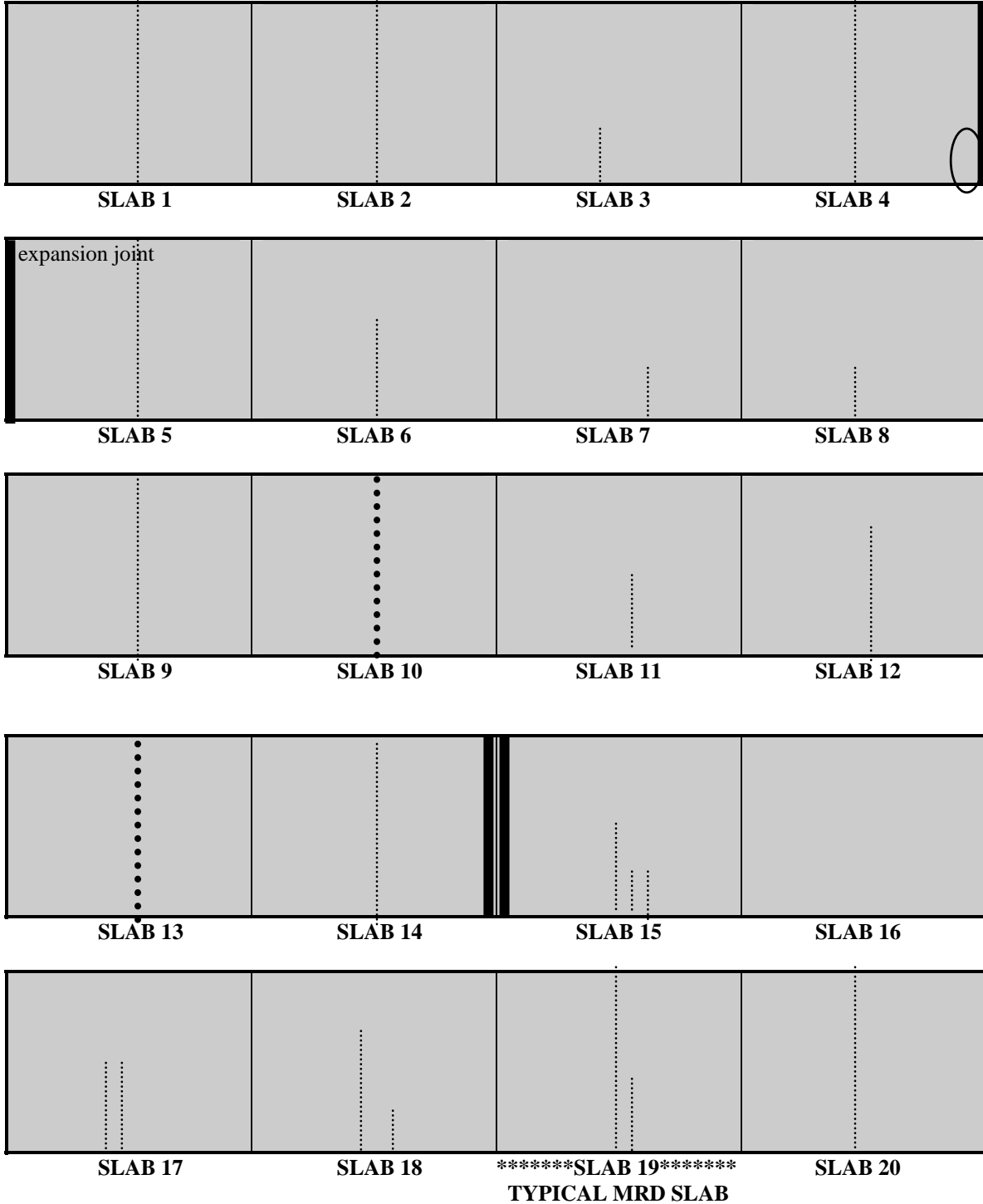
Site 1

DATE: 7/24/1999

SITE #: 1

LOCATION: Route: US-23 SB; Starts @ Sta 328+13; 54' south of MP 4; Section B of MDOT Aggregate Study

JOINT SPACING: 27' (8.2 m), 10' (3.0 m) tied concrete shoulders



KEY: Transverse Cracking

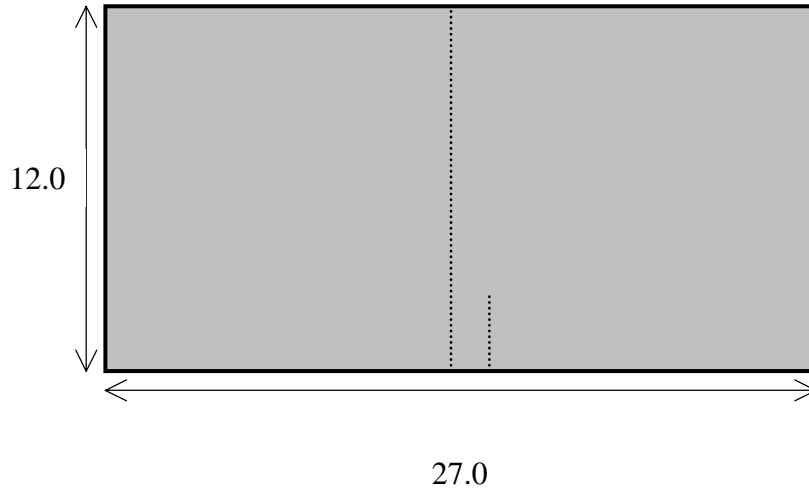
- Low
- Moderate
- High

COMMENTS: Small hole in Slab 7, Construction repairs (exopy) on Slab 15; Slag Coarse Aggregate

CRACK SPACINGS:

<u>Slab 1</u>	<u>Slab 2</u>	<u>Slab 3</u>	<u>Slab 4</u>
J ₁ -C ₁ 14.5'	J ₂ -C ₁ 12.0'	J ₃ -C ₁ 12.0'	J ₄ -C ₁ 12.0'
C ₁ -C ₂	C ₁ -C ₂	C ₁ -C ₂	C ₁ -C ₂
C ₂ -C ₃	C ₂ -C ₃	C ₂ -C ₃	C ₂ -C ₃
<u>Slab 5</u>	<u>Slab 6</u>	<u>Slab 7</u>	<u>Slab 8</u>
J ₁ -C ₁ 14.0'	J ₂ -C ₁ 13.0'	J ₃ -C ₁ 19.0'	J ₄ -C ₁ 15.0'
C ₁ -C ₂	C ₁ -C ₂	C ₁ -C ₂	C ₁ -C ₂
C ₂ -C ₃	C ₂ -C ₃	C ₂ -C ₃	C ₂ -C ₃
<u>Slab 9</u>	<u>Slab 10</u>	<u>Slab 11</u>	<u>Slab 12</u>
J ₁ -C ₁ 11.0'	J ₂ -C ₁ 12.0'	J ₃ -C ₁ 15.0'	J ₄ -C ₁ 13.0'
C ₁ -C ₂	C ₁ -C ₂	C ₁ -C ₂	C ₁ -C ₂
C ₂ -C ₃	C ₂ -C ₃	C ₂ -C ₃	C ₂ -C ₃
<u>Slab 13</u>	<u>Slab 14</u>	<u>Slab 15</u>	<u>Slab 16</u>
J ₁ -C ₁ 14.5'	J ₂ -C ₁ 12.0'	J ₃ -C ₁ 12.5'	J ₄ -C ₁
C ₁ -C ₂	C ₁ -C ₂	C ₁ -C ₂ 1.5'	C ₁ -C ₂
C ₂ -C ₃	C ₂ -C ₃	C ₂ -C ₃ 1.0'	C ₂ -C ₃
<u>Slab 17</u>	<u>Slab 18</u>	<u>Slab 19</u>	<u>Slab 20</u>
J ₁ -C ₁ 10.5'	J ₂ -C ₁ 12.0'	J ₃ -C ₁ 13.0'	J ₄ -C ₁ 12.0'
C ₁ -C ₂ 1.0'	C ₁ -C ₂ 4.0'	C ₁ -C ₂ 2.0'	C ₁ -C ₂
C ₂ -C ₃	C ₂ -C ₃	C ₂ -C ₃	C ₂ -C ₃

TYPICAL MRD SLAB: Slab 19



COMMENTS: A slight amount of staining on Crack 2

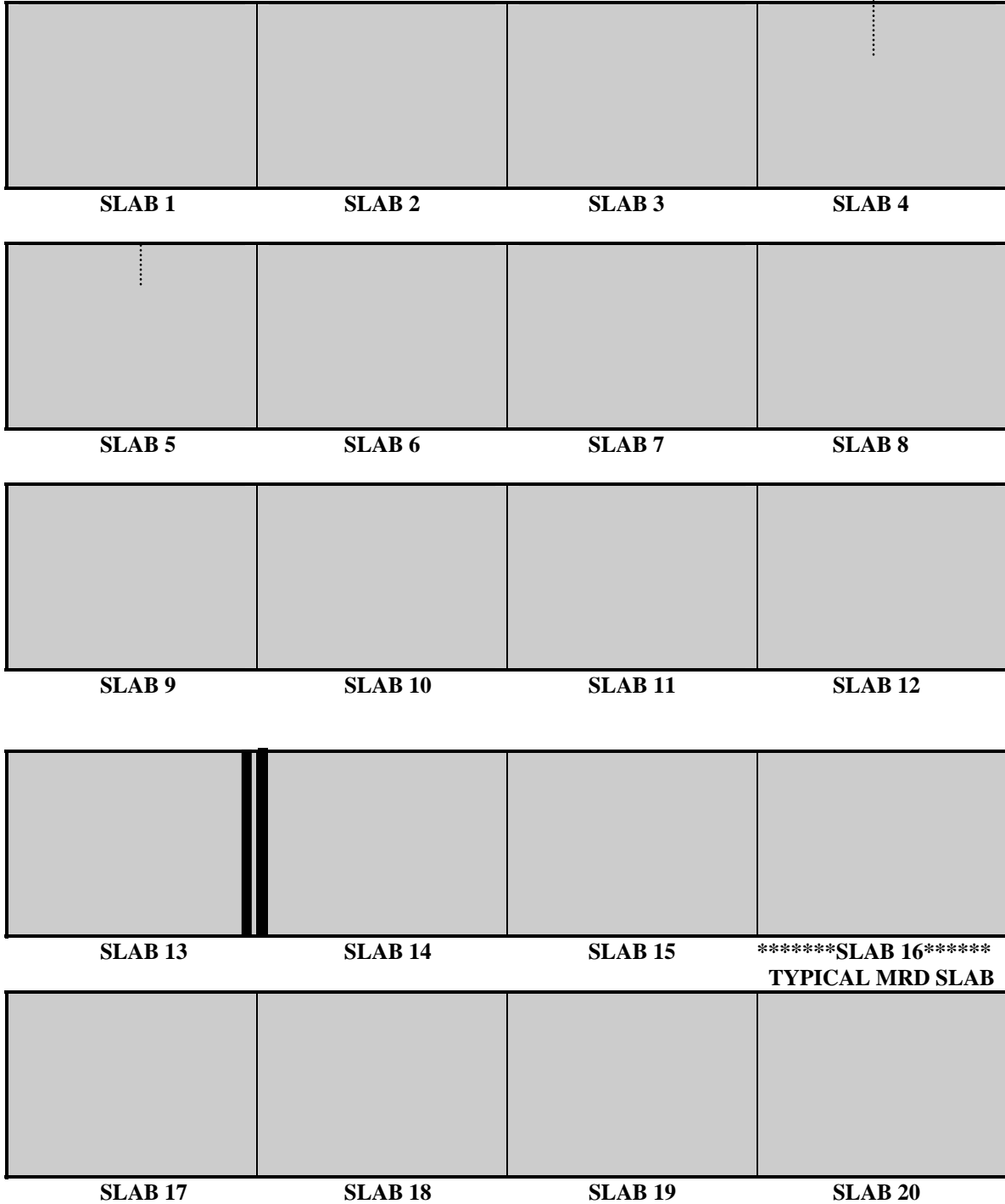
Site 2

DATE: 7/24/1999

SITE #: 2

LOCATION: Route: US-23 SB; Starts @ Sta 314+92; 8' south of "Start C" sign; Section C of MDOT Aggregate Study

JOINT SPACING: 27' (8.2 m), 10' (3.0 m) tied concrete shoulders



KEY: Transverse Cracking

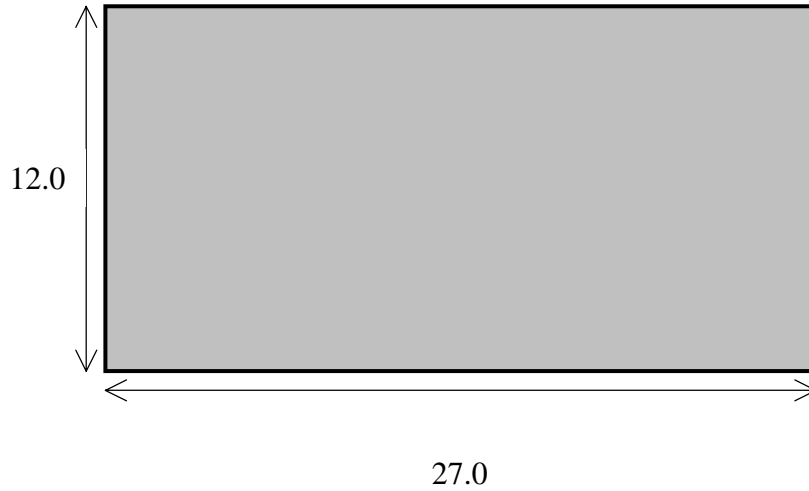
- Low
- Moderate
- High

COMMENTS: Stain on Crack 1 of Slab 5, Poor construction grooving on entire site, Coring hole on Slab 10, Construction repairs (exopy) on Slabs 13 and 14; Natural Gravel Coarse Aggregate

CRACK SPACINGS:

<u>Slab 1</u>	<u>Slab 2</u>	<u>Slab 3</u>	<u>Slab 4</u>
J ₁ -C ₁ C ₁ -C ₂ C ₂ -C ₃	J ₂ -C ₁ C ₁ -C ₂ C ₂ -C ₃	J ₃ -C ₁ C ₁ -C ₂ C ₂ -C ₃	J ₄ -C ₁ 12.5' C ₁ -C ₂ C ₂ -C ₃
<u>Slab 5</u>	<u>Slab 6</u>	<u>Slab 7</u>	<u>Slab 8</u>
J ₁ -C ₁ 12.0' C ₁ -C ₂ C ₂ -C ₃	J ₂ -C ₁ C ₁ -C ₂ C ₂ -C ₃	J ₃ -C ₁ C ₁ -C ₂ C ₂ -C ₃	J ₄ -C ₁ C ₁ -C ₂ C ₂ -C ₃
<u>Slab 9</u>	<u>Slab 10</u>	<u>Slab 11</u>	<u>Slab 12</u>
J ₁ -C ₁ C ₁ -C ₂ C ₂ -C ₃	J ₂ -C ₁ C ₁ -C ₂ C ₂ -C ₃	J ₃ -C ₁ C ₁ -C ₂ C ₂ -C ₃	J ₄ -C ₁ C ₁ -C ₂ C ₂ -C ₃
<u>Slab 13</u>	<u>Slab 14</u>	<u>Slab 15</u>	<u>Slab 16</u>
J ₁ -C ₁ C ₁ -C ₂ C ₂ -C ₃	J ₂ -C ₁ C ₁ -C ₂ C ₂ -C ₃	J ₃ -C ₁ C ₁ -C ₂ C ₂ -C ₃	J ₄ -C ₁ C ₁ -C ₂ C ₂ -C ₃
<u>Slab 17</u>	<u>Slab 18</u>	<u>Slab 19</u>	<u>Slab 20</u>
J ₁ -C ₁ C ₁ -C ₂ C ₂ -C ₃	J ₂ -C ₁ C ₁ -C ₂ C ₂ -C ₃	J ₃ -C ₁ C ₁ -C ₂ C ₂ -C ₃	J ₄ -C ₁ C ₁ -C ₂ C ₂ -C ₃

TYPICAL MRD SLAB: Slab 16



COMMENTS: Surface texture irregularities; popouts: 2-3 per m²

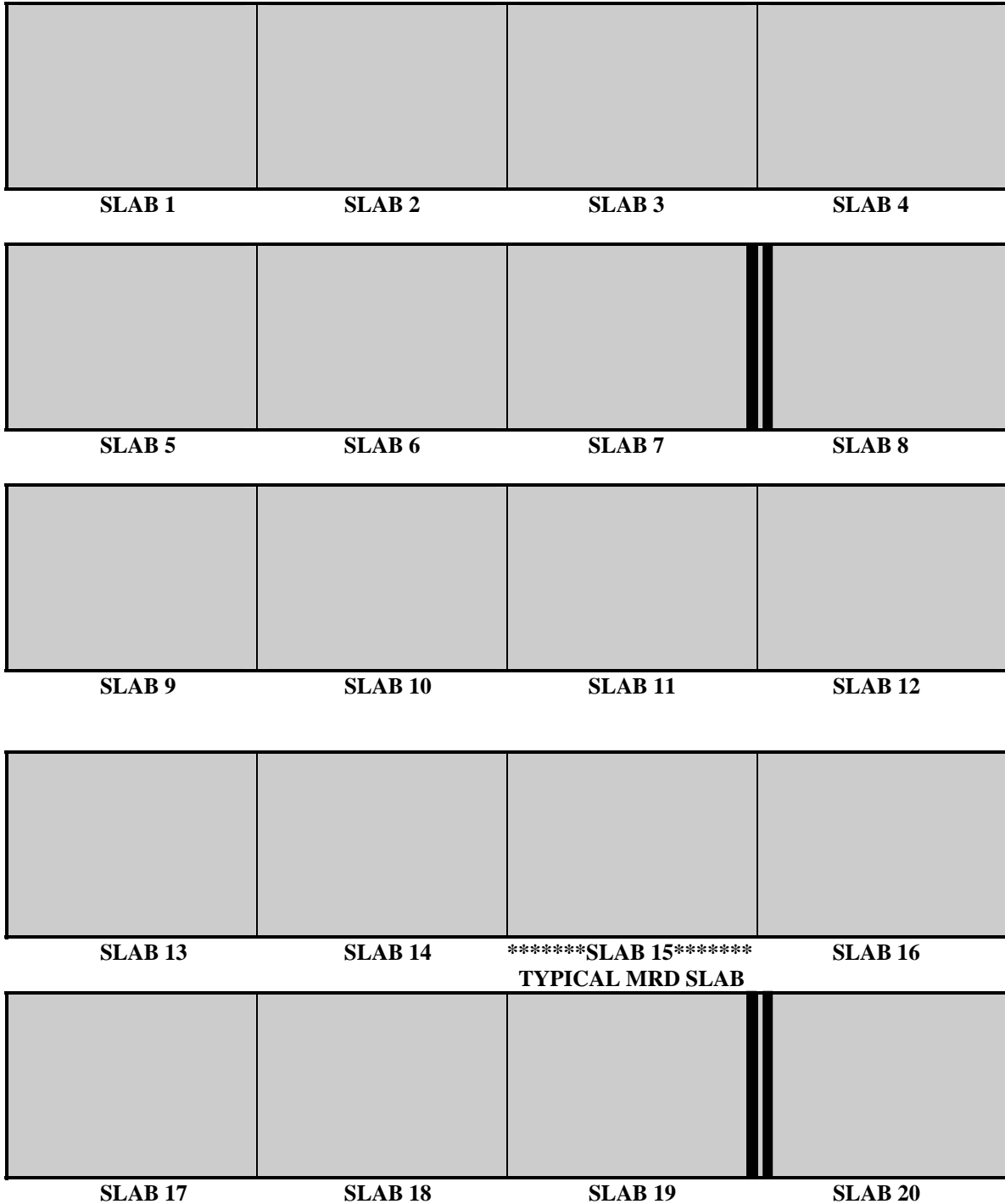
Site 3

DATE: 7/24/1999

SITE #: 3

LOCATION: Route: US-23 SB; Starts @ Sta 243+69; Section D of MDOT Aggregate Study

JOINT SPACING: 27' (8.2 m), 10' (3.0 m) tied concrete shoulders



KEY: Transverse Cracking

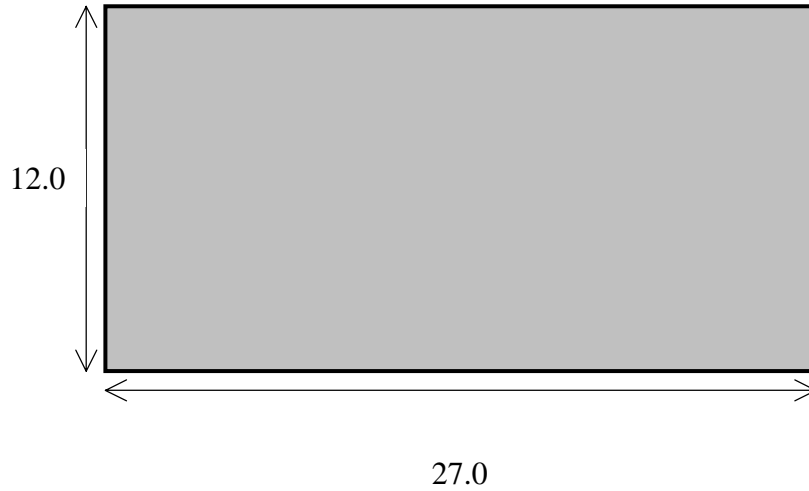
- Low
- Moderate
- High

COMMENTS: Joint sealant drop between Slabs 14 and 15, Poor construction grooving on entire site, Coring hole on Slab 9, Possible dowel misalignment cracks on Slabs 2 and 3; Crushed Limestone Coarse Aggregate

CRACK SPACINGS:

<u>Slab 1</u>	<u>Slab 2</u>	<u>Slab 3</u>	<u>Slab 4</u>
J ₁ -C ₁ C ₁ -C ₂ C ₂ -C ₃	J ₂ -C ₁ C ₁ -C ₂ C ₂ -C ₃	J ₃ -C ₁ C ₁ -C ₂ C ₂ -C ₃	J ₄ -C ₁ C ₁ -C ₂ C ₂ -C ₃
<u>Slab 5</u>	<u>Slab 6</u>	<u>Slab 7</u>	<u>Slab 8</u>
J ₁ -C ₁ C ₁ -C ₂ C ₂ -C ₃	J ₂ -C ₁ C ₁ -C ₂ C ₂ -C ₃	J ₃ -C ₁ C ₁ -C ₂ C ₂ -C ₃	J ₄ -C ₁ C ₁ -C ₂ C ₂ -C ₃
<u>Slab 9</u>	<u>Slab 10</u>	<u>Slab 11</u>	<u>Slab 12</u>
J ₁ -C ₁ C ₁ -C ₂ C ₂ -C ₃	J ₂ -C ₁ C ₁ -C ₂ C ₂ -C ₃	J ₃ -C ₁ C ₁ -C ₂ C ₂ -C ₃	J ₄ -C ₁ C ₁ -C ₂ C ₂ -C ₃
<u>Slab 13</u>	<u>Slab 14</u>	<u>Slab 15</u>	<u>Slab 16</u>
J ₁ -C ₁ C ₁ -C ₂ C ₂ -C ₃	J ₂ -C ₁ C ₁ -C ₂ C ₂ -C ₃	J ₃ -C ₁ C ₁ -C ₂ C ₂ -C ₃	J ₄ -C ₁ C ₁ -C ₂ C ₂ -C ₃
<u>Slab 17</u>	<u>Slab 18</u>	<u>Slab 19</u>	<u>Slab 20</u>
J ₁ -C ₁ C ₁ -C ₂ C ₂ -C ₃	J ₂ -C ₁ C ₁ -C ₂ C ₂ -C ₃	J ₃ -C ₁ C ₁ -C ₂ C ₂ -C ₃	J ₄ -C ₁ C ₁ -C ₂ C ₂ -C ₃

TYPICAL MRD SLAB: Slab 15



COMMENTS: Shrinkage cracking typically 6-8" apart and very tight, predominantly transverse;
Popouts: ~ 1 per m²

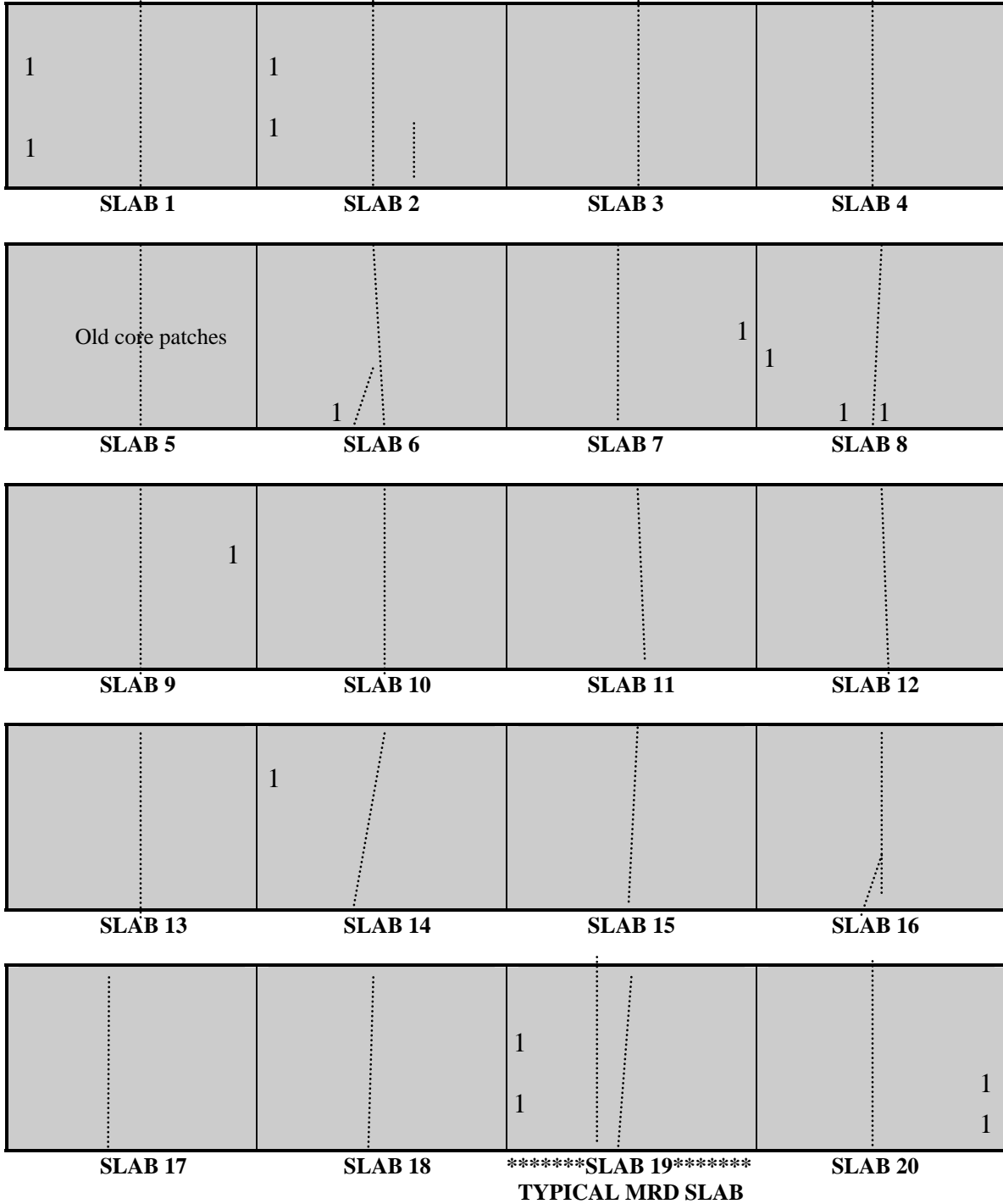
Site 4




DATE: 10/5/1999

SITE #: 4

LOCATION: Route: US-23 SB; Starts @ Sta 610+56; South of Hill Road; Between MP 89 & 90

JOINT SPACING: 27' (8.2 m), 10' (3.0 m) tied concrete shoulders



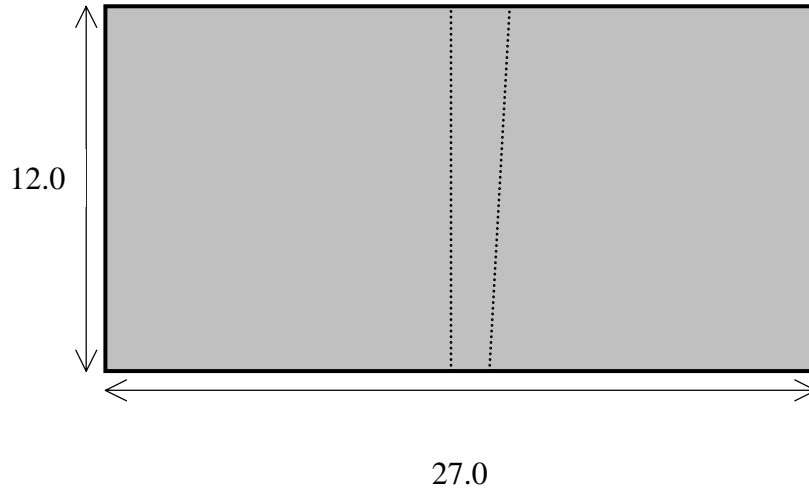
KEY: <i>Transverse Cracking</i>	<i>Patching</i>		1. Spalling	5. High steel
Low	Full-depth Concrete		2. D-Cracking	6. Polished agg
Moderate ●●●●●	Asphalt Patch		3. Poor sealant	7. Faulting
High ●●●●	Expansion joint		4. ASR	8. Long. crack

COMMENTS: ASR-like cracking in shoulder near joints; ASR-like cracking on entire mainline pavement; All joints sealants are deficient; Slag coarse aggregate

CRACK SPACINGS:

<u>Slab 1</u>	<u>Slab 2</u>	<u>Slab 3</u>	<u>Slab 4</u>
J ₁ -C ₁ 16.0'	J ₂ -C ₁ 10.0'	J ₃ -C ₁ 16.0'	J ₄ -C ₁ 15.0'
C ₁ -C ₂	C ₁ -C ₂ 4.0'	C ₁ -C ₂	C ₁ -C ₂
C ₂ -C ₃	C ₂ -C ₃	C ₂ -C ₃	C ₂ -C ₃
<u>Slab 5</u>	<u>Slab 6</u>	<u>Slab 7</u>	<u>Slab 8</u>
J ₁ -C ₁ 14.0'	J ₂ -C ₁ 12.0'	J ₃ -C ₁ 12.0'	J ₄ -C ₁ 14.0'
C ₁ -C ₂	C ₁ -C ₂	C ₁ -C ₂	C ₁ -C ₂
C ₂ -C ₃	C ₂ -C ₃	C ₂ -C ₃	C ₂ -C ₃
<u>Slab 9</u>	<u>Slab 10</u>	<u>Slab 11</u>	<u>Slab 12</u>
J ₁ -C ₁ 17.0'	J ₂ -C ₁ 14.0'	J ₃ -C ₁ 13.0'	J ₄ -C ₁ 13.0'
C ₁ -C ₂	C ₁ -C ₂	C ₁ -C ₂	C ₁ -C ₂
C ₂ -C ₃	C ₂ -C ₃	C ₂ -C ₃	C ₂ -C ₃
<u>Slab 13</u>	<u>Slab 14</u>	<u>Slab 15</u>	<u>Slab 16</u>
J ₁ -C ₁ 13.0'	J ₂ -C ₁ 10.0'	J ₃ -C ₁ 12.0'	J ₄ -C ₁ 13.0'
C ₁ -C ₂	C ₁ -C ₂	C ₁ -C ₂	C ₁ -C ₂
C ₂ -C ₃	C ₂ -C ₃	C ₂ -C ₃	C ₂ -C ₃
<u>Slab 17</u>	<u>Slab 18</u>	<u>Slab 19</u>	<u>Slab 20</u>
J ₁ -C ₁ 12.0'	J ₂ -C ₁ 12.0'	J ₃ -C ₁ 14.0'	J ₄ -C ₁ 12.0'
C ₁ -C ₂	C ₁ -C ₂	C ₁ -C ₂ 2.0'	C ₁ -C ₂
C ₂ -C ₃	C ₂ -C ₃	C ₂ -C ₃	C ₂ -C ₃

TYPICAL MRD SLAB: Slab 19



COMMENTS: Longitudinal cracking (~ 6" spacing) in slab due to connecting ASR-like cracks; Severe ASR-like cracking throughout entire slab; Popouts: 0.5 per m²

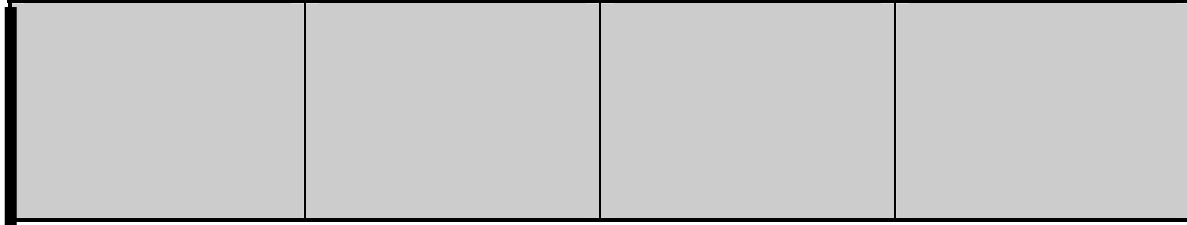
Site 4A

DATE: 10/13/1999

SITE #: 4A

LOCATION: Route: US-23 SB; Starts @ Sta 176+36; Right at MP 1; Section E of MDOT Aggregate Study

JOINT SPACING: 27' (8.2 m), 10' (3.0 m) tied concrete shoulders



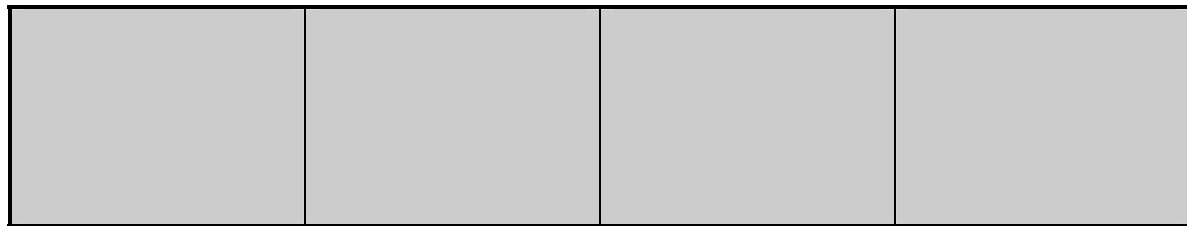
SLAB 1

SLAB 2

SLAB 3

*****SLAB 4*****

TYPICAL MRD SLAB

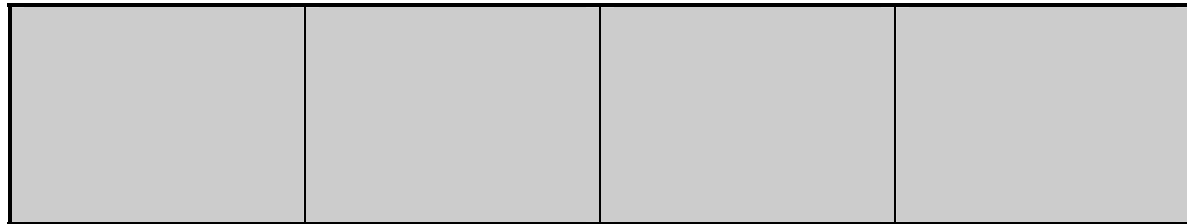


SLAB 5

SLAB 6

SLAB 7

SLAB 8

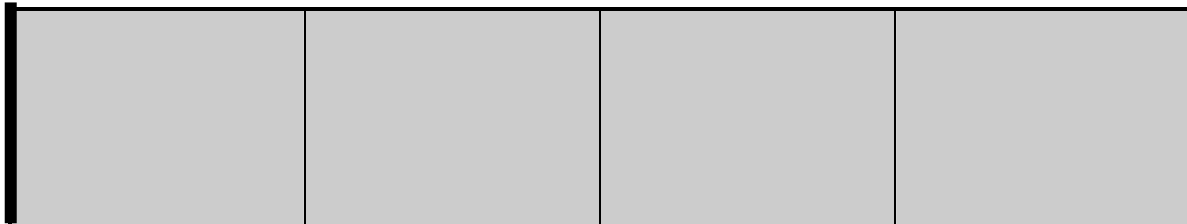


SLAB 9

SLAB 10

SLAB 11

SLAB 12



SLAB 13

SLAB 14

SLAB 15

SLAB 16






SLAB 17

SLAB 18

SLAB 19

SLAB 20

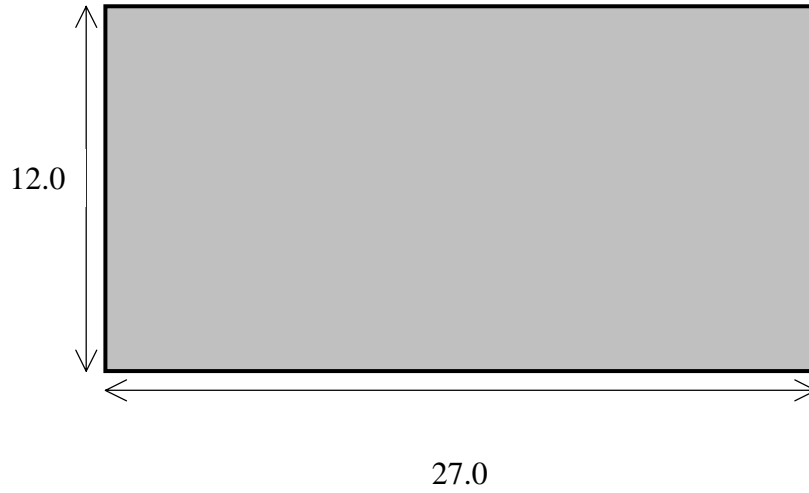
KEY: <i>Transverse Cracking</i>	<i>Patching</i>		1. Spalling	5. High steel
Low Moderate High ●●●●	Full-depth Concrete Asphalt Patch	 	2. D-Cracking 3. Poor sealant	6. Polished agg 7. Faulting
	Expansion joint		4. ASR	8. Long. crack

COMMENTS: Some popouts; no other distinguishable distresses

CRACK SPACINGS:

<u>Slab 1</u>	<u>Slab 2</u>	<u>Slab 3</u>	<u>Slab 4</u>
J ₁ -C ₁ C ₁ -C ₂ C ₂ -C ₃	J ₂ -C ₁ C ₁ -C ₂ C ₂ -C ₃	J ₃ -C ₁ C ₁ -C ₂ C ₂ -C ₃	J ₄ -C ₁ C ₁ -C ₂ C ₂ -C ₃
<u>Slab 5</u>	<u>Slab 6</u>	<u>Slab 7</u>	<u>Slab 8</u>
J ₁ -C ₁ C ₁ -C ₂ C ₂ -C ₃	J ₂ -C ₁ C ₁ -C ₂ C ₂ -C ₃	J ₃ -C ₁ C ₁ -C ₂ C ₂ -C ₃	J ₄ -C ₁ C ₁ -C ₂ C ₂ -C ₃
<u>Slab 9</u>	<u>Slab 10</u>	<u>Slab 11</u>	<u>Slab 12</u>
J ₁ -C ₁ C ₁ -C ₂ C ₂ -C ₃	J ₂ -C ₁ C ₁ -C ₂ C ₂ -C ₃	J ₃ -C ₁ C ₁ -C ₂ C ₂ -C ₃	J ₄ -C ₁ C ₁ -C ₂ C ₂ -C ₃
<u>Slab 13</u>	<u>Slab 14</u>	<u>Slab 15</u>	<u>Slab 16</u>
J ₁ -C ₁ C ₁ -C ₂ C ₂ -C ₃	J ₂ -C ₁ C ₁ -C ₂ C ₂ -C ₃	J ₃ -C ₁ C ₁ -C ₂ C ₂ -C ₃	J ₄ -C ₁ C ₁ -C ₂ C ₂ -C ₃
<u>Slab 17</u>	<u>Slab 18</u>	<u>Slab 19</u>	<u>Slab 20</u>
J ₁ -C ₁ C ₁ -C ₂ C ₂ -C ₃	J ₂ -C ₁ C ₁ -C ₂ C ₂ -C ₃	J ₃ -C ₁ C ₁ -C ₂ C ₂ -C ₃	J ₄ -C ₁ C ₁ -C ₂ C ₂ -C ₃

TYPICAL MRD SLAB: Slab 4



COMMENTS: Popouts: 3 per m²

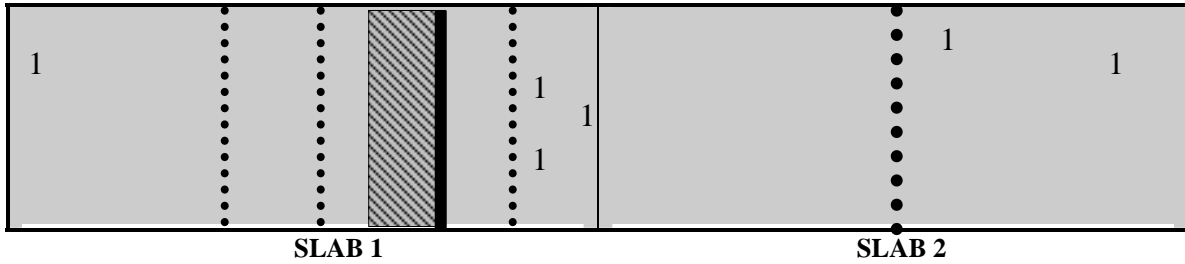
Site 6

DATE: 10/5/1999

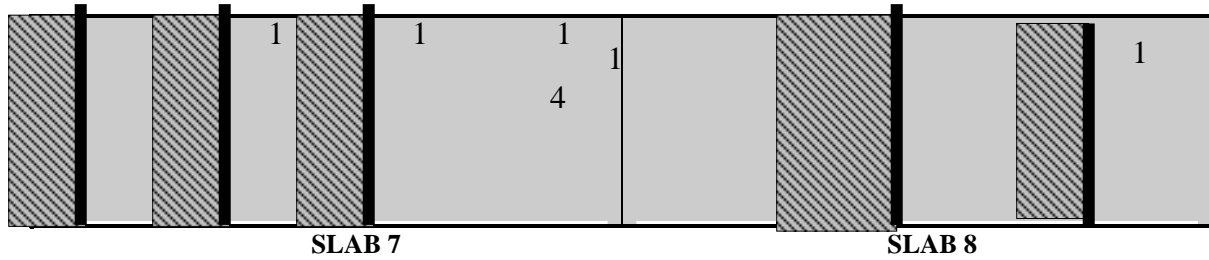
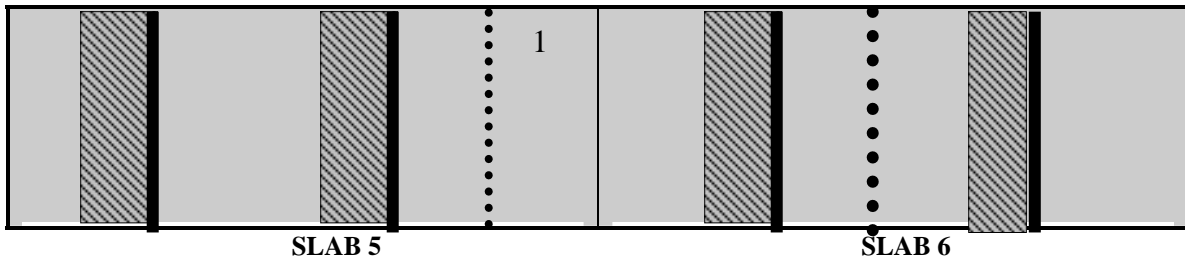
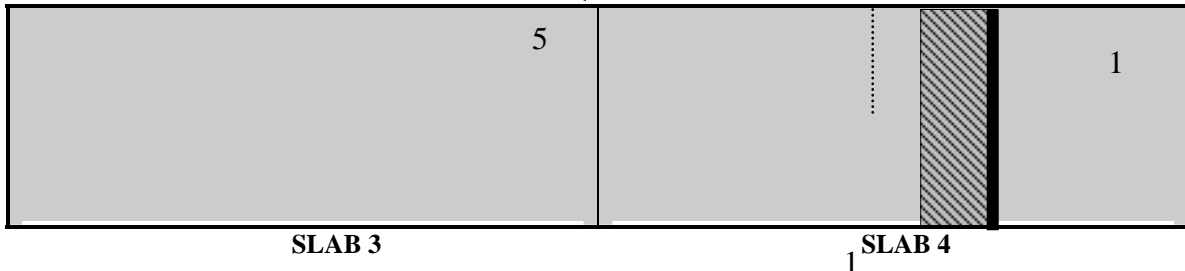
SITE #: 6




LOCATION: Route: I-69 EB; Starts @ Sta 1534+93; Between MP 154 & 155; Just East of Turnaround; East of Exit 153

JOINT SPACING: 71' (21.6 m), asphalt shoulders



*****TYPICAL MRD SLAB*****



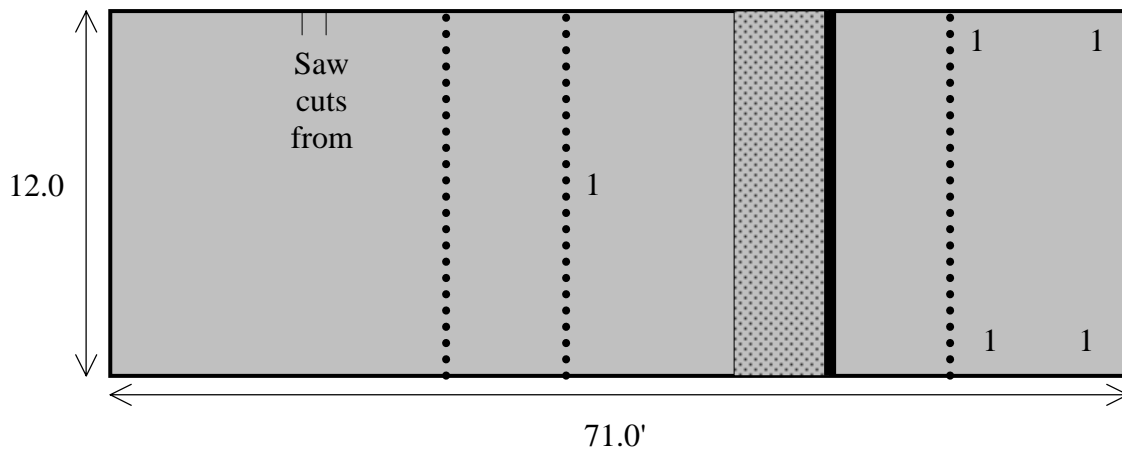
KEY: <i>Transverse Cracking</i>	<i>Patching</i>		1. Spalling	5. High steel
Low 	Full-depth Concrete		2. D-Cracking	6. Polished agg
Moderate 	Asphalt Patch		3. Poor sealant	7. Faulting
High •••••	Expansion joint		4. ASR	8. Long. crack

COMMENTS: Lane-shoulder dropoff; polished agg in wheelpath; popouts; lane-lane faulting; tar and chip repair throughout the entire site (especially near longitudinal joint); natural gravel pavement

CRACK SPACINGS:

<u>Slab 1</u>	<u>Slab 2</u>	<u>Slab 3</u>	<u>Slab 4</u>
J ₁ -C ₁ 31.0'	J ₂ -C ₁ 38.0'	J ₃ -C ₁	J ₄ -C ₁ 38.0'
C ₁ -C ₂ 10.0'			C ₁ -P ₁ 9.0'
C ₂ -P ₁ 5.0'			
P ₁ -P ₁ 6.0'			
P ₁ -C ₃ 9.0'			
<u>Slab 5</u>	<u>Slab 6</u>	<u>Slab 7</u>	<u>Slab 8</u>
J ₅ -P ₁ 10.0'	J ₆ -P ₁ 14.0'	J ₇ -P ₁ 0.0'	J ₈ -P ₁ 17.0'
P ₁ -P ₁ 6.0'	P ₁ -P ₁ 6.0'	P ₁ -P ₁ 6.0'	P ₁ -P ₁ 15.0'
P ₁ -P ₂ 20.0'	P ₁ -C ₁ 14.0'	P ₁ -P ₂ 6.0'	P ₁ -P ₂ 11.0'
P ₂ -P ₂ 6.0'	C ₁ -P ₂ 15.0'	P ₂ -P ₂ 6.0'	
P ₂ -C ₁ 10.0'		P ₂ -P ₃ 14.0'	

TYPICAL MRD SLAB: Slab 1



COMMENTS: General comments apply; Chip and seal repairs extensive along longitudinal joint; Polished agg (severe) in wheelpath; Popouts: ~ 2.5 per m²

Site 11

DATE: 9/10/1999

SITE #: 11

LOCATION: Route: US-27 NB; Starts @ Sta 521+16; Past Rest Area as well as ramp for West 10 to 115; Past MP 179; 13' north of "27 North" sign

JOINT SPACING: 99' (30.2 m), asphalt shoulders



SLAB 1



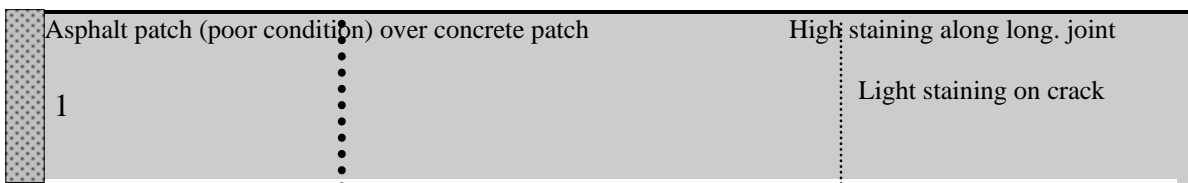
SLAB 2



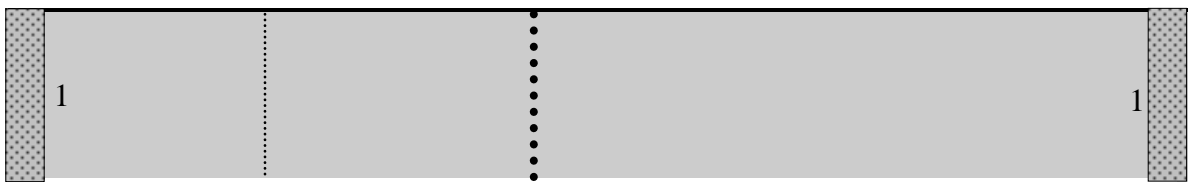
SLAB 3



SLAB 4



SLAB 5



SLAB 6

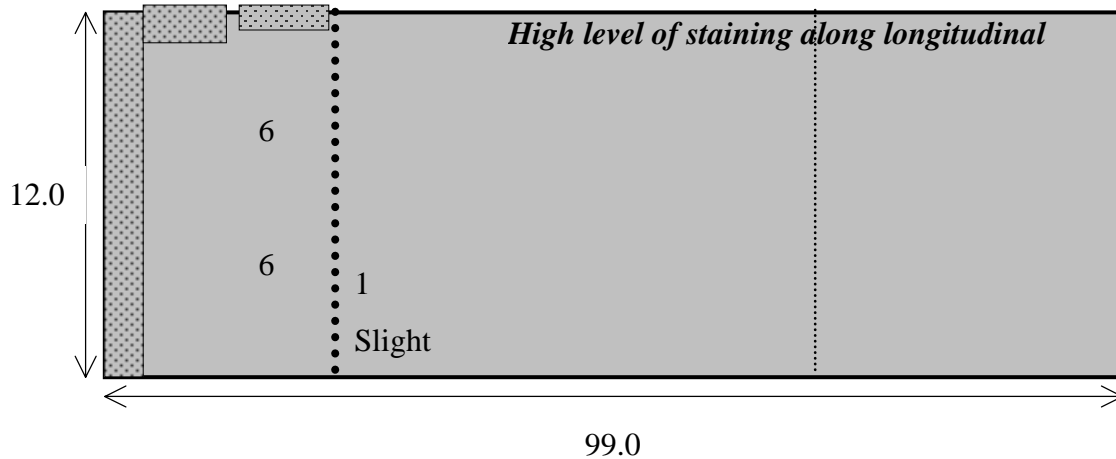
KEY: <i>Transverse Cracking</i>	<i>Patching</i>	1. Spalling	5. High steel
Low	Full-depth Concrete	2. D-Cracking	6. Polished agg
Moderate ●●●●●	Asphalt Patch	3. Popouts	7. Faulting
High ●●●●	Expansion joint	4. ASR	8. Long. crack

COMMENTS: Longitudinal joint is completely spalled and asphalt repaired in many spots; high steel in a few areas; large amount of polished aggregate; many popouts throughout site; large amount of small, tight cracks (possibly old shrinkage cracks)

CRACK SPACINGS:

<u>Slab 1</u>	<u>Slab 2</u>	<u>Slab 3</u>
J ₁ -C ₁ 84.0'	J ₂ -C ₁ 65.0'	J ₃ -C ₁ 19.0'
		C ₂ -C ₂ 12.0'
<u>Slab 4</u>	<u>Slab 5</u>	<u>Slab 6</u>
	J ₅ -C ₁ 26.0'	J ₆ -C ₁ 22.0'
	C ₁ -C ₂ 46.0'	C ₁ -P ₆ 24.0'

TYPICAL MRD SLAB: Slab 5



COMMENTS: Shrinkage-like cracking which is very tough to see, predominantly transverse; Polished agg (severe) in wheelpath; Popouts: ~ 2-3 per m²

Site 12

DATE: 9/10/1999

SITE #: 12

LOCATION: Route: US-27 SB; Starts @ Sta 843+45 (stationing in passing lane); Next to North Star Golf Course (next to 1st green and pond); across street from 4143 US-27 NB (white house with barn); Site ends a Rainbow Lake billboard, before Hayes Road and North Star driving range

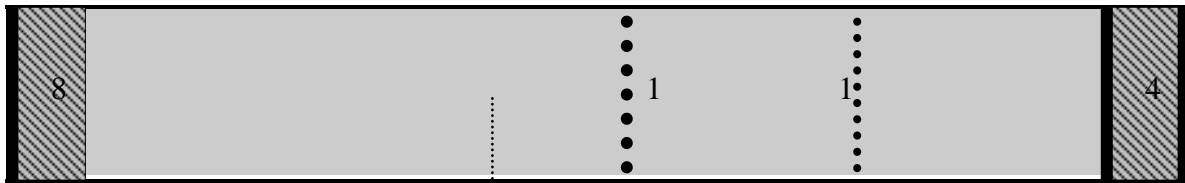
JOINT SPACING: 99' (30.2 m), asphalt shoulders



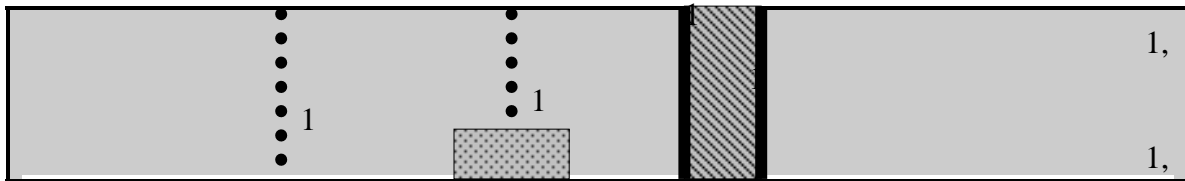
SLAB 1



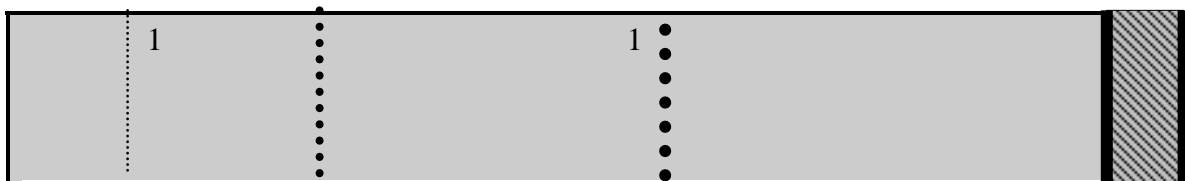
SLAB 2



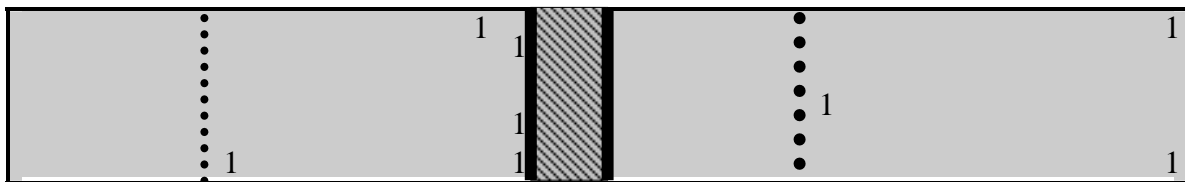
SLAB 3




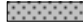

SLAB 4



SLAB 5



SLAB 6

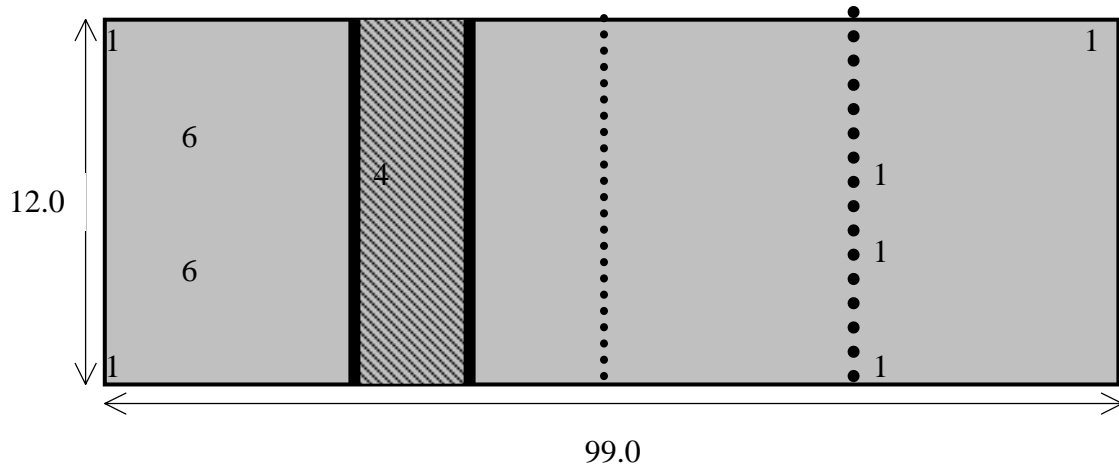
KEY: <i>Transverse Cracking</i>	<i>Patching</i>		1. Spalling	5. High steel
Low 	Full-depth Concrete 		2. D-Cracking	6. Polished agg
Moderate 	Asphalt Patch 		3. Popouts	7. Faulting
High •••••	Expansion joint 		4. ASR	8. Long. crack

COMMENTS: Polished agg and tiny cracks (possibly old shrinkage cracking) throughout site

CRACK SPACINGS:

<u>Slab 1</u>		<u>Slab 2</u>		<u>Slab 3</u>	
J ₁ -C ₁	8.0'	J ₂ -P ₁	17.0'	J ₃ -P ₂	0.0'
C ₁ -C ₂	82.0'	P ₁ -P ₁	6.0'	P ₂ -P ₂	6.0'
C ₂ -J ₂	9.0'	P ₁ -C ₂	12.0'	P ₂ -C ₁	41.0'
		C ₂ -C ₃	38.0'	C ₁ -C ₂	11.0'
		C ₃ -J ₃	26.0'	C ₂ -C ₃	23.0'
				C ₃ -P ₃	15.0'
				P ₃ -P ₃	5.0'
				P ₃ -J ₄	0.0'
<u>Slab 4</u>		<u>Slab 5</u>		<u>Slab 6</u>	
J ₄ -C ₁	21.0'	J ₅ -C ₁	13.0'	J ₆ -C ₁	15.0'
C ₁ -C ₂	19.0'	C ₁ -C ₂	13.0'	C ₁ -P ₆	28.0'
C ₂ -P ₄	15.0'	C ₂ -C ₃	?	P ₆ -P ₆	6.0'
P ₄ -P ₄	7.0'	C ₃ -P ₅	?	P ₆ -C ₂	15.0'
P ₂ -J ₅	35.0'	P ₅ -P ₅	6.0'	C ₂ -C ₃	23.0'
		P ₃ -J ₆	0.0'	C ₃ -J ₇	35.0'

TYPICAL MRD SLAB: Slab 2



COMMENTS: Shrinkage-like cracking which is very tough to see, predominantly transverse; Popouts: ~ 3 per m²

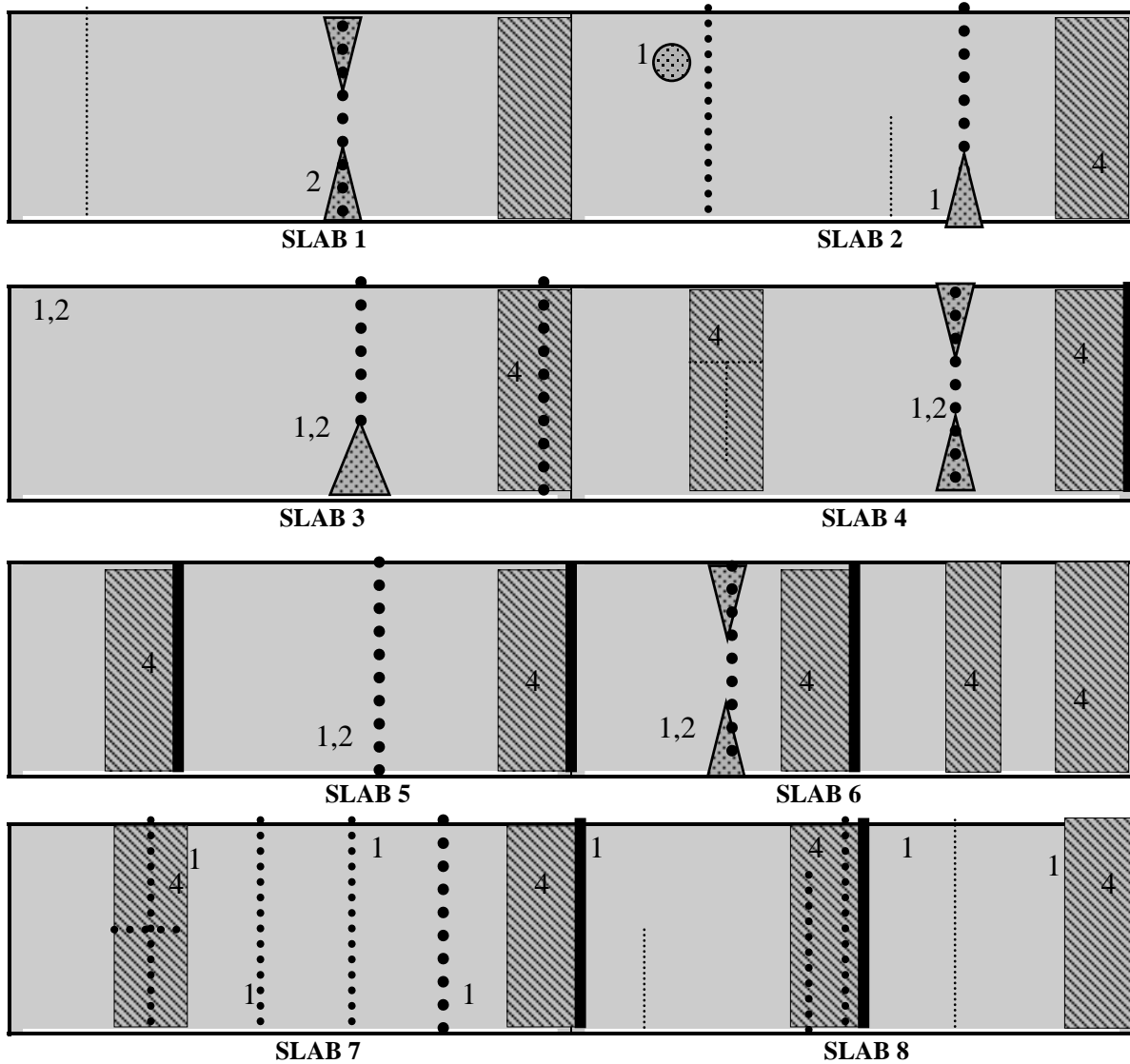
Site 13


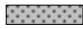

DATE: 9/10/1999

SITE #: 13

LOCATION: Route: M-46 EB; Starts @ Sta 170+18; West of Edmore; East of "Reduced Speed 40 mph" sign; approximately 1/4 mile east of Edmore Auto Sales; One lane each way, no turn lane for traffic control purposes, fairly wide shoulder

JOINT SPACING: Approximately 75' (22.9 m), asphalt shoulders



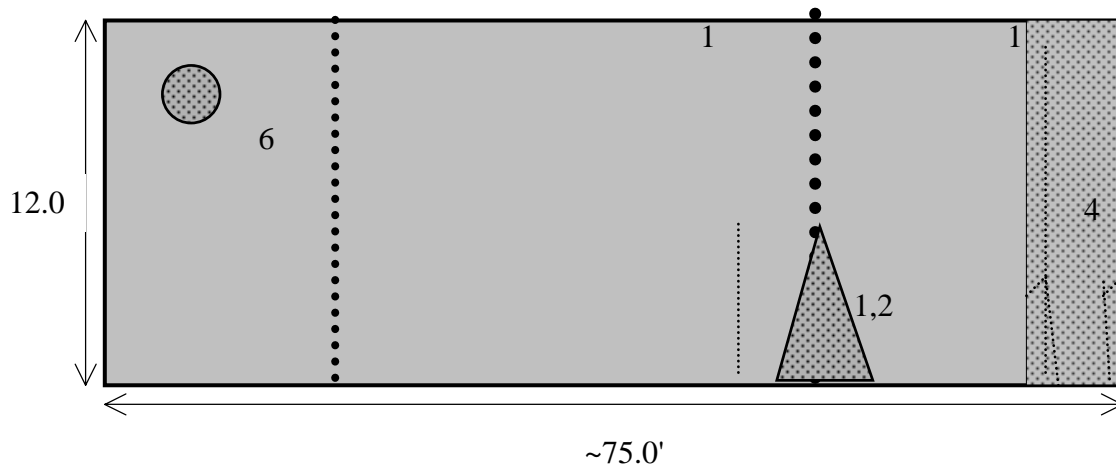
KEY: <i>Transverse Cracking</i>	<i>Patching</i>		1. Spalling	5. High steel
Low	Full-depth Concrete		2. D-Cracking	6. Polished agg
Moderate•••••	Asphalt Patch		3. Popouts	7. Faulting
High•••••	Expansion joint		4. ASR	8. Long. crack

COMMENTS: All joints have been repaired by a full-depth patch, making joint spacing difficult to determine; ASR in most concrete patches; D-cracking on many severe cracks; Many popouts, high steel, and polished aggregate in the wheelpaths

CRACK SPACINGS:

<u>Slab 1</u>	<u>Slab 2</u>	<u>Slab 3</u>	<u>Slab 4</u>
J ₁ -C ₁ 12.0'	J ₂ -C ₁ 9.0'	J ₃ -C ₁ 50.0'	J ₄ -P ₁ 21.0'
C ₁ -C ₂ 44.0'	C ₁ -C ₂ 41.0'		P ₁ -C ₁ 39.0'
	C ₂ -C ₃ 5.0'		
<u>Slab 5</u>	<u>Slab 6</u>	<u>Slab 7</u>	<u>Slab 8</u>
J ₅ -P ₁ 14.0'	J ₆ -C ₁ 14.0'	J ₇ -P ₁ 9.0'	J ₈ -P ₁ 6.0'
P ₁ -C ₁ 38.0'	C ₁ -P ₁ 13.0'	P ₁ -P ₁ 14.0'	P ₁ -C ₁ 49.0'
		P ₁ -C ₁ 9.0'	
		C ₁ -C ₂ 6.0'	
		C ₂ -C ₃ 9.0'	

TYPICAL MRD SLAB: Slab 2



COMMENTS: ASR in patch; D-cracking near major crack; Polished agg (severe) in wheelpath; Popouts: ~ 3 per m²

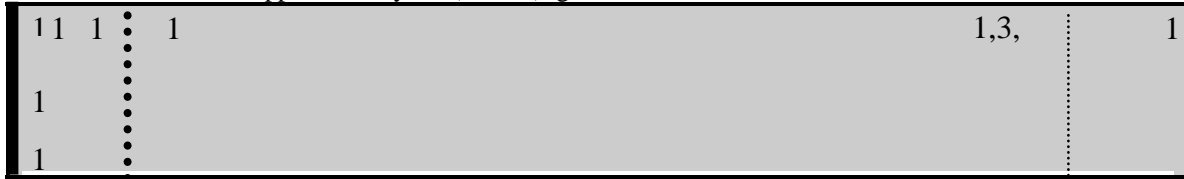
Site 14

DATE: 10/5/1999

SITE #: 14

LOCATION: Route: M-81 EB; No station numbering; East of Caro; Starts 160' East of intersection of M-81 and Mcgregory/Lazell Road; Approximately 4.7 miles of M-81/M-24 intersection in Caro; One lane each way, no turn lane for traffic control purposes, gravel shoulder on rising grade

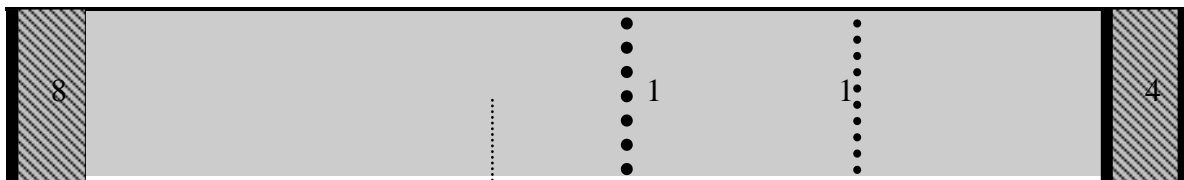
JOINT SPACING: Approximately 99' (30.2 m), gravel shoulders



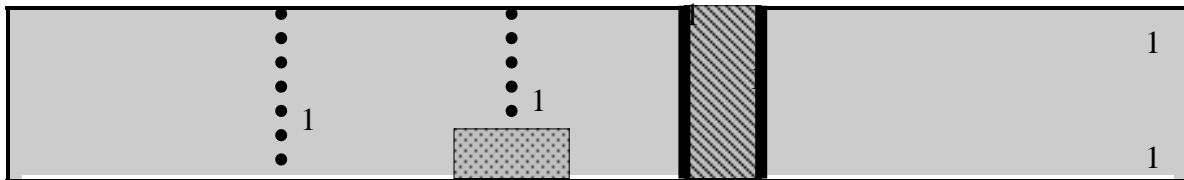
SLAB 1



SLAB 2



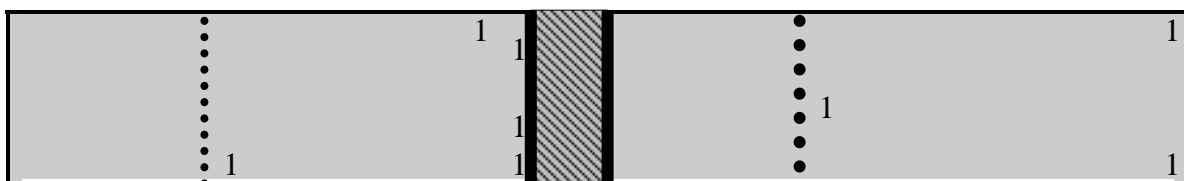
SLAB 3






SLAB 4



SLAB 5



SLAB 6

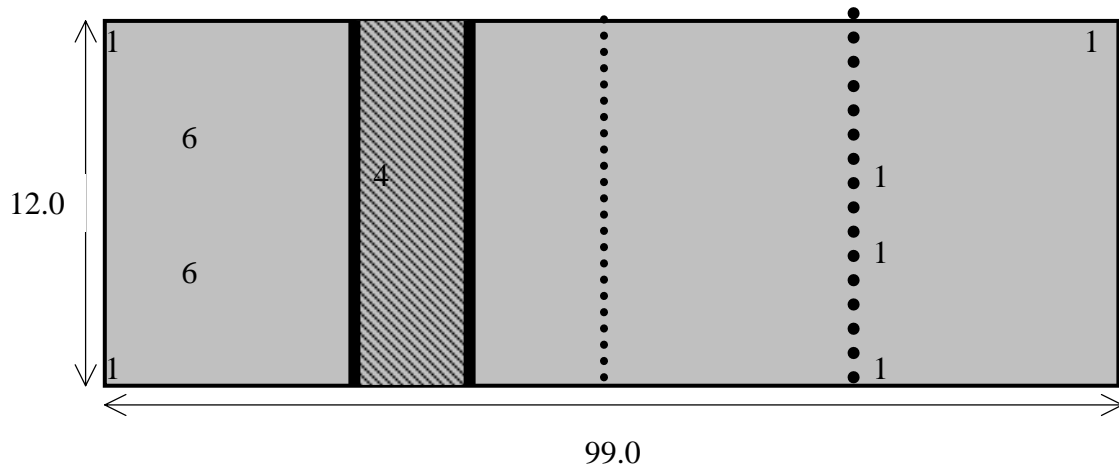
KEY: <i>Transverse Cracking</i>	<i>Patching</i>		1. Spalling	5. High steel
Low	Full-depth Concrete		2. D-Cracking	6. Polished agg
Moderate ●●●●●●	Asphalt Patch		3. Popouts	7. Faulting
High ●●●●	Expansion joint		4. ASR	8. Long. crack

COMMENTS: Polished agg and tiny cracks (possibly old shrinkage cracking) throughout site

CRACK SPACINGS:

<u>Slab 1</u>		<u>Slab 2</u>		<u>Slab 3</u>	
J ₁ -C ₁	8.0'	J ₂ -P ₁	17.0'	J ₃ -P ₂	0.0'
C ₁ -C ₂	82.0'	P ₁ -P ₁	6.0'	P ₂ -P ₂	6.0'
C ₂ -J ₂	9.0'	P ₁ -C ₂	12.0'	P ₂ -C ₁	41.0'
		C ₂ -C ₃	38.0'	C ₁ -C ₂	11.0'
		C ₃ -J ₃	26.0'	C ₂ -C ₃	23.0'
				C ₃ -P ₃	15.0'
				P ₃ -P ₃	5.0'
				P ₃ -J ₄	0.0'
<u>Slab 4</u>		<u>Slab 5</u>		<u>Slab 6</u>	
J ₄ -C ₁	21.0'	J ₅ -C ₁	13.0'	J ₆ -C ₁	15.0'
C ₁ -C ₂	19.0'	C ₁ -C ₂	13.0'	C ₁ -P ₆	28.0'
C ₂ -P ₄	15.0'	C ₂ -C ₃	?	P ₆ -P ₆	6.0'
P ₄ -P ₄	7.0'	C ₃ -P ₅	?	P ₆ -C ₂	15.0'
P ₂ -J ₅	35.0'	P ₅ -P ₅	6.0'	C ₂ -C ₃	23.0'
		P ₃ -J ₆	0.0'	C ₃ -J ₇	35.0'

TYPICAL MRD SLAB: Slab 2



COMMENTS: Shrinkage-like cracking, which is very tough to see, predominantly transverse; Popouts: ~ 3 per m²

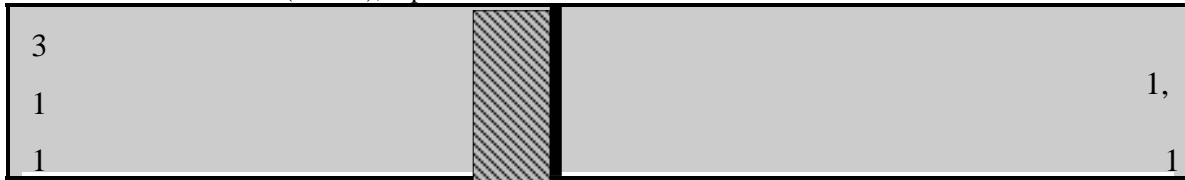
Site 17

DATE: 9/21/1999

SITE #: 17

LOCATION: Route: US-31 SB; South of Grand Haven; Just south of Hayes Street Light; 32' south of turnaround sign "Hayes St East, North 31"; Next to "Michigan Apples 4 Miles on Right at Light" sign; No station numbers (diamond ground) or MP numbers

JOINT SPACING: 99' (30.2 m), asphalt shoulders



SLAB 1



SLAB 2



SLAB 3






SLAB 4



SLAB 5



SLAB 6

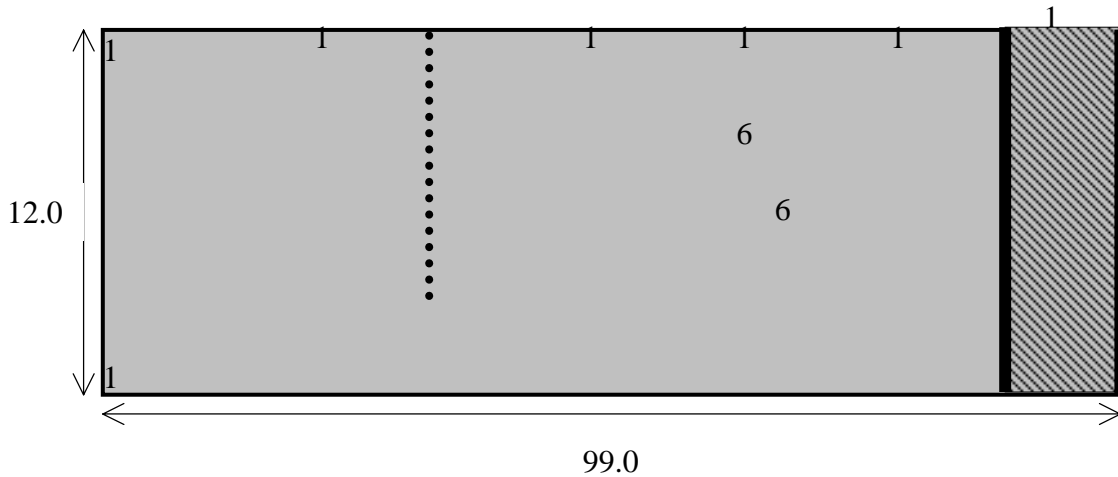
KEY: <i>Transverse Cracking</i>	<i>Patching</i>		1. Spalling	5. High steel
Low	Full-depth Concrete		2. D-Cracking	6. Polished agg
Moderate•••••	Asphalt Patch		3. Poor sealant	7. Faulting
High•••••	Expansion joint		4. ASR	8. Long. crack

COMMENTS: Entire site is diamond ground, shrinkage cracking throughout site (tough to see due to surface texture after grinding)

CRACK SPACINGS:

<u>Slab 1</u>	<u>Slab 2</u>	<u>Slab 3</u>
J ₁ -P ₁ 42.0'	J ₂ -P ₁ 93.0'	J ₃ -C ₁ 35.0'
		C ₁ -C ₂ 21.0'
		C ₂ -C ₃ 15.0'
		C ₃ -P ₁ 22.0'
<u>Slab 4</u>	<u>Slab 5</u>	<u>Slab 6</u>
J ₄ -P ₁ 93.0'	J ₅ -P ₁ 93.0'	J ₆ -C ₁ 35.0'
	C ₁ -C ₂ 13.0'	C ₁ -P ₁ 58.0'

TYPICAL MRD SLAB: Slab 6



COMMENTS: Shrinkage-like cracking throughout slab; Popouts: ~ 1.5 per m² - could be due to diamond grinding; joint before patch is completely missing sealant.

Site 18

DATE: 9/21/1999

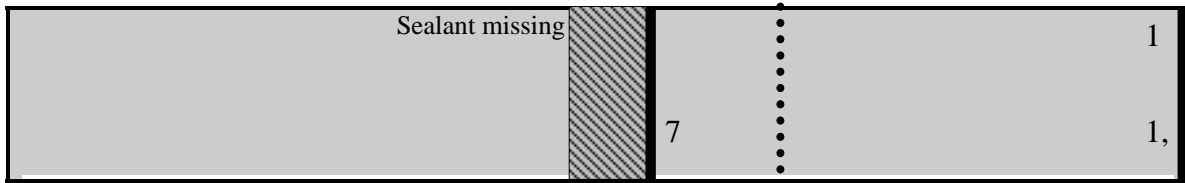
SITE #: 18

LOCATION: Route: I-196 SB; South of Holland; Just south of MP 42; Starts @ Station 517+54; Next to "Saugatuck Dunes State Park" sign

JOINT SPACING: 99' (30.2 m), asphalt shoulders



SLAB 1



SLAB 2



SLAB 3






SLAB 4



SLAB 5



SLAB 6

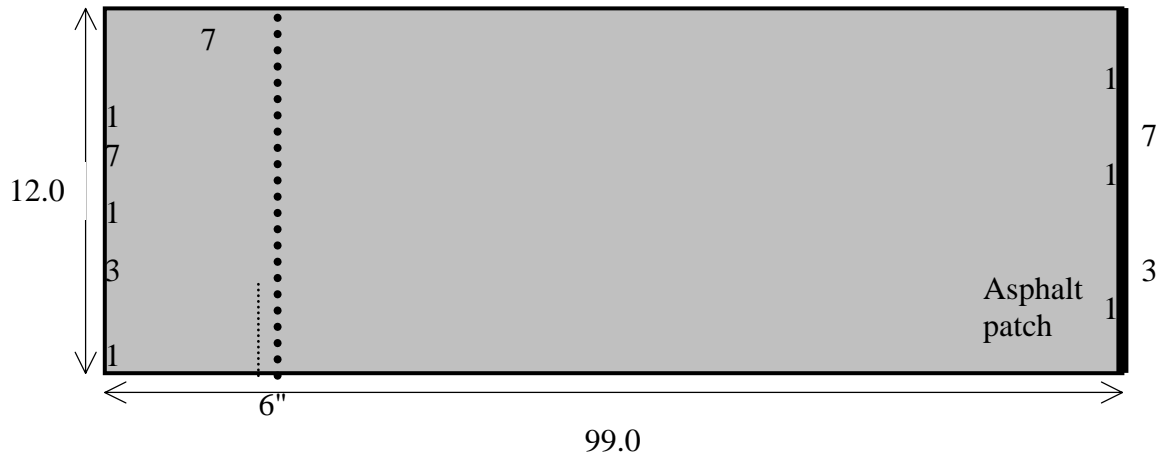
KEY: <i>Transverse Cracking</i>	<i>Patching</i>		1. Spalling	5. High steel
Low 	Full-depth Concrete 		2. D-Cracking	6. Polished agg
Moderate 	Asphalt Patch 		3. Poor sealant	7. Faulting
High •••••	Expansion joint 		4. ASR	8. Long. crack

COMMENTS: Large amount of shrinkage cracking and polished agg throughout site

CRACK SPACINGS:

<u>Slab 1</u>	<u>Slab 2</u>	<u>Slab 3</u>
J ₁ -C ₁ 60.0'?	J ₂ -P ₁ 48.0'	
	P ₁ -C ₁ 14.0'	
<u>Slab 4</u>	<u>Slab 5</u>	<u>Slab 6</u>
J ₄ -C ₁ 16.0'		J ₆ -P ₁ 93.0'

TYPICAL MRD SLAB: Slab 4



COMMENTS: Shrinkage-like cracking throughout slab; Popouts: ~ 0.5 per m²; Polished agg in wheelpath

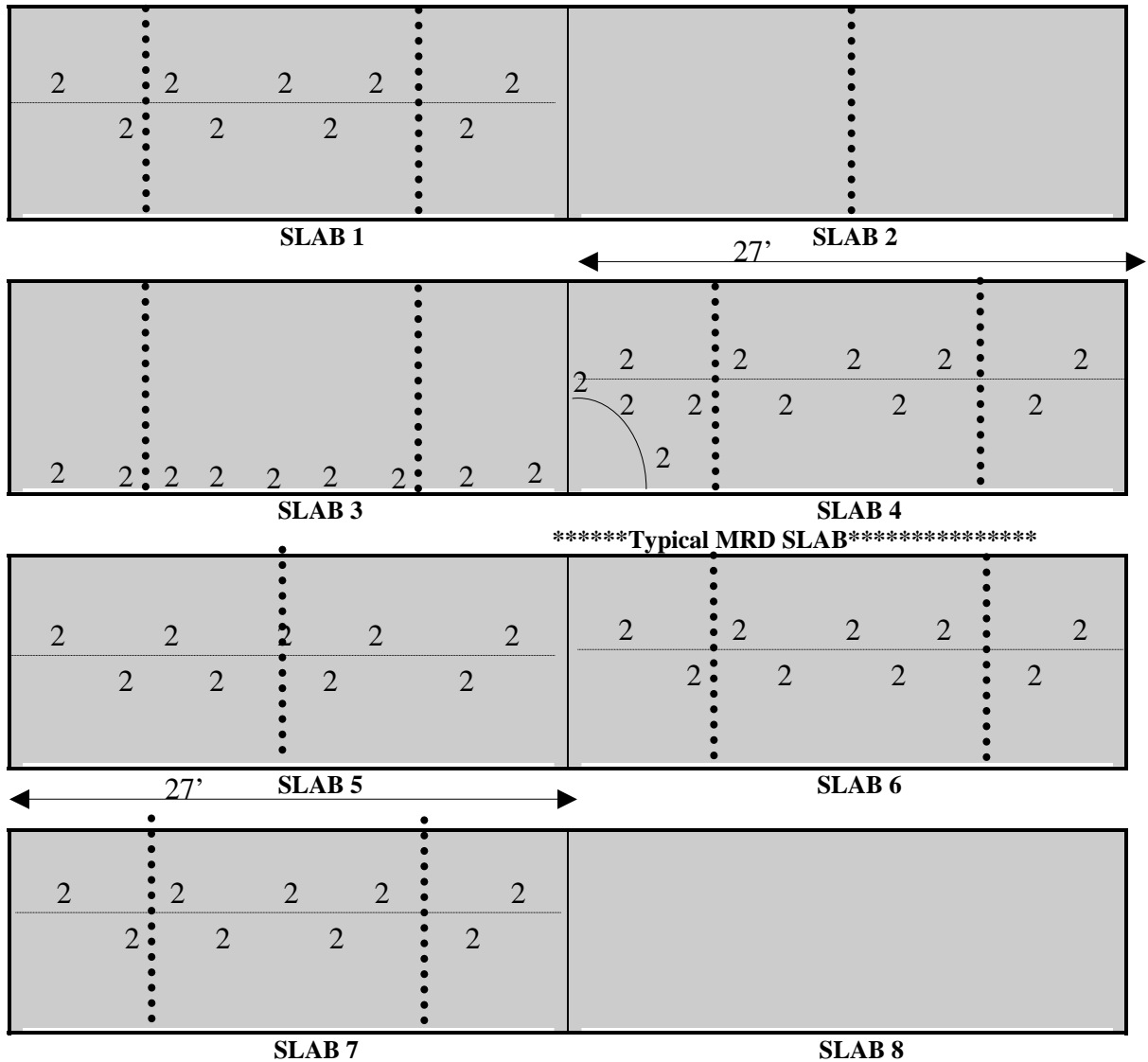
Site 19


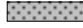

DATE: 08/21/2000

SITE #: 19

LOCATION: M-53 North; Starts @ Sta 517+57; Between 17th and 18th Mile Road, Just in front of Total Gas station.

JOINT SPACING: 71' (21.6 m), asphalt shoulders



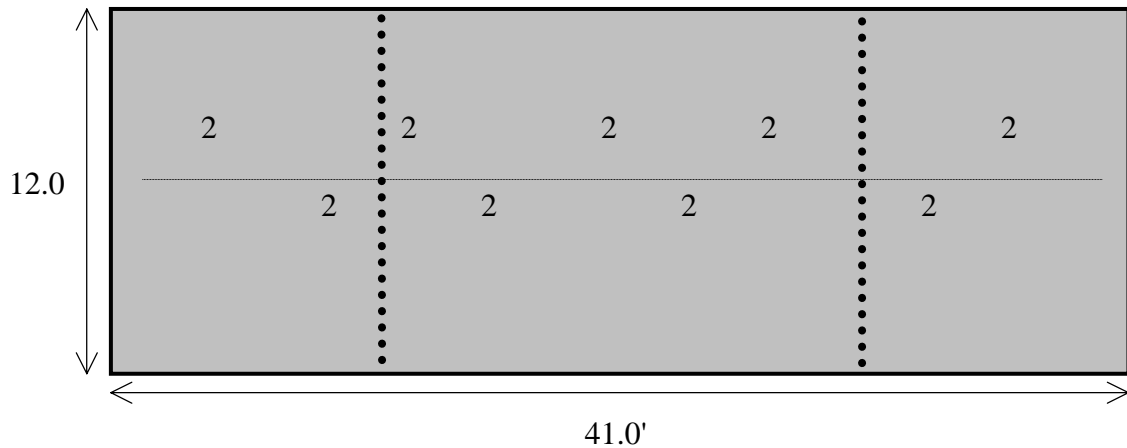
KEY: <i>Transverse Cracking..</i>	<i>Patching</i>		1. Spalling	5. High steel
Low	Full-depth Concrete		2. D-Cracking	6. Polished agg
Moderate	Asphalt Patch		3. Poor sealant	7. Faulting
High	Expansion joint		4. ASR	8. Long. crack

COMMENTS: Third point cracking in every slab; ASR kind of cracking is visible along the longitudinal crack and by the edge of the pavement.

CRACK SPACINGS:

<u>Slab 1</u>	<u>Slab 2</u>	<u>Slab 3</u>	<u>Slab 4</u>
J ₁ -C ₁ 13'0"	J ₂ -C ₁ 14'0"	J ₃ -C ₁ 14'0"	J ₄ -C ₁
C ₁ -C ₂ 14'0"		C ₁ -C ₂ 26'0"	C ₁ -P ₁
Edge-LC 6'5"			
<u>Slab 5</u>	<u>Slab 6</u>	<u>Slab 7</u>	
J ₅ -P ₁ 16'0"	J ₆ -C ₁ 13'6"	J ₇ -C ₁ 12'10"	
	C ₁ -C ₂ 13'8"	C ₁ -C ₂ 14'2"	
		P ₁ -P ₂	
		P ₂ -P ₂	
		P ₂ -P ₃	

TYPICAL MRD SLAB: Slab 4



COMMENTS: General comments apply. Longitudinal crack at the middle of the slab and D-cracking is observed along the longitudinal crack.

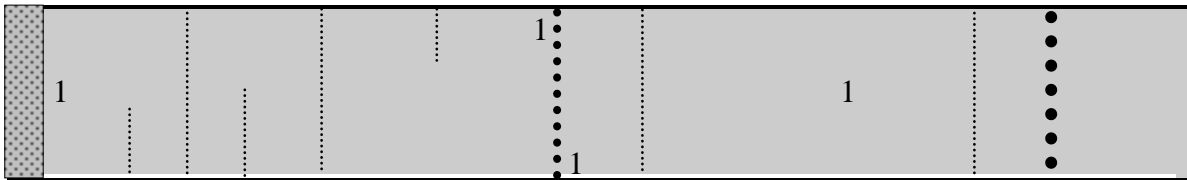
Site 22




DATE: 5/16/2000

SITE #: 22

LOCATION: Route: I-75 NB; Starts @ Sta 277+21; North of Mackinaw Bridge and North of MP 349;

JOINT SPACING: 99' (30.2 m), asphalt shoulders



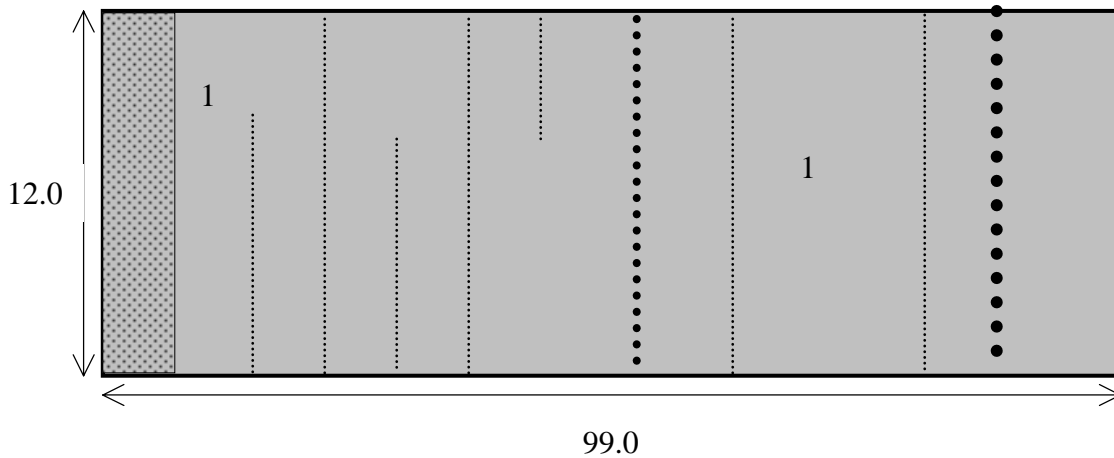
KEY: <i>Transverse Cracking</i>	<i>Patching</i>		1. Spalling	5. High steel
Low 	Full-depth Concrete		2. D-Cracking	6. Polished agg
Moderate 	Asphalt Patch		3. Popouts	7. Faulting
High •••••	Expansion joint		4. ASR	8. Long. crack

COMMENTS: Longitudinal joint is completely spalled; large amount of polished aggregate; many popouts throughout site; large amount of small, tight cracks (possibly old shrinkage cracks)

CRACK SPACINGS:

<u>Slab 1</u>	<u>Slab 2</u>	<u>Slab 3</u>
J ₁ -C ₁	J ₂ -C ₁	J ₃ -C ₁ C ₂ -C ₂
<u>Slab 4</u>	<u>Slab 5</u>	<u>Slab 6</u>
	J ₅ -C ₁ C ₁ -C ₂	J ₆ -C ₁ C ₁ -P ₆

TYPICAL MRD SLAB: Slab 1



COMMENTS: Shrinkage-like cracking which is very tough to see, predominantly transverse; Polished agg (severe) in wheelpath; Popouts: ~ 1 per m²

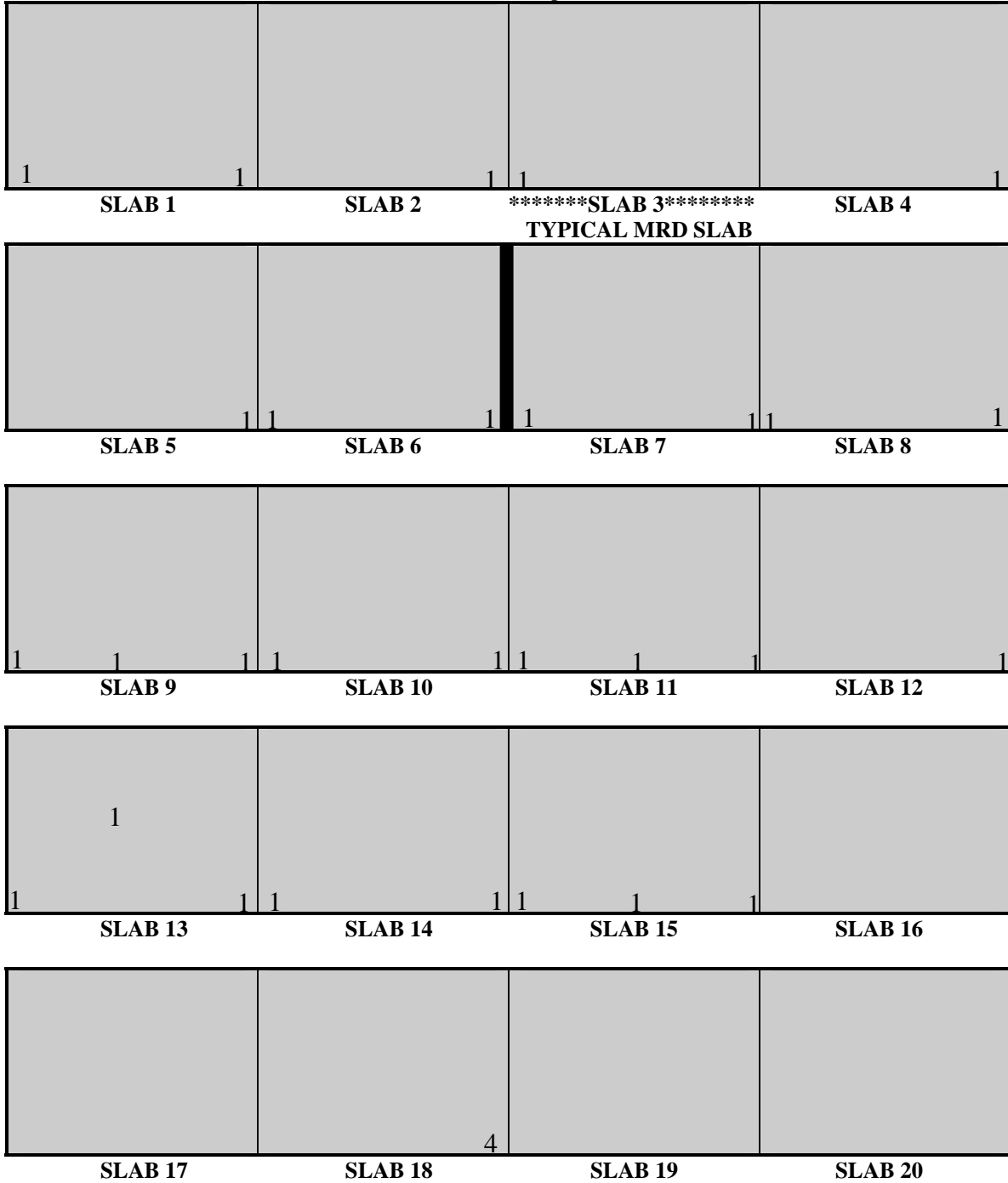
Site 26A




DATE: 5/4/2000

SITE #: 26A

LOCATION: Route: US-10 WB; Starts @ Sta 137+08; Before Next Right Sign;

JOINT SPACING: Varied Between 18', 12', 13' with Asphalt Concrete shoulders



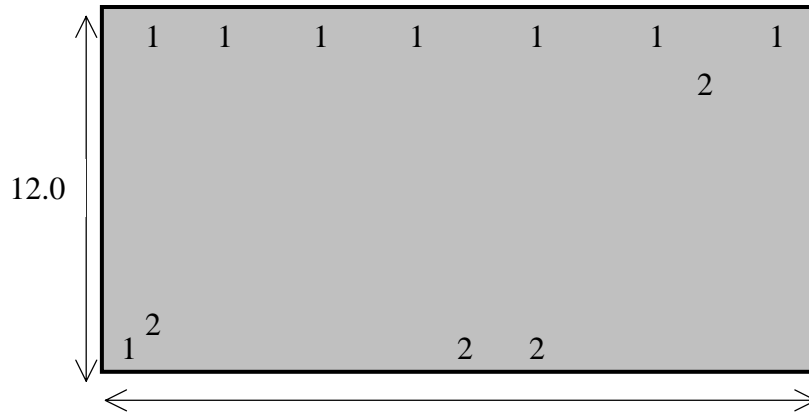
KEY: <i>Transverse Cracking</i>	<i>Patching</i>		1. Spalling	5. High steel
Low	Full-depth Concrete		2. D-Cracking	6. Polished agg
Moderate ●●●●●	Asphalt Patch		3. Poor sealant	7. Faulting
High ●●●●	Expansion joint		4. ASR	8. Long. crack

COMMENTS: Longitudinal joint completely spalled, Possible D-cracking at joints and cracks, Popouts: ~2 per m²

CRACK SPACINGS:

<u>Slab 1</u>	<u>Slab 2</u>	<u>Slab 3</u>	<u>Slab 4</u>
J ₁ -C ₁ C ₁ -C ₂ C ₂ -C ₃	J ₂ -C ₁ C ₁ -C ₂ C ₂ -C ₃	J ₃ -C ₁ C ₁ -C ₂ C ₂ -C ₃	J ₄ -C ₁ C ₁ -C ₂ C ₂ -C ₃
<u>Slab 5</u>	<u>Slab 6</u>	<u>Slab 7</u>	<u>Slab 8</u>
J ₁ -C ₁ C ₁ -C ₂ C ₂ -C ₃	J ₂ -C ₁ C ₁ -C ₂ C ₂ -C ₃	J ₃ -C ₁ C ₁ -C ₂ C ₂ -C ₃	J ₄ -C ₁ C ₁ -C ₂ C ₂ -C ₃
<u>Slab 9</u>	<u>Slab 10</u>	<u>Slab 11</u>	<u>Slab 12</u>
J ₁ -C ₁ C ₁ -C ₂ C ₂ -C ₃	J ₂ -C ₁ C ₁ -C ₂ C ₂ -C ₃	J ₃ -C ₁ C ₁ -C ₂ C ₂ -C ₃	J ₄ -C ₁ C ₁ -C ₂ C ₂ -C ₃
<u>Slab 13</u>	<u>Slab 14</u>	<u>Slab 15</u>	<u>Slab 16</u>
J ₁ -C ₁ C ₁ -C ₂ C ₂ -C ₃	J ₂ -C ₁ C ₁ -C ₂ C ₂ -C ₃	J ₃ -C ₁ C ₁ -C ₂ C ₂ -C ₃	J ₄ -C ₁ C ₁ -C ₂ C ₂ -C ₃
<u>Slab 17</u>	<u>Slab 18</u>	<u>Slab 19</u>	<u>Slab 20</u>
J ₁ -C ₁ C ₁ -C ₂ C ₂ -C ₃	J ₂ -C ₁ C ₁ -C ₂ C ₂ -C ₃	J ₃ -C ₁ C ₁ -C ₂ C ₂ -C ₃	J ₄ -C ₁ C ₁ -C ₂ C ₂ -C ₃

TYPICAL MRD SLAB: Slab 3



13.0

COMMENTS: Longitudinal joint completely spalled; Possible D-cracking at joints; Map cracking near joint and shoulder; Popouts: ~2 per m²

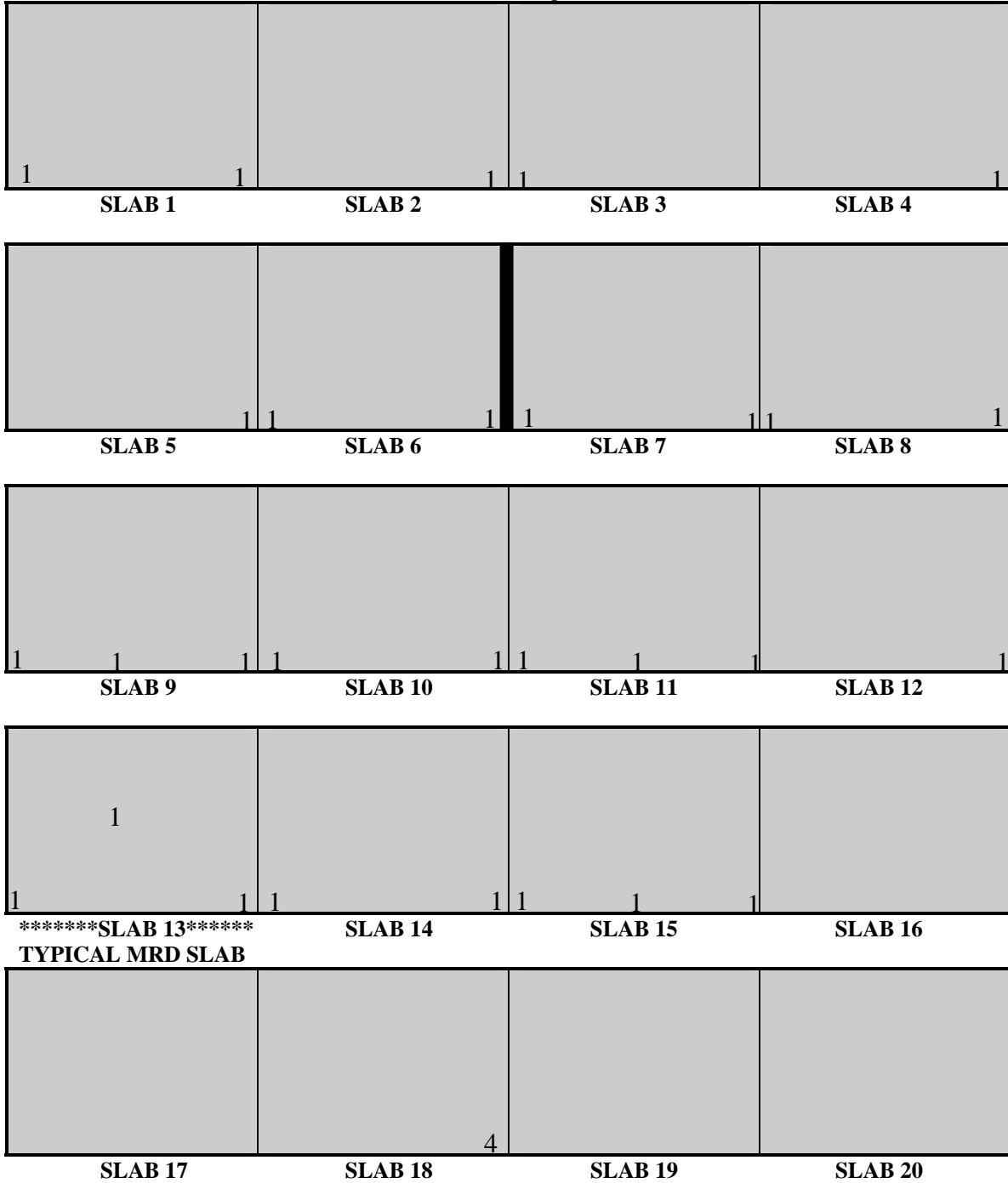
Site 26B




DATE: 5/4/2000

SITE #: 26B

LOCATION: Route: US-10 WB; Starts @ Sta 137+08; Before Next Right Sign;

JOINT SPACING: Varied Between 18', 12', 13' with Asphalt Concrete shoulders



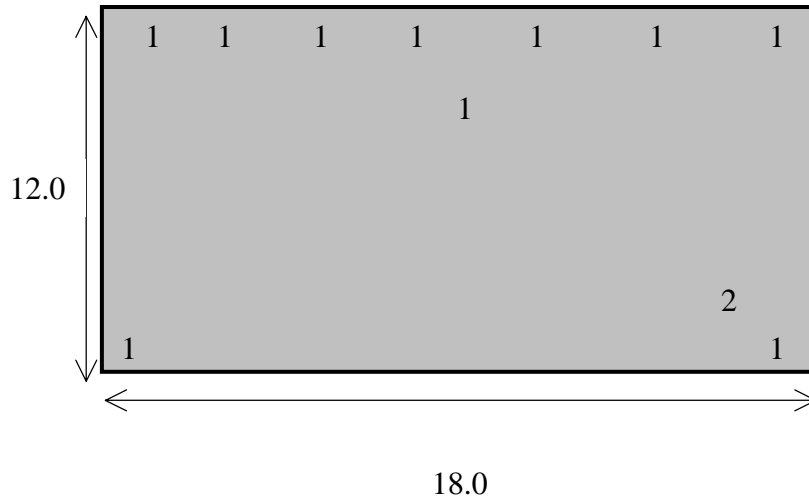
KEY: <i>Transverse Cracking</i>	<i>Patching</i>		1. Spalling	5. High steel
Low 	Full-depth Concrete 		2. D-Cracking	6. Polished agg
Moderate 	Asphalt Patch 		3. Poor sealant	7. Faulting
High •••••	Expansion joint 		4. ASR	8. Long. crack

COMMENTS: Longitudinal joint completely spalled, Possible D-cracking at joints and cracks, Popouts: ~2 per m²

CRACK SPACINGS:

<u>Slab 1</u>	<u>Slab 2</u>	<u>Slab 3</u>	<u>Slab 4</u>
J ₁ -C ₁ C ₁ -C ₂ C ₂ -C ₃	J ₂ -C ₁ C ₁ -C ₂ C ₂ -C ₃	J ₃ -C ₁ C ₁ -C ₂ C ₂ -C ₃	J ₄ -C ₁ C ₁ -C ₂ C ₂ -C ₃
<u>Slab 5</u>	<u>Slab 6</u>	<u>Slab 7</u>	<u>Slab 8</u>
J ₁ -C ₁ C ₁ -C ₂ C ₂ -C ₃	J ₂ -C ₁ C ₁ -C ₂ C ₂ -C ₃	J ₃ -C ₁ C ₁ -C ₂ C ₂ -C ₃	J ₄ -C ₁ C ₁ -C ₂ C ₂ -C ₃
<u>Slab 9</u>	<u>Slab 10</u>	<u>Slab 11</u>	<u>Slab 12</u>
J ₁ -C ₁ C ₁ -C ₂ C ₂ -C ₃	J ₂ -C ₁ C ₁ -C ₂ C ₂ -C ₃	J ₃ -C ₁ C ₁ -C ₂ C ₂ -C ₃	J ₄ -C ₁ C ₁ -C ₂ C ₂ -C ₃
<u>Slab 13</u>	<u>Slab 14</u>	<u>Slab 15</u>	<u>Slab 16</u>
J ₁ -C ₁ C ₁ -C ₂ C ₂ -C ₃	J ₂ -C ₁ C ₁ -C ₂ C ₂ -C ₃	J ₃ -C ₁ C ₁ -C ₂ C ₂ -C ₃	J ₄ -C ₁ C ₁ -C ₂ C ₂ -C ₃
<u>Slab 17</u>	<u>Slab 18</u>	<u>Slab 19</u>	<u>Slab 20</u>
J ₁ -C ₁ C ₁ -C ₂ C ₂ -C ₃	J ₂ -C ₁ C ₁ -C ₂ C ₂ -C ₃	J ₃ -C ₁ C ₁ -C ₂ C ₂ -C ₃	J ₄ -C ₁ C ₁ -C ₂ C ₂ -C ₃

TYPICAL MRD SLAB: Slab 13



COMMENTS: Longitudinal joint completely spalled; Possible D-cracking at joints; Map cracking near joint and shoulder; Popouts: ~2 per m²

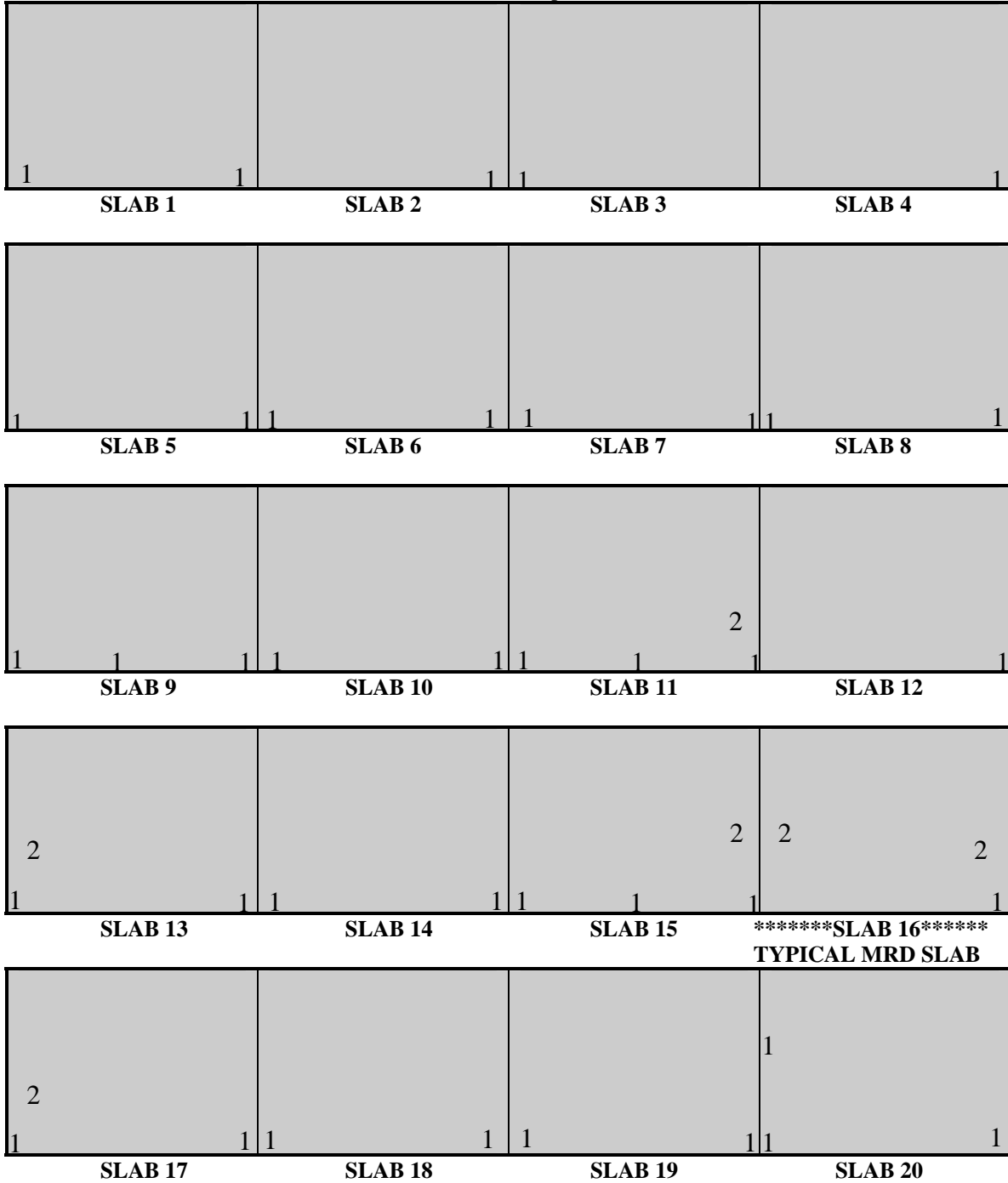
Site 27




DATE: 5/4/2000

SITE #: 27

LOCATION: Route: US-10 WB; Starts @ Sta 114+00; After Next Right Sign;

JOINT SPACING: Varied Between 18', 12', 13' with Asphalt Concrete shoulders



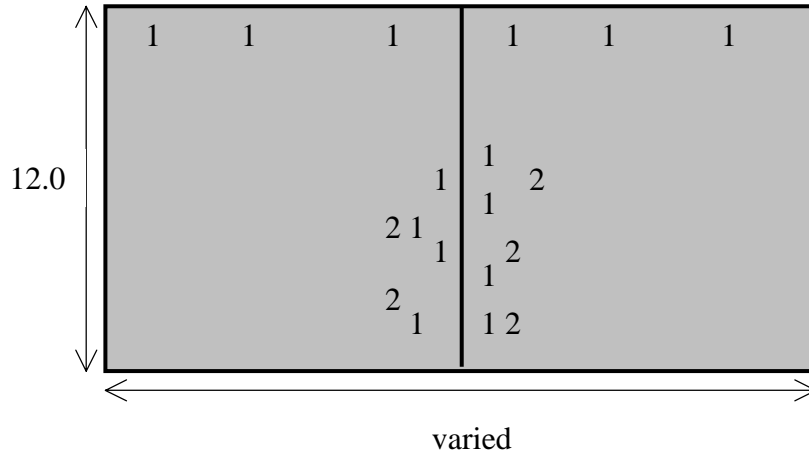
KEY: <i>Transverse Cracking</i>	<i>Patching</i>		1. Spalling	5. High steel
Low	Full-depth Concrete		2. D-Cracking	6. Polished agg
Moderate ●●●●●	Asphalt Patch		3. Poor sealant	7. Faulting
High ●●●●	Expansion joint		4. ASR	8. Long. crack

COMMENTS: Same as 26A and B although the spalling is more severe.

CRACK SPACINGS:

<u>Slab 1</u>	<u>Slab 2</u>	<u>Slab 3</u>	<u>Slab 4</u>
J ₁ -C ₁ C ₁ -C ₂ C ₂ -C ₃	J ₂ -C ₁ C ₁ -C ₂ C ₂ -C ₃	J ₃ -C ₁ C ₁ -C ₂ C ₂ -C ₃	J ₄ -C ₁ C ₁ -C ₂ C ₂ -C ₃
<u>Slab 5</u>	<u>Slab 6</u>	<u>Slab 7</u>	<u>Slab 8</u>
J ₁ -C ₁ C ₁ -C ₂ C ₂ -C ₃	J ₂ -C ₁ C ₁ -C ₂ C ₂ -C ₃	J ₃ -C ₁ C ₁ -C ₂ C ₂ -C ₃	J ₄ -C ₁ C ₁ -C ₂ C ₂ -C ₃
<u>Slab 9</u>	<u>Slab 10</u>	<u>Slab 11</u>	<u>Slab 12</u>
J ₁ -C ₁ C ₁ -C ₂ C ₂ -C ₃	J ₂ -C ₁ C ₁ -C ₂ C ₂ -C ₃	J ₃ -C ₁ C ₁ -C ₂ C ₂ -C ₃	J ₄ -C ₁ C ₁ -C ₂ C ₂ -C ₃
<u>Slab 13</u>	<u>Slab 14</u>	<u>Slab 15</u>	<u>Slab 16</u>
J ₁ -C ₁ C ₁ -C ₂ C ₂ -C ₃	J ₂ -C ₁ C ₁ -C ₂ C ₂ -C ₃	J ₃ -C ₁ C ₁ -C ₂ C ₂ -C ₃	J ₄ -C ₁ C ₁ -C ₂ C ₂ -C ₃
<u>Slab 17</u>	<u>Slab 18</u>	<u>Slab 19</u>	<u>Slab 20</u>
J ₁ -C ₁ C ₁ -C ₂ C ₂ -C ₃	J ₂ -C ₁ C ₁ -C ₂ C ₂ -C ₃	J ₃ -C ₁ C ₁ -C ₂ C ₂ -C ₃	J ₄ -C ₁ C ₁ -C ₂ C ₂ -C ₃

TYPICAL MRD SLAB: Slab 15/16



COMMENTS: Same as 26A and B although the spalling is more severe.

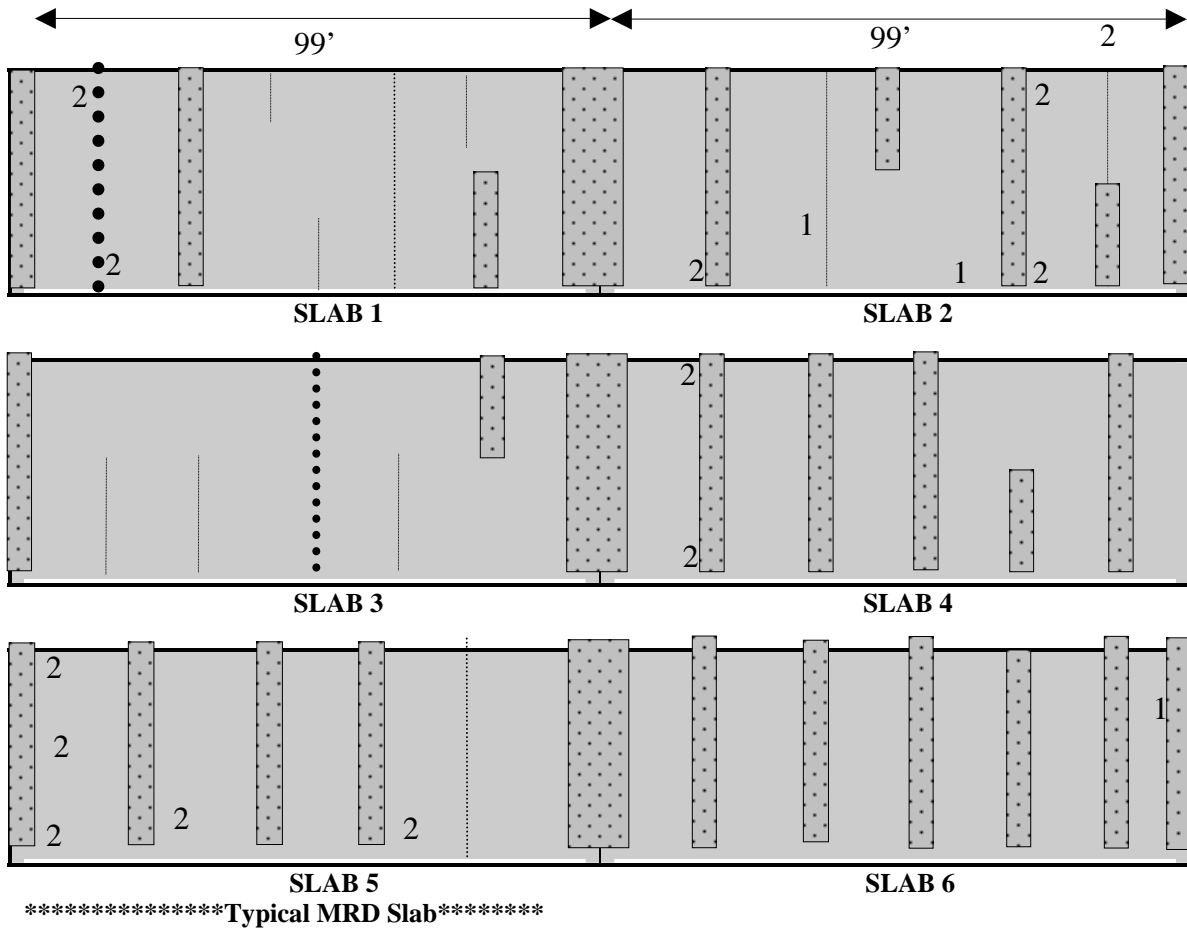
Site 28




DATE: 05/23/2000

SITE #: 28

LOCATION: Route: US-27 SB; Starts @ Sta 519+07; Between MP 155 & 156; Just North of Entrance Ramp;

JOINT SPACING: 99', asphalt shoulders



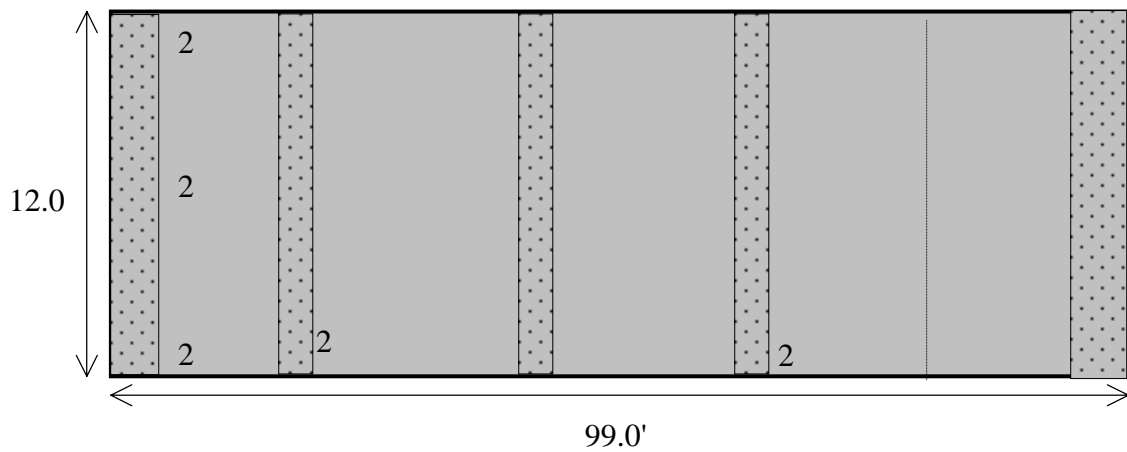
KEY: Transverse Cracking	Low ●●●●●	Patching		1. Spalling	5. High steel
	Moderate	●●●●	Full-depth Concrete		2. D-Cracking	6. Polished agg
High	●●●●	Asphalt Patch		3. Poor sealant	7. Faulting	
		Expansion joint		4. ASR	8. Long. crack	

COMMENTS: Most of the Transverse Cracks are asphalt patched. Spalling on the Longitudinal joints (every 6 feet) but already been patched too. Popouts occurred here and there.

CRACK SPACINGS:

<u>Slab 1</u>	<u>Slab 2</u>	<u>Slab 3</u>	<u>Slab 4</u>
J ₁ -C ₁	J ₂ -C ₁ 38.0'	J ₃ -C ₁	J ₄ -C ₁ 38.0'
C ₁ -C ₂			C ₁ -P ₁ 9.0'
C ₂ -P ₁			
P ₁ -P ₁			
P ₁ -C ₃			
<u>Slab 5</u>	<u>Slab 6</u>		
J ₅ -P ₁	J ₅ -P ₁		
P ₁ -P ₁	P ₁ -P ₁		
P ₁ -P ₂	P ₁ -P ₂		
P ₂ -P ₂ 6.0'	P ₂ -P ₂ 6.0'		
P ₂ -C ₁ 10.0'	P ₂ -C ₁ 10.0'		

TYPICAL MRD SLAB: Slab 3



COMMENTS: General comments apply; Chip and seal repairs extensive along longitudinal joint; Polished agg (severe) in wheelpath; Popouts: ~ 1-2 per m²

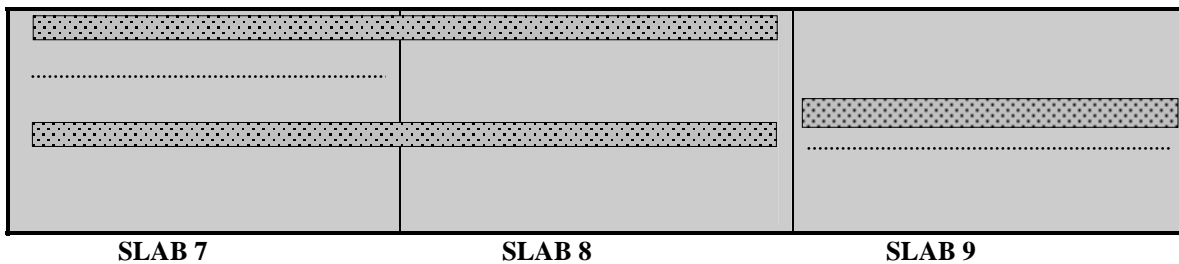
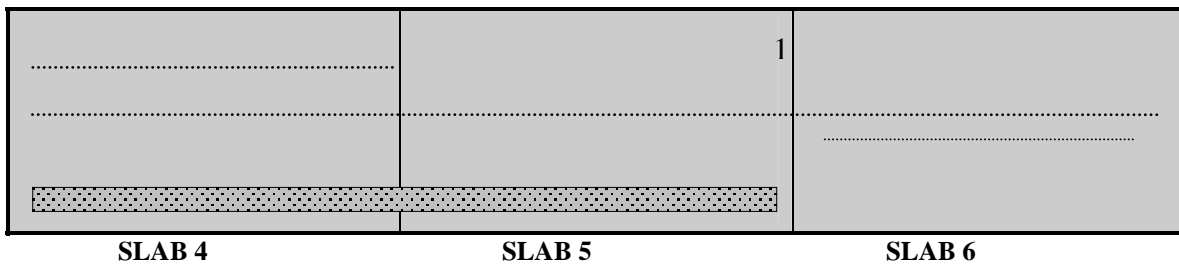
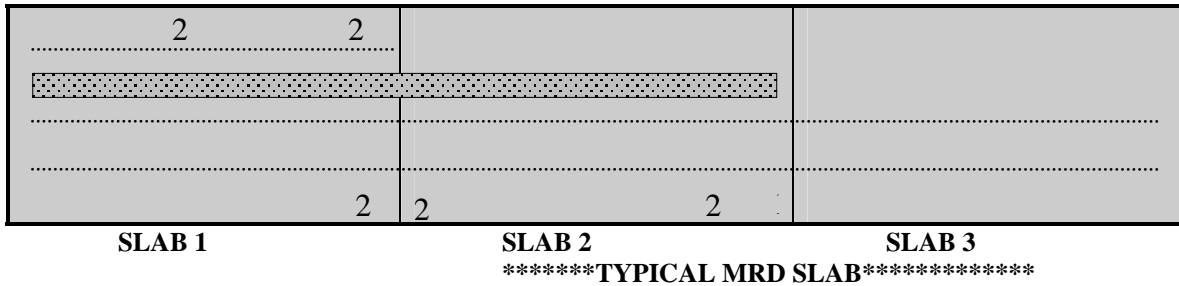
Site 29





DATE: 06/29/2000

SITE #: 29

LOCATION: I-275 SB, Exit 11A, South Huron Road towards East and ends at Willow Metropark. Three lanes road is approaching toward the park.

JOINT SPACING: 74' and 10' concrete shoulder.



KEY: <i>Trans./Lon. Cracking</i>	<i>Patching</i>		1. Spalling	5. High steel
Low	Full-depth Concrete		2. D-Cracking	6. Polished agg
Moderate ●●●●●	Asphalt Patch		3. Poor sealant	7. Faulting
High ●●●●	Expansion joint		4. ASR	8. Long. crack

COMMENTS: Each of the longitudinal cracking exhibits D-Cracking. Most of the slab has D-Cracking at Longitudinal cracking and at longitudinal joints. Some of the cracks are asphalt patched.

CRACK SPACINGS:

Slab 1

J₁-C₁
C₁-C₂
C₂-P₁
P₁-C₃

Slab 2

J₂-C₁
C₁-C₂
C₂-C₃

Slab 3

J₃-C₁
C₁-C₂
C₂-C₃

Slab 4

J₄-C₁
C₁-C₂
C₂-C₃

Slab 5

J₁-C₁
C₁-C₂
C₂-C₃

Slab 6

J₂-C₁
C₁-C₂
C₂-C₃

Slab 7

J₃-C₁
C₁-C₂
C₂-C₃

Slab 8

J₄-C₁
C₁-C₂
C₂-C₃

Slab 9

J₁-C₁
C₁-C₂
C₂-C₃

Slab 10

J₂-C₁
C₁-C₂
C₂-C₃

Slab 11

J₃-C₁
C₁-C₂
C₂-C₃

Slab 12

J₄-C₁
C₁-C₂
C₂-C₃

Slab 13

J₁-C₁
C₁-C₂
C₂-C₃

Slab 14

J₂-C₁
C₁-C₂
C₂-C₃

Slab 15

J₃-C₁
C₁-C₂
C₂-C₃

Slab 16

J₄-C₁
C₁-C₂
C₂-C₃

Slab 17

J₁-C₁
C₁-C₂
C₂-C₃

Slab 18

J₂-C₁
C₁-C₂
C₂-C₃

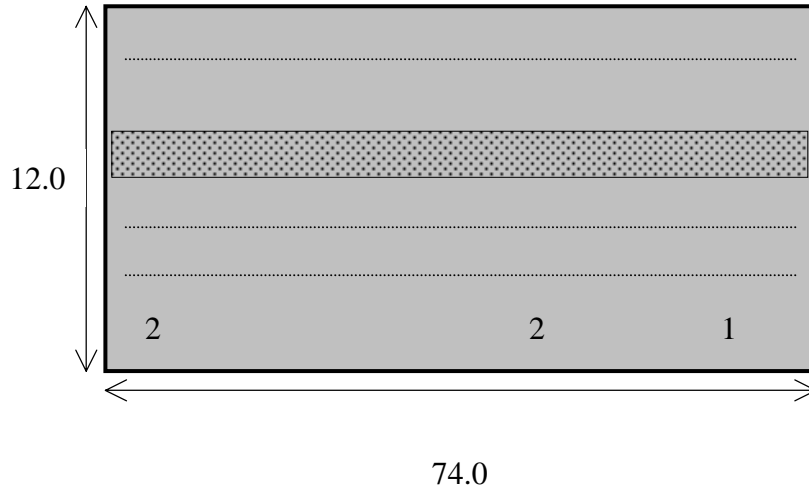
Slab 19

J₃-C₁
C₁-C₂
C₂-C₃

Slab 20

J₄-C₁
C₁-C₂
C₂-C₃

TYPICAL MRD SLAB: Slab 2/3



COMMENTS: Longitudinal cracking in slab due to connecting ASR-like cracks; Severe ASR-like cracking throughout entire slab; Popouts: 0.5 per m².

APPENDIX C: AIR-VOID ANALYSIS DATA

	O	1	2	3	4A	4	Site Number		22	26A	26B	27	28	29
							12	19						
raw data														
area analyzed (cm ²)	151.46	94.9	151.56	70	86.01	94.9	90.47	69.385	156.87	69.85	87.6	74.2	152.64	100.20
air stops	217	116	180	88	113	117	136	133	98	65	120	96	139	150
paste stops	732	304	734	349	264	294	471	466	302	368	389	336	239	429
aggregate stops	2006	921	2044	929	1055	921	1156	747	1154	913	1202	1011	1128	841
secondary ettringite stops	5	9	4	2	1	18	5	10	10	19	1	7	15	5
total stops	2960	1350	2962	1368	1433	1350	1768	1356	1564	1365	1712	1450	1521	1425
traverse length (mm)	7731.5	4133.7	7736.7	3573.2	4053.9	4133.7	4618.0	3541.9	5719.5	3565.4	4471.7	3787.4	5563.8	4363.4
# of air void intercepts	3728	1275	2376	892	1626	1318	1752	1066	1278	772	1496	1435	1819	1878
# of secondary ettringite filled intercepts	207	170	288	80	5	448	113	77	92	399	72	197	14	404
results														
vol% aggregate	67.8	68.2	69.0	67.9	73.6	68.2	65.4	55.1	73.8	66.9	70.2	69.7	74.2	59.0
vol% air original	7.5	9.3	6.2	6.6	8.0	10.0	8.0	10.5	6.9	6.2	7.1	7.1	10.1	10.9
vol% air existing	7.3	8.6	6.1	6.4	7.9	8.7	7.7	9.8	6.3	4.8	7.0	6.6	9.1	10.5
vol% paste original	24.7	22.5	24.8	25.5	18.4	21.8	26.6	34.4	19.3	27.0	22.7	23.2	15.7	30.1
vol% paste existing	24.9	23.2	24.9	25.7	18.5	23.1	26.9	35.1	19.9	28.4	22.8	23.7	16.7	30.5
original void frequency (voids/m)	509	350	344	272	402	427	404	323	240	328	351	431	329	523
existing void frequency (voids/m)	482	308	307	250	401	319	379	301	223	217	335	379	327	430
original avg. chord length (mm)	0.147	0.265	0.180	0.242	0.198	0.234	0.197	0.327	0.288	0.187	0.202	0.165	0.307	0.208
existing avg. chord length (mm)	0.152	0.279	0.198	0.258	0.197	0.272	0.203	0.326	0.280	0.220	0.210	0.175	0.280	0.245
original specific surface (mm ⁻¹)	27.1	15.1	22.2	16.5	20.2	17.1	20.3	12.2	13.9	21.3	19.8	24.3	13.0	19.2
existing specific surface (mm ⁻¹)	26.3	14.4	20.2	15.5	20.3	14.7	19.7	12.3	14.3	18.2	19.1	22.9	14.3	16.4
original paste/air ratio	3.3	2.4	4.0	3.9	2.3	2.2	3.3	3.3	2.8	4.4	3.2	3.3	1.6	2.8
existing paste/air ratio	3.4	2.7	4.1	4.0	2.3	2.7	3.5	3.6	3.2	6.0	3.3	3.6	1.8	2.9
original spacing factor (mm)	0.121	0.161	0.180	0.234	0.114	0.127	0.165	0.266	0.202	0.204	0.162	0.134	0.119	0.144
existing spacing factor (mm)	0.129	0.188	0.203	0.257	0.115	0.181	0.177	0.292	0.223	0.276	0.170	0.156	0.128	0.177

APPENDIX D: TEST SITE PORTFOLIOS

SITES 0, 1, 2, 3, AND 4A: MDOT US-23 AGGREGATE TEST SITE

INTRODUCTION

The cores received from the MDOT US-23 Aggregate Test Site are from pavements in good condition constructed in the years 1993 and 1994. The cores represent pavements with five different coarse aggregate types: two carbonate sources, two natural gravel sources, and one blast furnace slag source. Table D-1 summarizes the mix design information for the five sites. Figure D-1 depicts the mix volumetrics for the five sites. From Table D-1 and Figure D-1, it is apparent that coarse aggregate type is not the only variable that changed between the different mixture designs. For example, the water to cementitious ratio (w/cm) varies from 0.41 to 0.49, and, the volumes of aggregate vary considerably. The pavements with natural gravel contain considerably less fine aggregate, and the pavement with slag contains considerably more fine aggregate. However, the cement paste volumes remain relatively constant between the five sites.

To investigate the sites, slabs were cut from the cores in a plane perpendicular to the pavement surface. Some of the slabs were polished and used for chemical staining and stereo OM, other slabs were cut into billets and prepared in thin section, and the rest of the slabs were crushed into powder to perform chemical extractions. Figures D-2 through D-6 are provided to give a general overview of the different pavements. It is interesting to note that the interface with the cement paste appears different for some of the coarse aggregate types. In the carbonate-bearing pavements, there is often a light colored zone in the cement paste surrounding the coarse aggregate, and sometimes the coarse aggregates have darkened rims in contact with the cement paste. In the slag-bearing pavement, there is often a dark colored zone in the cement paste surrounding the coarse aggregate.

CHEMICAL STAINING

A solution of sodium cobaltinitrite was applied to the polished slab surfaces to stain potassium-bearing alkali-silica gels yellow. The alkali-silica gel stain primarily affected the chert and siltstone constituents of the fine aggregate common to the five sites. Figure D-7 shows an example of a yellow-stained chert particle, and Figure D-8 shows an example of a yellow-stained siltstone particle. Figure D-9 shows a carbonate coarse aggregate where the stain affected the rim in contact with the cement paste. A solution of barium chloride and potassium permanganate was used to stain sulfate-bearing minerals pink. The sulfate stain assisted with the identification of entrained air voids filled with secondary ettringite deposits observed during the ASTM C457 Modified Point Count. Figures D-10 and D-11 depict some pink-stained secondary ettringite filled air voids near a slag coarse aggregate. Note the dark coloration of the cement paste near the slag aggregate.

Table D-1. Summary of volume percentage computed from mix designs for Test Site Nos. 0, 1, 2, 3, and 4A.

Site No.	0	1	2	3	4A
Coarse Agg. Type	carbonate	blast furnace slag	natural gravel	carbonate	natural gravel
kg/m ₃ Cement	307	285	307	285	307
kg/m ₃ Fly Ash	46	43	46	43	46
kg/m ₃ Water	169	162	144	157	150
kg/m ₃ Coarse	1003	830	1211	1026	1165
kg/m ₃ Fine	796	918	670	843	689
w/cm	0.48	0.49	0.41	0.48	0.42
Vol % Cement Paste	27.1	25.5	25.1	25.1	25.6
Vol % Coarse Agg.	37.2	34.4	43.3	37.5	42.3
Vol % Fine Agg.	29.3	33.6	25.1	30.9	25.7
Vol % Air	6.5	6.5	6.5	6.5	6.5
Cement Source	Type I Medusa	Type I Medusa	Type I Medusa	Type I Medusa	Type I Medusa
Fly Ash	Type F	Type F	Type F	Type F	Type F
Coarse Agg. No.	93-03	82-22	30-35	58-08	63-97
Fine Agg. No.	30-35	30-35	30-35	30-35	30-35

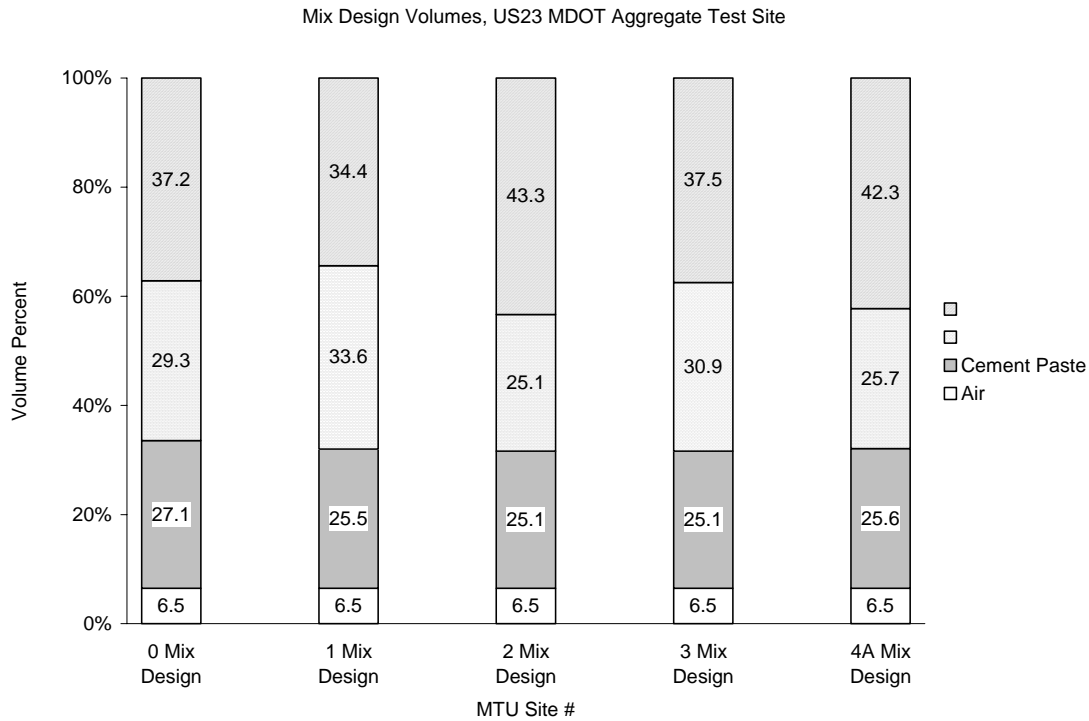


Figure D-1. Volume percentages computed from mix design information for Test Site Nos. 0, 1, 2, 3, and 4A.

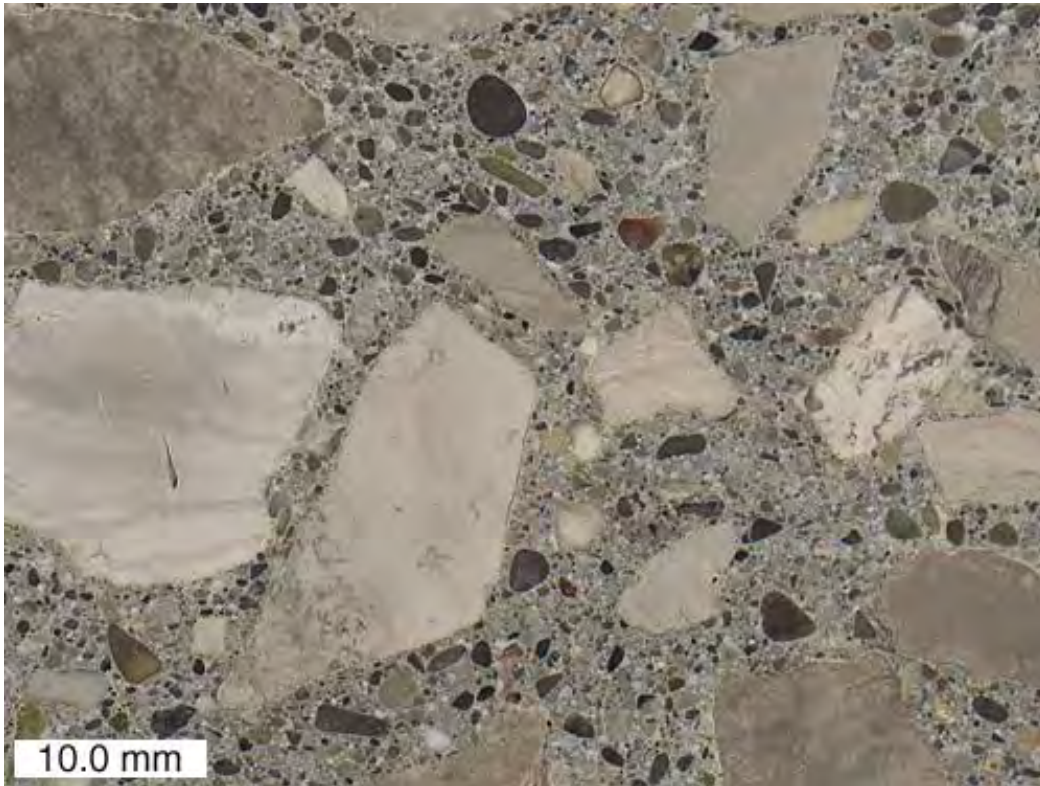


Figure D-2. View of polished surface from Core 0-A.

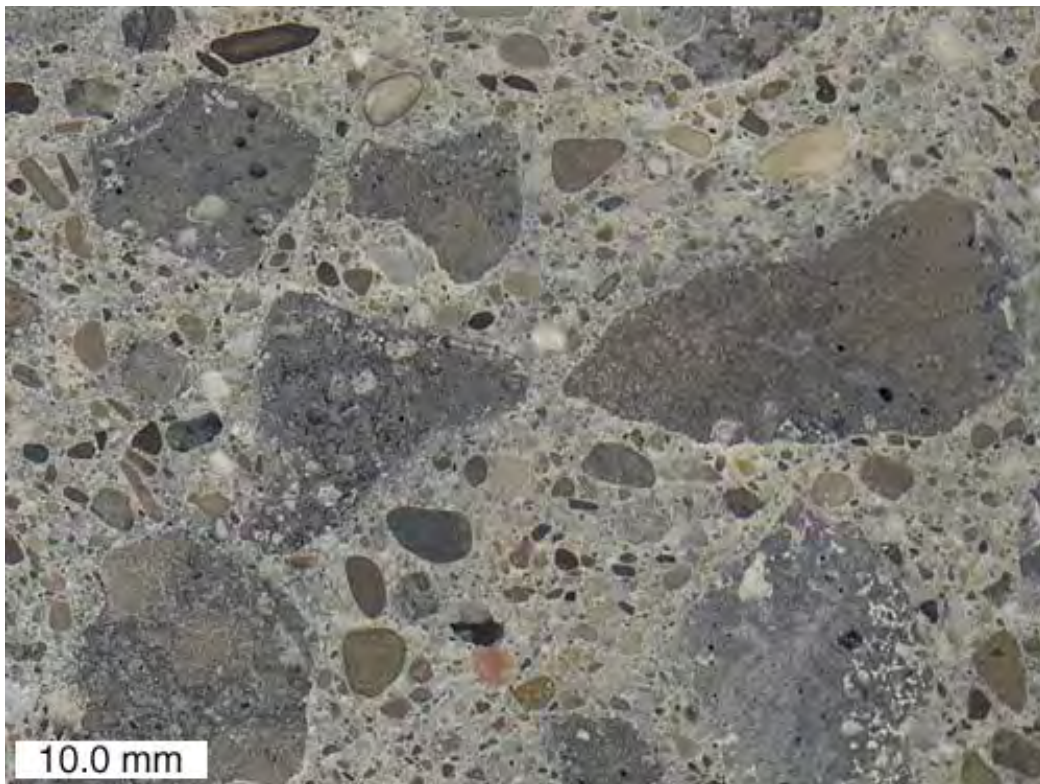


Figure D-3. View of polished surface from Core 1-A.

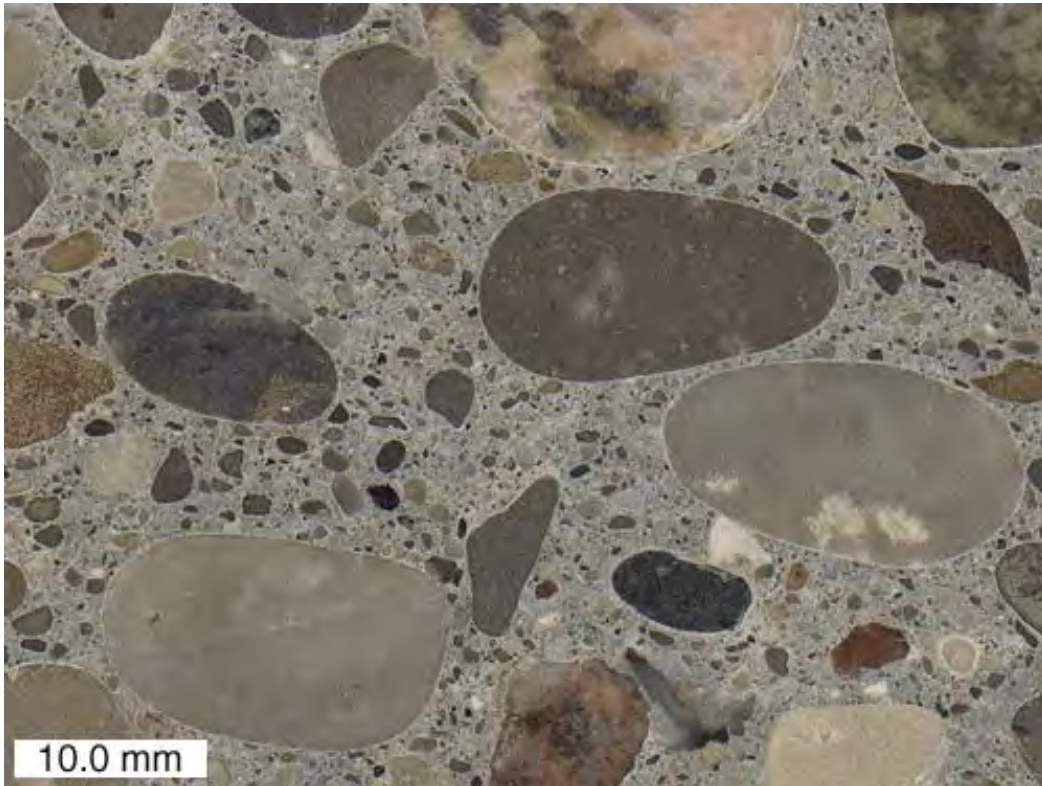


Figure D-4. View of polished surface from Core 2-A.

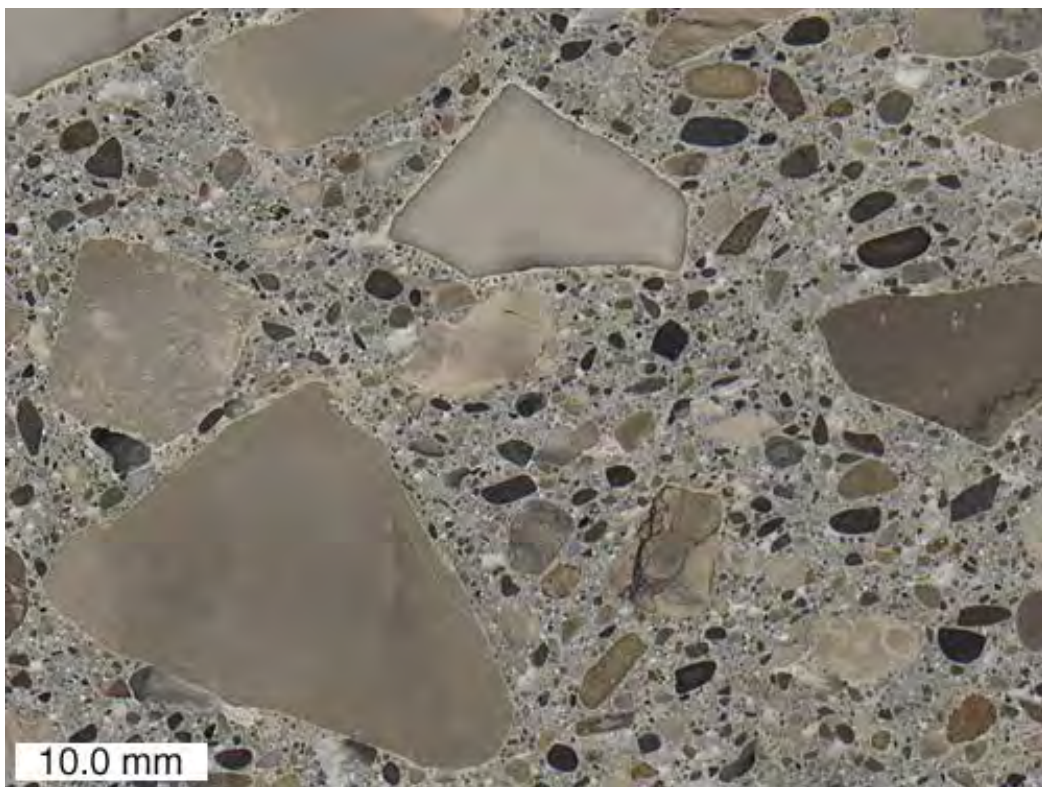


Figure D-5. View of polished surface from Core 3-A.

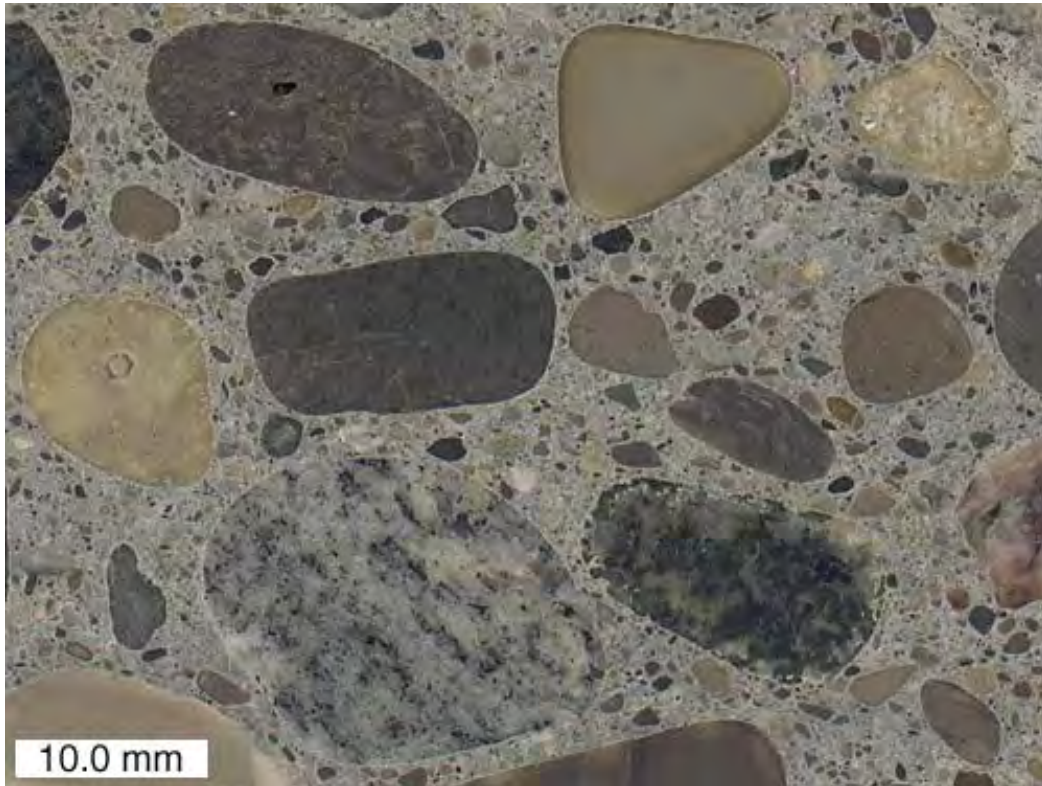


Figure D-6. View of polished surface from Core 4A-B.



Figure D-7. Yellow stained chert sand particle from Core O-A.



Figure D-8. Yellow stained siltstone sand particle from Core 3-A.

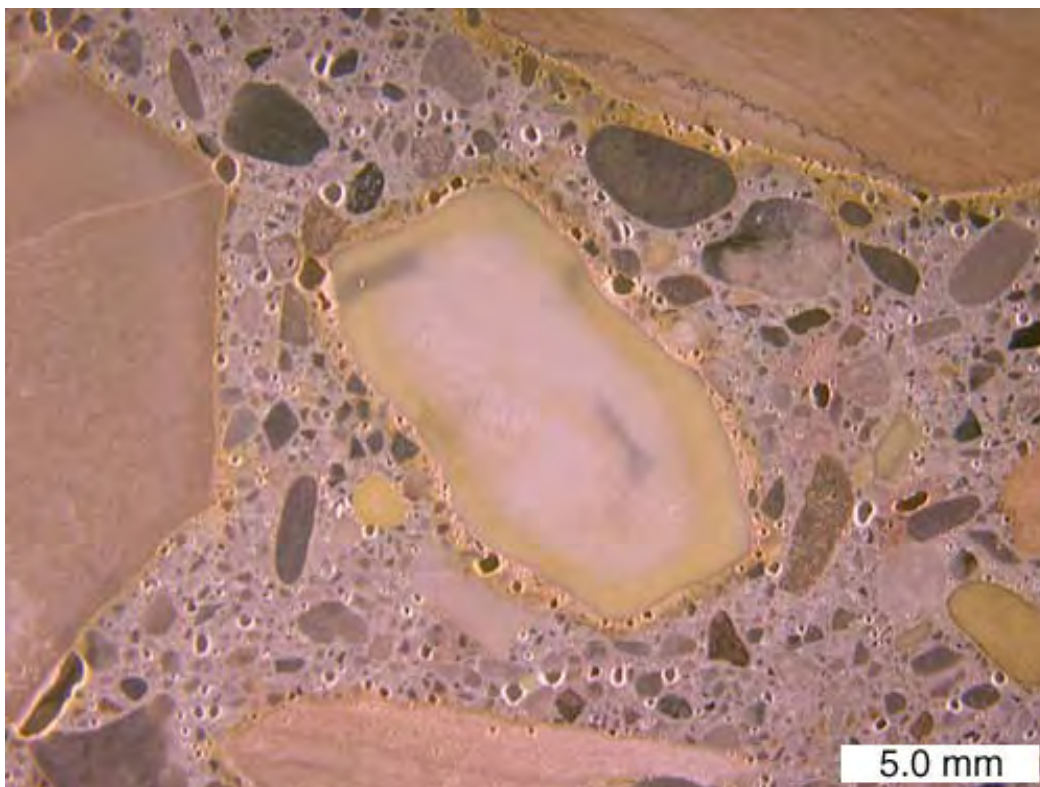


Figure D-9. Yellow stained dolomite coarse aggregate particle from Core 3-A.

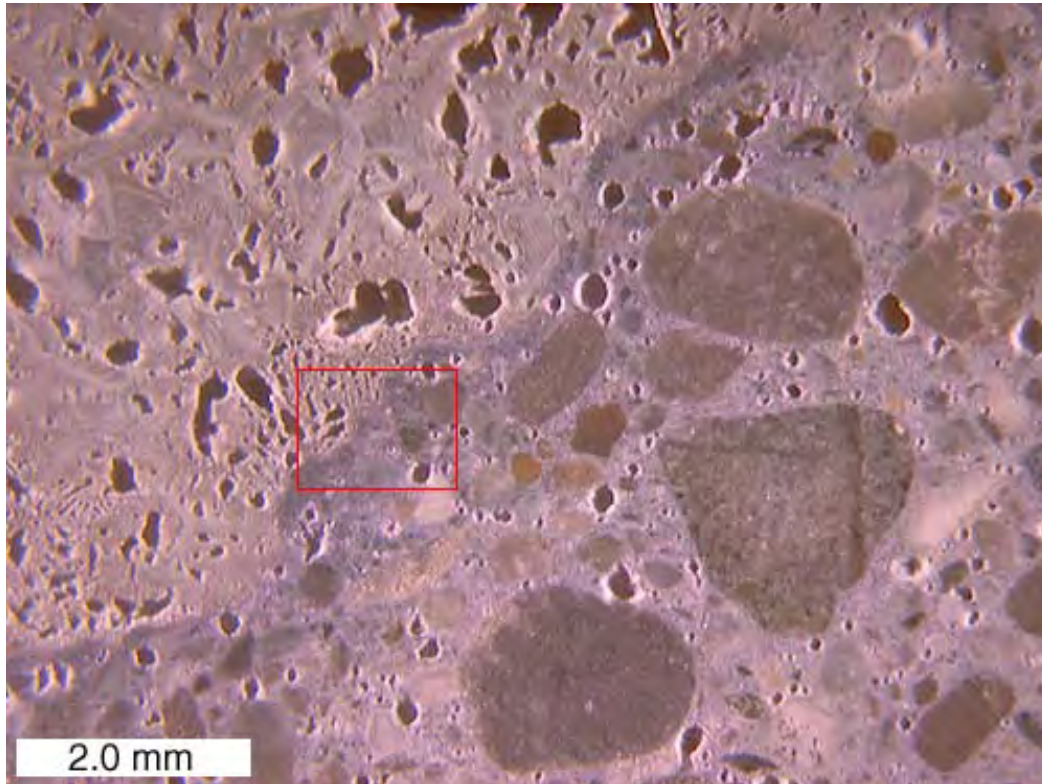


Figure D-10. A polished surface stained for sulfate minerals from Core 1-A. The red box shows the location of the close-up in Figure D-11.

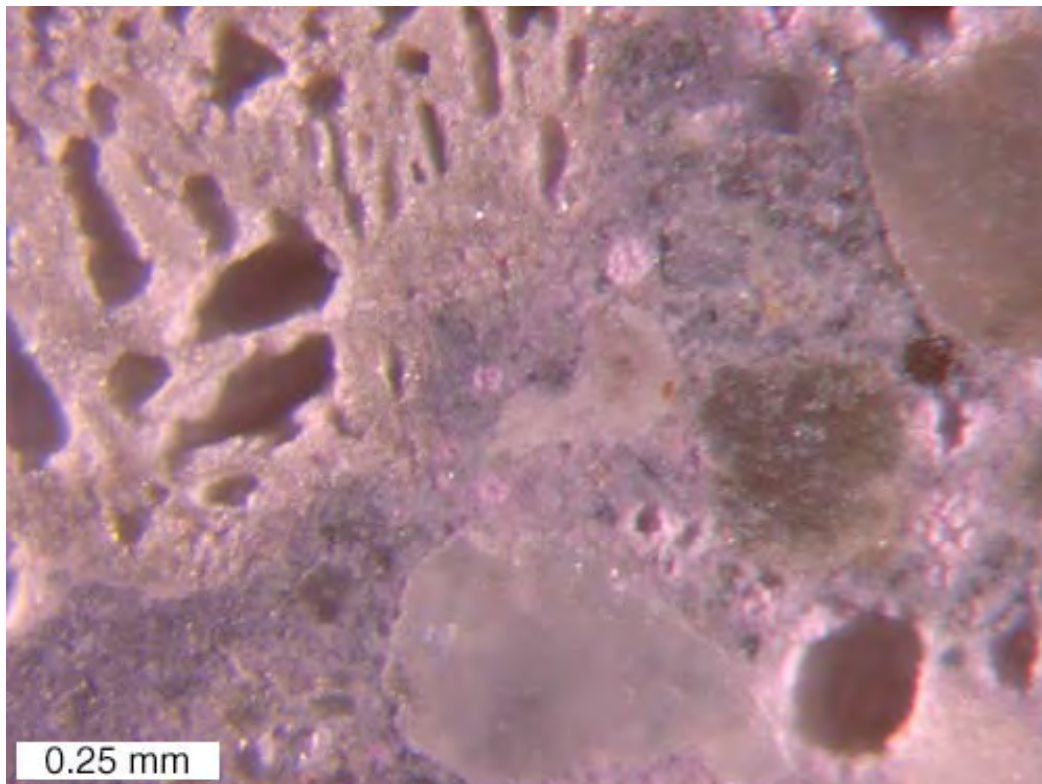


Figure D-11. Close-up of area from Figure D-10 showing ettringite filled air voids.

THIN SECTIONS

Two types of reactive fine aggregate particles were identified during the chemical staining procedures. Figures D-12a, D-12b, and D-12c show an example of a reactive chert particle. Note that there is no cracking associated with the chert. The presence of a dense rim in contact with the cement paste, and a lack of any cracking is typical of the chert particles in all five of the test sites. Figures D-13a, D-13b, and D-13c show an example of a reactive siltstone particle. Siliceous fossils within the siltstone appear to be the reactive constituent. The siltstone particle shown is cracked, but the cracks do not extend into the surrounding cement paste. The siltstone particle shown in Figures D-13a, D-13b, and D-13c is typical of the siltstone particles in all five of the pavements.

The cement paste/coarse aggregate interface was also examined in thin section. Figures D-14a, D-14b, and D-14c are an example of the interface between a carbonate coarse aggregate and the cement paste. From the cross-polarized image in Figure D-14b, it can be seen the cement paste within about 0.2 millimeters of the coarse aggregate appears carbonated. From the fluorescent image in Figure D-14c, it can be seen that the carbonated zone of cement paste is relatively porous, and that the rim of the coarse aggregate in contact with the cement paste is denser than the interior of the aggregate. Figure D-15 contains a series of elemental maps made using an SEM equipped with an EDS detector. Figures D-16a, D-16b, and D-16c are optical images of the same area. From Figure D-15, it can be seen that the carbonate aggregate contains calcium and magnesium, and is a dolomite. Also from Figure D-15, it can be seen that the cement paste in contact with the aggregate appears depleted in potassium. Furthermore, potassium bearing regions within the dolomite are associated with silicon, which suggests that the darkened rim may be due to an alkali-silica reaction where chert impurities in the dolomite have reacted with potassium from the cement paste. However, the darkened rims do not appear to be associated with any cracking or deterioration.

Figures D-17a and D-17b are an example of the interface between a slag coarse aggregate and the cement paste. From the plane-polarized image in Figure D-17a, it appears that the concentration of partially hydrated fly ash and cement particles is higher near the slag aggregate. From the fluorescent image in Figure D-17b the cement paste appears denser near the slag aggregate. Figure D-18 is a close-up view of the partially hydrated fly ash and cement near the slag aggregate. In Figure D-18, a green coloration is associated with the fly ash and the ferrite phase of the cement particles. It is suspected that the green color is due to the reduction of the iron in these materials, and is perhaps related to the calcium sulfide in the slag aggregate. Figures D-19a, D-19b, and D-19c are close-up in-situ views of the Class F fly ash particles common to the five sites. As can be seen in Figures D-19a, D-19b, and D-19c, many of the fly ash particles are composed of highly reflective opaque minerals. Figures D-20a and D-20b are close-up views of calcium sulfide dendrites in the slag coarse aggregate.

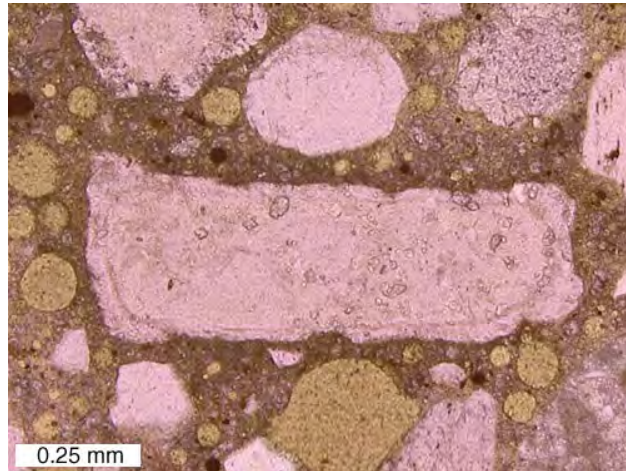


Figure D-12a. Thin-section view of a reactive chert sand particle from Core 1-A, plane-polarized light.

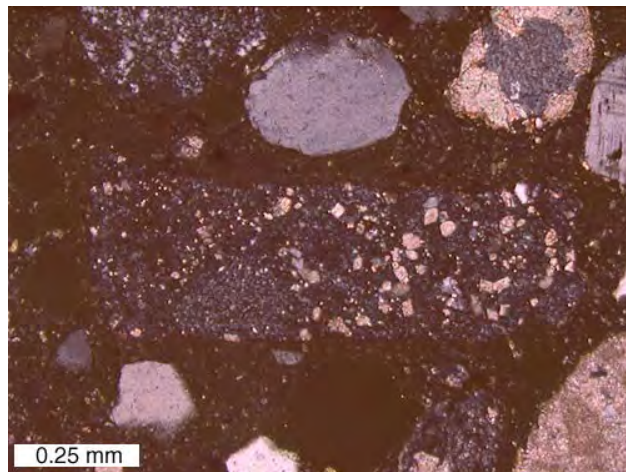


Figure D-12b. Thin-section view of a reactive chert sand particle from Core 1-A, cross-polarized light.

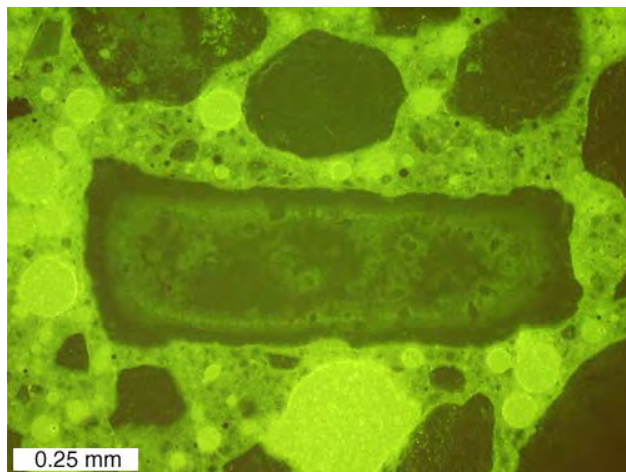


Figure D-12c. Thin-section view of a reactive chert sand particle from Core 1-A, epifluorescent mode.

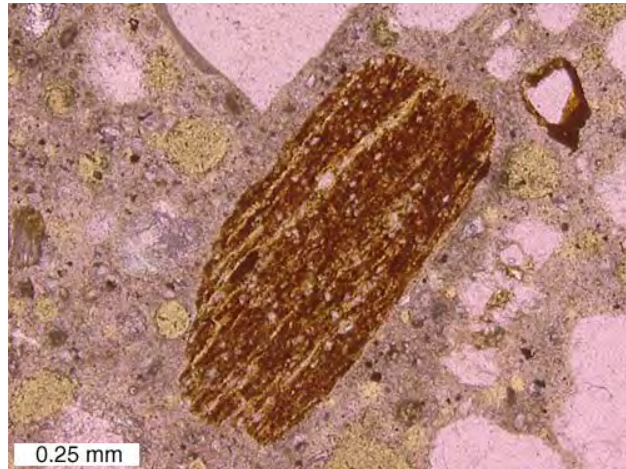


Figure D-13a. Thin-section view of a reactive siltstone sand particle from Core 1-A, plane-polarized light.

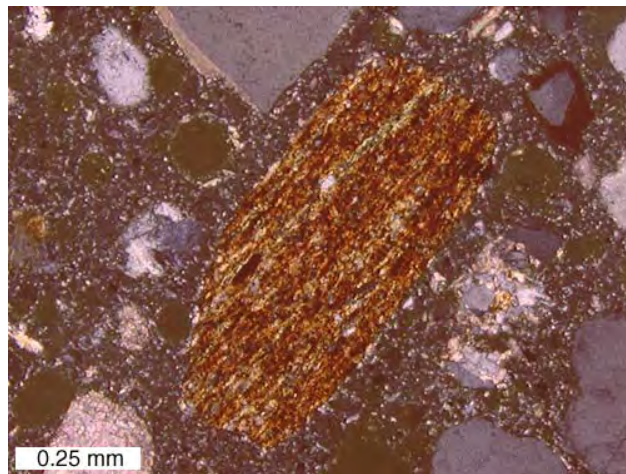


Figure D-13b. Thin-section view of a reactive siltstone sand particle from Core 1-A, cross-polarized light.

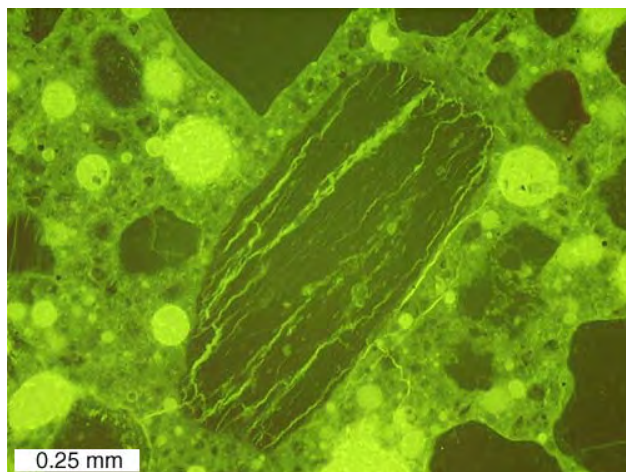


Figure D-13c. Thin-section view of a reactive siltstone sand particle from Core 1-A, epifluorescent mode.

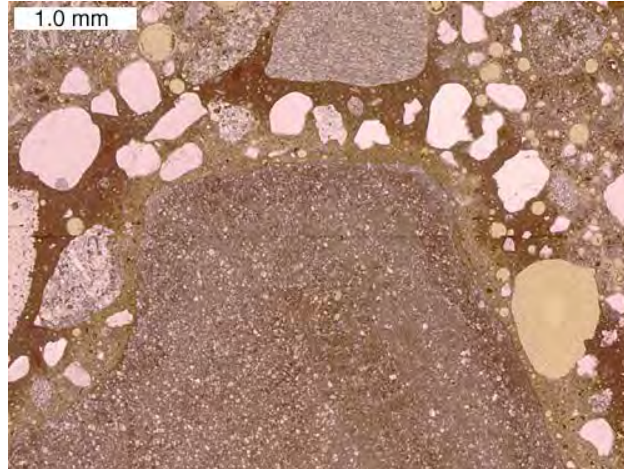


Figure D-14a. Thin-section view of a cement paste/coarse aggregate interface from Core 3-A, plane-polarized light.

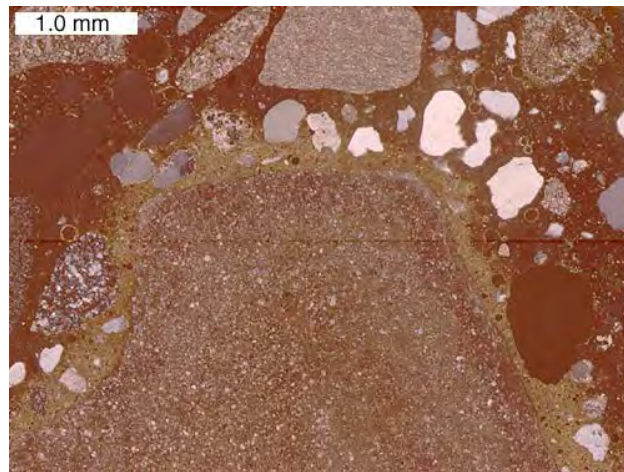


Figure D-14b. Thin-section view of a cement paste/coarse aggregate interface from Core 3-A, cross-polarized light.

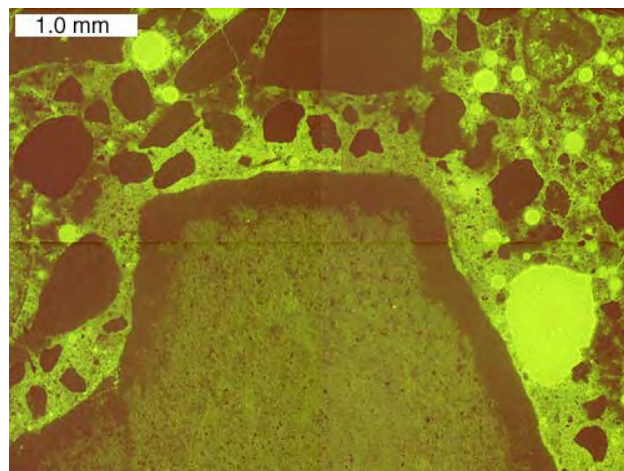


Figure D-14c. Thin-section view of a cement paste/coarse aggregate interface from Core 3-A, epifluorescent mode.

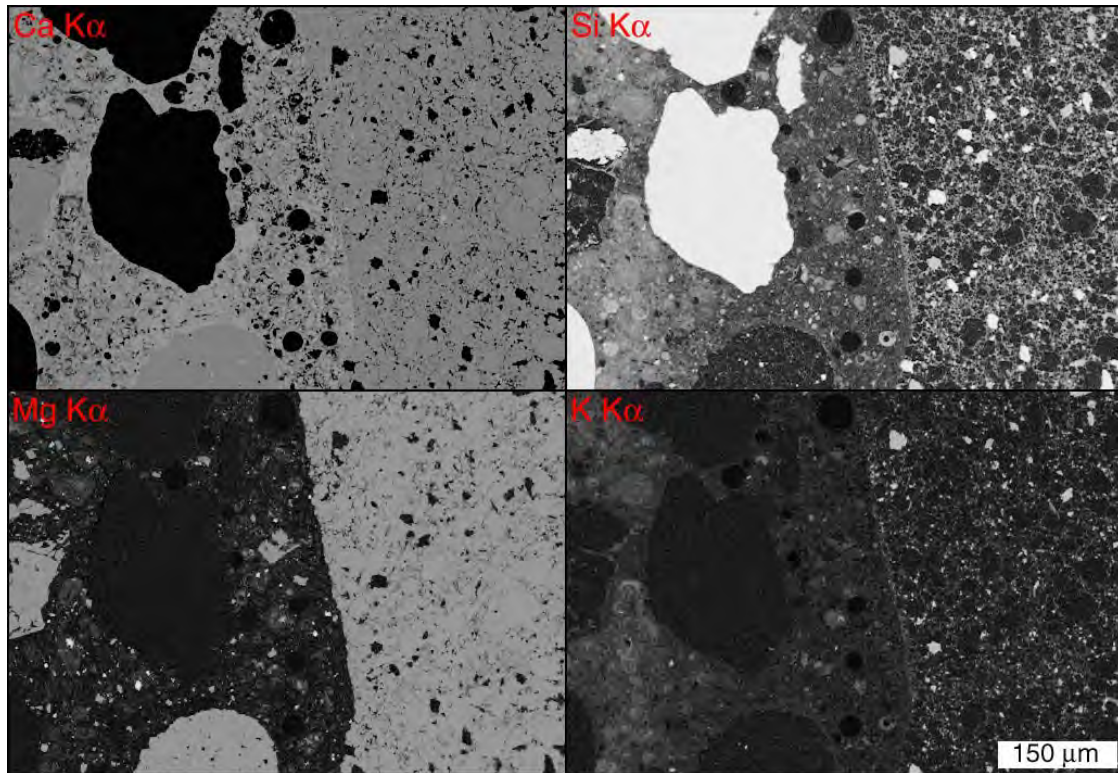


Figure D-15. Elemental maps made using an SEM equipped with an EDS detector. Brighter areas indicate a higher counts for that element.

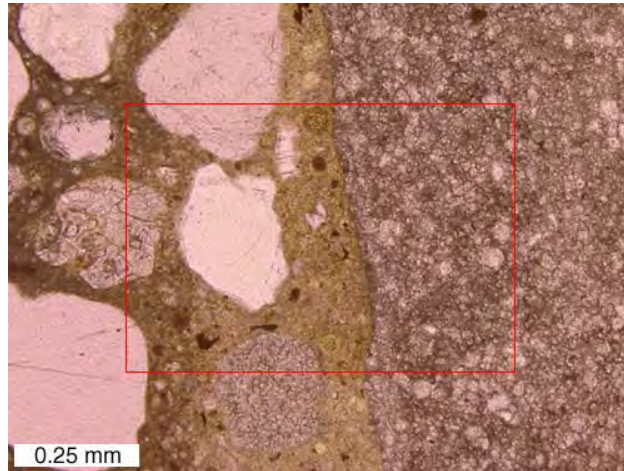


Figure D-16a. Thin-section view of a cement paste/coarse aggregate interface from Core 3-A, plane-polarized light. The red box shows the location from Figure D-15.

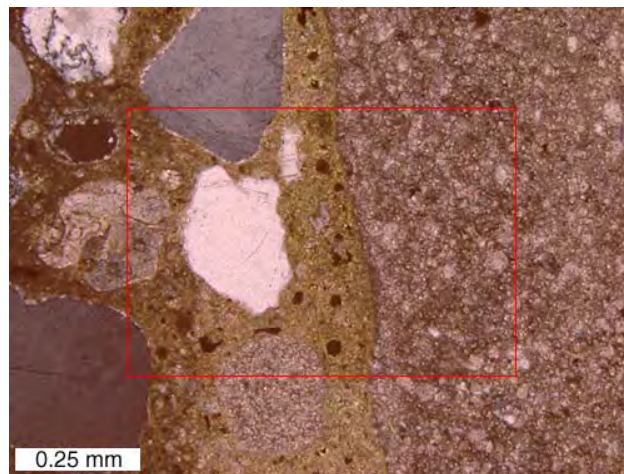


Figure D-16b. Thin-section view of a cement paste/coarse aggregate interface from Core 3-A, cross-polarized light. The red box shows the location from Figure D-15.

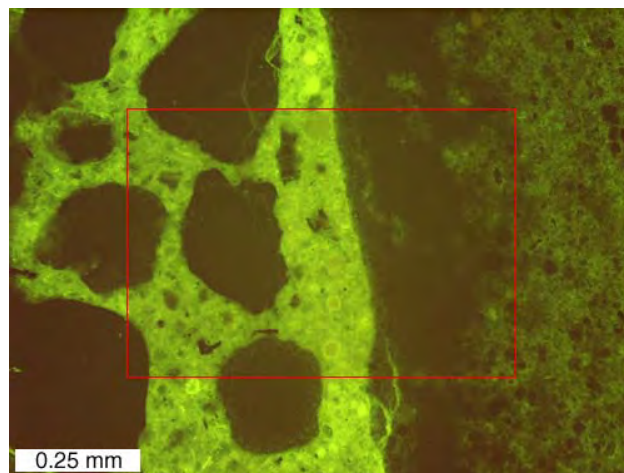


Figure D-16c. Thin-section view of a cement paste/coarse aggregate interface from Core 3-A, epifluorescent mode. The red box shows the location of the maps from Figure D-15.

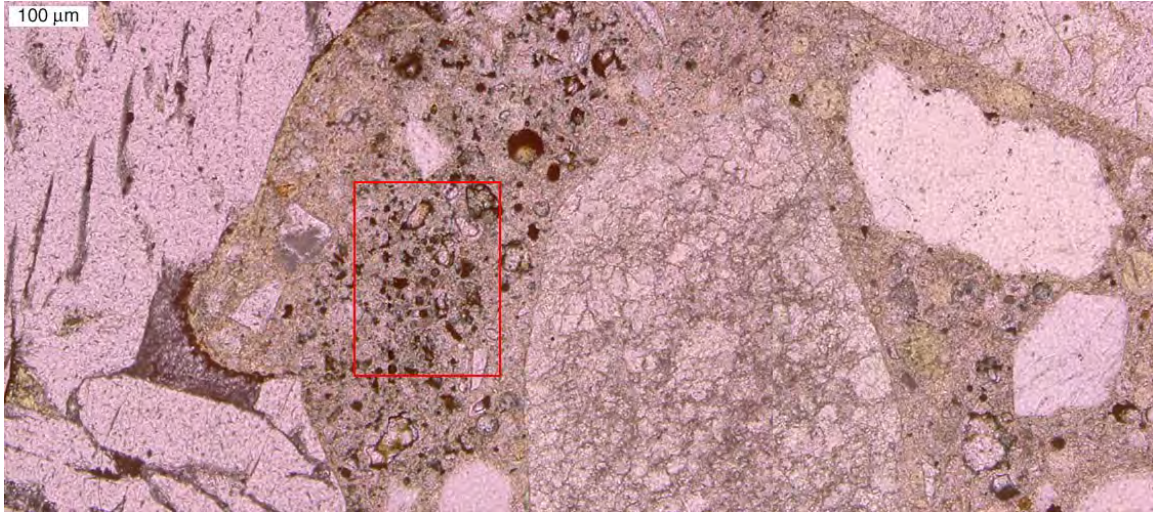


Figure D-17a. Thin-section view of a cement paste/coarse aggregate interface from Core 1-A, plane-polarized light. The red box shows the location of close-up in Figure D-18.

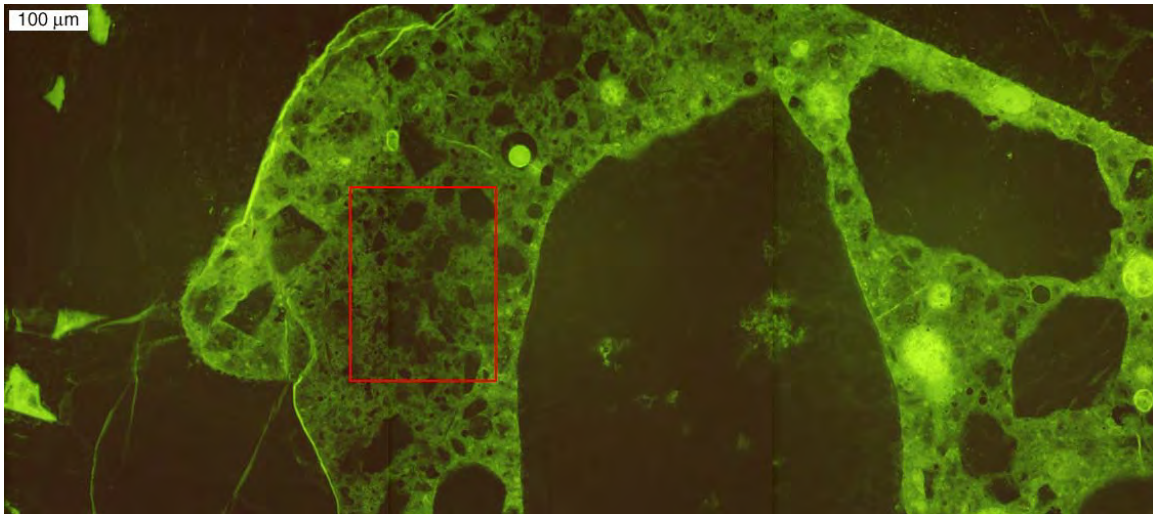


Figure D-17b. Thin-section view of a cement paste/coarse aggregate interface from Core 1-A, epifluorescent mode. The red box shows the location of close-up in Figure D-18.

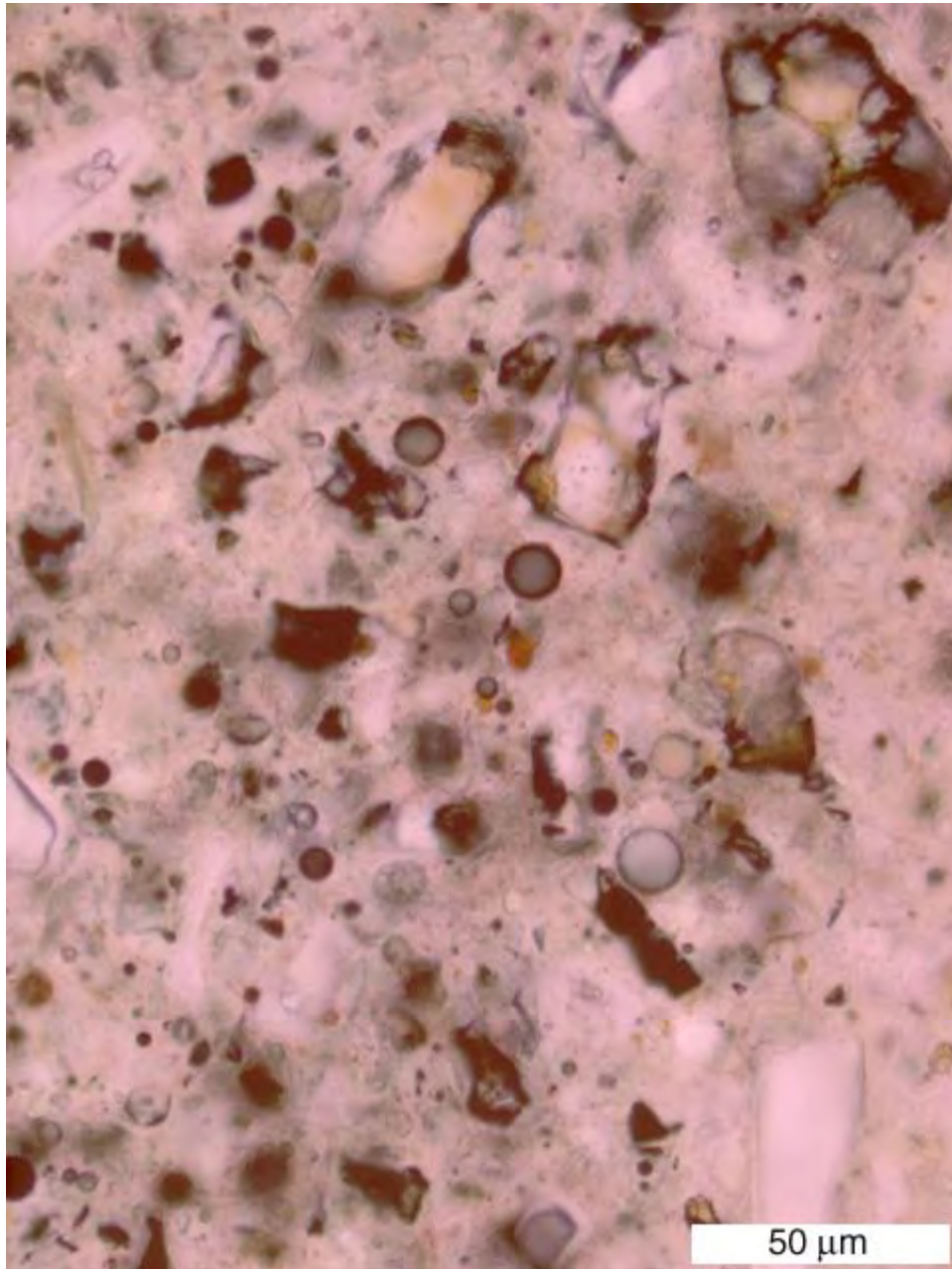


Figure D-18. Thin-section view of cement paste near contact with slag aggregate, a close-up from area outlined in red in Figures D-17a and D-17b.



Figure D-19a. Thin section view of fly ash particles from Core 0-A, combined transmitted plane-polarized light and reflected light.

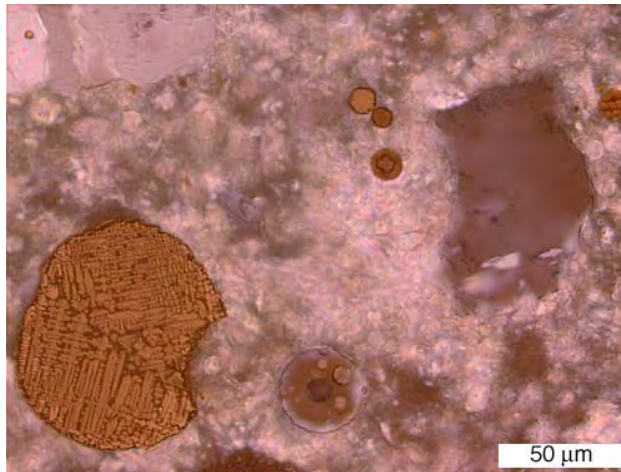


Figure D-19b. Thin section view of fly ash particles from Core 0-A, combined transmitted cross-polarized light and reflected light.

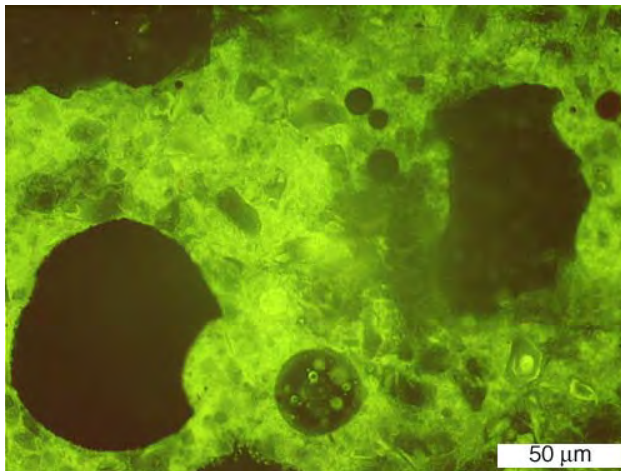


Figure D-19c. Thin section view of fly ash particles from Core 0-A, epifluorescent mode.

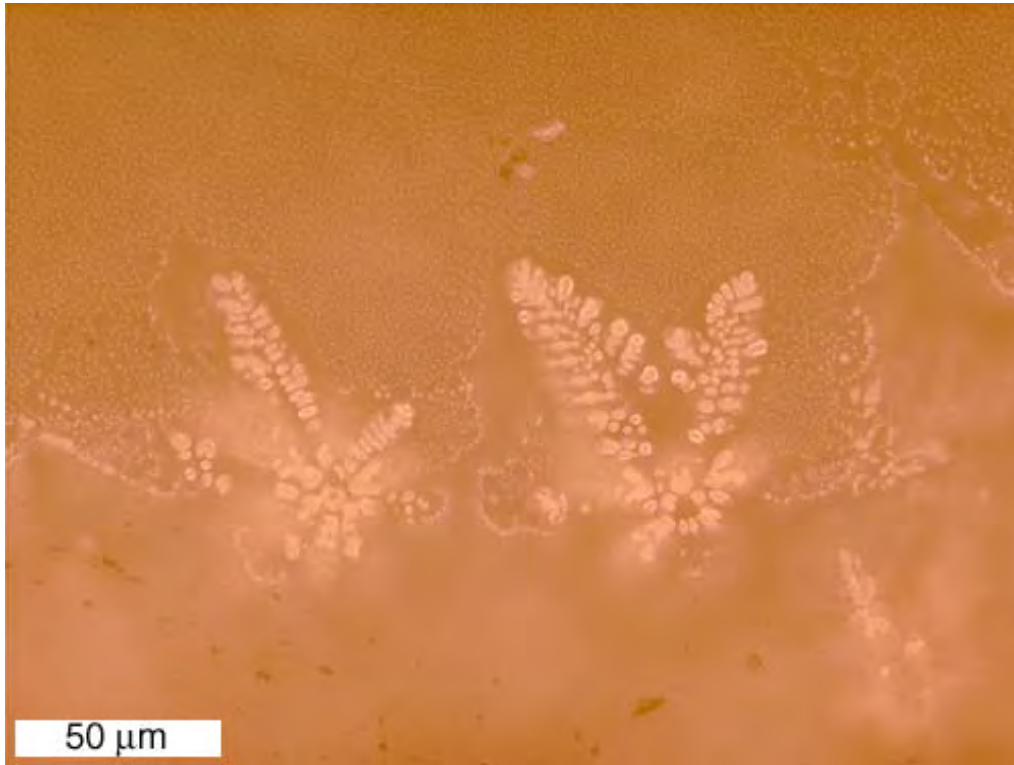


Figure D-20a. Thin section view of calcium sulfide dendrites in slag aggregate from Core 1-A, plane-polarized light.

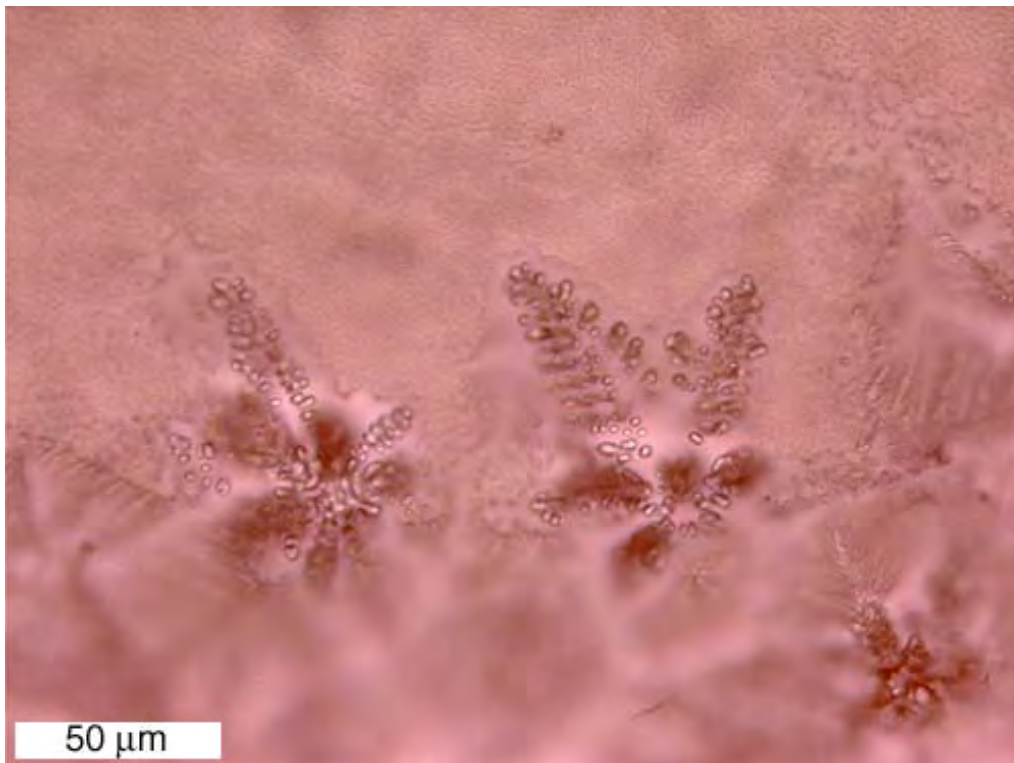


Figure D-20b. Thin section view of calcium sulfide dendrites in slag aggregate from Core 1-A, reflected light.

CHEMICAL EXTRACTIONS

A gravimetric procedure of sulfate determination was used according to British Standard 1881:Part 124. Methods for Analysis of Hardened Concrete: 1988. The weight percent SO_3 computed from the mix design assumes 3.5% by weight SO_3 for the cement and 4.5% by weight of the fly ash. The results of the sulfate determinations, expressed in terms of SO_3 , are presented in Table D-2. Figure D-21 plots the computed SO_3 wt% next to the extracted SO_3 wt% for each of the sites. Neither of sites that contain natural gravel coarse aggregate have extraction values that exceed the computed value. One of the sites that contains carbonate coarse aggregate has an extraction value that exceeds the computed value, (Test Site No. 3) while the other site that contains carbonate coarse aggregate, (Test Site No. 0) does not exceed the computed value. Site 1, the only site that contains slag coarse aggregate, has an extraction value that exceeds the computed value.

A standard technique for alkali extraction from hardened concrete was not available, so an ammonium acetate extraction technique developed for the determination of exchangeable and soluble sodium and potassium in soils was adopted. The concentrations of potassium and sodium were determined by an inductively coupled plasma emission spectrophotometer. The results from the test are expressed in weight percent elemental sodium and weight percent elemental potassium. In Table D-3, the results were converted to the industry convention of kilograms of “ Na_2O equivalent” per cubic meter of concrete, based on the total mass from the mix designs. The recalculation to kilograms of “ Na_2O equivalent” per cubic meter of concrete allows comparisons to be made with industry standards for limiting total alkalis in the mixture. The Canadian standards specifying a maximum of 3.0 kg/m^3 Na_2O equivalent for mild protection, 2.2 kg/m^3 Na_2O equivalent for moderate protection, and 1.7 kg/m^3 Na_2O equivalent for strong protection. Figure D-22 plots the Na_2O equivalent values from extraction for all of the sites, along with dotted lines showing the Canadian protection levels.

AIR VOID CHARACTERISTICS

Slabs from each pavement were polished and examined under a stereo microscope in accordance with ASTM C457 Procedure B – Modified Point-Count Method. In addition to the standard procedure, the slabs were stained with a solution of potassium permanganate and barium chloride. The chemicals stain sulfate-bearing minerals, such as ettringite, pink. Over time, such minerals commonly occur as secondary growths in the entrained air voids. Often, entrained air voids in deteriorated concrete are completely filled with secondary ettringite. The stain assists in the identification of filled air voids that may otherwise be mistaken for hardened cement paste. In the equations used to determine the air-void system parameters, filled air voids that are identified as paste would be considered to offer no protection to freeze-thaw damage. It is controversial whether filled air voids can protect the paste against freeze-thaw damage, and thus, air-void system parameters are computed for both the concrete in its original state, and the concrete in its existing state. Table D-4 shows the results of the Modified Point-Count for the five sites. Figure D-23 plots the spacing factors for each site, along with dotted

Table D-2. Results of sulfate extractions.

MTU Core ID	Computed wt% SO ₃	Extracted wt% SO ₃
O-A	0.55	0.47
1-A	0.53	0.61
2-A	0.54	0.49
3-A	0.51	0.67
4A-B	0.54	0.48

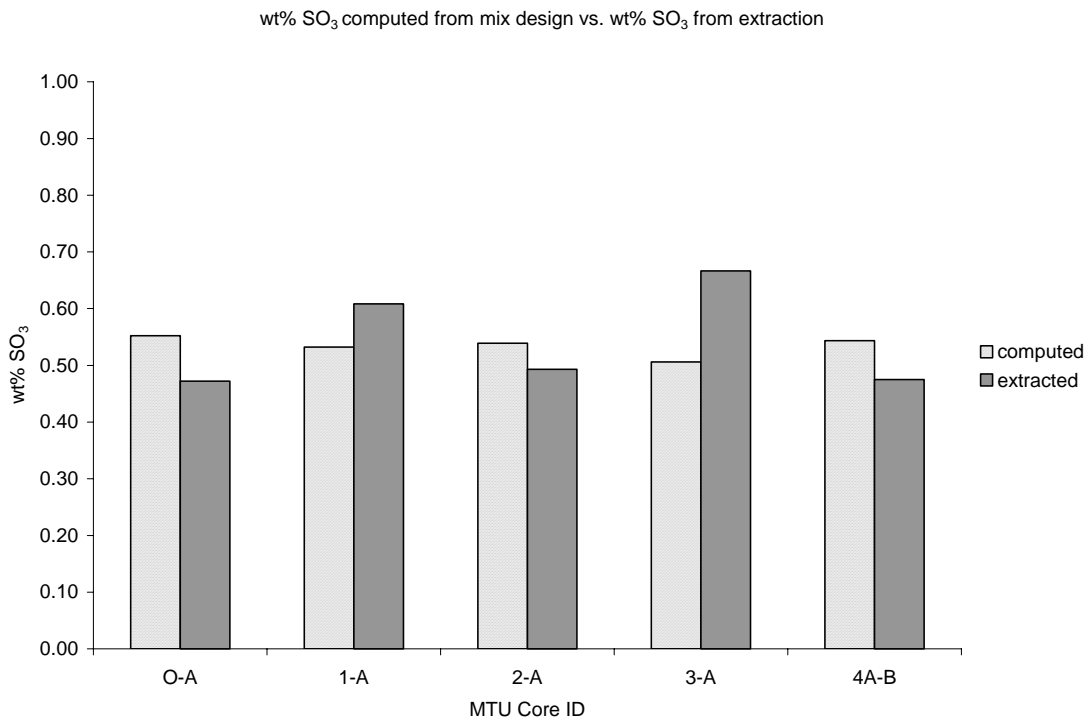


Figure D-21. Wt% SO₃ values from extraction compared to wt% SO₃ values computed from the mix design.

Table D-3. Results of alkali extractions.

MTU Core ID	Wt% Na	Wt% K	Na ₂ O Equivalent kg/m ³
O-A	0.021	0.036	1.29
1-A	0.026	0.038	1.46
2-A	0.021	0.038	1.35
3-A	0.021	0.033	1.27
4A-B	0.020	0.043	1.42

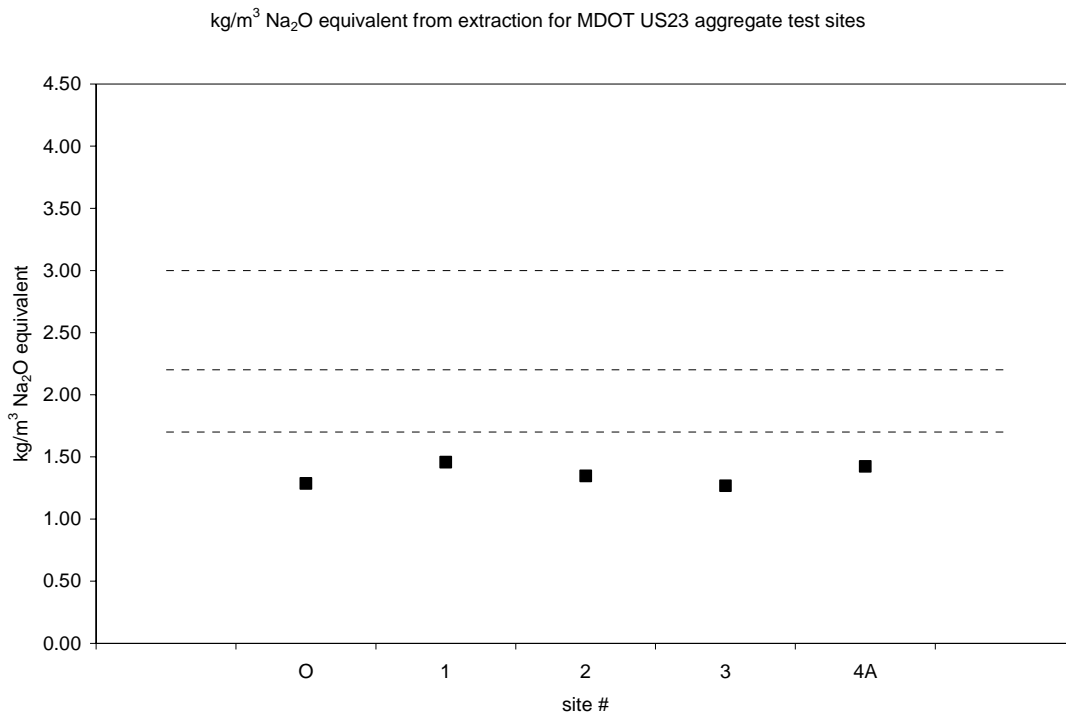


Figure D-22. Na₂O equivalent kg/m³ values from extraction compared to Na₂O equivalent kg/m³ values computed from the mix design.

Table D-4. Results of ASTM C457 Modified Point Counts.

MTU Core ID	0-C	1-A	2-C	3-C	4A-C
Raw Data					
area analyzed (cm ²)	151.5	94.9	151.6	70.0	86.0
air stops	217	116	180	88	113
paste stops	732	304	734	349	264
aggregate stops	2006	921	2044	929	1055
secondary ettringite stops	5	9	4	2	1
total stops	2960	1350	2962	1368	1433
traverse length (mm)	7732	4134	7737	3573	4054
# of air void intercepts	3728	1275	2376	892	1626
# of secondary ettringite filled intercepts	207	170	288	80	5
Results					
vol% aggregate	67.8	68.2	69.0	67.9	73.6
vol% air original	7.5	9.3	6.2	6.6	8.0
vol% air existing	7.3	8.6	6.1	6.4	7.9
vol% paste original	24.7	22.5	24.8	25.5	18.4
vol% paste existing	24.9	23.2	24.9	25.7	18.5
original void frequency (voids/m)	509	350	344	272	402
existing void frequency (voids/m)	482	308	307	250	401
original avg. chord length (mm)	0.147	0.265	0.180	0.242	0.198
existing avg. chord length (mm)	0.152	0.279	0.198	0.258	0.197
original specific surface (mm ⁻¹)	27.1	15.1	22.2	16.5	20.2
existing specific surface (mm ⁻¹)	26.3	14.4	20.2	15.5	20.3
original paste/air ratio	3.3	2.4	4.0	3.9	2.3
existing paste/air ratio	3.4	2.7	4.1	4.0	2.3
original spacing factor (mm)	0.121	0.161	0.180	0.234	0.114
existing spacing factor (mm)	0.129	0.188	0.203	0.257	0.115

lines to represent the suggested range according to ASTM C457. Figure D-24 plots the void frequency for each site, along with dotted lines to represent the suggested range according to ASTM C457. Figure D-25 compares the aggregate, cement paste and air volume percentages as determined by point count to the volume percentages computed from the mix design.

CONCLUSIONS

The results of the evaluation of the cores received from the MDOT US-23 Aggregate Test Site are from pavements constructed in the years 1993 and 1994. The cores, representing five different coarse aggregate types (two carbonate sources, two natural gravel sources, and one blast furnace slag source), are all from pavements in good condition. As would be assumed, differences in the microstructure exist in the concrete from the various test sites, primarily as a result of the coarse aggregate. These differences can be summarized as follows:

- In Test Site No. 3, the rims where the dolomite aggregates (Pit No. 58-08) contacted the paste stained positively for alkali-silica reaction product, a finding that is confirmed by petrographic analysis. Further, this reaction is associated with increased porosity and carbonation of the surrounding cement paste and densification of the aggregate rims. It seems that the darkened rims are due to an alkali-silica reaction where chert impurities in the dolomite have reacted with potassium from the cement paste. However, the darkened rims do not appear to be associated with any cracking or deterioration.
- It appears that the concentration of partially hydrated fly ash and cement particles is higher near the slag aggregate than in the bulk paste, with a corresponding increase in paste density. In addition, a green coloration is associated with the fly ash and the ferrite phase of the cement particles. It is suspected that the green color is due to the reduction of the iron in these materials, and is perhaps related to the calcium sulfide in the slag aggregate.
- The results of the sulfate extraction found that the measured sulfate content was lower than the predicted in 3 of the 4 mixtures containing natural aggregates. In the case of mixtures made with the slag (Pit No. 82-22) and the dolomite (Pit No. 58-08) coarse aggregate, the measured sulfate contents were higher than predicted. This finding, which was confirmed through repeating the test, suggests that slag and some natural aggregates may provide a source of internal sulfate.

In addition to differences observed between the mixtures due to the coarse aggregate type, the following observations were made:

- Two types of reactive fine aggregate particles were identified during the chemical staining procedures and petrographic analysis. One type is reactive chert that stained yellow after treatment with sodium cobaltinitrite and developed dense rims in contact with the cement paste. There was no cracking associated with the chert particles in any of the five of the test sites. The second reactive fine aggregate particle is a reactive siltstone that contains siliceous fossils that appear to be the reactive

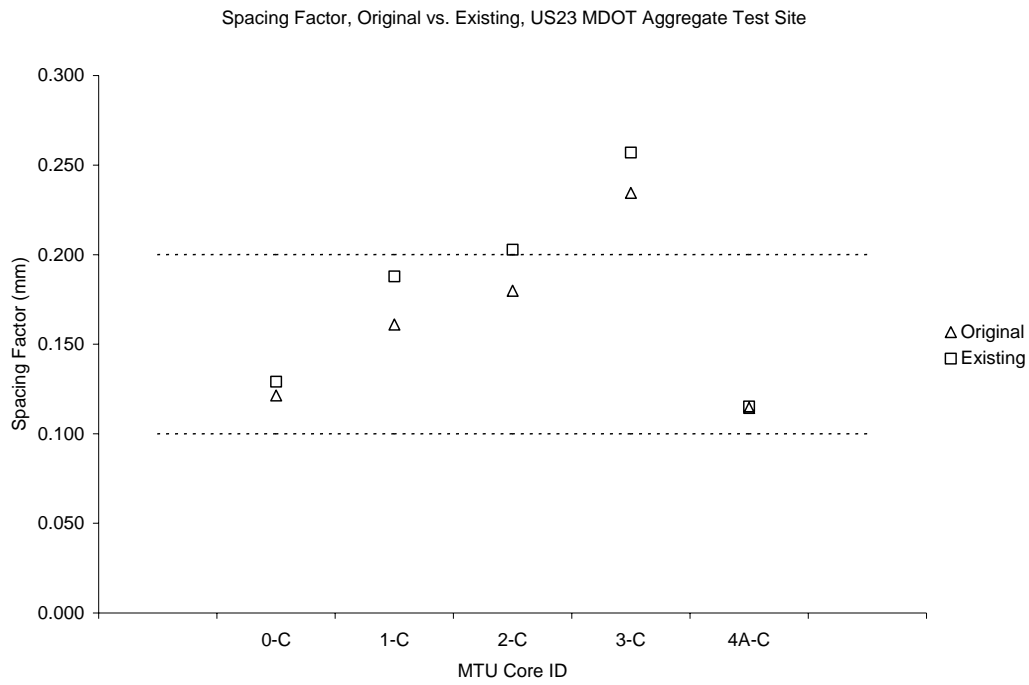


Figure D-23. Spacing factors plotted with dotted lines showing suggested values from ASTM C457.

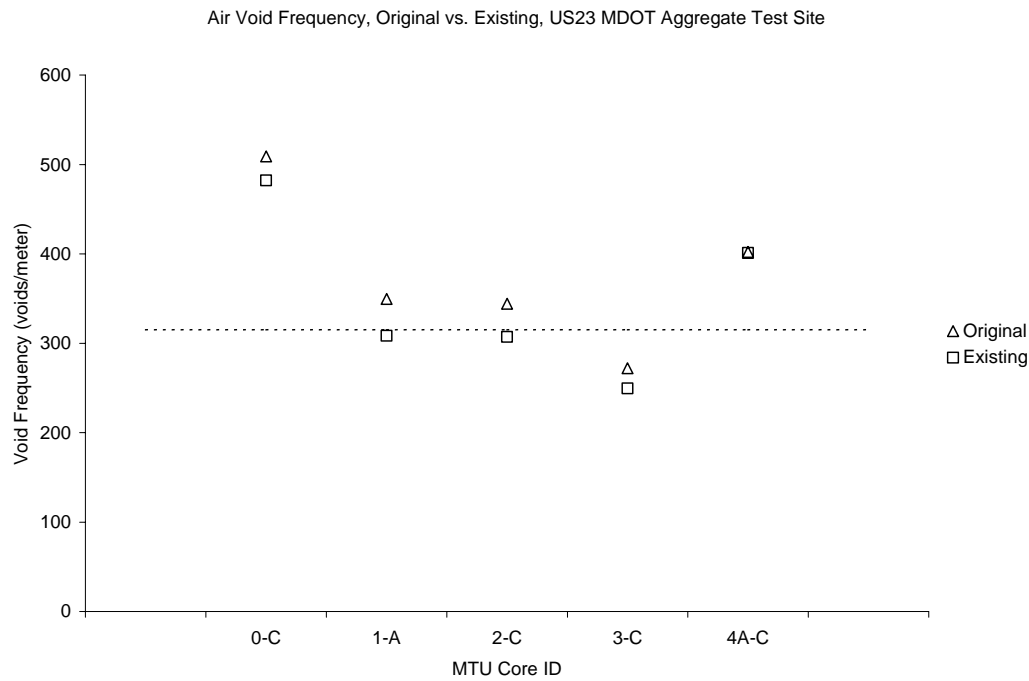


Figure D-24. Void frequencies plotted with dotted lines showing suggested values from ASTM C457.

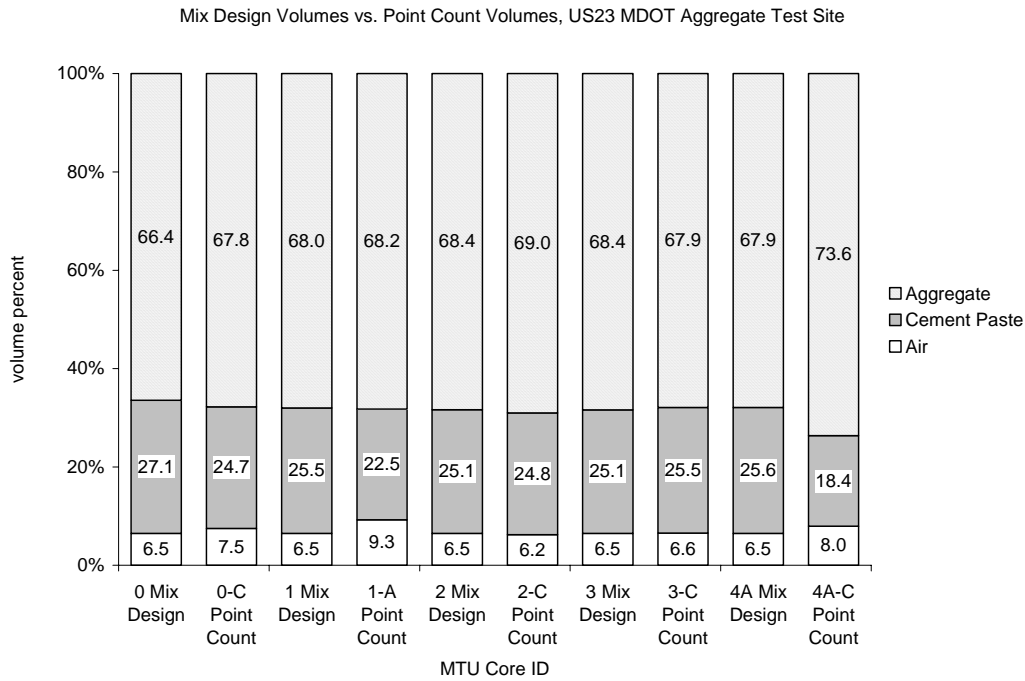


Figure D-25. Volume percentages from point counts compared to volume percentages computed from mix designs.

constituent. Typically, the siltstone particles are cracked, but the cracks do not extend into the surrounding cement paste. This is typical of the siltstone particles in all five of the pavements.

- The Class F fly ash, which is largely composed of highly reflective opaque minerals, is common to all five sites. It is interesting to note that in the presence of this fly ash, that none of the potential ASR was deleterious and that the higher than expected sulfate levels in two of the sites had no apparent ill effect. Also, the overall alkali levels in the mixtures were well below that needed to protect the concrete against ASR.

SITES 26A, 26B, AND 27: THE MDOT US10 CLARE TEST SITE

INTRODUCTION

The cores received from the MDOT US10 Clare Test Site are from pavements in poor condition. The three sites all have the same mix design, which is shown in Table D-5. However, the subbase materials used at the sites were not the same. Both Test Sites Nos. 26A and 26B utilized an asphalt treated permeable base, while Test Site No. 27 was supported on an aggregate base. To investigate the sites, slabs were cut from the cores in a plane perpendicular to the pavement surface. Some of the slabs were polished and used for chemical staining and stereo OM, other slabs were cut into billets and prepared in thin section.

CHEMICAL STAINING

A solution of sodium cobaltinitrite was applied to the polished slab surfaces to stain potassium-bearing alkali-silica gels yellow. A variety of aggregate types picked up the yellow stain, including cherts, impure cherty carbonates, and sandstones. Figures D-26 through D-28 depict some cracked coarse aggregates where alkali-silica reaction product in the cracks has picked up the yellow stain. A solution of barium chloride and potassium permanganate was used to stain sulfate-bearing minerals pink. The sulfate stain assisted with the identification of entrained air voids filled with secondary ettringite deposits observed during the ASTM C457 Modified Point Count. Figure D-29 depicts some pink-stained secondary ettringite filled air voids from core 27-B.

THIN SECTIONS

Figures D-30a, D-30b, and D-30c show some cracked coarse aggregates from core 26B-C. Figures D-31a, D-31b, and D-31c are a close-up view of the alkali-silica reaction product that fills the crack. Measurements of the capillary porosity of the cement paste from the three sites were made using fluorescence microscopy. To make the measurements, thin sections were made from cores 26A-C, 26B-C, and 27-C at representative depths of 5 cm, 10 cm, and 15 cm from the pavement surface. From each thin section, six regions of cement paste and fine aggregate were sampled, for a total of 18 images for each site. Each image consists of the 8-bit G band from the complete 24-bit RGB image originally captured from the microscope. Figures D-32, D-33, and D-34 consist of a composite image showing all of the images used from each site. In the figures, the dark areas are fine aggregate particles, the bright areas are entrained air bubbles, and the intermediately bright areas are the cement paste. Figure D-35 shows the summary brightness histogram for the three sites. For each site, the histogram shows three distinct peaks: a large peak in the dark region for the fine aggregates, a broad peak in the middle for the cement paste, and a small peak in the bright region for the entrained air bubbles. From Figure D-35, it appears that the cement paste from core 26A-C is slightly more dense (darker) than the cement paste from the other two cores, 26B-C, and 27-C. One explanation for this observation is that the w/cm for Test Site 26A was lower than for the other two test sites.

Table D-5. Mix design information for Test Site Nos. 26A, 26B, and 27.

Site No.	26A, 26B, and 27
kg/m ³ Cement	252
kg/m ³ Fly Ash	0
kg/m ³ Water	121
kg/m ³ Coarse	1158
kg/m ³ fine	629
w/cm	0.48
Vol% Cement Paste	21.3
Vol% Coarse Agg.	46.5
Vol% Fine Agg.	25.7
Vol% Air	6.5
Coarse Agg. No.	67-02
Fine Agg. No.	67-02

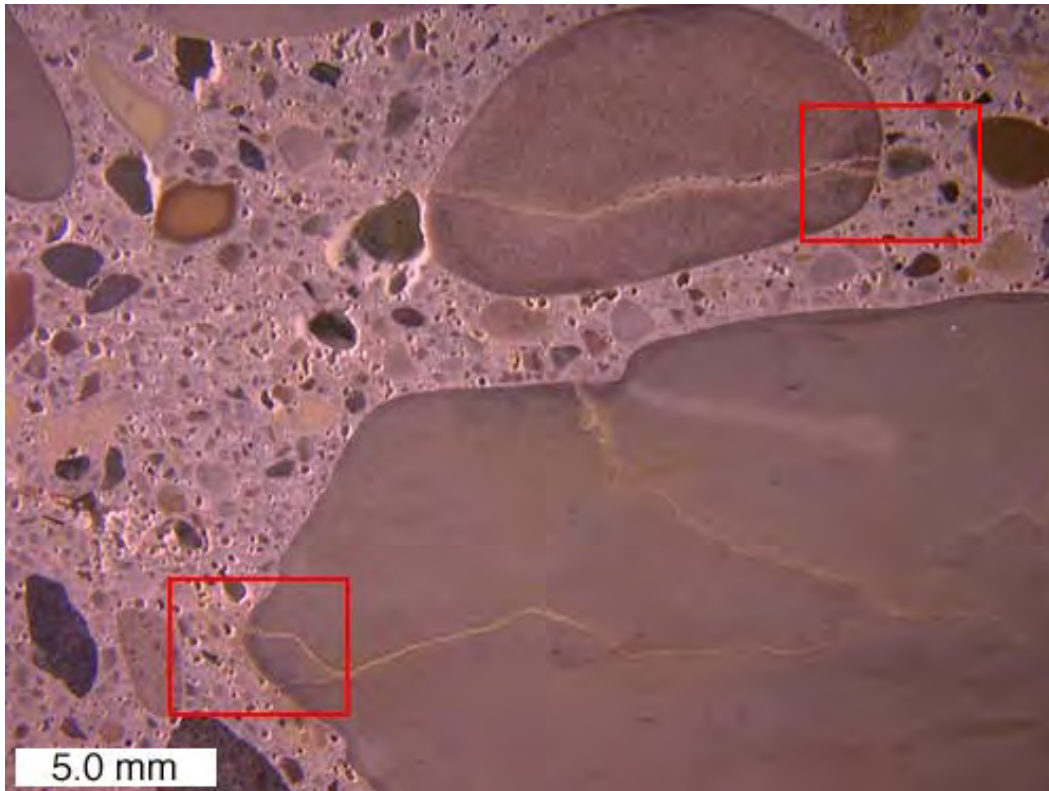


Figure D-26. Cracked coarse aggregates where alkali-silica gel product in the cracks has picked up the yellow sodium cobaltinitrite stain in Core 27-B. Red boxes show close-up areas depicted in Figures D-27 and D-28.

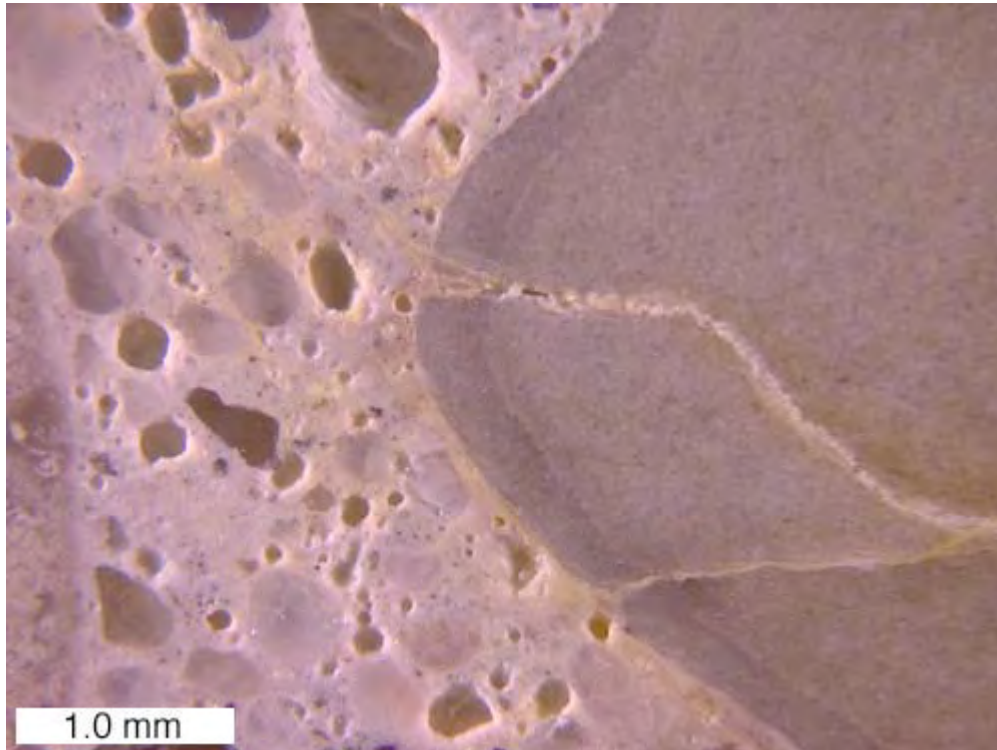


Figure D-27. Alkali-silica reaction product in cracks that has picked up the yellow sodium cobaltinitrite stain, close-up of area outlined in red in Figure D-26.

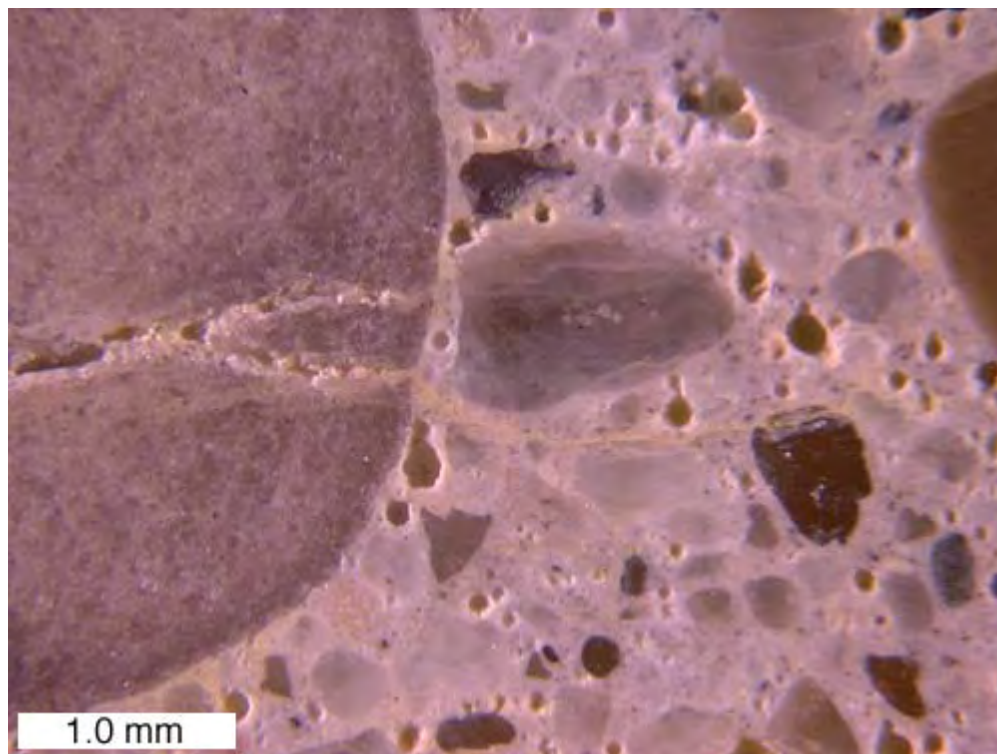


Figure D-28. Alkali-silica reaction product in cracks that has picked up the yellow sodium cobaltinitrite stain, close-up of area outlined in red in Figure D-26.

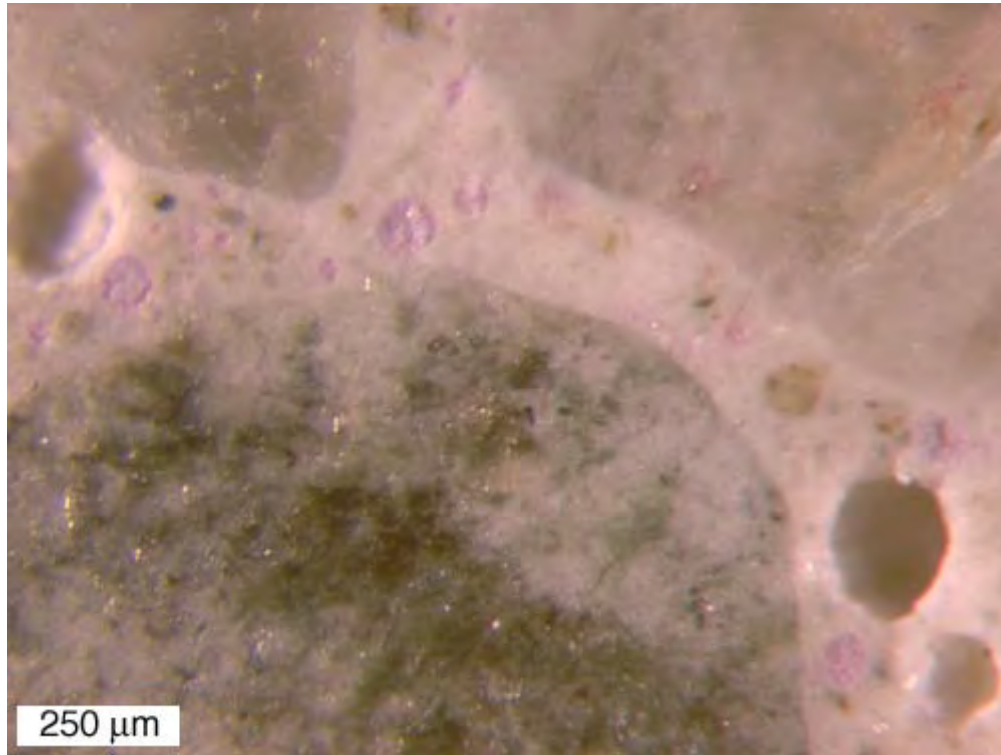


Figure D-29. Ettringite filled entrained air voids stained pink from core 27-B.

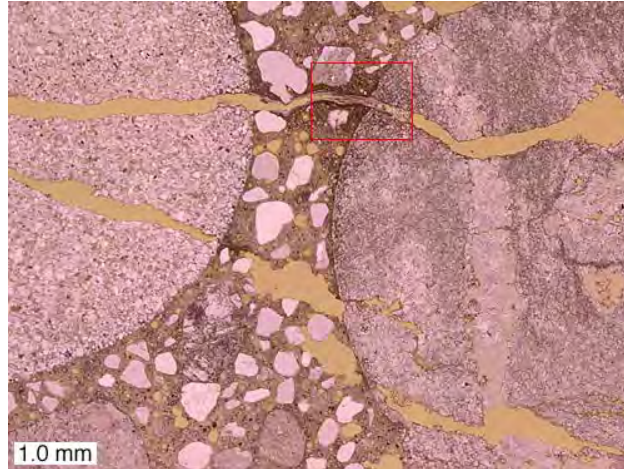


Figure D-30a. Thin-section view of cracked coarse aggregates from Core 26B-C, plane-polarized light. Red box shows area of close-up view in Figure D-31a.

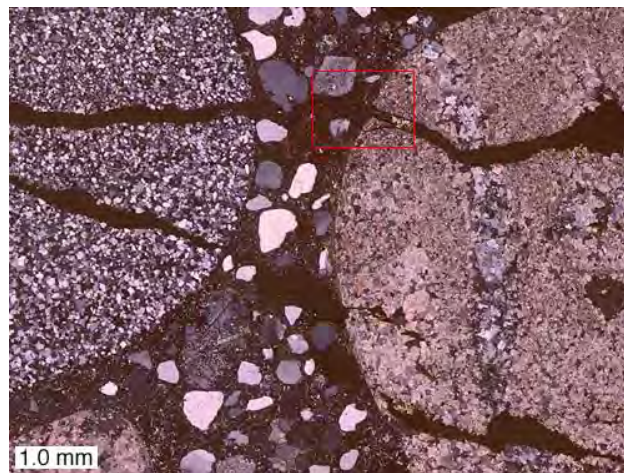


Figure D-30b. Thin-section view of cracked coarse aggregates from Core 26B-C, cross-polarized light. Red box shows area of close-up view in Figure D-31b.

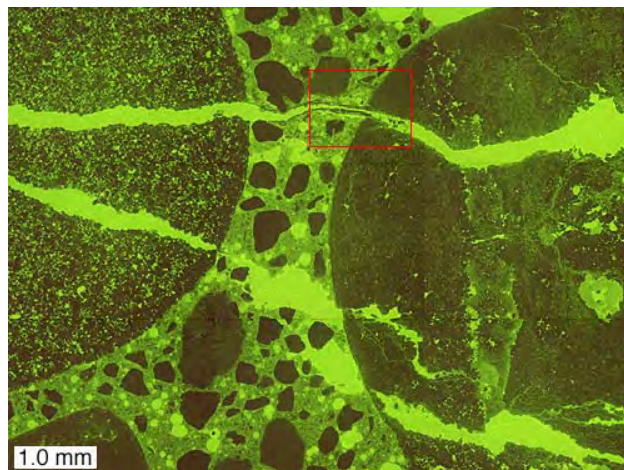


Figure D-30c. Thin-section view of cracked coarse aggregates from Core 26B-C, epifluorescent mode. Red box shows area of close-up view in Figure D-31c.

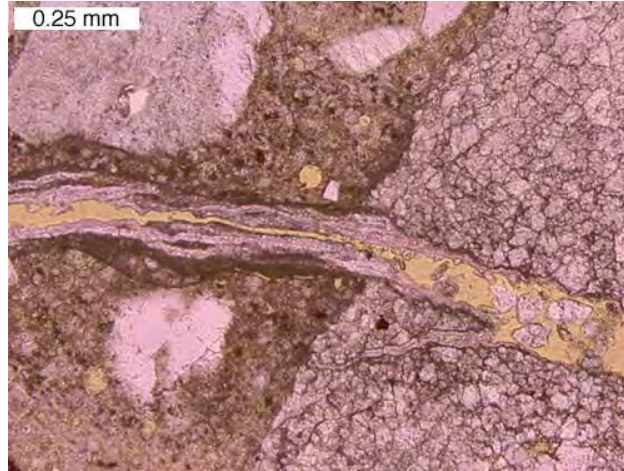


Figure D-31a. Thin section view of alkali-silica reaction product in crack, plane-polarized light, close-up of area outlined in red in Figure D-30a.

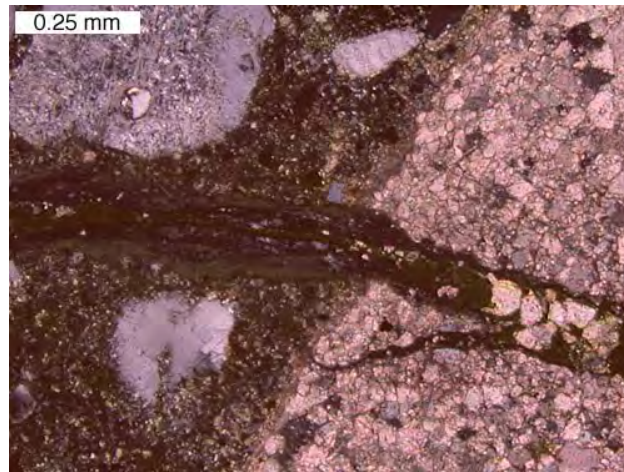


Figure D-31b. Thin section view of alkali-silica reaction product in crack, cross-polarized light, close-up of area outlined in red in Figure D-30b.

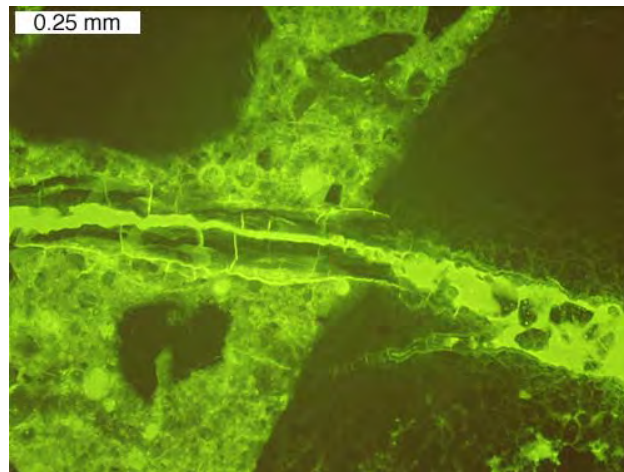


Figure D-31c. Thin section view of alkali-silica reaction product in crack, epifluorescent mode, close-up of area outlined in red in Figure D-30c.

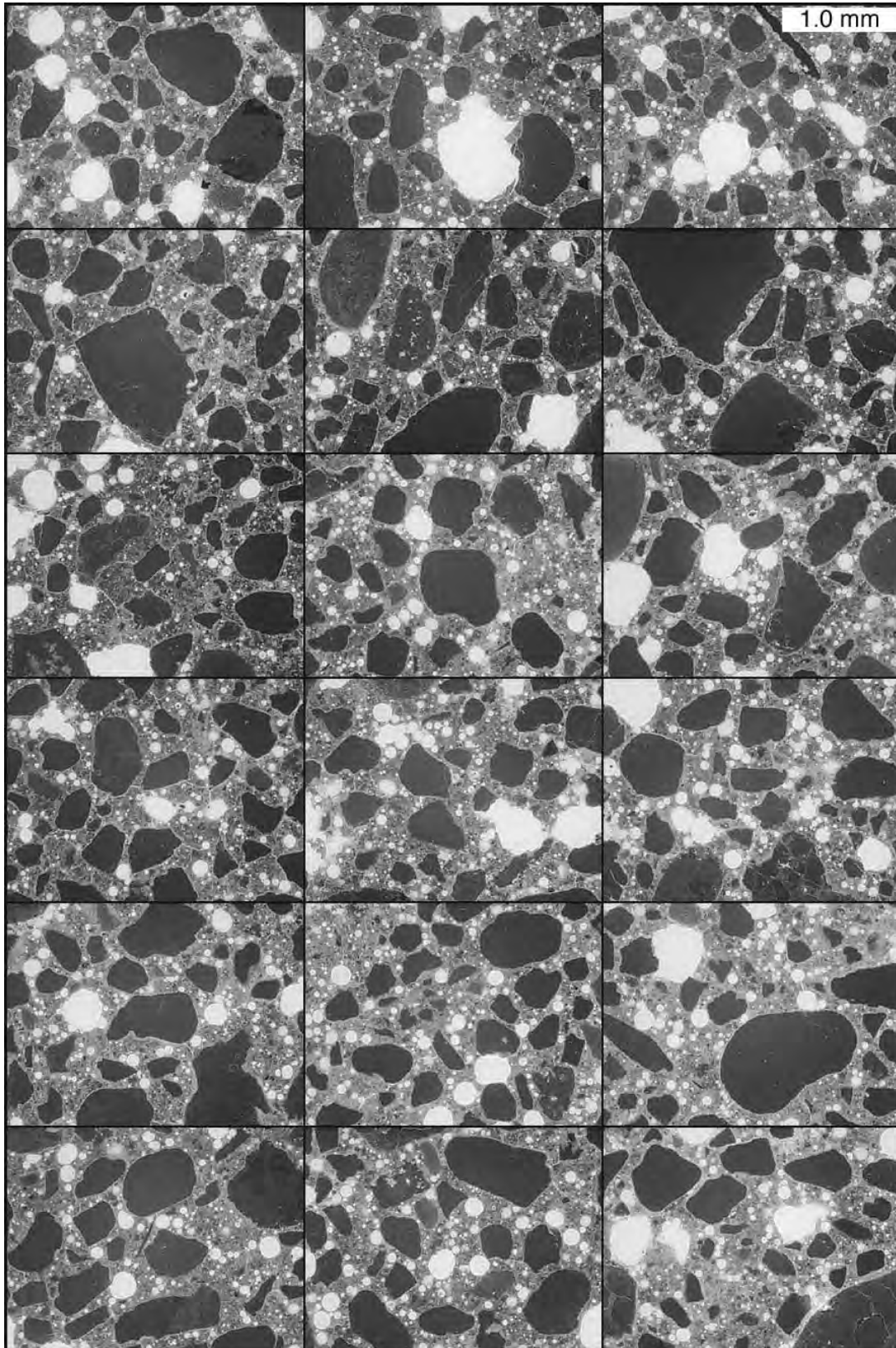


Figure D-32. Composite of 18 epifluorescent mode images used to measure cement paste capillary porosity in Core 26A-C.

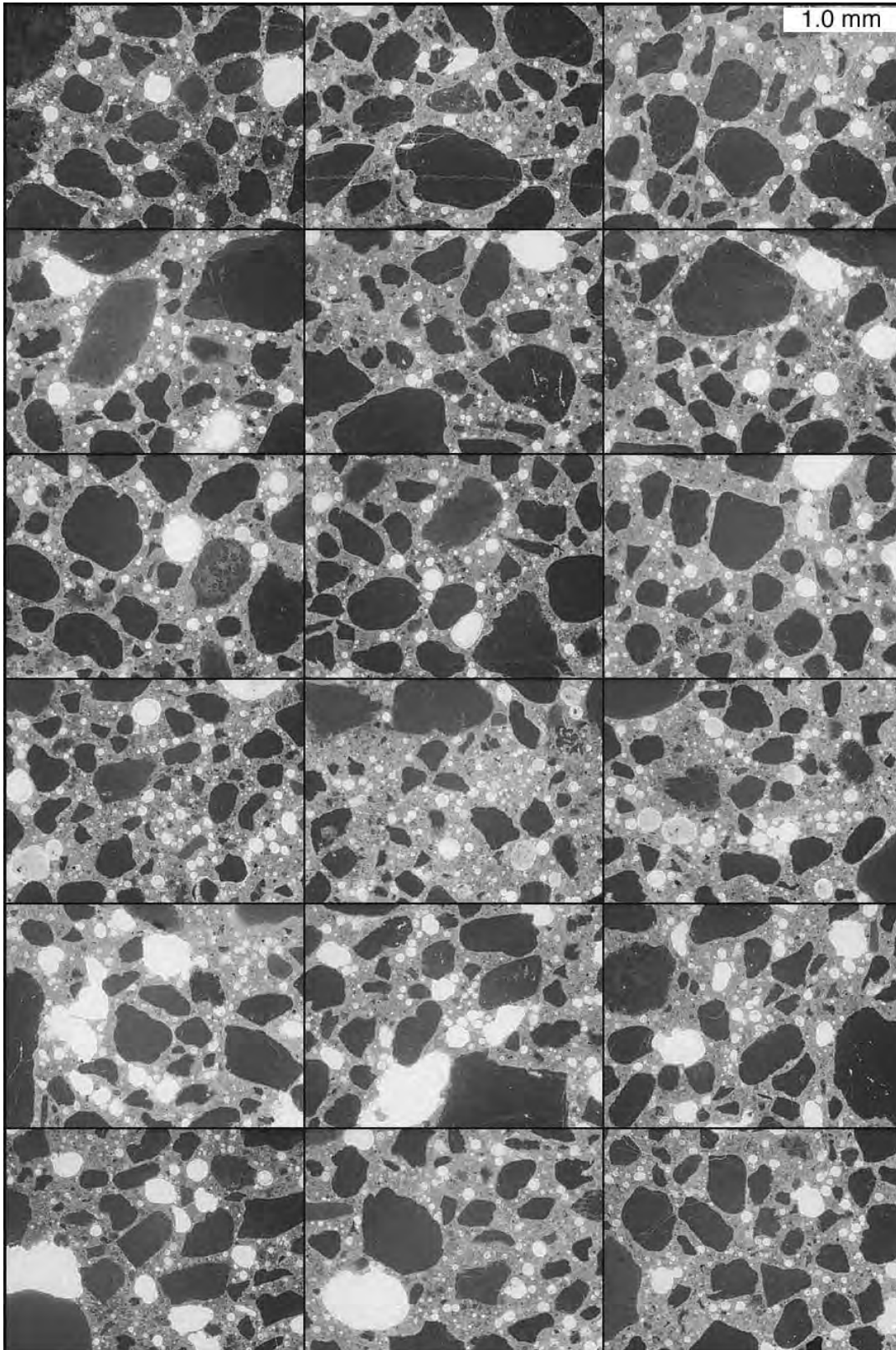


Figure D-33. Composite of 18 epifluorescent mode images used to measure cement paste capillary porosity in Core 26B-C.

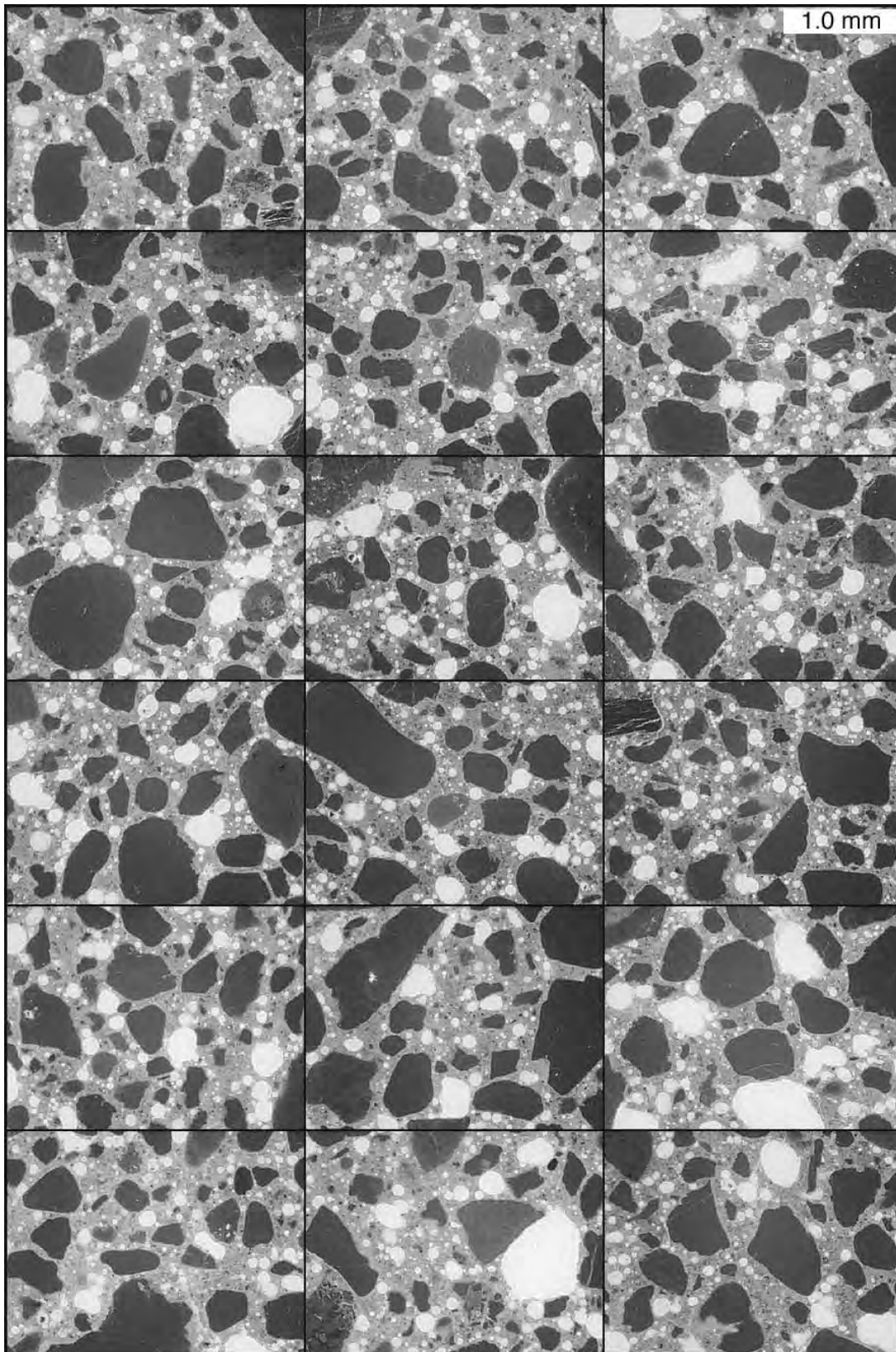


Figure D-34. Composite of 18 epifluorescent mode images used to measure cement paste capillary porosity in Core 27-C.

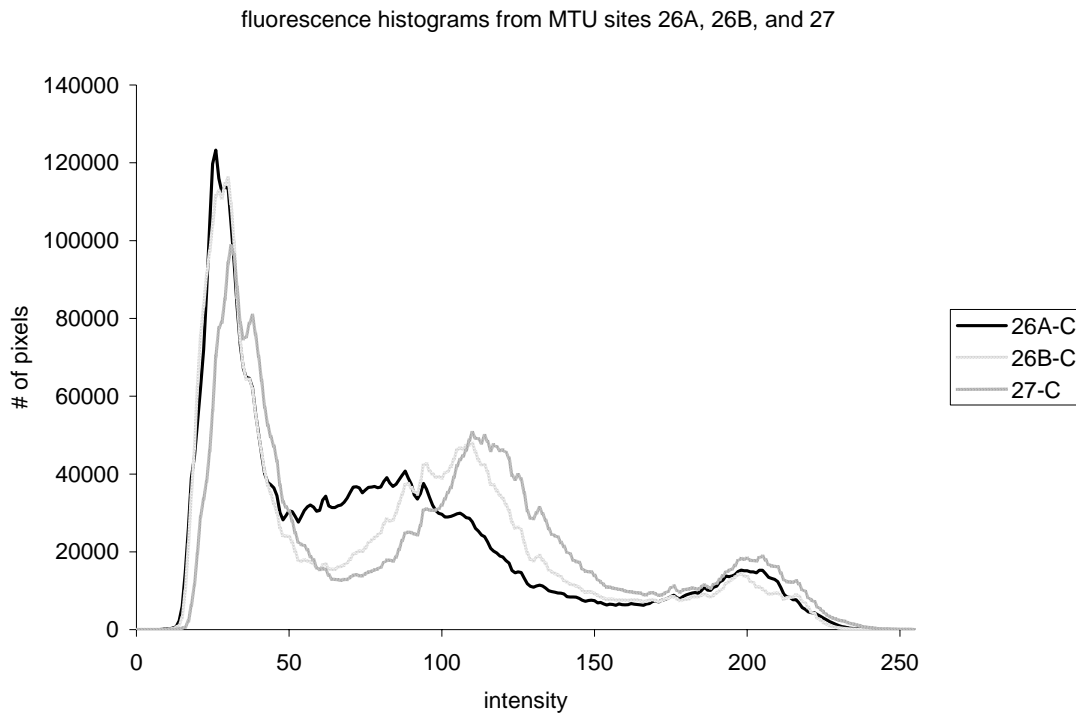


Figure D-35. Brightness histograms for epifluorescent mode images from Figures D-32 through D-34.

AIR VOID CHARACTERISTICS

Slabs from each pavement were polished and examined under a stereo OM in accordance with ASTM C457 Procedure B – Modified Point-Count Method. In addition to the standard procedure, the slabs were stained with a solution of potassium permanganate and barium chloride. The chemicals stain sulfate-bearing minerals, such as ettringite, pink. Over time, such minerals commonly occur as secondary growths in the entrained air voids. Often, entrained air voids in deteriorated concrete are completely filled with secondary ettringite. The stain assists in the identification of filled air voids that may otherwise be mistaken for hardened cement paste. In the equations used to determine the air-void system parameters, filled air voids that are identified as paste would be considered to offer no protection to freeze-thaw damage. It is controversial whether filled air voids can protect the paste against freeze-thaw damage, and thus, air-void system parameters are computed for both the concrete in its original state, and the concrete in its existing state. Table D-6 shows the results of the Modified Point-Count for the three sites. Figure D-36 plots the spacing factors for each site, along with dotted lines to represent the suggested range according to ASTM C457. Figure D-37 plots the void frequency for each site, along with dotted lines to represent the suggested range according to ASTM C457. Figure D-38 compares the aggregate, cement paste and air volume percentages as determined by point count to the volume percentages computed from the mix design.

Table D-6. Results of air void analyses for cores 26A-C, 26B-C, and 27-C.

MTU Core ID	26A-C	26B-D	27-C
Raw Data			
area analyzed (cm ²)	69.9	87.6	74.2
air stops	65	120	96
paste stops	368	389	336
aggregate stops	913	1202	1011
secondary ettringite stops	19	1	7
total stops	1365	1712	1450
traverse length (mm)	3565	4472	3787
# of air void intercepts	772	1496	1435
# of secondary ettringite filled intercepts	399	72	197
Results			
vol% aggregate	66.9	70.2	69.7
vol% air original	6.2	7.1	7.1
vol% air existing	4.8	7.0	6.6
vol% paste original	27.0	22.7	23.2
vol% paste existing	28.4	22.8	23.7
original void frequency (voids/m)	328	351	431
existing void frequency (voids/m)	217	335	379
original avg. chord length (mm)	0.187	0.202	0.165
existing avg. chord length (mm)	0.220	0.210	0.175
original specific surface (mm ⁻¹)	21.3	19.8	24.3
existing specific surface (mm ⁻¹)	18.2	19.1	22.9
original paste/air ratio	4.4	3.2	3.3
existing paste/air ratio	6.0	3.3	3.6
original spacing factor (mm)	0.204	0.162	0.134
existing spacing factor (mm)	0.276	0.170	0.156

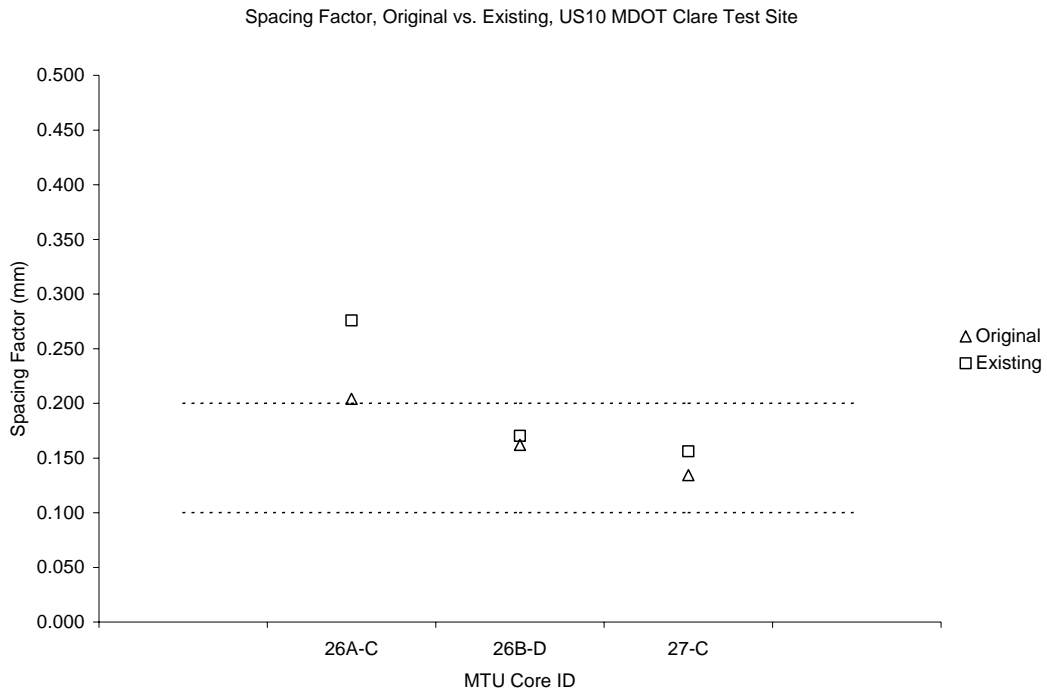


Figure D-36. Spacing factors plotted with dotted lines showing suggested values from ASTM C457.

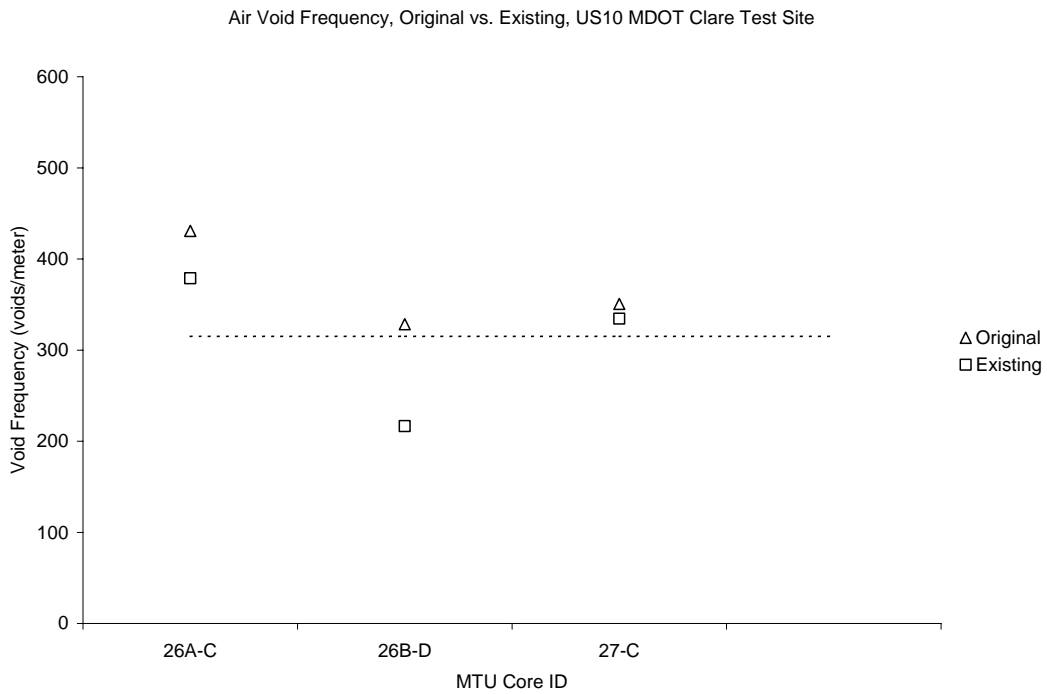


Figure D-37. Void frequencies plotted with dotted lines showing suggested values from ASTM C457.

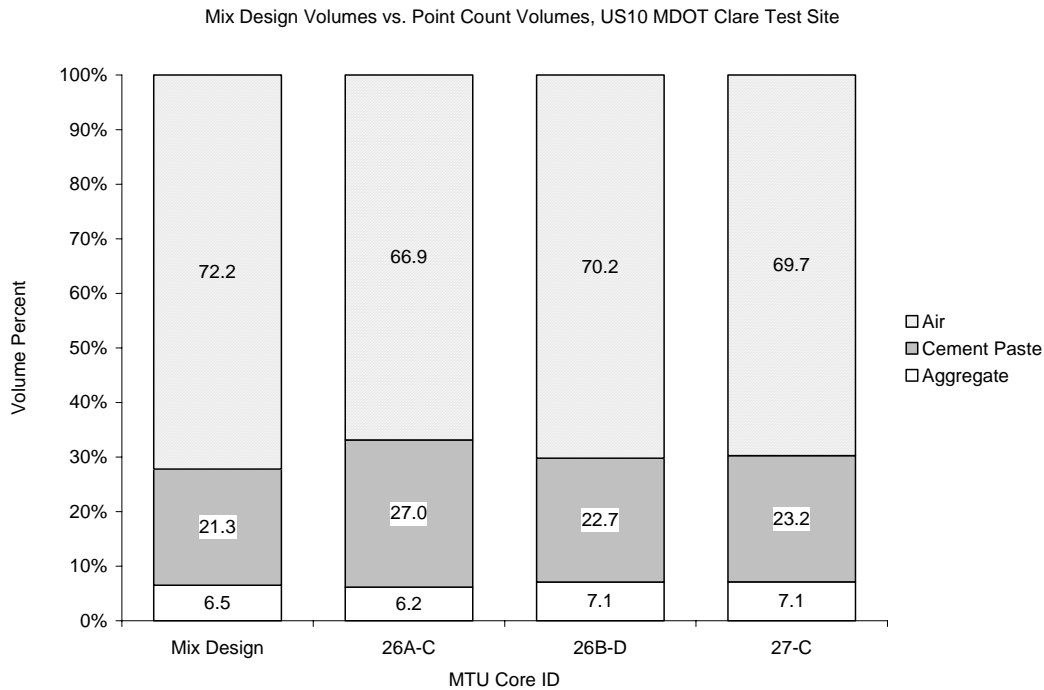


Figure D-38. Volume percentages from point counts compared to volume percentages computed from mix designs.

CONCLUSIONS

The MDOT US10 Clare Test Site was developed to evaluate various pavement design elements, and as such, the concrete used was designed to be the same throughout. Although the three sites all have the same mix design, the subbase materials used at the sites were not the same. Both Test Sites Nos. 26A and 26B utilized an asphalt treated permeable base, while Test Site No. 27 was supported on an aggregate base. The pavements are all currently in relatively poor condition, suffering joint deterioration that has been commonly been classified as “D-cracking.” The following summarizes the microstructural observations made for these three test sites:

- Although the concrete was supposed to be the same, there are some noticeable differences between that in Test Site 26A and the other two test sites. The first observation is that the hydrated cement paste in Test Site 26A appears to be more dense, indicating that the w/cm for this site may have been less than for the other two sites. In addition, the overall original air content at Test Site 26A was also less than that at the other two sites.
- One primary distress mechanism appears to be ASR associated with the various cherts, impure cherty carbonates, and sandstones coarse aggregate particles. These aggregate particles have cracked, and copious quantities of alkali-silica reaction product are observed to be filling these cracks, which extend into the paste.

- A potentially contributing factor is aggregate freeze-thaw distress, since many of the cracked coarse aggregates are fine-grained and porous, sharing similar properties to aggregates known to be susceptible to freeze-thaw deterioration. Thus, it is possible that the cracking in the coarse aggregate is a result of freeze-thaw deterioration, and that the alkali-silica reaction occurred once the concrete fabric was compromised.
- Infilling of the air-void system with ettringite is common, but more so in Test Site No. 26A. In this case, a marginal air-void system is becoming less capable of providing protection against freeze-thaw damage. Such infilling is a common feature in distress concrete, and it is unlikely that it is related to the initiation of the observed distress. Yet, it may contribute to the continuation of the distress once it has been initiated.

SITES 4, 19, AND 29: PAVEMENTS WITH BLAST FURNACE SLAG COARSE AGGREGATE

INTRODUCTION

The cores received from Test Site Nos. 4, 19, and 29 were from distressed pavements made with iron blast furnace slag coarse aggregate. Table D-7 summarizes the mix design information for the three sites. To investigate the sites, slabs were cut from the cores in a plane perpendicular to the pavement surface. Some of the slabs were polished and used for chemical staining and stereo OM, other slabs were cut into billets and prepared in thin section, and the rest of the slabs were crushed into powder to perform chemical extractions. Note that Test Site No. 4 is part of a special study, the report of which is presented in Appendix E.

CHEMICAL STAINS

A solution of sodium cobaltinitrite was applied to the polished slab surfaces to stain potassium-bearing alkali-silica gels yellow. The alkali-silica gel stain primarily affected the chert fine aggregate common to the three sites. Figure D-39 shows an example of a yellow-stained chert particle. A solution of barium chloride and potassium permanganate was used to stain sulfate-bearing minerals pink. The sulfate stain assisted with the identification of entrained air voids filled with secondary ettringite deposits observed during the ASTM C457 Modified Point Count. Figure D-40 depicts some pink-stained secondary ettringite filled air voids.

THIN SECTIONS

Two types of reactive fine aggregate particles were identified during the chemical staining procedures. Figures D-41a, D-41b, and D-41c show an example of a cracked reactive chert particle. The presence of a dense rim in contact with the cement paste, and cracks extending into the cement paste is typical of the chert particles in all three of the pavements. In addition to the chert particles, Test Site No. 29 had abundant siltstone fine aggregate particles similar to those of the fine aggregate from the US-23 MDOT Aggregate Test Site (Test Site Nos. 0 through 4A). Figures D-42a, D-42b, and D-42c show an example of a reactive siltstone particle between two chert particles. Siliceous fossils within the siltstone appear to be the reactive constituent. The siltstone particle shown is cracked, but the cracks do not extend into the surrounding cement paste.

Test Site No. 19 had the most severe cracking of the hydrated cement paste of the three sites. The cracks were often filled with alkali-silica reaction product. Figures D-43a, D-43b, and D-43c show some alkali-silica reaction product filled cracks with the gel apparently originating from a large chert particle. Figures D-44a, D-44b, and D-44c show a close-up of the crack filled with alkali-silica reaction product. Figure D-45 shows a back-scattered electron image of the same crack, and Figure D-46 is an x-ray energy spectrum collected from the alkali-silica reaction product shown in Figure D-45 with peaks for carbon, oxygen, aluminum, silicon, sulfur, chlorine, potassium, and calcium.

Table D-7. Volume percentage values computed from mix designs.

Test Site No.	4	19	29
Year Constructed	1992	1988/89	1976
kg/m ³ Cement	480	553	516
kg/m ³ Fly Ash	72	none	none
kg/m ³ Water	260	248	295
kg/m ³ Coarse	1399	2147	1427
kg/m ³ Fine	1551	1094	1679
w/cm	0.47	0.45	0.57
Vol% Cement Paste	25.6	24.4	26.1
Vol% Coarse Agg.	42.3	46.0	30.7
Vol% Fine Agg.	25.7	24.1	36.7
Vol% Air	6.5	5.5	6.5
Coarse Agg. No.	82-19	47-03	Trenton
Fine Agg. No.	63-54	63-04 63-47	81-57



Figure D-39. Yellow stained chert sand particle from Core 4-A.

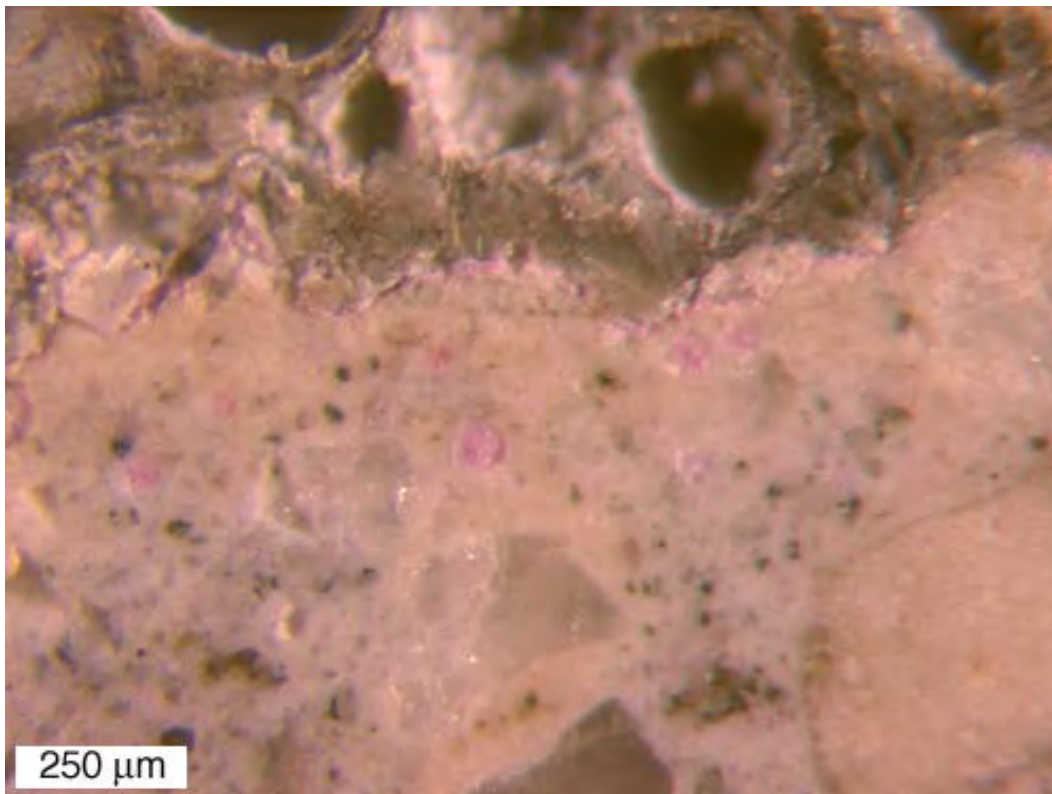


Figure D-40. A polished surface stained for sulfate minerals from Core 19-B.

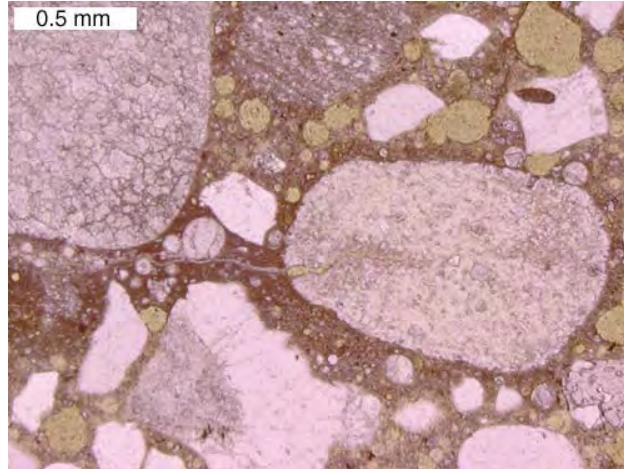


Figure D-41a. Thin-section view of a reactive chert sand particle from Core 4-A, plane-polarized light.

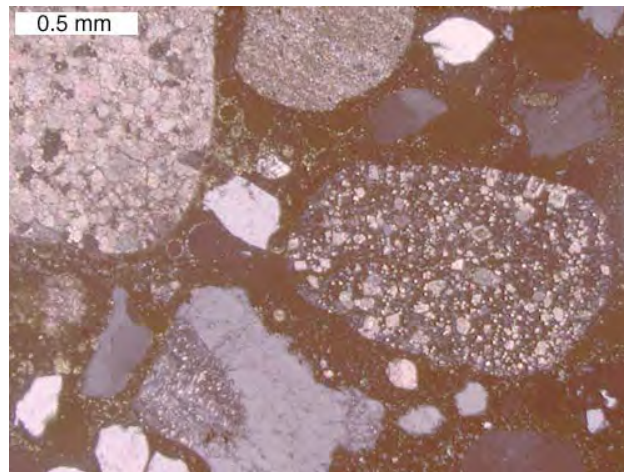


Figure D-41b. Thin-section view of a reactive chert sand particle from Core 4-A, cross-polarized light.

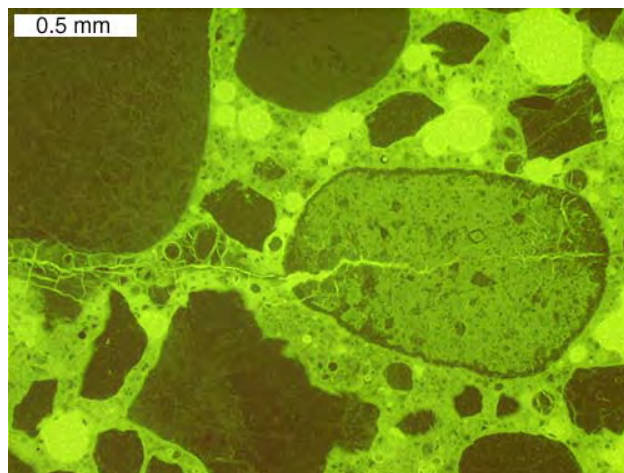


Figure D-41c. Thin-section view of a reactive chert sand particle from Core 4-A, epifluorescent mode.

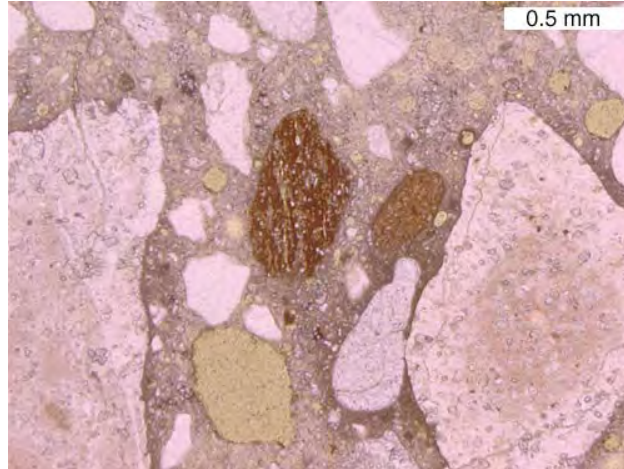


Figure D-42a. Thin-section view of a reactive siltstone sand particle, (center) with reactive chert particles on either side, Core 4-A, plane-polarized light.

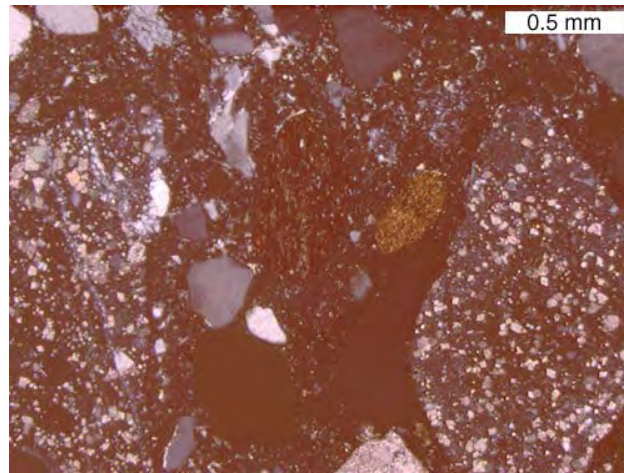


Figure D-42b. Thin-section view of a reactive siltstone sand particle, (center) with reactive chert particles on either side, Core 4-A, cross-polarized light.

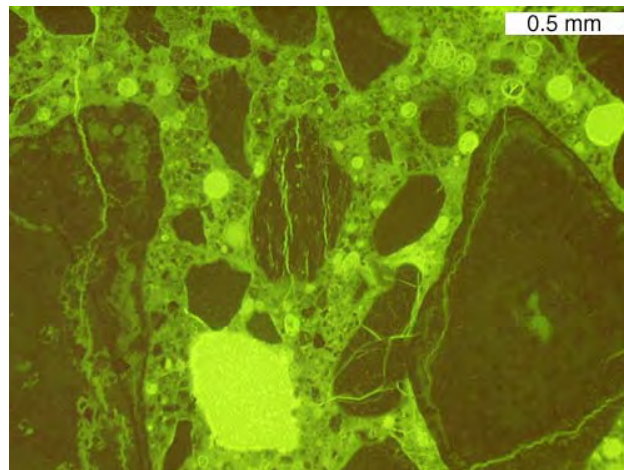


Figure D-42c. Thin-section view of a reactive siltstone sand particle, (center) with reactive chert particles on either side, Core 4-A, epifluorescent mode.

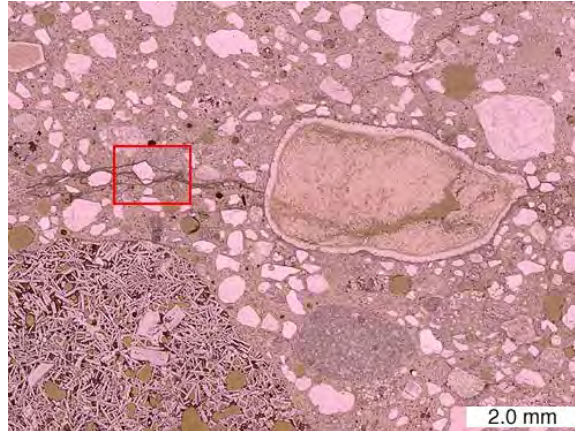


Figure D-43a. Thin-section view of a reactive chert sand particle with cracks extending into surrounding cement paste, Core 19-B, red box shows area of close-up in Figure D-44a, plane-polarized light.

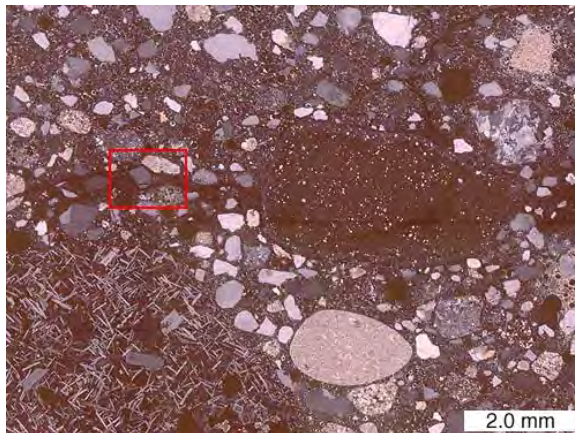


Figure D-43b. Thin-section view of a reactive chert sand particle with cracks extending into surrounding cement paste, Core 19-B, red box shows area of close-up in Figure D-44b, cross-polarized light.

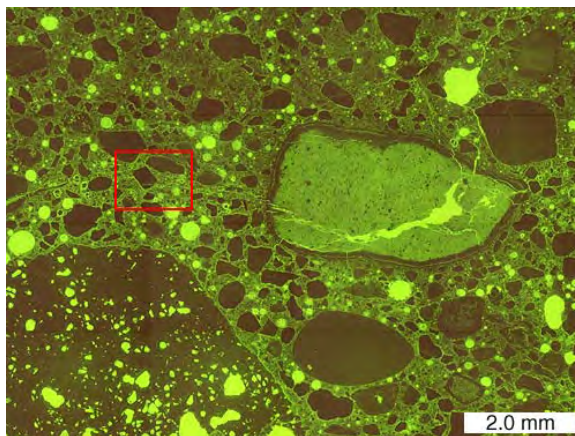


Figure D-43c. Thin-section view of a reactive chert sand particle with cracks extending far into the surrounding cement paste, Core 19-B, red box shows area of close-up in Figure D-44c, epifluorescent mode.

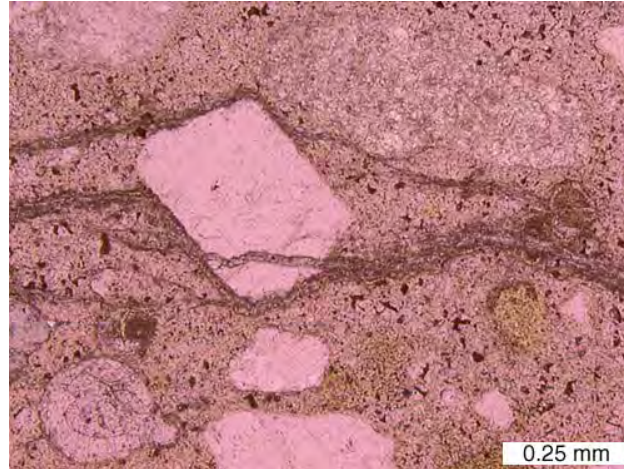


Figure D-44a. Close-up of area shown in Figure D-43a showing alkali-silica reaction product filled cracks and voids, Core 19-B, plane-polarized light.

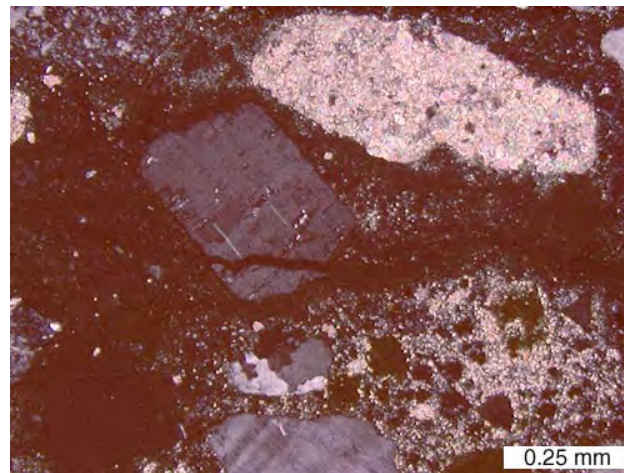


Figure D-44b. Close-up of area shown in Figure D-44b showing alkali-silica reaction product filled cracks and voids, Core 19-B, cross-polarized light.

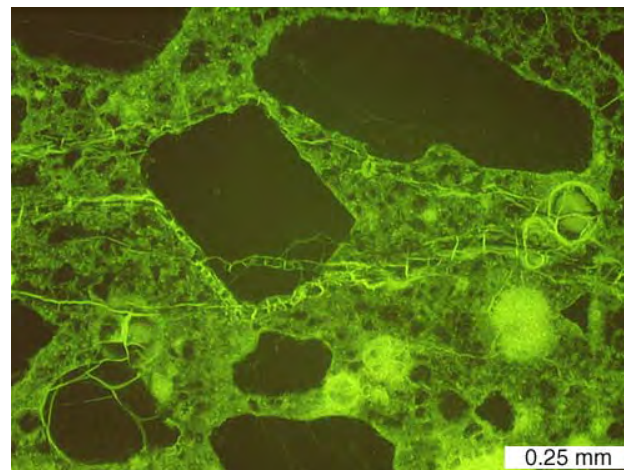


Figure D-44c. Close-up of area shown in Figure D-44c showing alkali-silica reaction product filled cracks and voids, Core 19-B, epifluorescent mode.

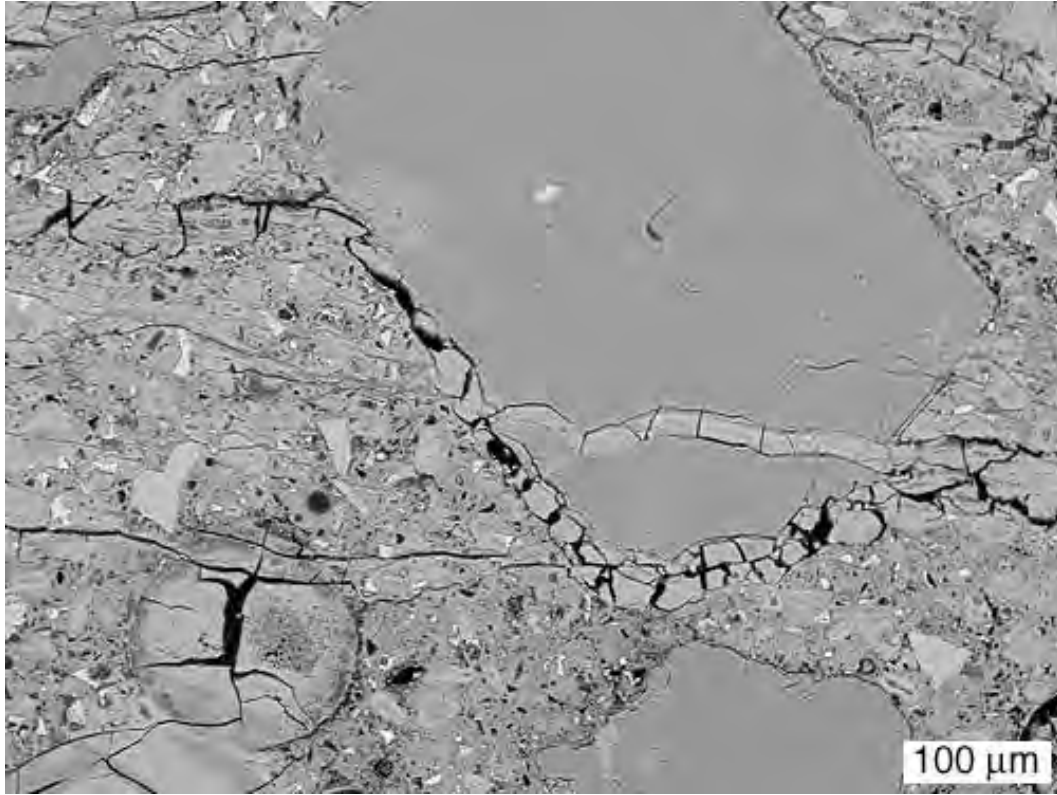


Figure D-45. Back-scattered electron image of cracks and void filled with alkali-silica reaction product, Core 19-B.

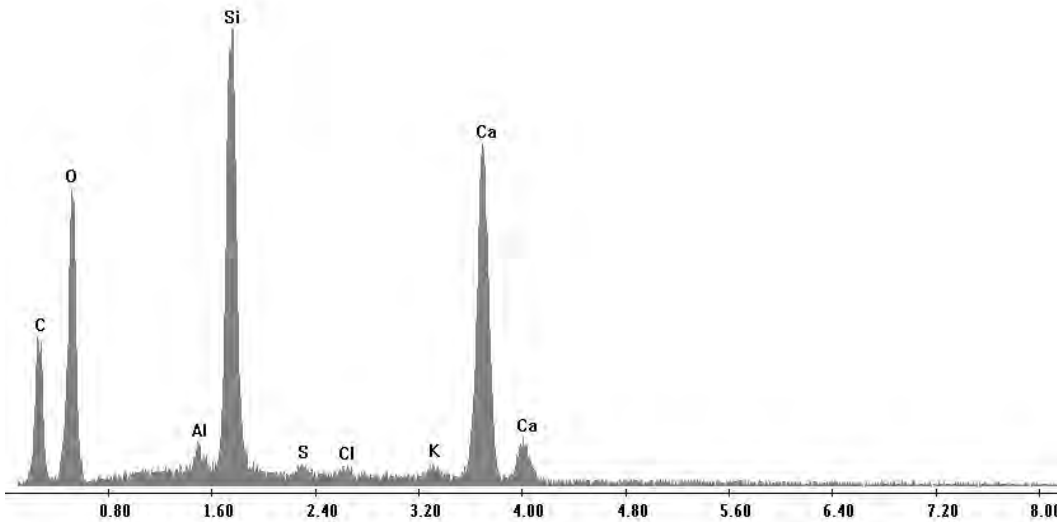


Figure D-46. X-ray energy spectrum collected from alkali-silica reaction product shown in Figure D-45.

It is noted that a peak for carbon is always present regardless of the concentration of carbon in the sample due to the thin layer of carbon that was evaporated on to the sample surface to prevent charge build-up during the electron microscope investigation.

In addition to the abundant alkali-silica reaction product filled cracks at Test Site No. 19, there were also many cracks filled with ettringite. Figures D-47a, D-47b, and D-47c show some ettringite filled cracks. Figures D-48 and D-49 are back-scattered electron images of large cracks running along the contact between slag coarse aggregate and the cement paste. Figure D-50 is an x-ray energy spectrum collected from the ettringite. Figure D-51 is a close-up of a region in Figure D-49 showing calcium sulfide dendrites in the slag aggregate.

Often, in all three pavements, the cement paste in the immediate vicinity of slag coarse aggregate particles appears darker than the rest of the cement paste. At the cement paste/slag aggregate interface the cement paste is denser and partially hydrated cement grains are very abundant. Calcium hydroxide crystals are also often found in the air voids near slag aggregate particles. Figures D-52a, D-52b, and D-52c show a cement paste/slag aggregate interface. The calcium hydroxide filled air voids appear bright yellow in Figure D-52b. Figures D-53a, D-53b, and D-53c are close-ups of a calcium hydroxide filled void and many partially hydrated cement grains. In Figure D-53a, a green coloration is associated with the ferrite and aluminates phases of the cement grains.

CHEMICAL EXTRACTIONS

A gravimetric procedure of sulfate determination was used according to British Standard 1881:Part 124. Methods for Analysis of Hardened Concrete: 1988. The weight percent SO_3 computed from the mix design assumes 3.5% by weight SO_3 for the cement and 4.5% by weight of the fly ash. The results of the sulfate determinations, expressed in terms of SO_3 , are presented in Table D-8. Figure D-54 plots the computed SO_3 wt% next to the extracted SO_3 wt% for each of the sites. In all three of the sites, the extraction values exceeded the computed values.

A standard technique for alkali extraction from hardened concrete was not available, so an ammonium acetate extraction technique developed for the determination of exchangeable and soluble sodium and potassium in soils was adopted. The concentrations of potassium and sodium were determined by an inductively coupled plasma emission spectrophotometer. The results from the test are expressed in weight percent elemental sodium and weight percent elemental potassium. In Table D-9, the results were converted to the industry convention of kilograms of “ Na_2O equivalent” per cubic meter of concrete, based on the total mass from the mix designs. The recalculation to kilograms of “ Na_2O equivalent” per cubic meter of concrete allows comparisons to be made with industry standards for limiting total alkalis in the mixture. The Canadian standards specifying a maximum of $3.0 \text{ kg/m}^3 \text{ Na}_2\text{O}$ equivalent for mild protection, $2.2 \text{ kg/m}^3 \text{ Na}_2\text{O}$ equivalent for moderate protection, and $1.7 \text{ kg/m}^3 \text{ Na}_2\text{O}$ equivalent for strong protection. Figure D-55 plots the Na_2O equivalent values from extraction for all of the sites, along with dotted lines showing the Canadian protection levels.

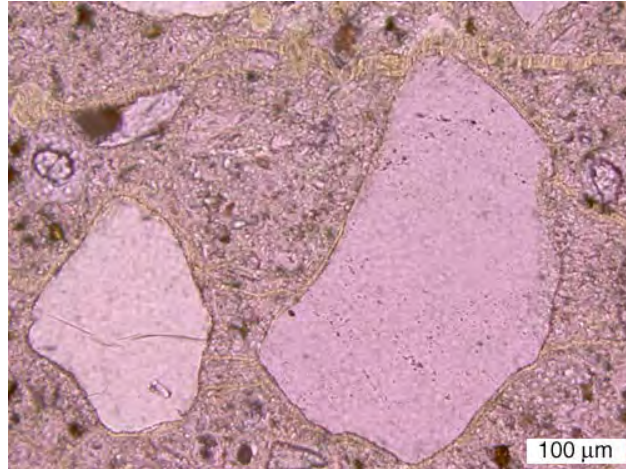


Figure D-47a. Thin-section view of ettringite filled crack along slag aggregate/cement paste interface, Core19-B, plane-polarized light.

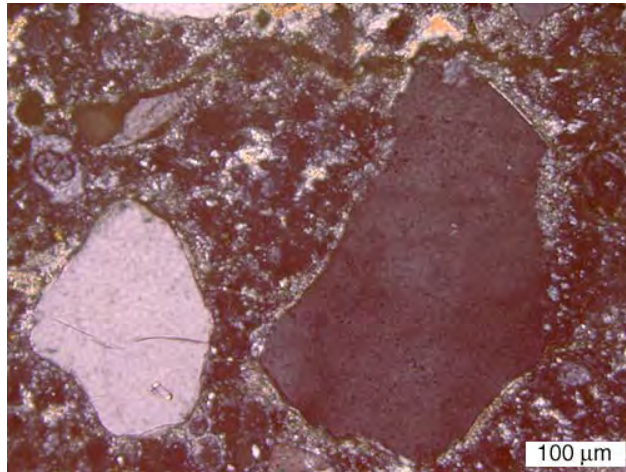


Figure D-47b. Thin-section view of ettringite filled crack along slag aggregate/cement paste interface, Core19-B, cross-polarized light.

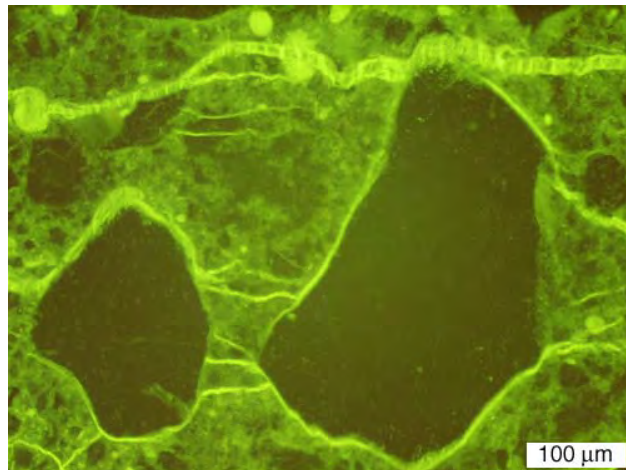


Figure D-47c. Thin-section view of ettringite filled crack along slag aggregate/cement paste interface, Core19-B, epifluorescent mode.

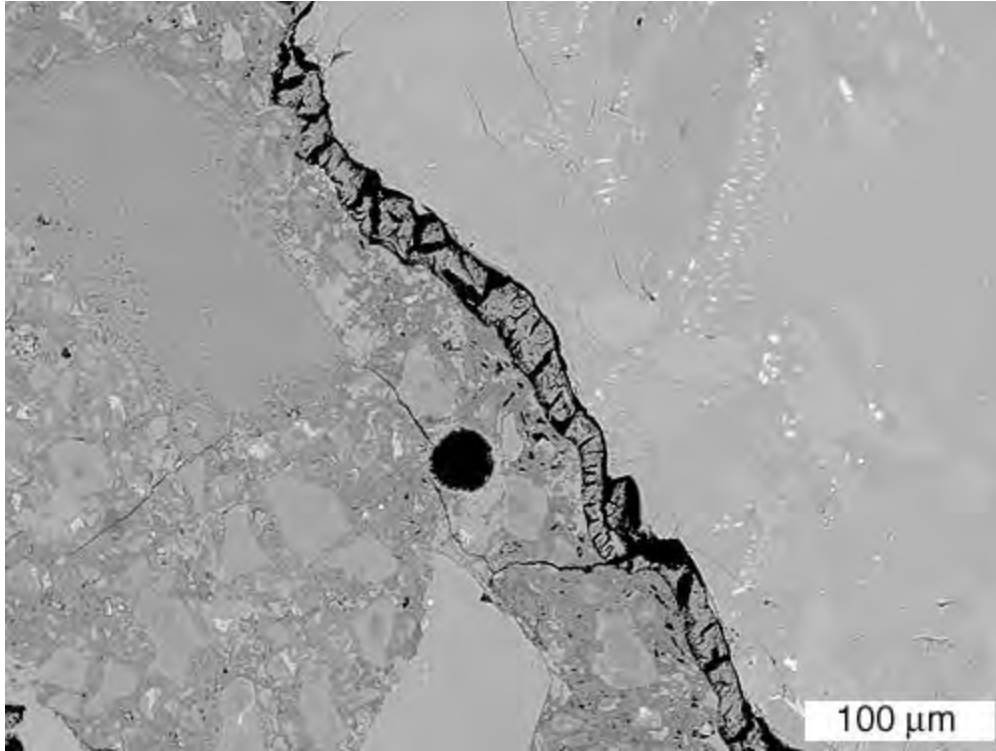


Figure D-48. Back-scattered electron image of ettringite filled crack along slag aggregate/cement paste interface, Core 19-B.

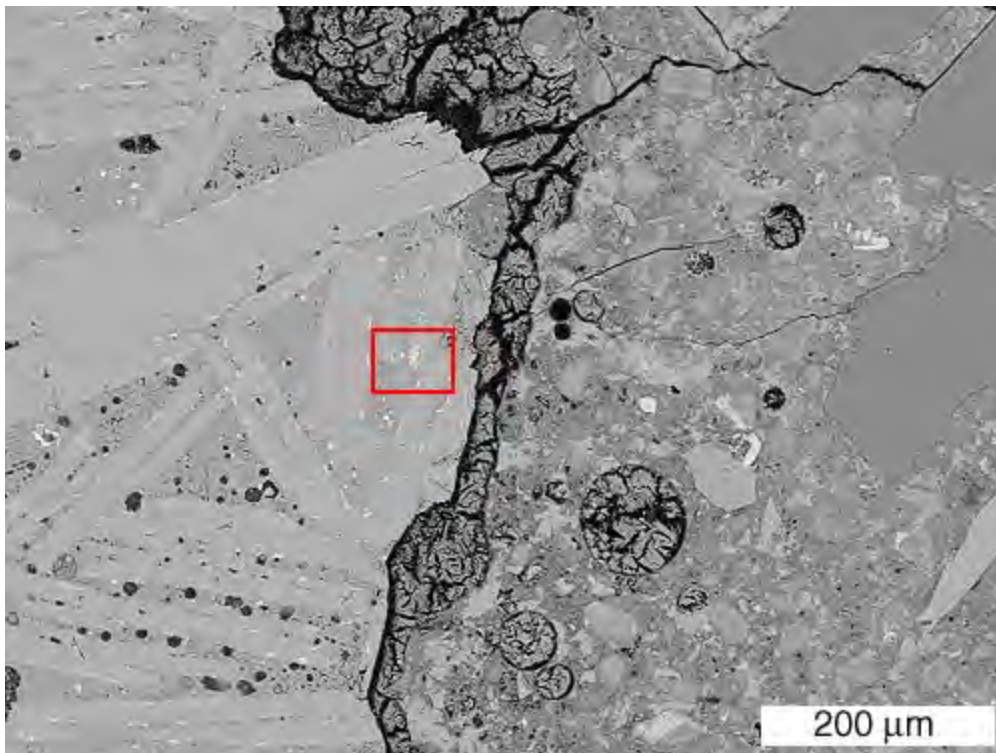


Figure D-49. Back-scattered electron image of ettringite filled crack along slag aggregate/cement paste interface in Core 19-B, red box shows area of close-up in Figure D-51.

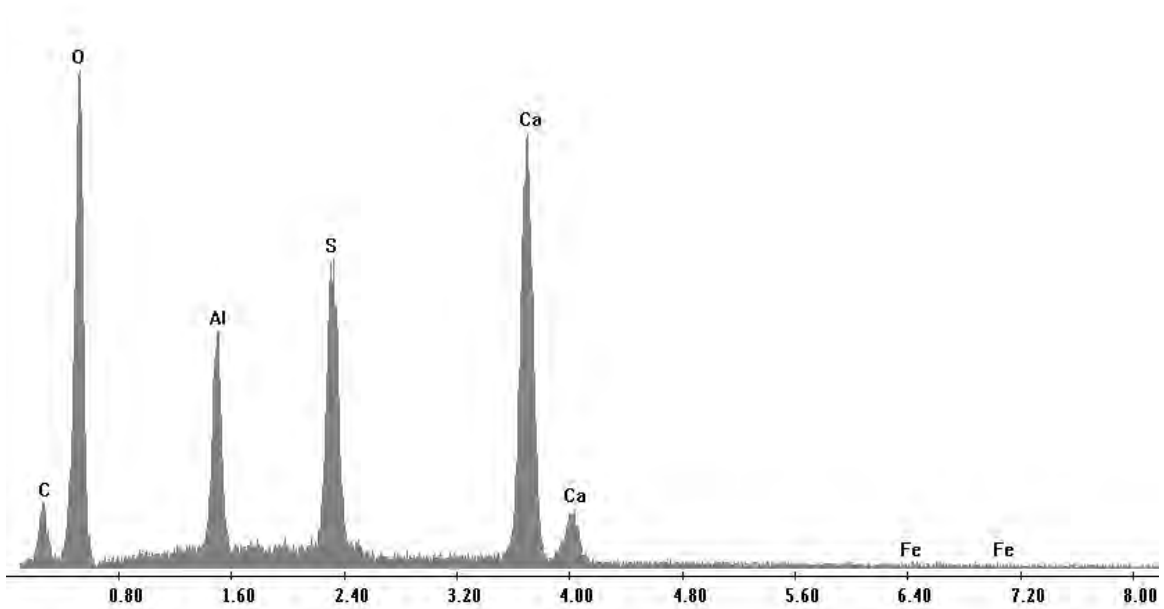


Figure D-50. X-ray energy spectrum collected from ettringite filled crack shown in Figure D-49.

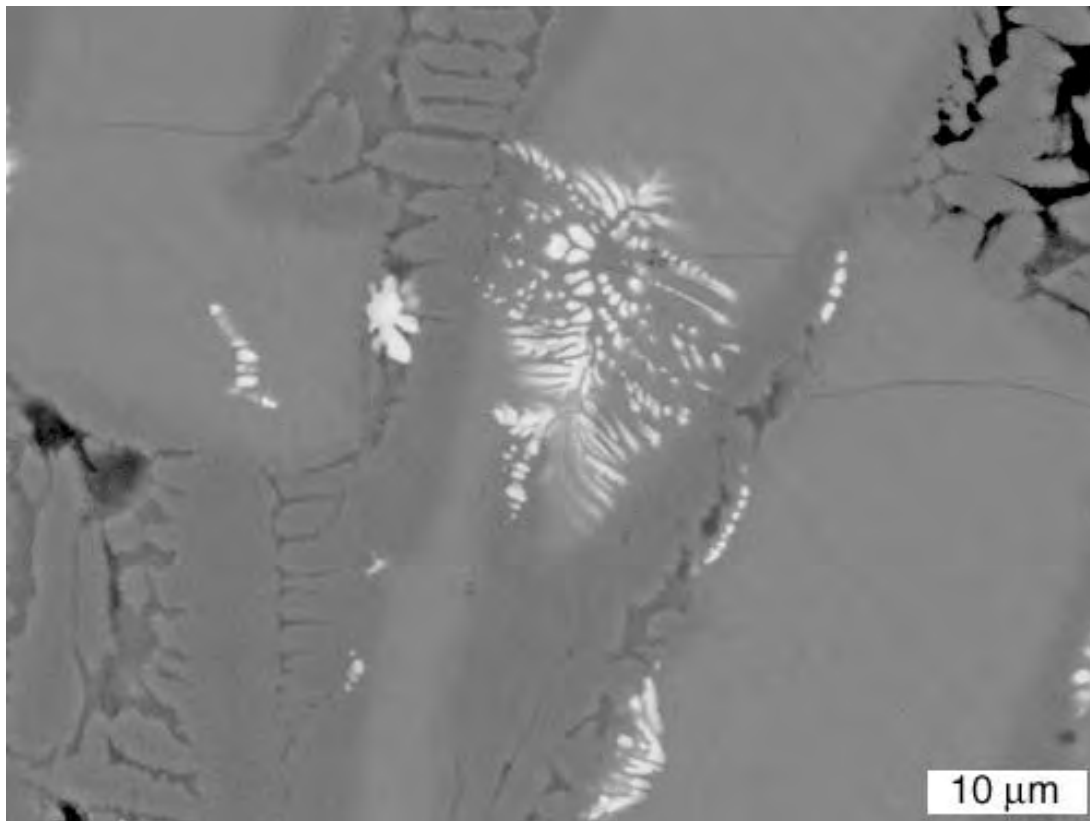


Figure D-51. Close-up of area outlined in red in Figure D-49 with calcium sulfide dendrites in slag aggregate, Core 19-B.

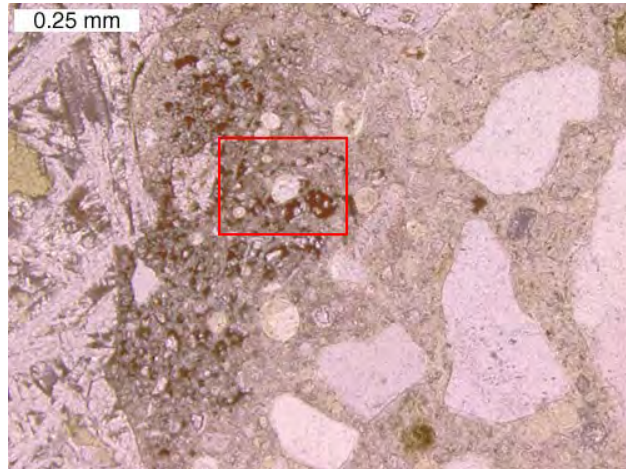


Figure D-52a. Thin-section view of cement paste near contact with slag aggregate, red box shows area of close-up in Figure D-53a, Core 29-A, plane-polarized light.

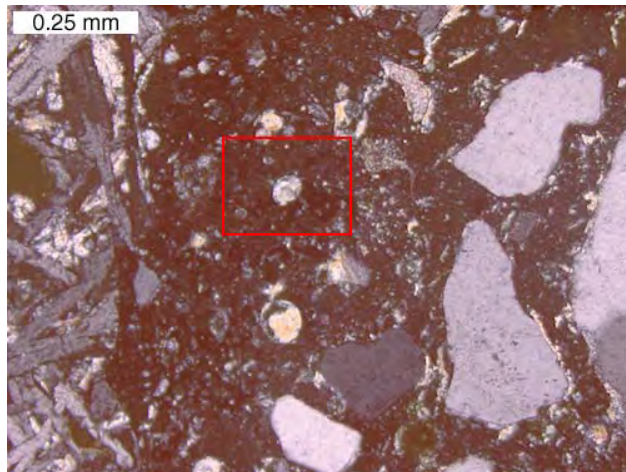


Figure D-52b. Thin-section view of cement paste near contact with slag aggregate, red box shows area of close-up in Figure D-53b, Core 29-A, cross-polarized light.

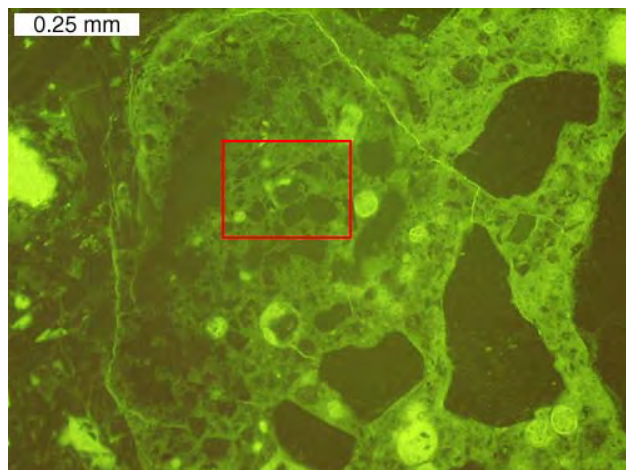


Figure D-52c. Thin-section view of cement paste near contact with slag aggregate, red box shows area of close-up in Figure D-53c, Core 29-A, epifluorescent mode.

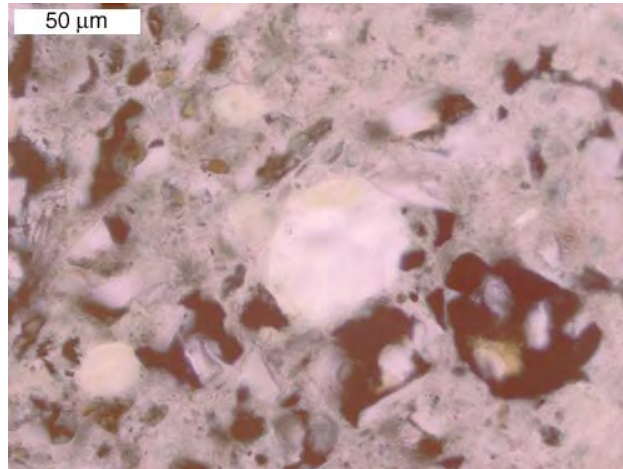


Figure D-53a. Close-up of area outlined in red in Figure D-52a, Core 29-A, plane-polarized light.

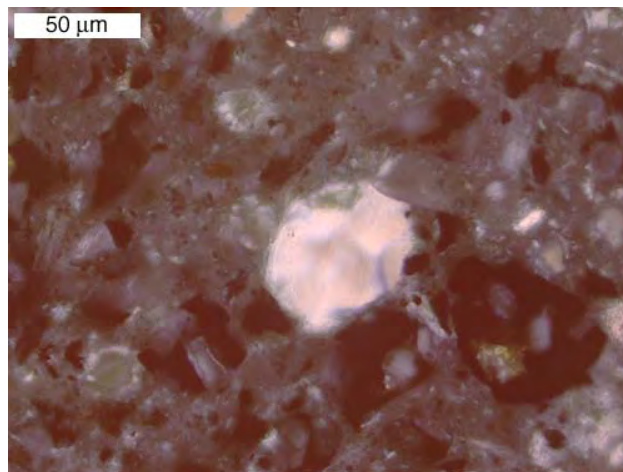


Figure D-53b. Close-up of area outlined in red in Figure D-52b, Core 29-A, cross-polarized light.

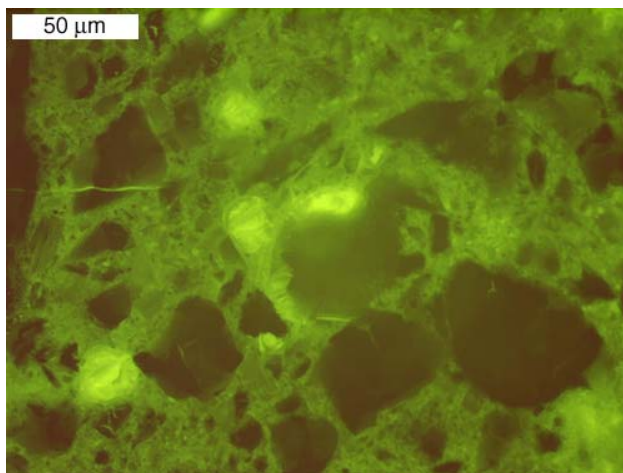


Figure D-53c. Close-up of area outlined in red in Figure D-52c, Core 29-A, epifluorescent mode.

Table D-8. Results of sulfate extractions.

MTU Core ID	Computed Wt% SO ₃	Extracted Wt% SO ₃
4-A	0.53	0.67
19-B	0.48	0.68
29-A	0.46	0.57

wt% SO₃ computed from mix design vs. wt% SO₃ from extraction

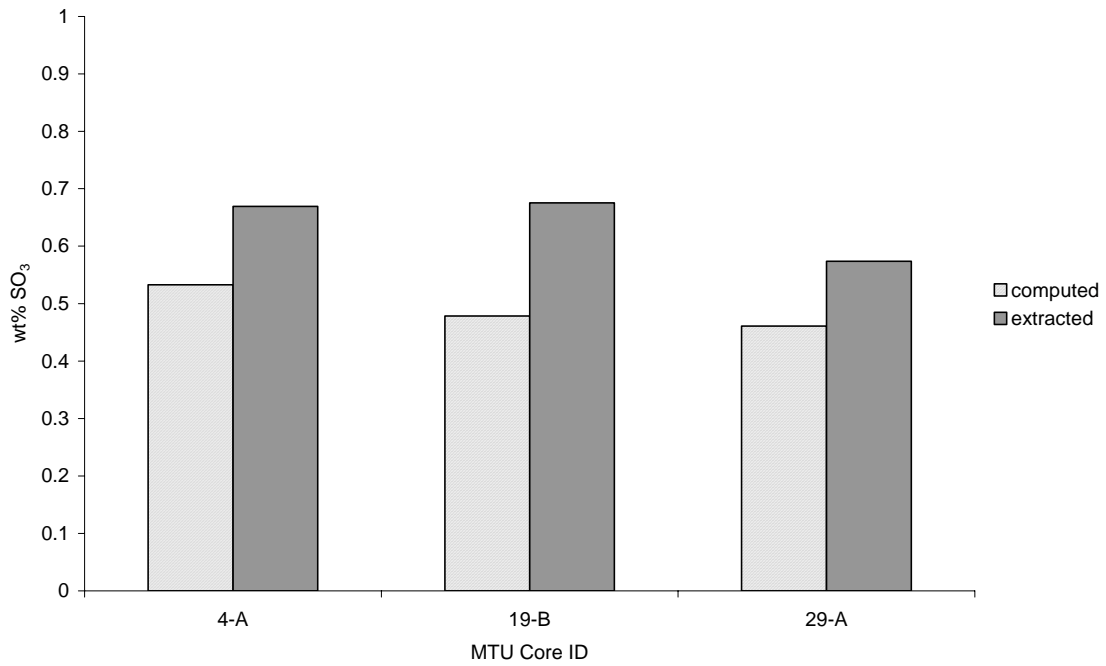


Figure D-54. Wt% SO₃ values from extraction compared to wt% SO₃ values computed from the mix design.

Table D-9. Results of alkali extractions.

MTU Core ID	Wt% Na	Wt% K	Na ₂ O Equivalent kg/m ³
4-A	0.054	0.025	2.05
19-B	0.032	0.044	1.87
29-A	0.030	0.038	1.62

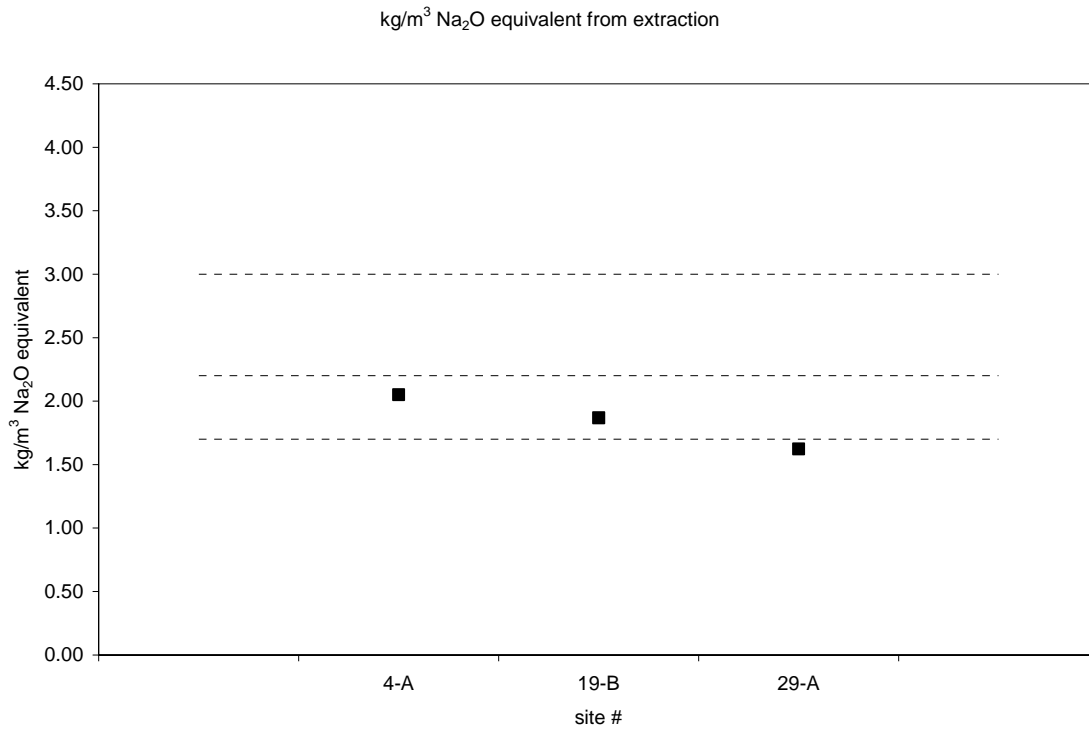


Figure D-55. Na₂O equivalent kg/m³ values from extraction compared to Na₂O equivalent kg/m₃ values computed from the mix design.

AIR VOID CHARACTERISTICS

Slabs from each pavement were polished and examined under a stereo OM in accordance with ASTM C457 Procedure B – Modified Point-Count Method. In addition to the standard procedure, the slabs were stained with a solution of potassium permanganate and barium chloride. The chemicals stain sulfate-bearing minerals, such as ettringite, pink. Over time, such minerals commonly occur as secondary growths in the entrained air voids. Often, entrained air voids in deteriorated concrete are completely filled with secondary ettringite. The stain assists in the identification of filled air voids that may otherwise be mistaken for hardened cement paste. In the equations used to determine the air-void system parameters, filled air voids that are identified as paste would be considered to offer no protection to freeze-thaw damage. It is controversial whether filled air voids can protect the paste against freeze-thaw damage, and thus, air-void system parameters are computed for both the concrete in its original state, and the concrete in its existing state.

Table D-10 shows the results of the Modified Point-Count for the three sites. Figure D-56 plots the spacing factors for each site, along with dotted lines to represent the suggested range according to ASTM C457. Figure D-57 plots the void frequency for each site, along with dotted lines to represent the suggested range according to ASTM C457. Figure D-58 compares the aggregate, cement paste and air volume percentages as determined by point count to the volume percentages computed from the mix design.

CONCLUSIONS

The cores received from Test Site Nos. 4, 19, and 29 were from distressed pavements made with iron blast furnace slag coarse aggregate. They were constructed between 1976 and 1992, and are located in the Southeastern part of the Lower Peninsula. One of the test sites (Test Site No. 4) was ultimately included in a special study, the report of which is presented in Appendix E. The results of the microstructural evaluation can be summarized as follows:

- In all three pavement sections, reactive chert particles that are a constituent in the fine aggregate were aggressively and deleteriously alkali-silica reactive, leading to the formation of significant reaction product and associated cracking in the hydrated cement paste. This was true even though the extracted alkali contents of the two of the three sections would indicate “moderate” protection against ASR. The third section (Test Site No. 29) had an even lower extracted alkali content that would offer “strong” protection against ASR, but it was built in 1976 which may indicate that ultimately the deleterious reaction with the chert will occur given enough time. Only one section had fly ash (Test Site No. 4) and this was a Class C fly ash.
- In all cases, the extracted sulfate contents were in excess of that predicted from the mixture design. In addition, the degree of crack and air void infilling with ettringite was high. It was also observed that in many cases the calcium sulfide dendrites located near the aggregate-hydrated cement paste interface were “empty”, indicating that potential dissolution of the calcium sulfide had occurred. This is one explanation

Table D-10. Results of ASTM C457 Modified Point Counts.

MTU Core ID	4-A	19-B	29-A
Raw Data			
area analyzed (cm ²)	94.9	69.4	100.2
air stops	117	133	150
paste stops	294	466	429
aggregate stops	921	747	841
secondary ettringite stops	18	10	5
total stops	1350	1356	1425
traverse length (mm)	4134	3542	4363
# of air void intercepts	1318	1066	1878
# of secondary ettringite filled intercepts	448	77	404
Results			
vol% aggregate	68.2	55.1	59.0
vol% air original	10.0	10.5	10.9
vol% air existing	8.7	9.8	10.5
vol% paste original	21.8	34.4	30.1
vol% paste existing	23.1	35.1	30.5
original void frequency (voids/m)	427	323	523
existing void frequency (voids/m)	319	301	430
original avg. chord length (mm)	0.234	0.327	0.208
existing avg. chord length (mm)	0.272	0.326	0.245
original specific surface (mm ⁻¹)	17.1	12.2	19.2
existing specific surface (mm ⁻¹)	14.7	12.3	16.4
original paste/air ratio	2.2	3.3	2.8
existing paste/air ratio	2.7	3.6	2.9
original spacing factor (mm)	0.127	0.266	0.144
existing spacing factor (mm)	0.181	0.292	0.177

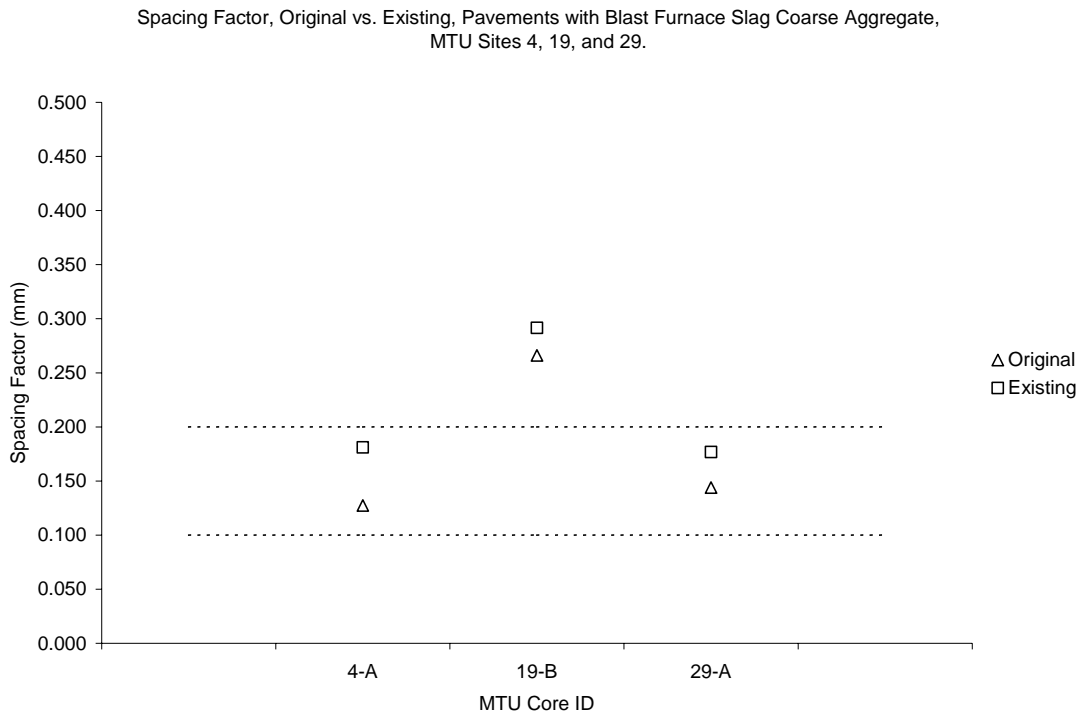


Figure D-56. Spacing factors plotted with dotted lines showing suggested values from ASTM C457.

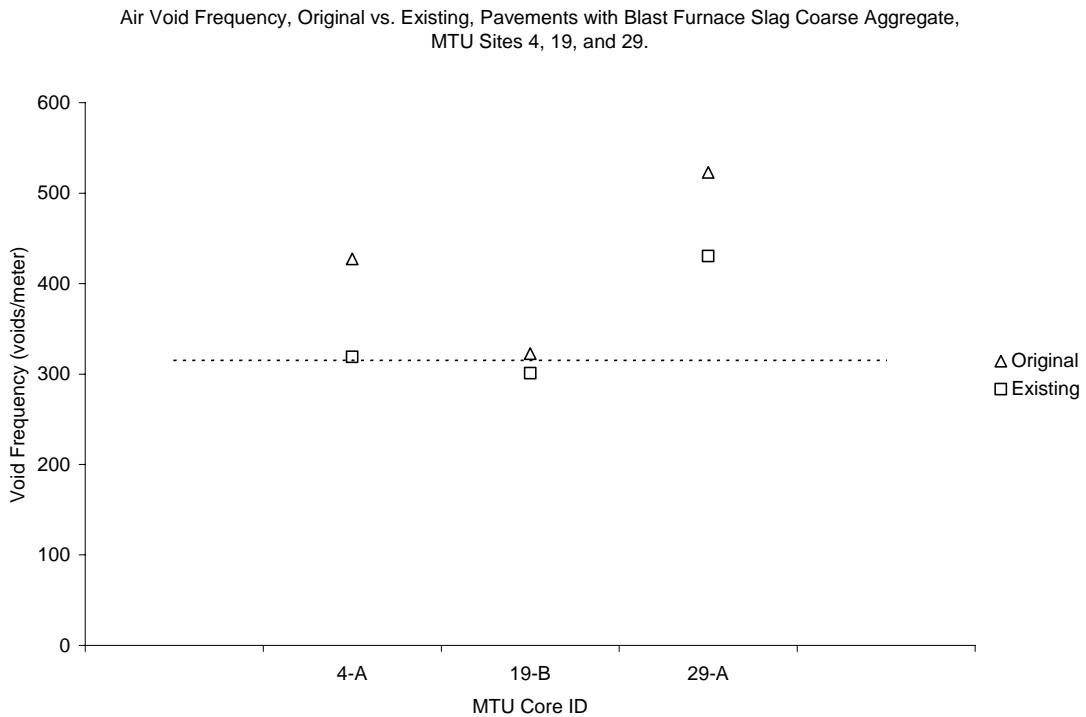


Figure D-57. Void frequencies plotted with dotted lines showing suggested values from ASTM C457.

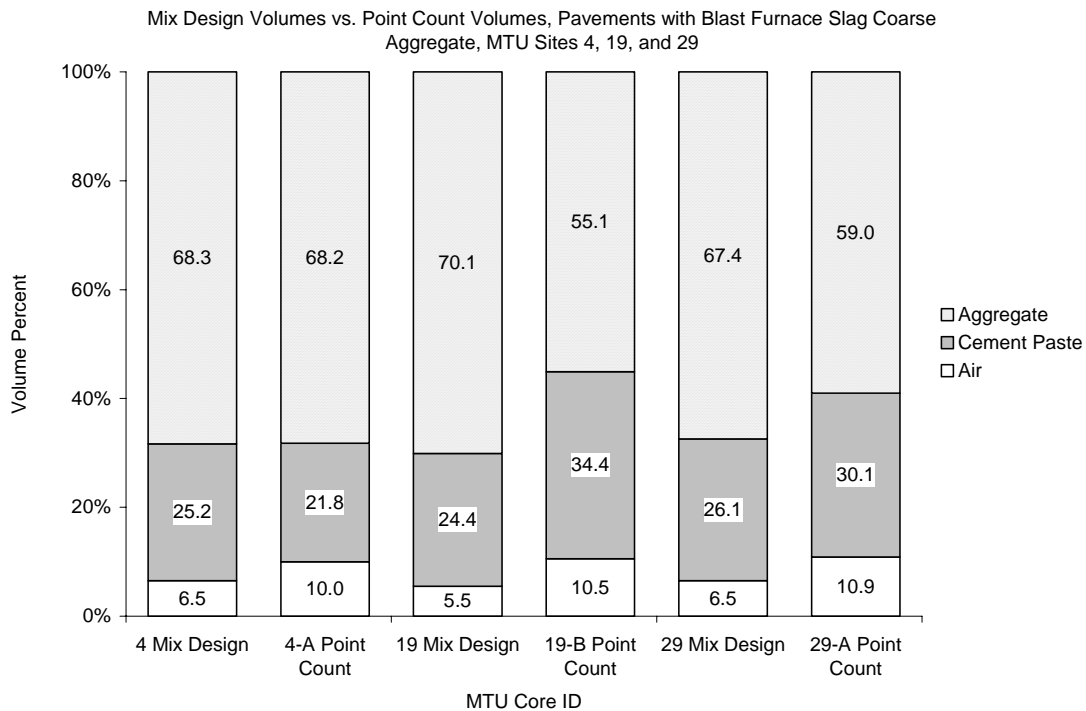


Figure D-58. Volume percentages from point counts compared to volume percentages computed from mix designs.

for the origination of the excess sulfates measured through extractions, although further work needs to be conducted to investigate this further.

- Often, in all three pavements, the cement paste in the immediate vicinity of slag coarse aggregate particles appears darker than the rest of the cement paste, primarily due to the presence of partially hydrated cement grains that are very abundant. In addition, calcium hydroxide crystals are also often found in the air voids near slag aggregate particles. Further, a green coloration is associated with the ferrite and aluminate phases of the cement grains near the interface. The implication of these findings is currently unknown, but without question some chemical interactions are occurring between the slag coarse aggregate and the hydrated cement paste/pore solution in the vicinity of the paste-aggregate interface.
- At all three test sites, the measured original air content was significantly higher than that specified (10 percent or greater). Even though, one test site (Test Site No. 19) had an original spacing factor that would provide only marginal protection against paste freeze-thaw damage. Further, the infilling with ettringite has significantly altered the measured air-void system parameters, potentially reducing paste freeze-thaw durability.

SITES 12, 22, AND 28, PAVEMENTS WITH NATURAL GRAVEL COARSE AGGREGATE

INTRODUCTION

The cores received from Test Site Nos. 12, 22, and 28 were from distressed pavements. Table D-11 summarizes the mix design information for the three sites. Figures D-59, D-60, and D-61 are provided to give a general overview of the different pavements. To investigate the sites, slabs were cut from the cores in a plane perpendicular to the pavement surface. The slabs were polished and used for chemical staining and stereo OM.

CHEMICAL STAINS

A solution of sodium cobaltinitrite was applied to the polished slab surfaces to stain potassium-bearing alkali-silica gels yellow. The slabs prepared from Test Site No. 22 were not significantly affected by the sodium cobaltinitrite stain. Chert particles, both in the fine and coarse aggregate fractions were stained yellow in slabs prepared from Test Site Nos. 12 and 28. Figure D-62 is an example of a yellow-stained chert particle. In general, cracking was not associated with the fine chert particles. However, cracking was sometimes associated with coarse chert particles. Figure D-63 shows an example of a yellow-stained chert coarse aggregate particle and related cracking. A solution of barium chloride and potassium permanganate was used to stain sulfate-bearing minerals pink. The sulfate stain assisted with the identification of entrained air voids filled with secondary ettringite deposits observed during the ASTM C457 Modified Point Count. Figure D-64 depicts some pink-stained secondary ettringite filled air voids.

MACRO-CRACKING

All of the sites contained large coarse aggregate particles (by today's standards) with an estimated top size estimated of least 38 mm (1.5 inches). Relatively porous carbonate aggregates of this size were frequently cracked. Figures D-65a and D-65b show cracking typical of the carbonate aggregates from Test Site No. 22. Figures D-66a and D-66b show an entire polished slab taken from the joint at Test Site No. 12. The core that provided the slab shown in Figures D-66a and D-66b was received in several pieces, and was epoxied together prior to slabbing. The length of the core shown in Figures D-66a and D-66b is not representative of the true pavement depth because the base of the pavement was so deteriorated that a complete intact core could not be retrieved. A large carbonate aggregate near the base of the slab is severely cracked.

AIR VOID CHARACTERISTICS

Slabs from each pavement were polished and examined under a stereo OM in accordance with ASTM C457 Procedure B – Modified Point-Count Method. In addition to the standard procedure, the slabs were stained with a solution of potassium permanganate and barium chloride. The chemicals stain sulfate-bearing minerals, such as ettringite,

Table D-11. Volume percentage values computed from mix designs.

Test Site No.	12	22	28
Year Constructed	1957	1957	1960
kg/m ³ Cement	300	301	231
kg/m ³ Fly Ash	0	0	0
kg/m ³ Water	155	162	108
kg/m ³ Coarse	1437	1260	998
kg/m ³ Fine	718	644	478
w/cm	0.52	0.54	0.47
Vol% cement paste	22.4	25.1	23.4
Vol% Coarse Agg.	47.4	45.5	47.7
Vol% Fine Agg.	24.7	23.4	23.0
Vol% Air	5.5	6.0	6.0
Coarse Agg. No.	34-36	49-44	67-02
Fine Agg. No.	34-36	49-44	67-02

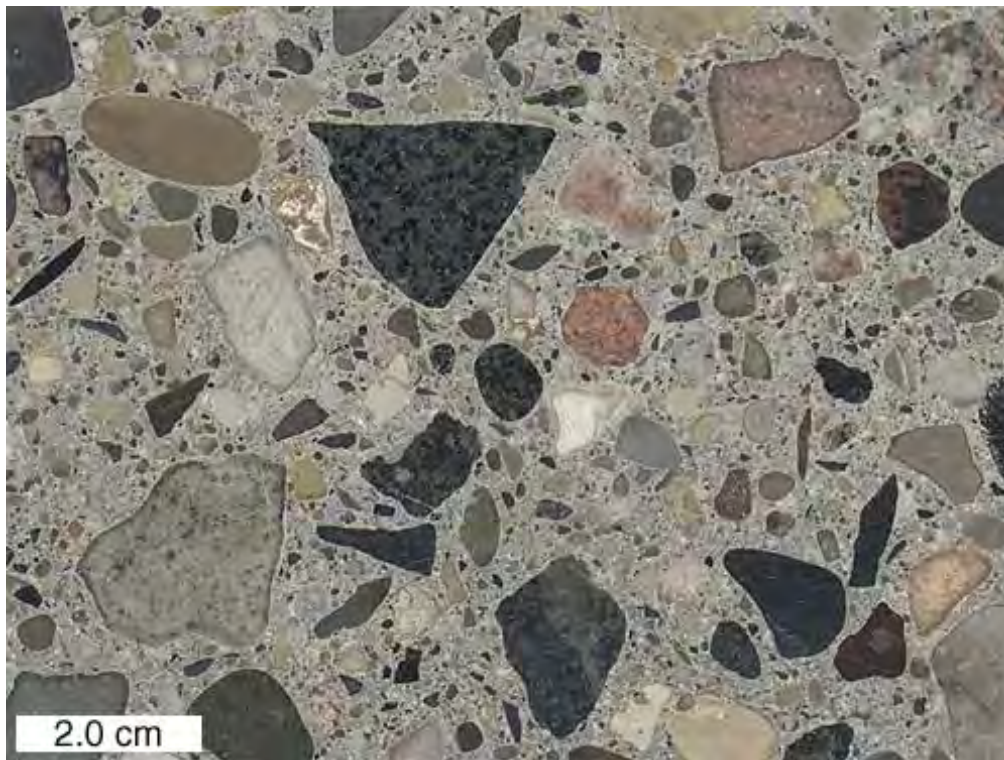


Figure D-59. View of polished slab from Core 12-C.



Figure D-60. View of polished slab from Core 22-C.

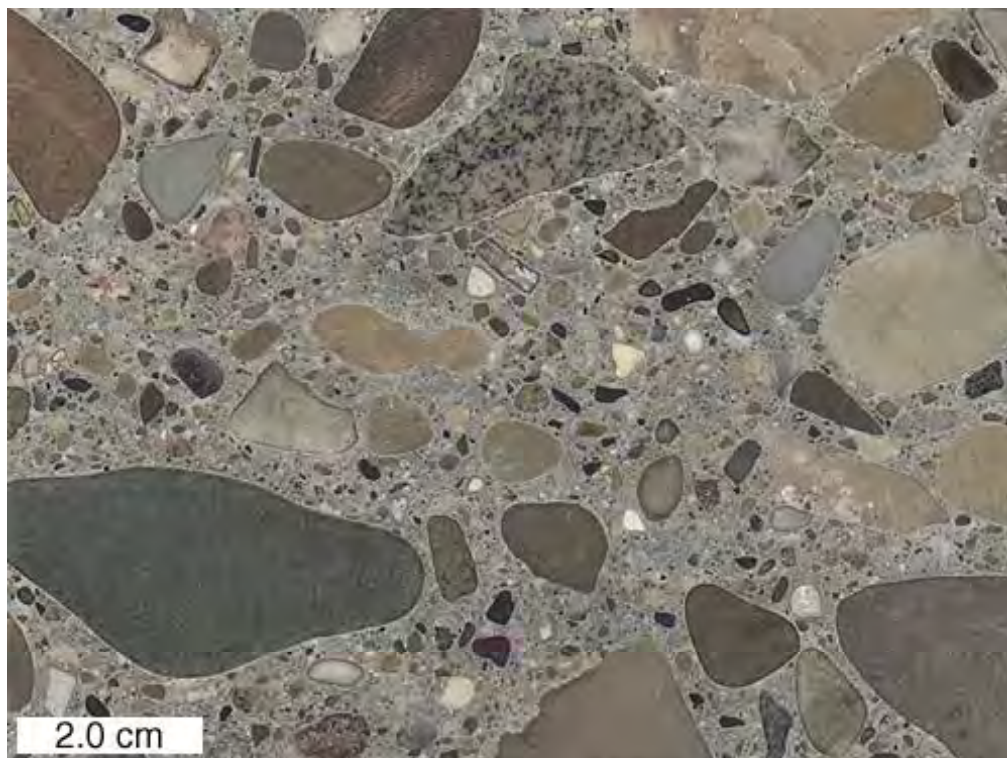


Figure D-61. View of polished slab from Core 28-B.

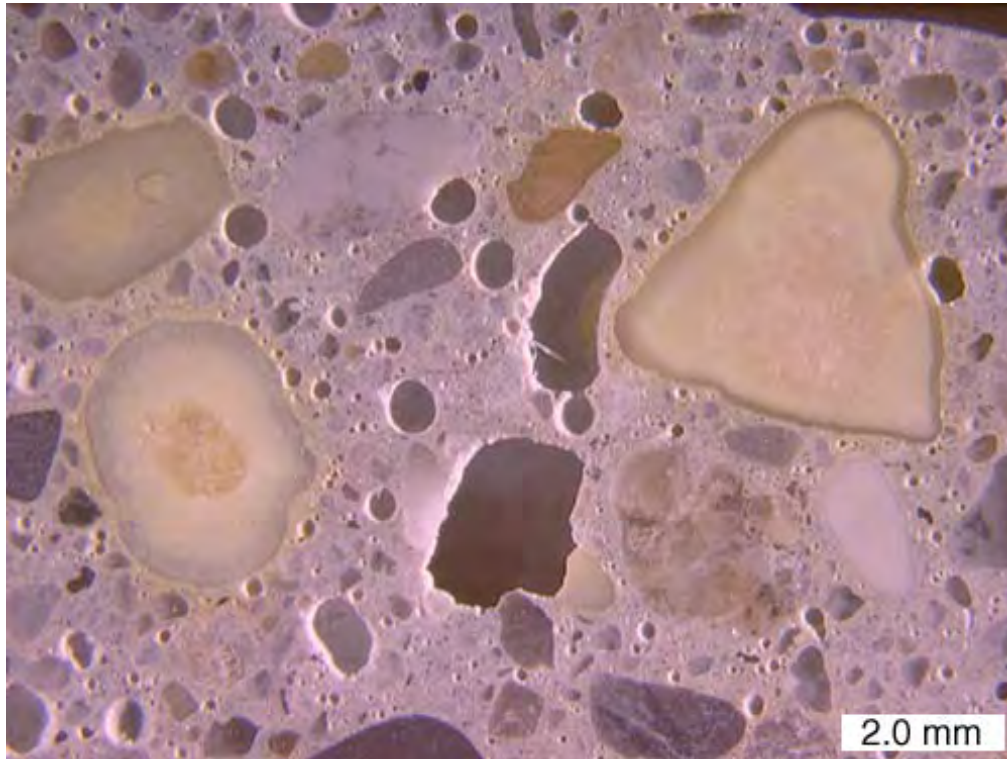


Figure D-62. Yellow stained chert fine aggregate particle, Core 28-B.

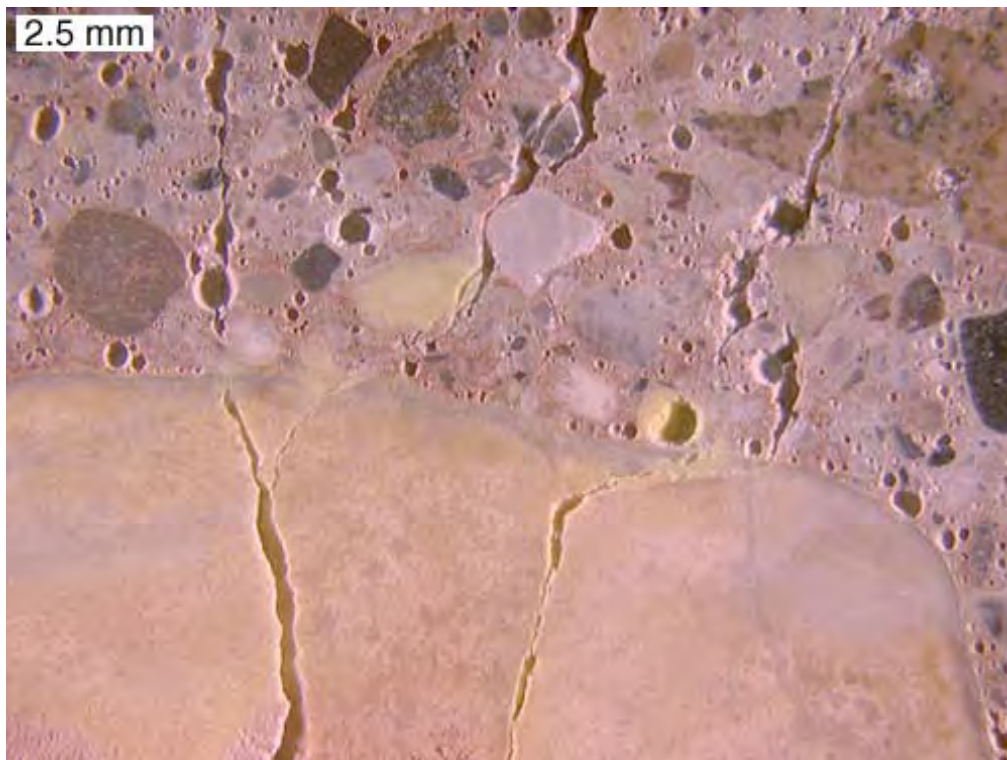


Figure D-63. Yellow stained chert coarse aggregate with cracks, core 12-C.

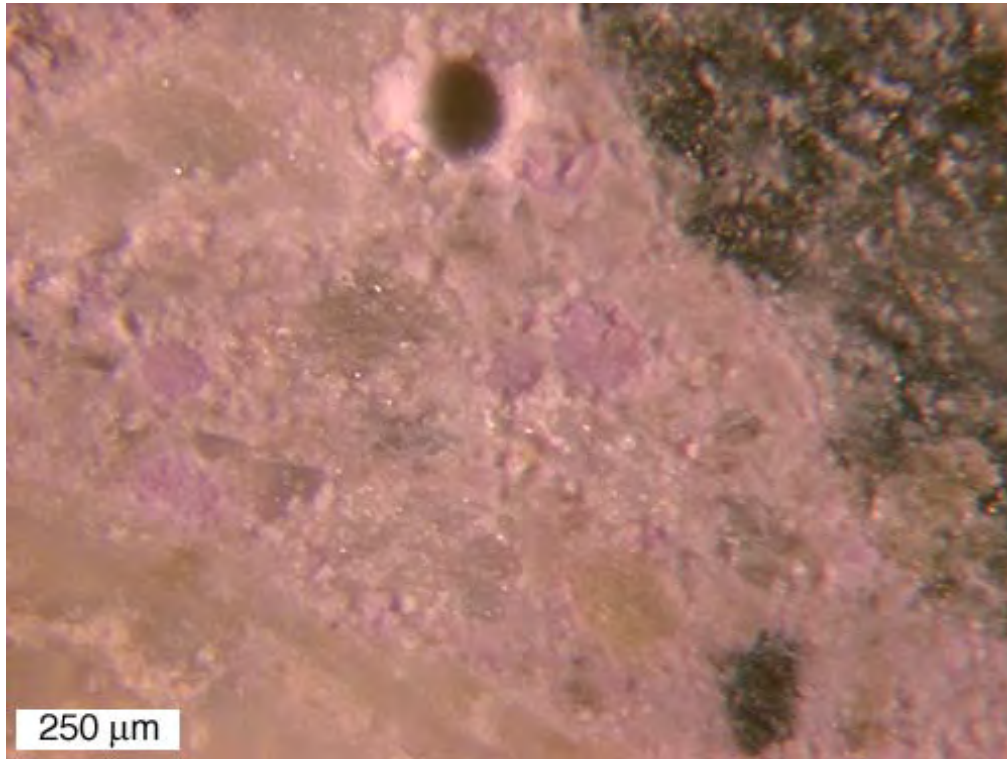


Figure D-64. Pink stained ettringite deposits in entrained air voids, Core 12-B.

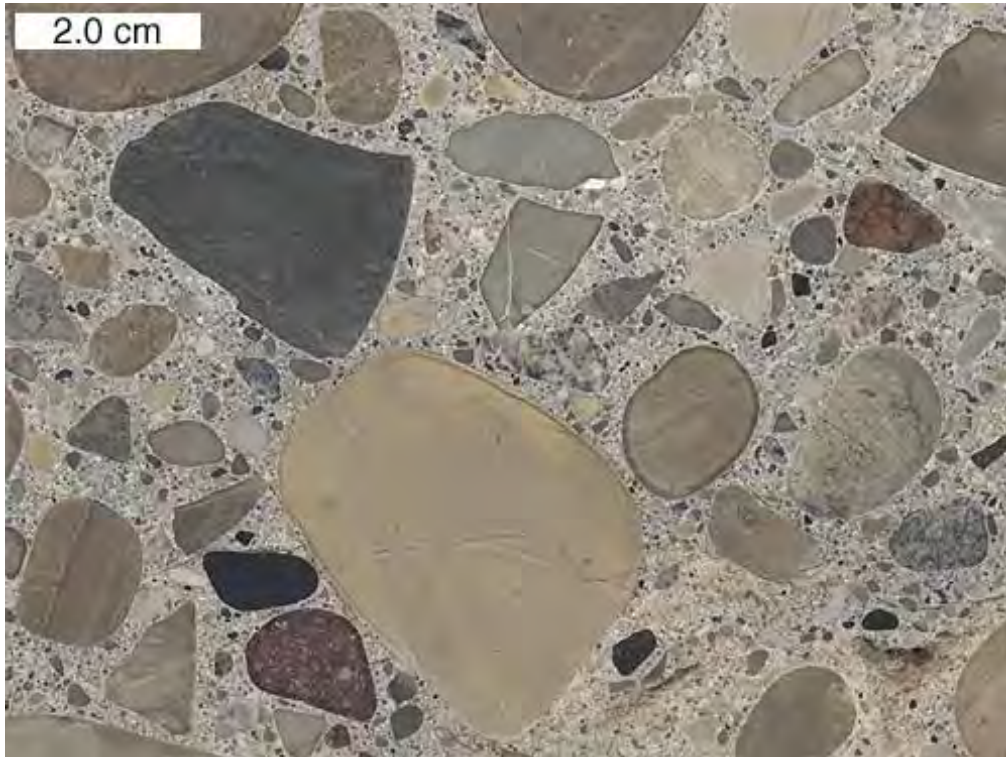


Figure D-65a. View of polished slab with cracked carbonate coarse aggregates, Core 22-B.

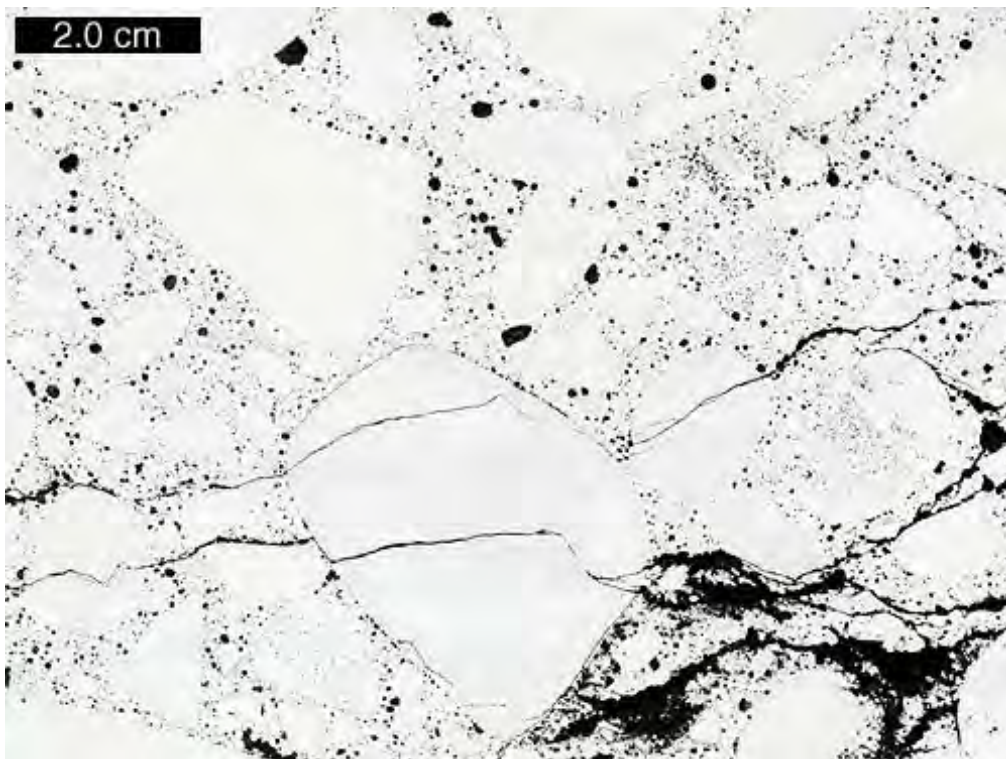


Figure D-65b. Negative image of area shown in Figure 7a after painting surface black and pressing with white powder to enhance cracks, Core 22-B.

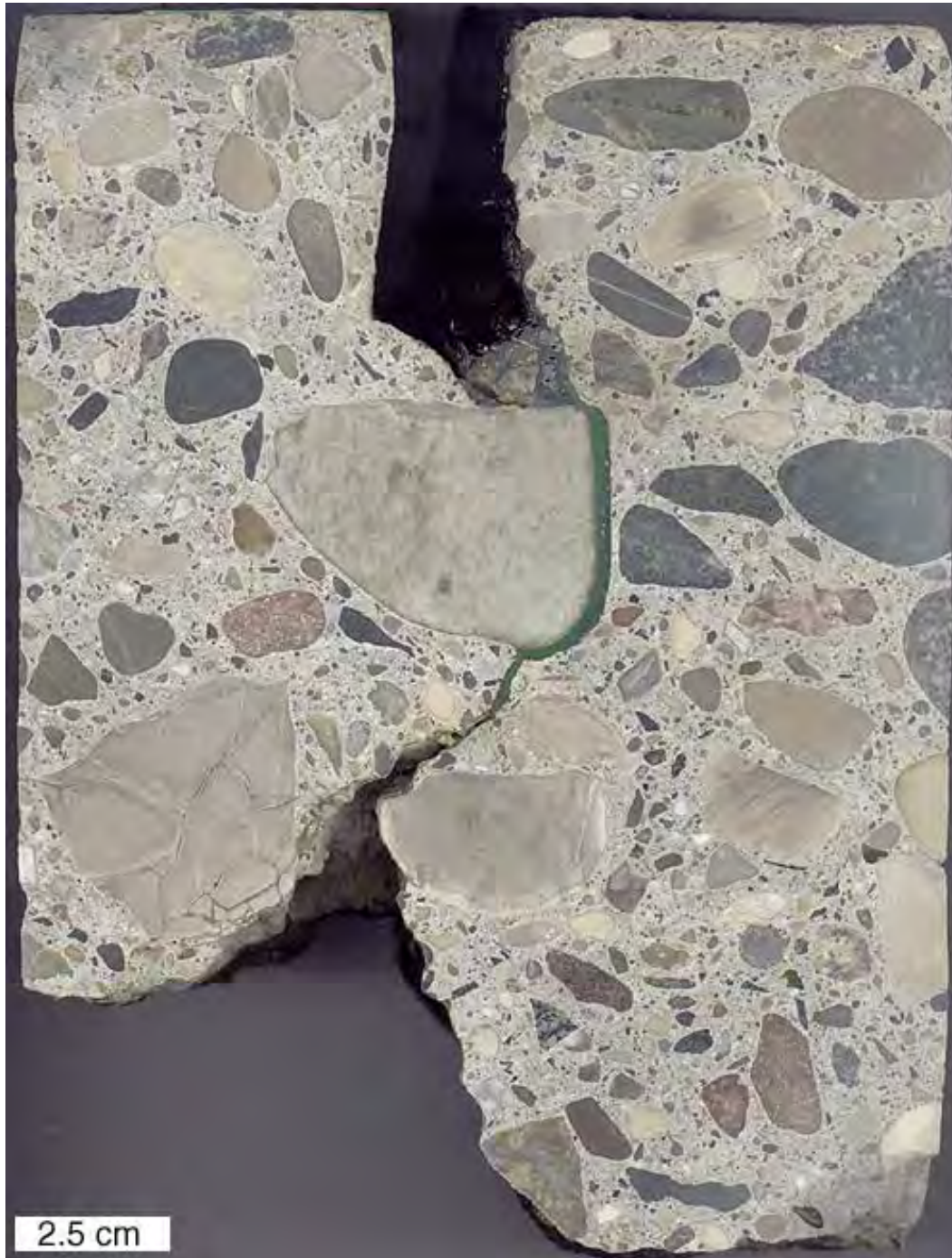


Figure D-66a. View of polished slab with cracked carbonate coarse aggregates, Core 12-B.



Figure D-66b. Negative image of area shown in Figure 8a after painting surface black and pressing with white powder to enhance cracks, Core 12-B.

pink. Over time, such minerals commonly occur as secondary growths in the entrained air voids. Often, entrained air voids in deteriorated concrete are completely filled with secondary ettringite. The stain assists in the identification of filled air voids that may otherwise be mistaken for hardened cement paste. In the equations used to determine the air-void system parameters, filled air voids that are identified as paste would be considered to offer no protection to freeze-thaw damage. It is controversial whether filled air voids can protect the paste against freeze-thaw damage, and thus, air-void system parameters are computed for both the concrete in its original state, and the concrete in its existing state. Table D-12 shows the results of the Modified Point-Count for the five sites. Figure D-67 plots the spacing factors for each site, along with dotted lines to represent the suggested range according to ASTM C457. Figure D-68 plots the void frequency for each site, along with dotted lines to represent the suggested range according to ASTM C457. Figure D-69 compares the aggregate, cement paste and air volume percentages as determined by point count to the volume percentages computed from the mix design.

CONCLUSIONS

Test Site Nos. 12, 22, and 28 were from distressed pavements made with natural gravel coarse aggregate. Two of these test sites were built in 1957, and the third in 1960, so they are over 40 years old, and were still in service at the time of inspection. It seems likely that these pavements would have continued in service for many more years if it were not for the MRD. In general, compared to the typical concrete mixture used today, the concrete mixtures have a low cement content and large maximum aggregate size. The results of the microstructural evaluation can be summarized as follows:

- Unlike the concrete in the test sites containing slag coarse aggregate, the fine aggregate chert constituents, although showing signs of reactivity, have not reacted in a deleterious fashion. There is no cracking associated with these fine chert particles.
- On the other hand, coarse aggregate chert particles present in the natural gravel used in Test Site Nos. 12 and 28 do show signs of being deleteriously reactive, being linked both to alkali-silica reaction product and cracking. These same aggregates have properties that would make them potentially susceptible to aggregate freeze-thaw deterioration.
- The large coarse aggregate carbonates particles are porous and show significant cracking in the vicinity of joints. These are classic “D-crackers”, having all the diagnostic features of suffering aggregate freeze-thaw deterioration.

Table D-12. Results of ASTM C457 Modified Point Counts.

MTU Core ID	12-B	22-D	28-C
Raw Data			
area analyzed (cm ²)	90.5	156.9	152.6
air stops	136	98	139
paste stops	471	302	239
aggregate stops	1156	1154	1128
secondary ettringite stops	5	10	15
total stops	1768	1564	1521
traverse length (mm)	4618	5720	5564
# of air void intercepts	1752	1278	1819
# of secondary ettringite filled intercepts	113	92	14
Results			
vol% aggregate	65.4	73.8	74.2
vol% air original	8.0	6.9	10.1
vol% air existing	7.7	6.3	9.1
vol% paste original	26.6	19.3	15.7
vol% paste existing	26.9	19.9	16.7
original void frequency (voids/m)	404	240	329
existing void frequency (voids/m)	379	223	327
original avg. chord length (mm)	0.197	0.288	0.307
existing avg. chord length (mm)	0.203	0.280	0.280
original specific surface (mm ⁻¹)	20.3	13.9	13.0
existing specific surface (mm ⁻¹)	19.7	14.3	14.3
original paste/air ratio	3.3	2.8	1.6
existing paste/air ratio	3.5	3.2	1.8
original spacing factor (mm)	0.165	0.202	0.119
existing spacing factor (mm)	0.177	0.223	0.128

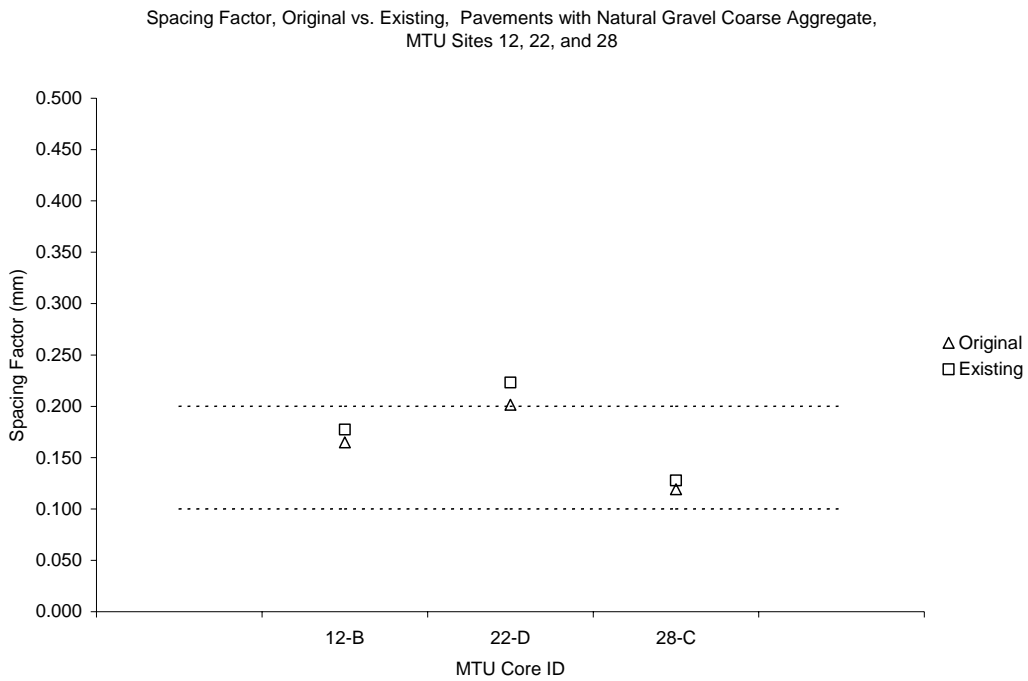


Figure D-67. Spacing factors plotted with dotted lines showing suggested values from ASTM C457.

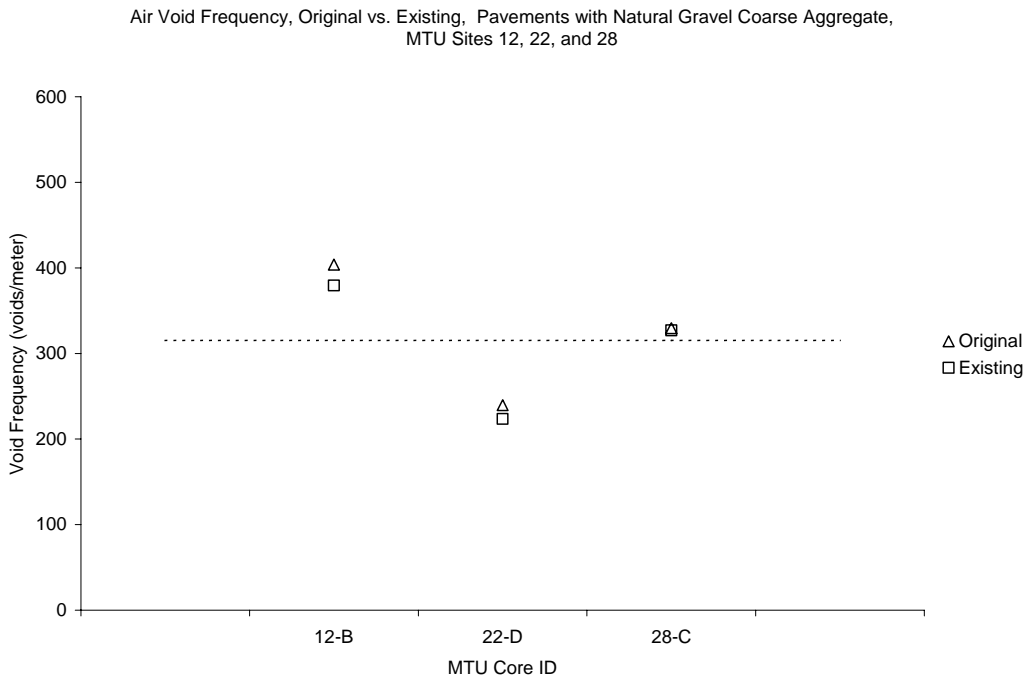


Figure D-68. Void frequencies plotted with dotted lines showing suggested values from ASTM C457.

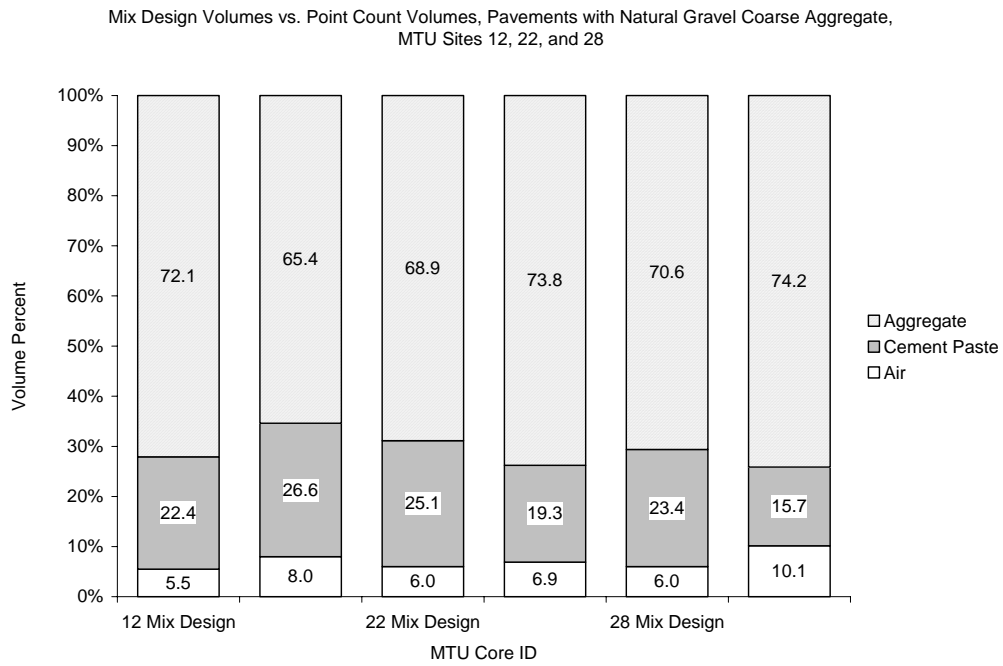


Figure D-69. Volume percentages from point counts compared to volume percentages computed from mix designs.

Appendix E

SPECIAL CASE STUDY FOR THE ASSESSMENT OF THE CAUSE OF DETERIORATION ON US-23 SOUTH OF FLINT, MICHIGAN

**Submitted to the Michigan Department of Transportation
by the Michigan Tech Transportation Institute
Michigan Tech Civil & Environmental Engineering Department**

Investigators:

**Karl R. Peterson, Research Scientist
Dr. Thomas Van Dam, P.E., Associate Professor
Dr. Lawrence L. Sutter, Assistant Professor**

June 30, 2002

Table of Contents

Introduction	3
Project Description	3
Experimental Methods	7
Air-Void System Parameters	7
Staining for Alkali Silica Reaction	11
Petrographic Examination	14
Sodium and Potassium Determination	14
Sulfate Determination	27
Discussion	30
Alkali-Silica Reactivity.....	31
Dissolution of Calcium Sulfide.....	32
Other Factors.....	34
Conclusions	35

Introduction

Sections of US-23 (referred to in this report as US-23N [CS 25031-30798A]) south of Flint are suffering extensive cracking and joint deterioration in spite of the fact that they were constructed only 10 years ago in 1992. Figures 1 through 4 show typically observed distress manifestations. An adjacent section constructed the following year (referred to as US-23S [CS 25031-31018A]) using comparable design features and materials remains in good condition with little sign of visual distress. In the spring of 2001, the Michigan Department of Transportation (MDOT) sent Michigan Tech a total of 18 cores taken from the pavement for analysis. The cores were representative of four of the mix designs used on US-23N, and two of the mix designs used on US-23S. In order to assess the discrepancy in performance between the US-23N and US-23S sections, a testing regime was developed to investigate several hypotheses that might explain the observed deterioration. Cores from four other pavements with mix designs similar to the pavement south of Flint were also included in this evaluation.

Project Description

The pavement section under study, US-23 south of Flint (CS 25031) is a jointed reinforced concrete pavement (JRCP) with 27 foot transverse joint spacing. The lane widths are 12 foot and are tied to a concrete shoulder. All transverse joints are doweled and longitudinal joints are tied. The slab is 10 inches thick, on a 4-inch thick asphalt treated open graded drainage course (5G crushed concrete) with a 3-inch thick aggregate separator course (22A crushed concrete). The 10-inch thick sand subbase is from the original construction. Underdrains were added in the most recent construction phase.

Table 1 contains information about the locations and conditions of all the pavements sampled. It is noted that cores 19b (CS 50011) and 29a (CS 82291), although from pavements in distressed condition, are older than those from the US-23 (CS 25031) sites. Table 2 contains information about the mix designs from the pavements sampled. Table 3 contains information about the sources of the materials used in the pavements sampled. Appendix A contains specific information regarding the core locations and mix designs for the US-23N and US-23S sections as provided to Michigan Tech by MDOT.



Figure 1. Spall at transverse joint (note paste disintegration).



Figure 2. Cracking running perpendicular to transverse joint.



Figure 3. Complete disintegration of shoulder at transverse joint.



Figure 4. Transverse joint deterioration and map cracking.

Table 1: Location and condition of pavements sampled.

Core ID	Yr. Const.	Route	CS	BMP	EMP	Job #	Direction	Condition
19b	1988/89	M-53	50011	4.8	8.4	25647A	NB	distressed
29a	1976	I-275	82291	2.9	6.0	09902A	NB – exit 11a	distressed
15	1992	US-23	25031	5.9	12.3	30798A	NB	distressed
22	1992	US-23	25031	5.9	12.3	30798A	NB	distressed
32	1992	US-23	25031	5.9	12.3	30798A	NB	distressed
38	1992	US-23	25031	5.9	12.3	30798A	NB	distressed
4a	1992	US-23	25031	5.9	12.3	30798A	SB	distressed
1	1993	US-23	25031	0.0	5.9	31018A	NB	fair
9	1993	US-23	25031	0.0	5.9	31018A	NB	fair
1a	1992	US-23	58034	0.0	6.0	32750A	SB – sec “B”	fair

Table 2: Mix designs from pavements sampled.

Core ID	Cement (kg/m ³)	Water (kg/m ³)	Coarse Agg. (kg/m ³)	Fine Agg. (kg/m ³)	Fly Ash (kg/m ³)	"Sacks Cement"	% Fly Ash
19b	328.0	147.0	1273.5	649.0	0.0	5.9	0
29a	306.0	175.0	846.8	996.2	0.0	5.5	0
15	501.9	166.1	905.9	653.2	0.0	9.0	0
22	284.8	154.3	830.0	920.2	42.7	5.9	13
32	312.1	154.8	830.0	939.8	0.0	5.6	0
38	251.0	120.4	885.8	789.7	83.7	6.0	25
4a	284.8	154.3	859.1	970.6	42.7	5.9	13
1	267.6	169.1	876.3	775.4	67.0	6.0	20
9	390.4	195.8	841.9	755.8	0.0	7.0	0
1a	285.0	162.0	830.0	918.0	43.0	5.9	13

Table 3: Material source information.

Core ID	Cement Source	Fly Ash Source	Coarse Aggregate Type	Inventory Source	Fine Aggregate Type	Inventory Source
19b	no data	no fly ash	slag	no data	natural sand	no data
29a	no data	no fly ash	slag	no data	natural sand	81-57
15	Type I Medusa	no fly ash	slag	82-19	natural sand	63-54
22	Type I Medusa	Detroit Edison Class C	slag	82-19	natural sand	63-54
32	Type I Medusa	no fly ash	slag	82-19	natural sand	63-54
38	Type I Medusa	Detroit Edison Class C	slag	82-19	natural sand	63-54
4a	Type I Medusa	Detroit Edison Class C	slag	82-19	natural sand	63-54
1	Type I St. Mary	US Ash Class F	slag	82-19	natural sand	63-54
9	Type I St. Mary	no fly ash	slag	82-19	natural sand	63-54
1a	Type I/ Medusa	Avon Lake Class F	slag	82-22	natural sand	30-35

In table 1, each pavement was classified as being either in “distressed” condition or “fair” condition. This condition rating is based on observed pavement distress, with distressed sections characterized by spalling, cracking, staining/exudate, or disintegration that is characteristic of MRD. Pavements considered in fair condition have no observed distress consistent with MRD.

Experimental Methods

One core, taken near a transverse pavement joint, was selected from each site. This core was cut in half in a plane parallel to the pavement surface, and the two halves were subsequently cut into slabs in a plane perpendicular to the pavement surface. The following tests were performed on these slabs:

- ASTM C457 Standard Test Method for Microscopical Determination of Parameters of the Air-Void System in Hardened Concrete.
- Chemical staining to detect the presence of secondary sulfate minerals in the entrained air voids.
- Chemical staining to detect alkali-silica reaction (ASR) product.
- Petrographic analysis of thin sections to observe the concrete microstructure.
- Chemical extraction to determine the levels of exchangeable and soluble potassium and sodium.
- Chemical extraction to determine the sulfate levels.

Air-Void System Parameters

One slab from the bottom half of each core was polished and examined under a stereo microscope in accordance with ASTM C457 Procedure B – Modified Point-Count Method. In addition to the standard procedure, the slabs were stained with a solution of potassium permanganate and barium chloride. The chemicals stain sulfate-bearing minerals, such as ettringite, pink. Over time, such minerals commonly occur as secondary growths in the entrained air voids. Often, entrained air voids in deteriorated concrete are completely filled with secondary ettringite. The stain assists in the identification of filled air voids that may otherwise be mistaken for hardened cement paste. In the equations used to determine the air-void system parameters, filled air voids that are identified as paste would be considered to offer no protection to freeze-thaw damage. It is controversial whether filled air voids can protect the paste against freeze-thaw damage, and thus, air-void system parameters are computed for both the concrete in its original state, and the concrete in its existing state.

Tables 4a and 4b summarize the results of the air-void system analysis. Figure 5 shows a chart comparing the spacing factor for the concrete in its original state and the spacing factor in its existing state. A spacing factor in the range of 0.1 to 0.2 mm is considered adequate to provide

freeze-thaw durability. For all cores, the spacing factor increases from the original state to the existing state due to the infilling of many of the air voids by secondary ettringite. Figure 6 consists of a chart comparing the void frequency for the concrete in its original state and in its existing state. For all of the cores, the number of air voids intercepted per unit length of linear traverse decreases from the original state to the existing state. The decrease is due to the complete infilling of many of the air voids by secondary ettringite. Generally, a value of greater than 315 voids intercepted per meter of linear traverse is considered likely to provide good freeze-thaw durability. Figure 7 depicts a typical scene encountered by an operator of an air-void analysis, where many of the smaller air voids are completely filled by ettringite.

Table 4a: Results of ASTM C457 Procedure B – Modified Point-Count Method.

Raw Data	19b	29a	4a	15	22
area analyzed (cm ²)	69.4	100.2	94.9	94.9	69.8
air void stops	133	150	117	117	102
cement paste stops	466	429	294	470	403
coarse aggr. stops	471	449	560	404	474
fine aggr. stops	276	392	361	299	371
ettringite stops	10	5	18	60	15
total stops	1356	1425	1350	1350	1365
traverse length (mm)	3541.9	4363.4	4133.7	4133.7	3565.4
air void intercepts	1066	1878	1318	1751	890
filled air void intercepts	77	404	448	424	465
Results					
vol % coarse aggr.	34.7	31.5	41.5	29.9	34.7
vol % fine aggr.	20.4	27.5	26.7	22.1	27.2
original vol % air voids	10.5	10.9	10.0	13.1	8.6
existing vol % air voids	9.8	10.5	8.7	8.7	7.5
original vol % cement paste	34.4	30.1	21.8	34.8	29.5
existing vol % cement paste	35.1	30.5	23.1	39.3	30.6
original void frequency (voids/m)	323	523	427	526	380
existing void frequency (voids/m)	301	430	319	424	250
original avg. chord length (mm)	0.327	0.208	0.234	0.249	0.226
existing avg. chord length (mm)	0.326	0.245	0.272	0.205	0.299
original air void specific surface (mm ⁻¹)	12.2	19.2	17.1	16.1	17.7
existing air void specific surface (mm ⁻¹)	12.3	16.4	14.7	19.6	13.4
original paste/air ratio	3.3	2.8	2.2	2.7	3.4
existing paste/air ratio	3.6	2.9	2.7	4.5	4.1
original spacing factor (mm)	0.266	0.144	0.127	0.165	0.194
existing spacing factor (mm)	0.292	0.177	0.181	0.226	0.307

Table 4b: Results of ASTM C457 Procedure B – Modified Point-Count Method.

Raw Data	32	38	1	9	1A
area analyzed (cm ²)	94.9	94.9	70.0	72.9	94.9
air void stops	120	126	100	150	116
cement paste stops	365	358	300	429	304
coarse aggr. stops	485	437	571	449	534
fine aggr. stops	380	415	396	392	387
ettringite stops	0	14	1	5	9
total stops	1350	1350	1368	1425	1350
traverse length (mm)	4133.7	4133.7	3573.2	3722.1	4133.7
air void intercepts	1466	1765	824	1878	1275
filled air void intercepts	290	331	137	404	170
Results					
vol % coarse aggr.	35.9	32.4	41.7	31.5	39.6
vol % fine aggr.	28.1	30.7	28.9	27.5	28.7
original vol % air voids	8.9	10.4	7.4	10.9	9.3
existing vol % air voids	8.9	9.3	7.3	10.5	8.6
original vol % cement paste	27.0	26.5	21.9	30.1	22.5
existing vol % cement paste	27.0	27.6	22.0	30.5	23.2
original void frequency (voids/m)	425	507	269	613	350
existing void frequency (voids/m)	355	427	231	505	308
original avg. chord length (mm)	0.209	0.205	0.275	0.177	0.265
existing avg. chord length (mm)	0.251	0.219	0.317	0.209	0.279
original air void specific surface (mm ⁻¹)	19.1	19.6	14.6	22.5	15.1
existing air void specific surface (mm ⁻¹)	16.0	18.3	12.6	19.2	14.4
original paste/air ratio	3.0	2.6	3.0	2.8	2.4
existing paste/air ratio	3.0	3.0	3.0	2.9	2.7
original spacing factor (mm)	0.159	0.131	0.204	0.123	0.161
existing spacing factor (mm)	0.191	0.161	0.239	0.151	0.188

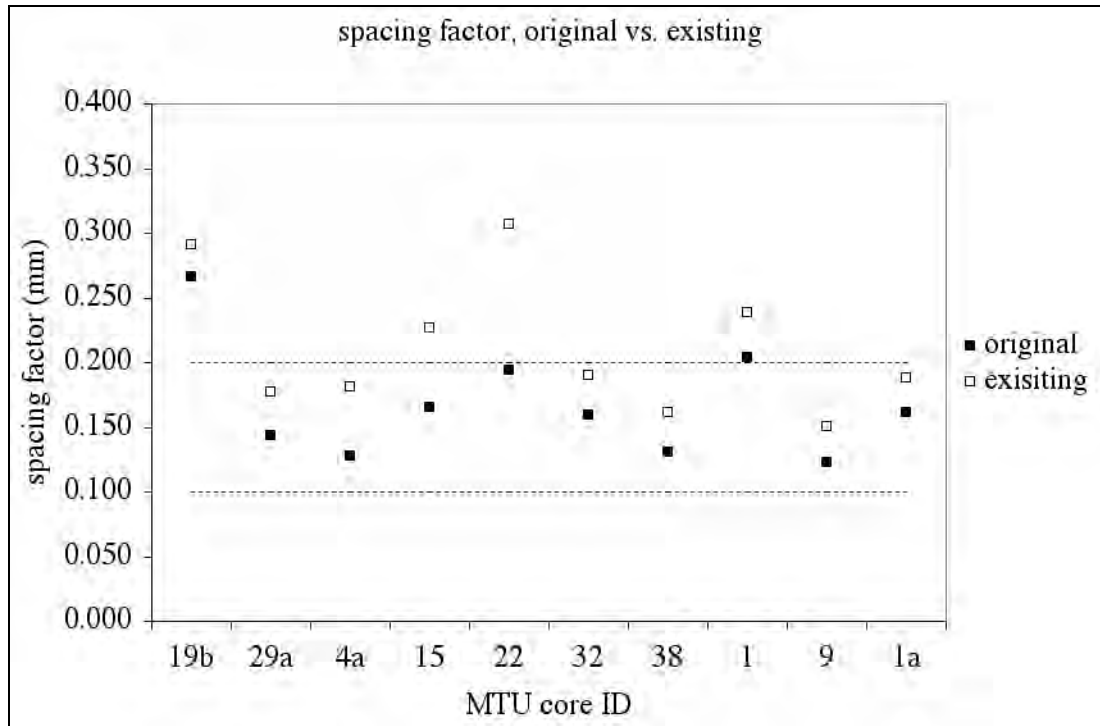


Figure 5: Chart depicting increase in spacing factor due to infilling of air voids by secondary ettringite. Dashed lines represent accepted range for freeze-thaw durability.

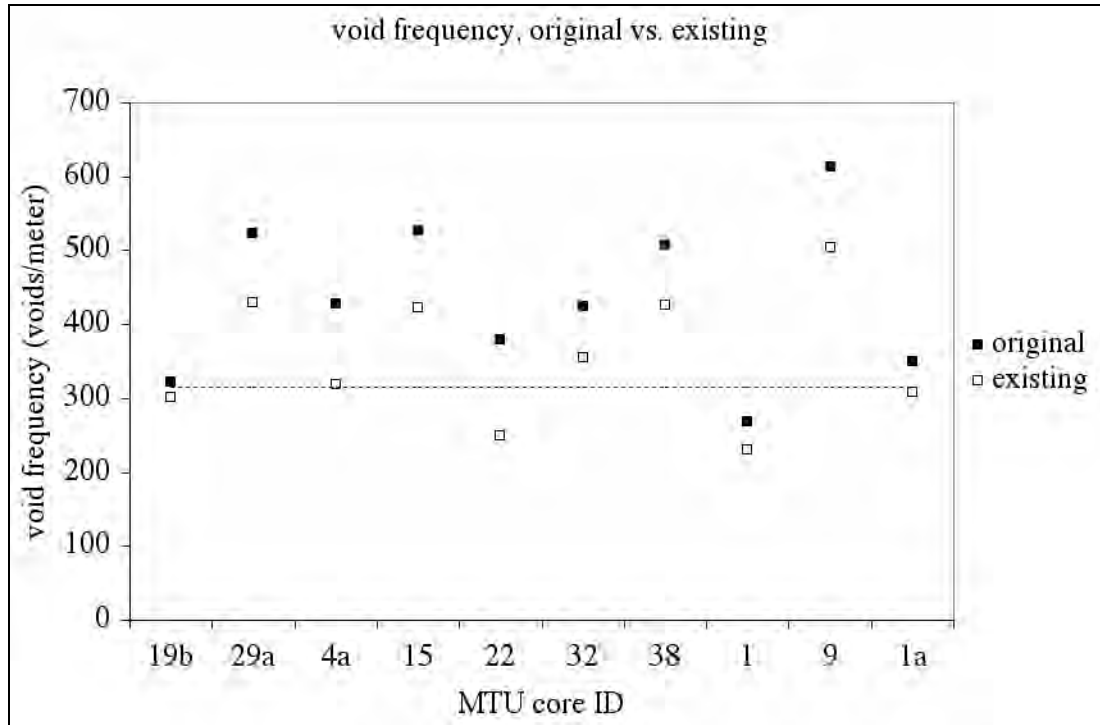


Figure 6: Chart depicting decrease in the number air voids intercepted per meter of linear traverse due to infilling of air voids by secondary ettringite. Values above dashed line are considered likely to ensure good freeze-thaw durability.

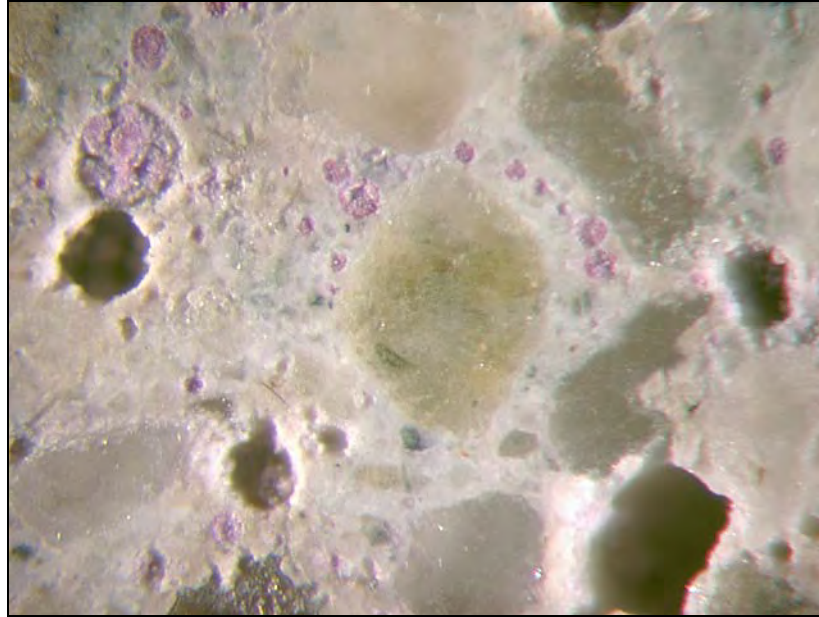


Figure 7: Microscope image of polished slab surface from core 29a (CS 82291) stained for sulfate minerals. Ettringite filled air voids are stained pink, magnified 83x.

Staining for Alkali Silica Reaction

One slab representing the top half of each core was polished and stained with a solution of sodium cobaltinitrite. The stain turns potassium bearing alkali silica gel yellow. In all the samples evaluated, some chert particles in the fine aggregate were stained yellow. Uniquely, in the pavements classified to be in distressed condition, the stained chert particles were also consistently cracked, often with cracks extending into the cement paste and interconnecting with other cracked chert particles. This was in contrast to the pavements classified to be in good condition, where the chert particles were stained yellow, but rarely exhibited any cracking. Figures 8a and 8b show a cracked chert particle typical of the pavements in distressed condition. Figures 9a and 9b show a chert particle that has picked up the yellow stain, but does not show cracking, typical of the pavements in good condition. It is extremely rare to find chert particles showing cracking in the fair sections versus almost universal cracking, with associated copious quantities of ASR reaction product, observed in the chert particles from cores obtained from the distressed sections. Although the difference between the distressed and fair sections is striking, it is noted that the “fair” sections are relatively young in age being constructed in 1993 and it is possible that deterioration may occur as they age.

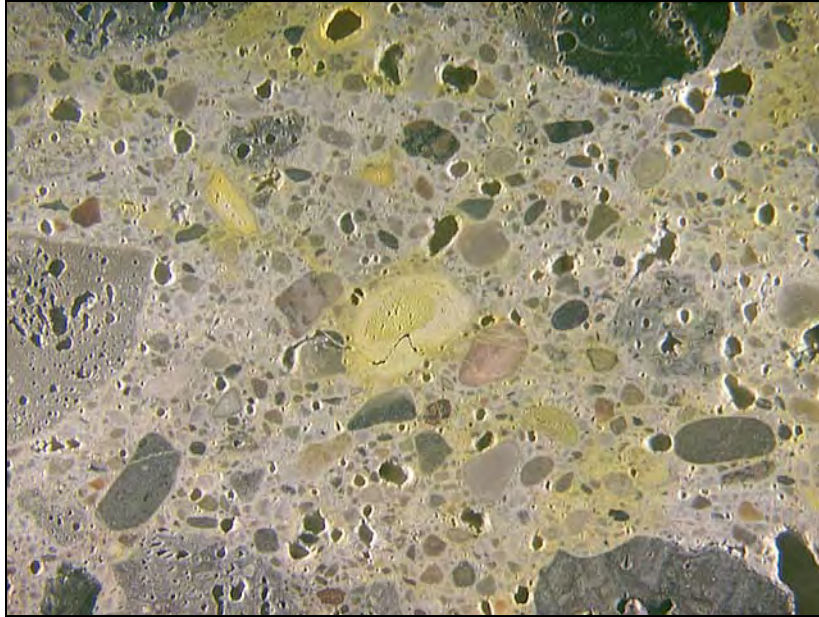


Figure 8a: Close-up of a polished and stained surface from core 22 (CS 25031-30798A). Alkali-silica reactive stained particles appear yellow and exhibit cracking, magnified 6x.

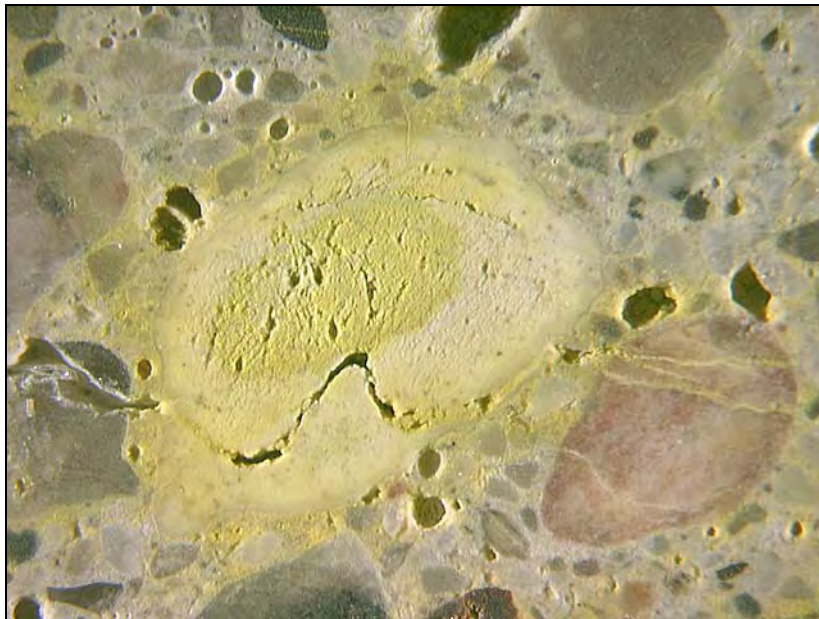


Figure 8b: A close-up of Figure 8a, showing cracked reactive chert particle, with cracks propagating through neighboring non-chert sand particles, magnified 15x.

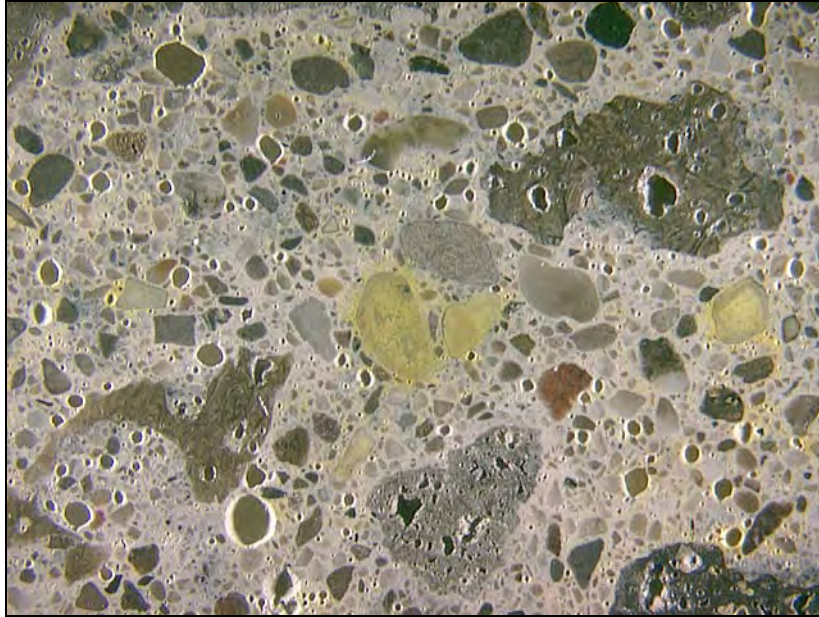


Figure 9a: Close-up of a polished and stained surface from core 9 (CS 25031-31018A). Alkali-silica reactive stained particles appear yellow but do not exhibit cracking, magnified 6x.

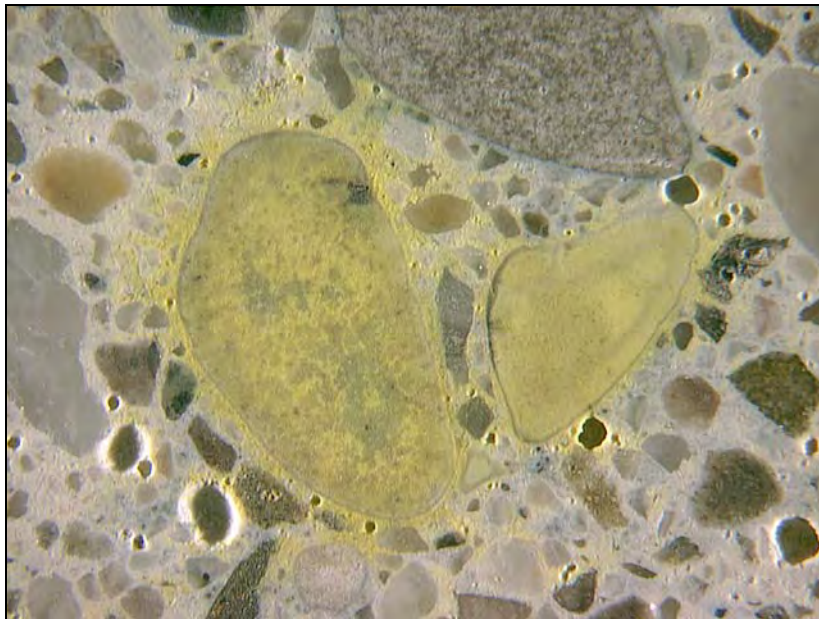


Figure 9b: A close-up of Figure 9a, showing yellow stained reactive chert particle, and the absence of any related cracking, magnified 15x.

Petrographic Examination

Fluorescent epoxy impregnated thin sections were made using slabs from each of the cores. At least four thin sections were made to represent each core, one directly at the pavement surface, one at the contact with the sub-base, and two or more at intermediate depths. Figures 10 through 16 show examples of the cracked reactive chert particles that are abundant in the cores from poorly performing sections. Cracks and air voids filled with alkali silica gel are often associated with these cracked chert particles. Figures 17 through 19 show examples of the reactive chert, but without the accompanying cracks and gel deposits, as is typical for the cores obtained from pavements in fair condition.

Sodium and Potassium Determination

Given the prevalence of alkali silica reactive chert, an effort was made to determine the alkali content of the concrete in the various pavements. Since there were no records available for alkali content in the fly ash and cement, and no standard method available for determining available alkalis in hardened concrete, an extraction technique developed for the determination of exchangeable and soluble sodium and potassium in soils was adopted. The slabs from each core were crushed to a fine powder, and the alkalis were extracted with an ammonium acetate solution. The concentrations of potassium and sodium were determined by an inductively coupled plasma emission spectrophotometer. The results from the test are expressed in weight percent elemental sodium and weight percent elemental potassium. In Table 6, the results were converted to the industry convention of kilograms of “Na₂O equivalent” per cubic meter of concrete, based on the total mass from the mix designs, with the exception of core 4a (CS 25031-30798A), which had no mix design information available. In this case, an approximation was used based on the mix design from core 22 (CS 25031-30798A).

The recalculation to kilograms of “Na₂O equivalent” per cubic meter of concrete allows comparisons to be made with industry standards for limiting total alkalis in the mixture. The Canadian standards specifying a maximum of 3.0 kg/m³ Na₂O equivalent for mild protection, 2.2 kg/m³ Na₂O equivalent for moderate protection, and 1.7 kg/m³ Na₂O equivalent for strong protection. As can be seen in Table 6, two of the distressed sections are above the recommended limits for “mild” protection whereas all three “fair” performing pavements are below the limit for “strong” protection.

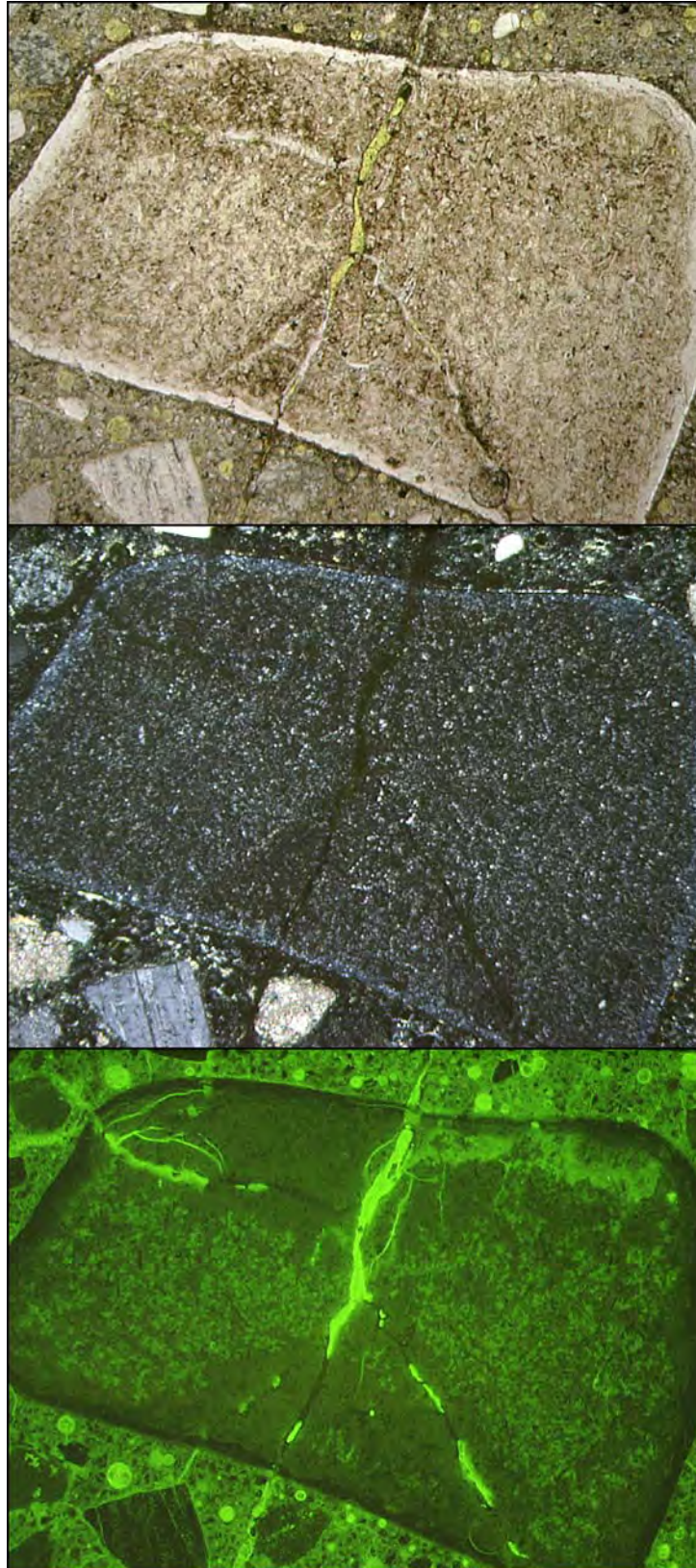


Figure 10: Example of cracked reactive chert from core 19b (CS 50011), magnified 40x. From top to bottom, plane polarized light, cross polarized light, and epifluorescent illumination.

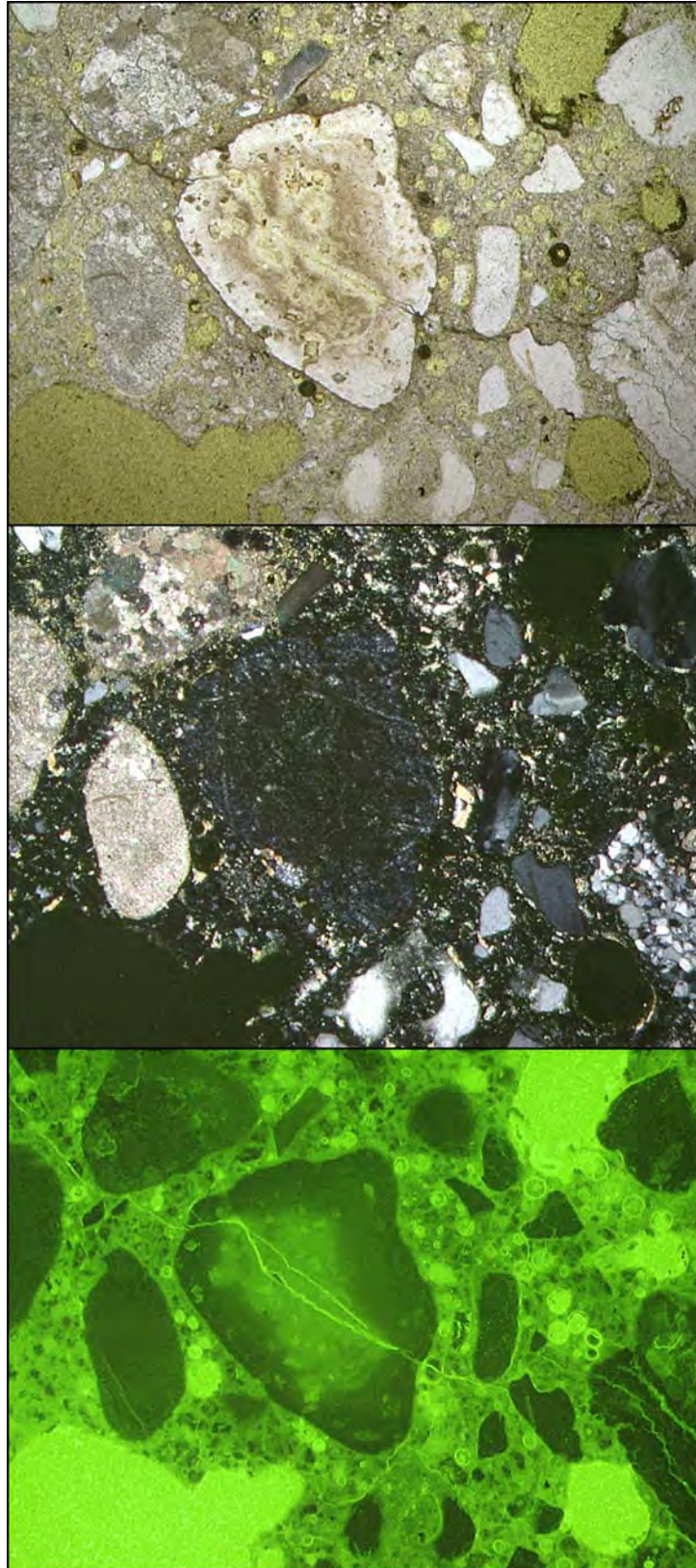


Figure 11: Example of cracked reactive chert from core 29a (CS 82291), magnified 40x. From top to bottom, plane polarized light, cross polarized light, and epifluorescent illumination.

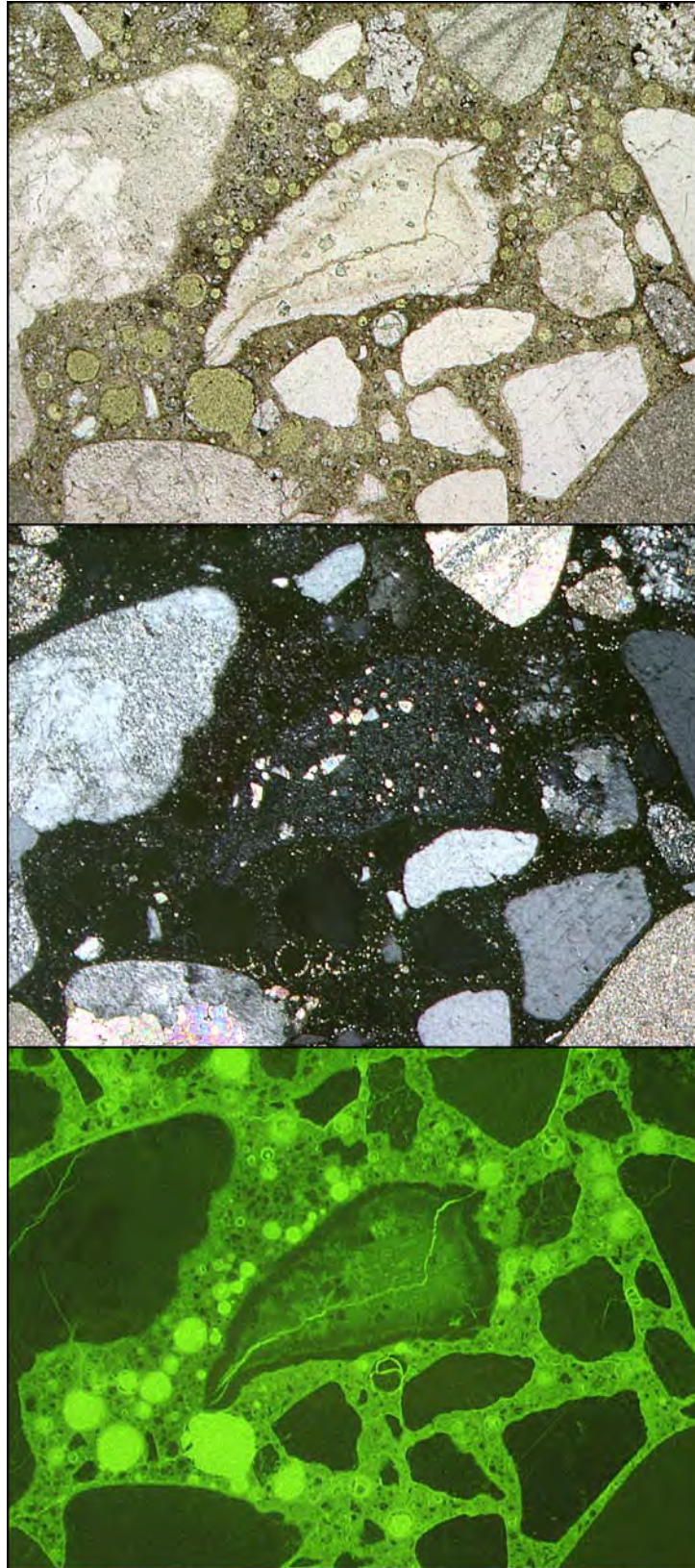


Figure 12: Example of cracked reactive chert from core 4a (CS 25031-30798A), magnified 40x. From top to bottom, plane polarized light, cross polarized light, and epifluorescent illumination.

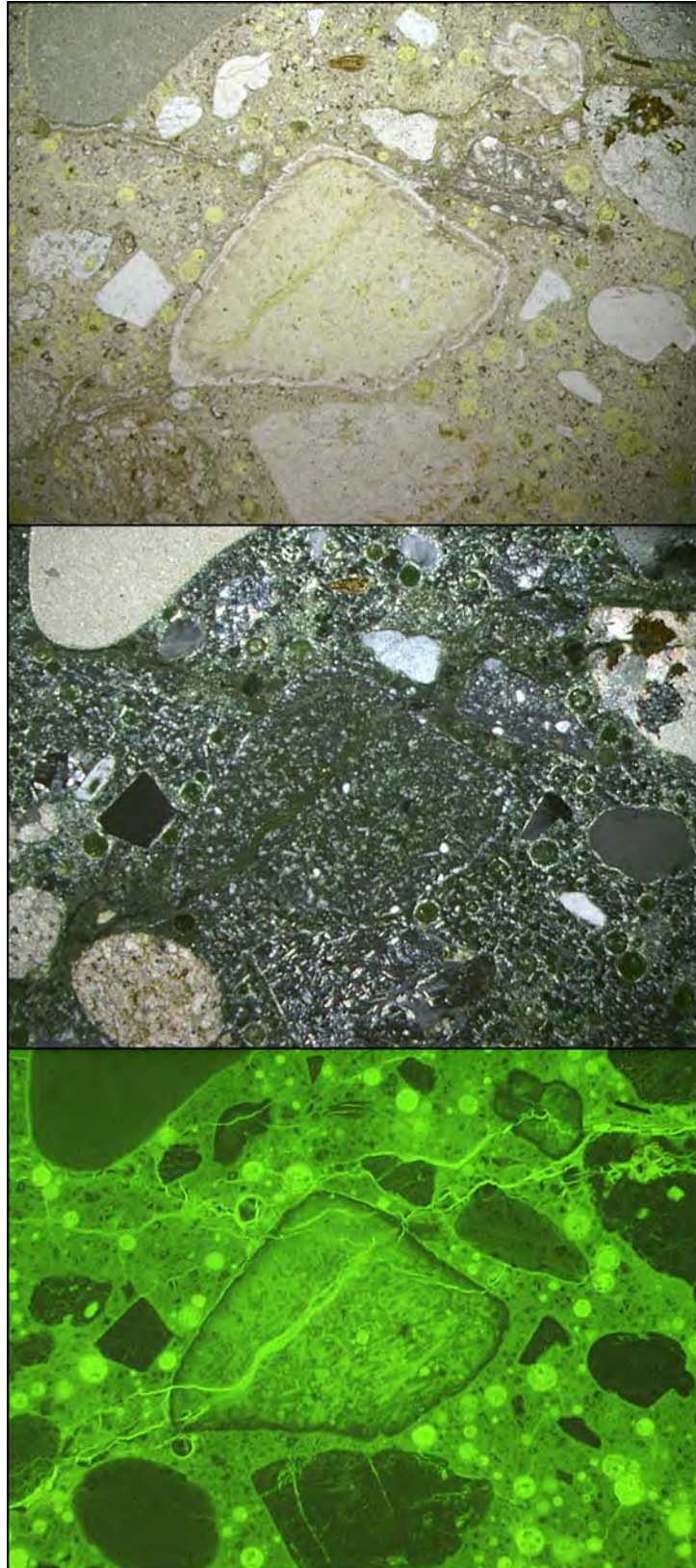


Figure 13: Example of cracked reactive chert from core 15 (CS 25031-30798A), magnified 40x. From top to bottom, plane polarized light, cross polarized light, and epifluorescent illumination.

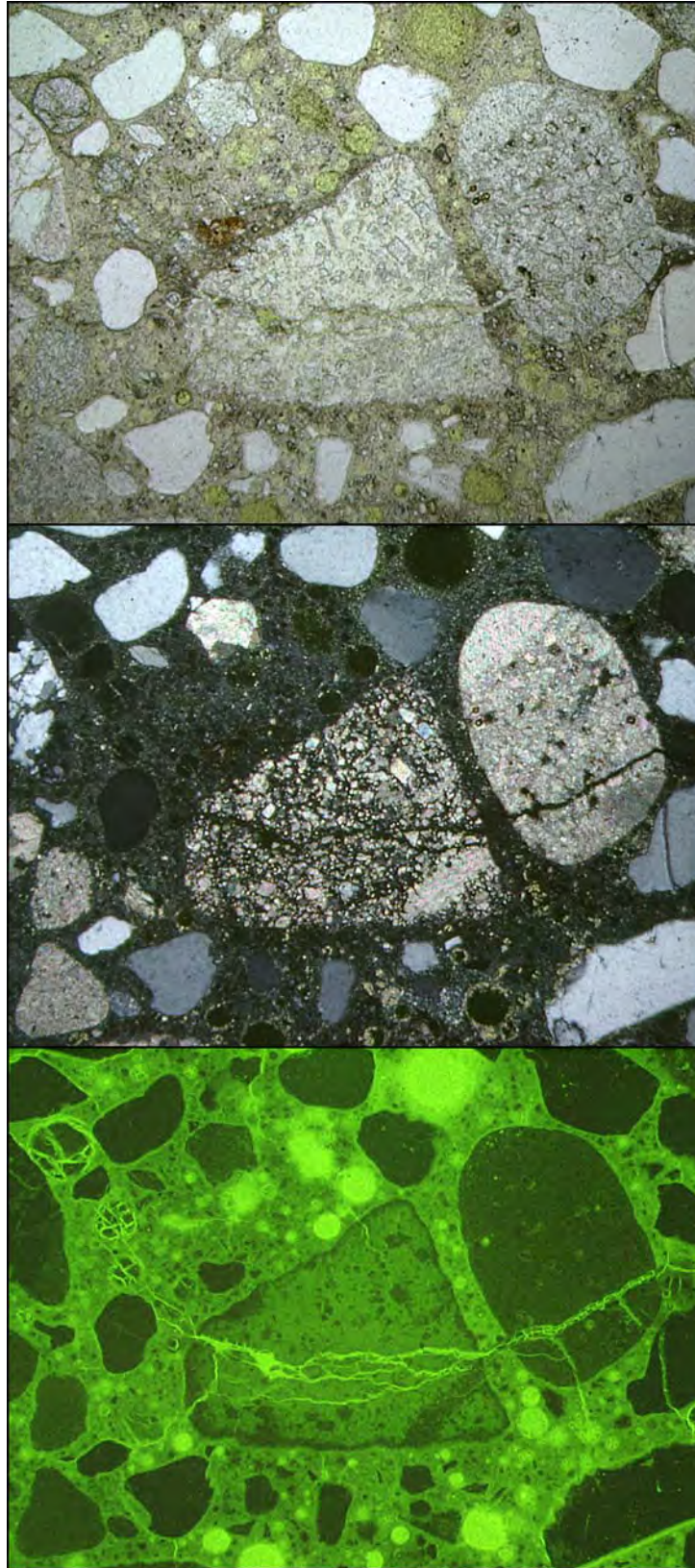


Figure 14: Example of cracked reactive chert from core 22 (CS 25031-30798A), magnified 40x. From top to bottom, plane polarized light, cross polarized light, and epifluorescent illumination.

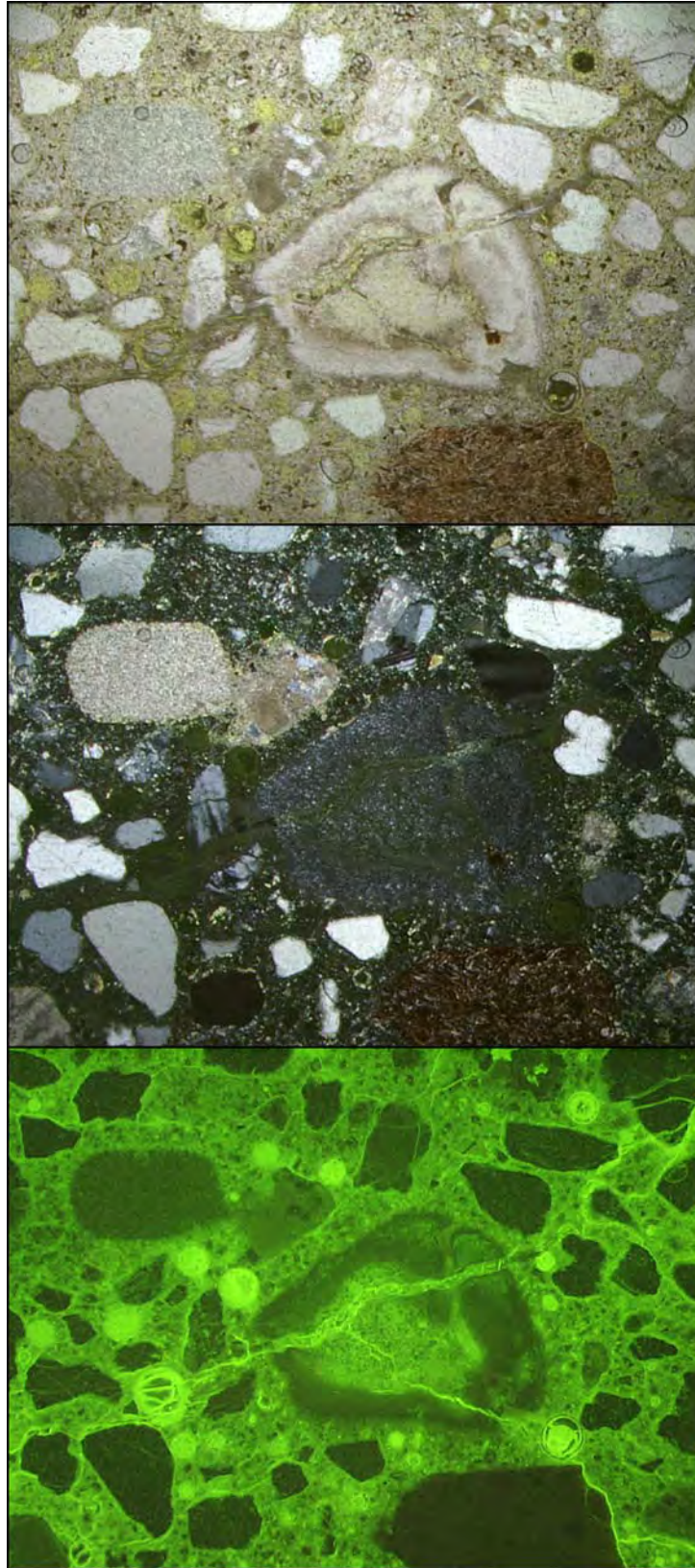


Figure 15: Example of cracked reactive chert from core 32 (CS 25031-30798A), magnified 40x. From top to bottom, plane polarized light, cross polarized light, and epifluorescent illumination.

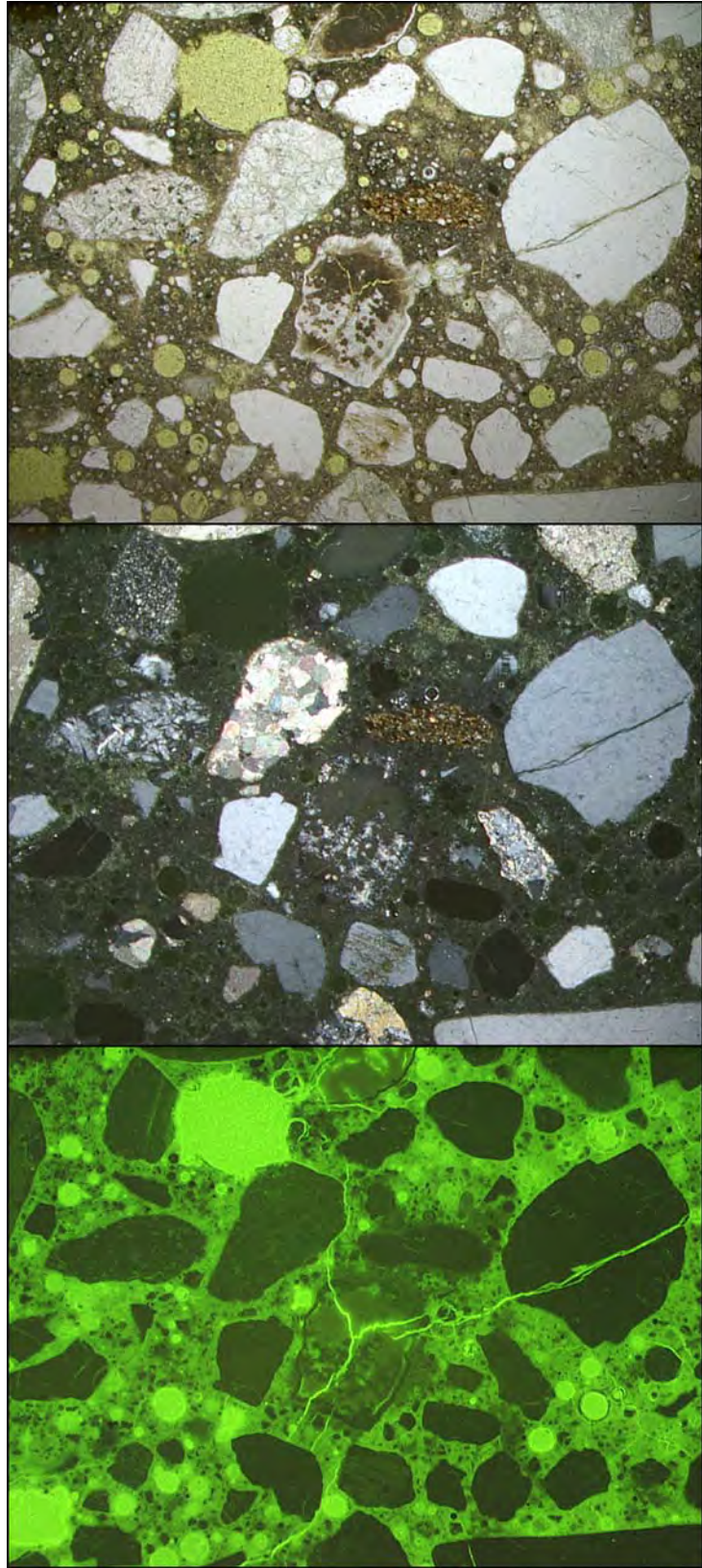


Figure 16: Example of cracked reactive chert from core 38 (CS 25031-30798A), magnified 40x. From top to bottom, plane polarized light, cross polarized light, and epifluorescent illumination.

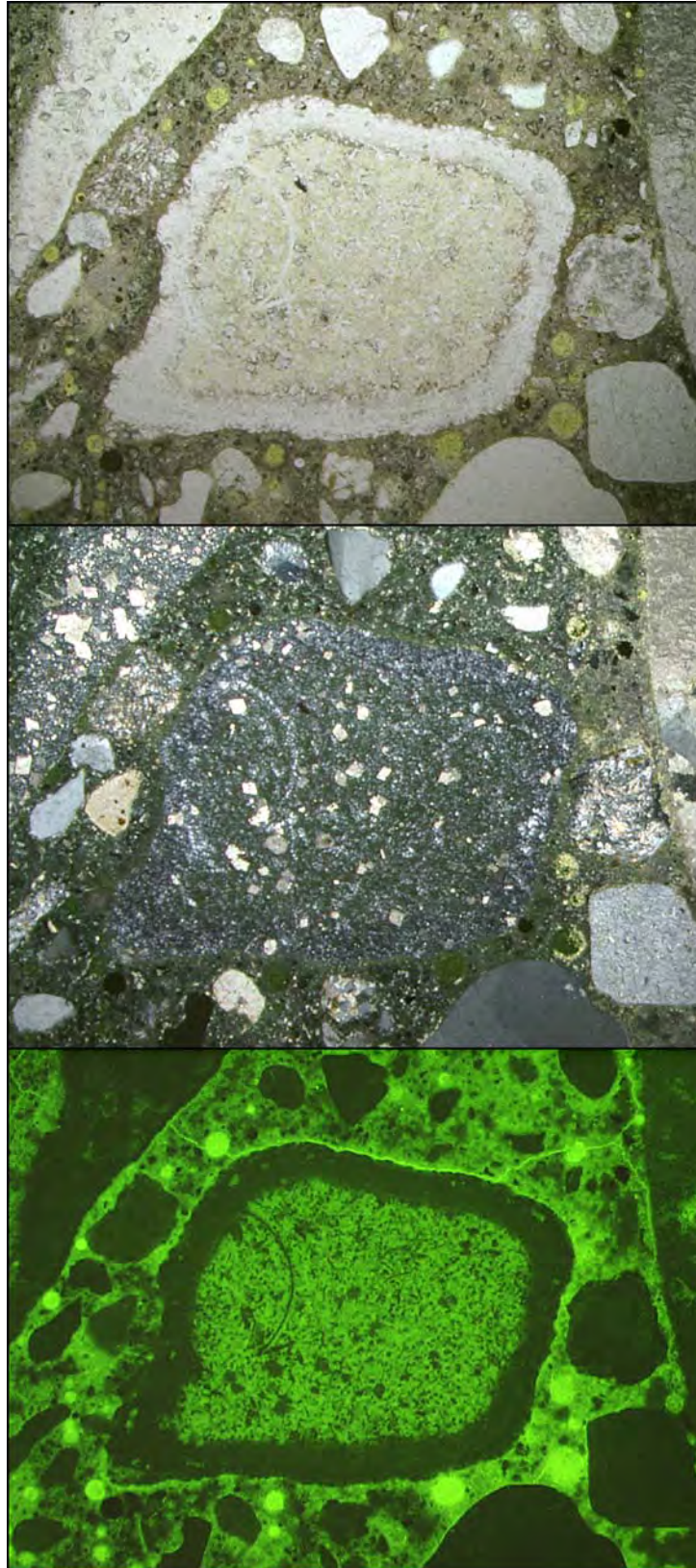


Figure 17: Example of reactive chert from core 1 (CS 25031-31018A), magnified 40x. From top to bottom, plane polarized light, cross polarized light, and epifluorescent illumination.

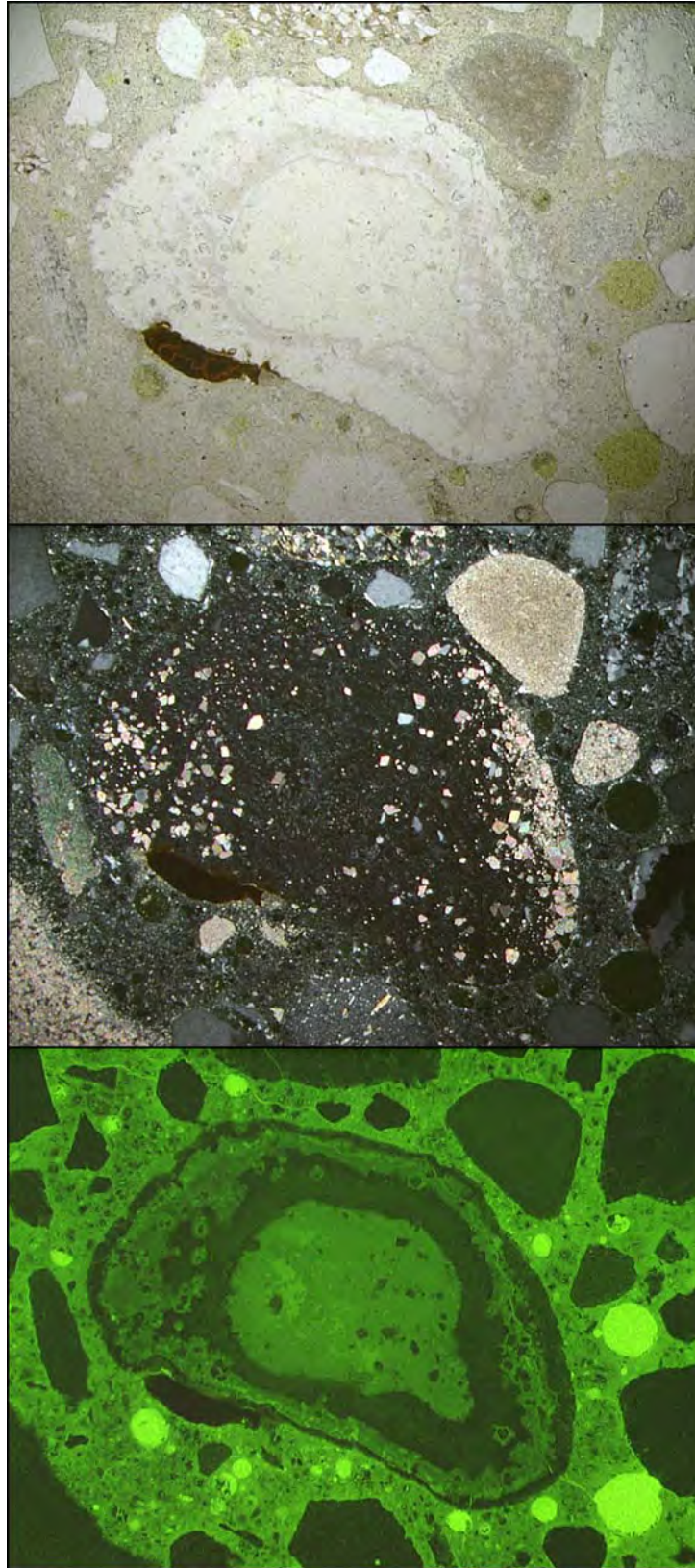


Figure 18: Example of reactive chert from core 9 (CS 25031-31018A), magnified 40x. From top to bottom, plane polarized light, cross polarized light, and epifluorescent illumination.

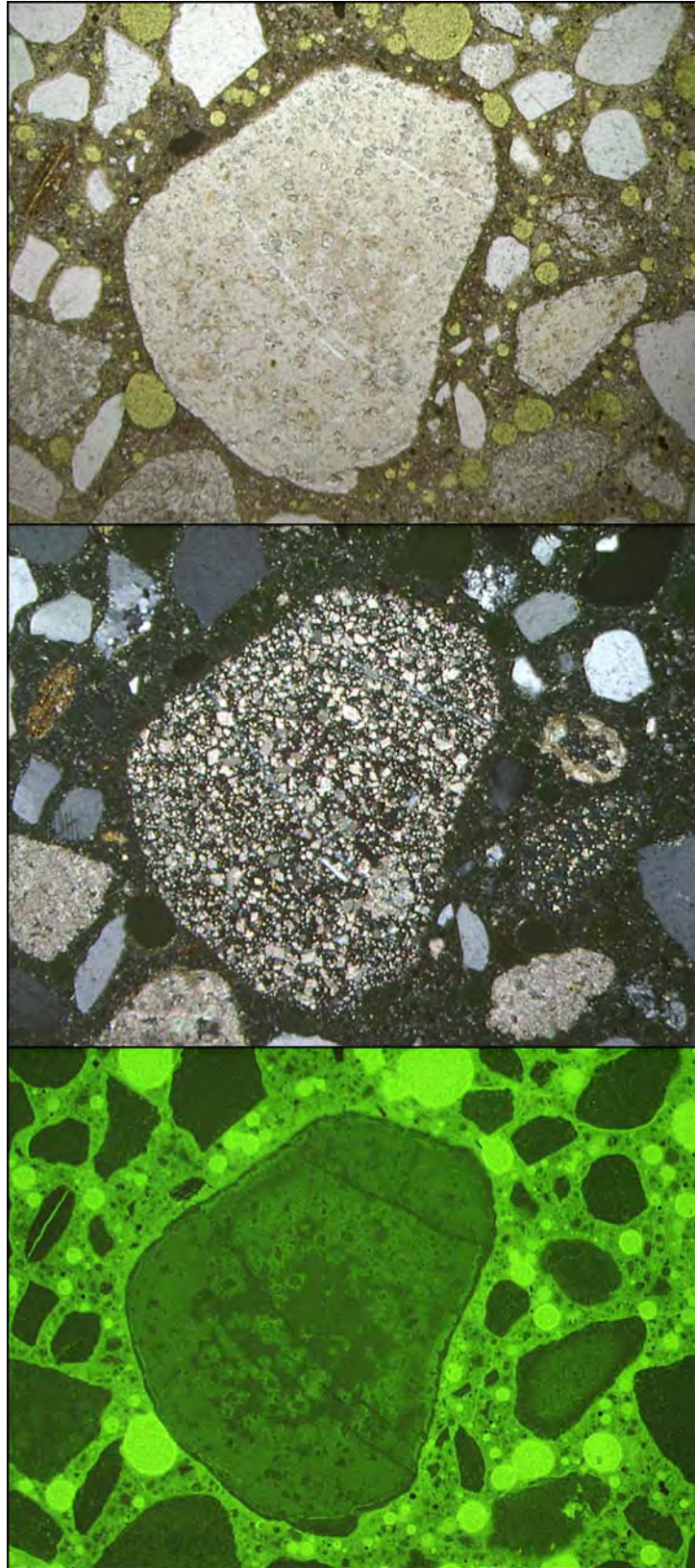


Figure 19: Example of reactive chert from core 1a (CS 58034), magnified 40x. From top to bottom, plane polarized light, cross polarized light, and epifluorescent illumination.

Table 6: Results of alkali extraction, combined with basic mix design information.

Core ID	Sacks of Cement	Percent Fly Ash	kg/m ³ Na ₂ O Equivalent	Condition	Canadian Alkali Limit
19b	5.9	0	1.9	distressed	“moderate” protection
29a	5.5	0	1.6	distressed	“strong” protection
15	9.0	0	2.1	distressed	“moderate” protection
22	5.9	13	3.1	distressed	above “mild” protection
32	5.6	0	1.7	distressed	“moderate” protection
38	6.0	25	4.3	distressed	above “mild” protection
4a	5.9	13	2.0	distressed	“moderate” protection
1	6.0	20	1.3	fair	“strong” protection
9	7.0	0	1.1	fair	“strong” protection
1a	5.9	13	1.5	fair	“strong” protection

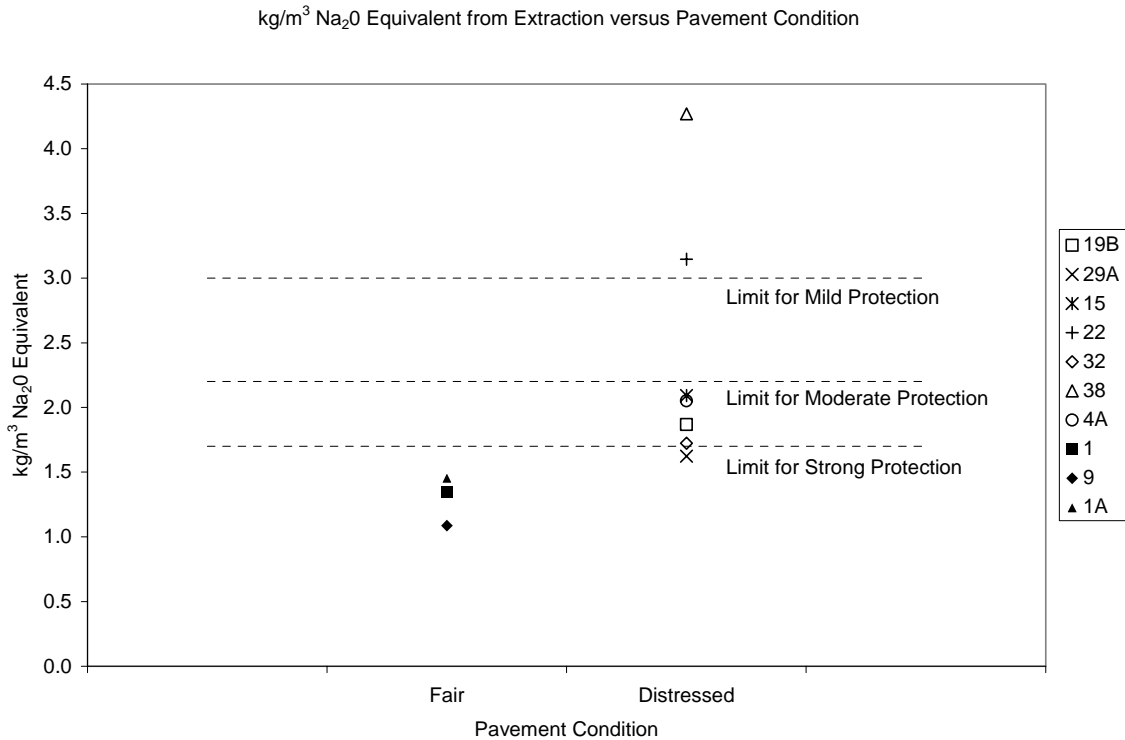


Figure 20: Available alkalis plotted against pavement condition.

Figure 20 depicts the results presented in Table 6 in terms of pavements in fair or distressed condition. Note that all the cores from pavements in fair condition had alkali levels below the limit for strong protection whereas all but one pavement in distressed condition exceeded this limit. Interestingly, the two cores with the highest alkali levels (38 and 22 [both CS 25031-30798A]) both contained a Detroit Edison Class C fly ash and the Medusa Type I cement. Although alkali test data on the fly ash is not available, it is common for Class C fly ashes to have fairly high alkali contents. Tied for the third highest measured total alkali content was core 4a (CS 25031-30798A), which is also suspected of containing the Detroit Edison Class C fly ash, although the specific mix design information is unknown. Core 4a was obtained from a distressed performing section on US-23N. Cores containing Class F fly ash (core 1 [CS 25031-31018A and core 1a [CS 58034]) were both from fair performing pavement sections and had low alkali levels.

This analysis suggests that the type and amount of fly ash may be contributing to the total amount of alkalis measured in the concrete, and to some degree, the amount of deterioration observed. It appears that concrete mixtures containing Class C fly ash have higher total alkalis than similar mixtures made with cement alone. It is also observed that mixtures made with the Class F fly ash have low alkali levels and little evidence of deleterious ASR as indicated by observed fracturing of chert particles or the presence of alkali-silica reaction product. But neither the total alkali content nor the presence of Class C fly ash can be primarily responsible for the observed deterioration. One section that contains no fly ash is suffering the most severe deterioration from the US-23N project (i.e. the section from which core 15 [CS 25031-30798A] was obtained) while the section with the highest total alkali content (from which core 38 [CS 25031-30798A] was obtained) has the least visible distress of the US-23N project. It is noted though that all of the cores obtained from the US-23N project have significant amounts of microcracking emanating from reacting chert particles, and it is likely only a matter of time before all sections progress towards serious distress.

Sulfate Determination

Secondary ettringite deposits in air voids are a common feature for all the cores evaluated in this study. Previous research conducted at Michigan Tech has indicated that calcium sulfide present in blast furnace slag aggregate may dissolve and oxidize to become a source of sulfate and calcium in the concrete, perhaps encouraging the formation of ettringite in the entrained air voids. A gravimetric procedure of sulfate determination was used according to British Standard 1881:Part 124. Methods for Analysis of Hardened Concrete: 1988. The weight percent SO₃ computed from the mix design assumes 3.5% by weight SO₃ for the cement and 4.5% by weight of the fly ash. The results of the sulfate determinations, expressed in terms of SO₃, are presented in Table 7. Graphical representations of the results are presented in Figures 21 and 22.

Table 7: Results of sulfate analysis.

Core ID	Wt% SO ₃ computed from mix design	Wt% SO ₃ from extraction	Difference	Percent Excess SO ₃ Above Computed	Condition
19b	0.48	0.68	0.20	41.1	distressed
29a	0.46	0.57	0.11	24.5	distressed
15	0.79	1.02	0.23	29.3	distressed
22	0.53	0.65	0.11	21.2	distressed
32	0.49	0.66	0.17	34.5	distressed
38	0.59	0.75	0.16	27.4	distressed
4a	0.53	0.67	0.14	25.6	distressed
1	0.57	0.65	0.07	12.9	fair
9	0.63	0.74	0.11	18.3	fair
1a	0.53	0.61	0.08	14.3	fair

It is noted that in all cases, the extraction of sulfate from field specimens exceeded the calculated sulfate levels. This is not unexpected since the calculated sulfate levels were based solely on the assumed sulfate in the cement and fly ash, and did not consider possible additional sulfates from aggregate and other sources. Table 7 presents the difference between the extracted weight percent SO₃ and the computed value and the percent difference that the extracted amount is above the computed. Figure 23 is a plot relating the percent excess SO₃ above the computed value to the pavement condition. Statistical analysis using a t-test finds that a significant difference exists between the excess SO₃ for pavements in fair and distressed conditions.

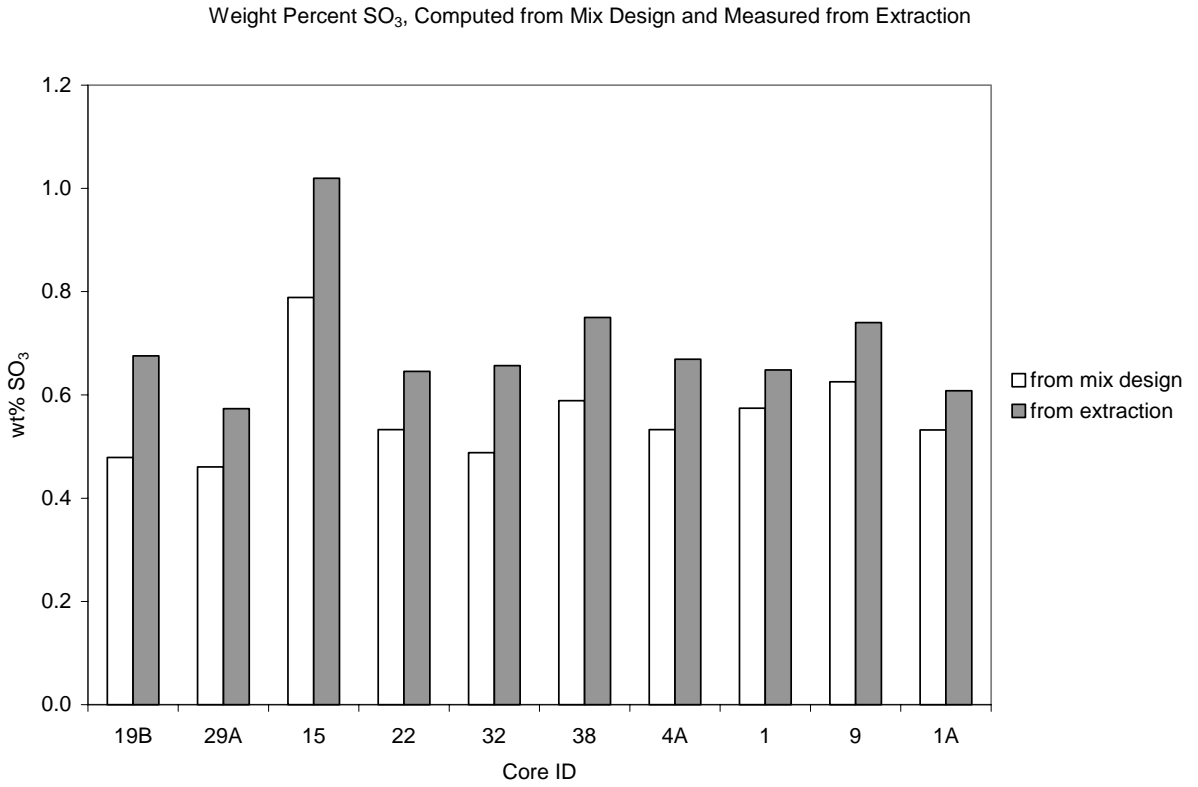


Figure 21. Results of sulfate analysis.

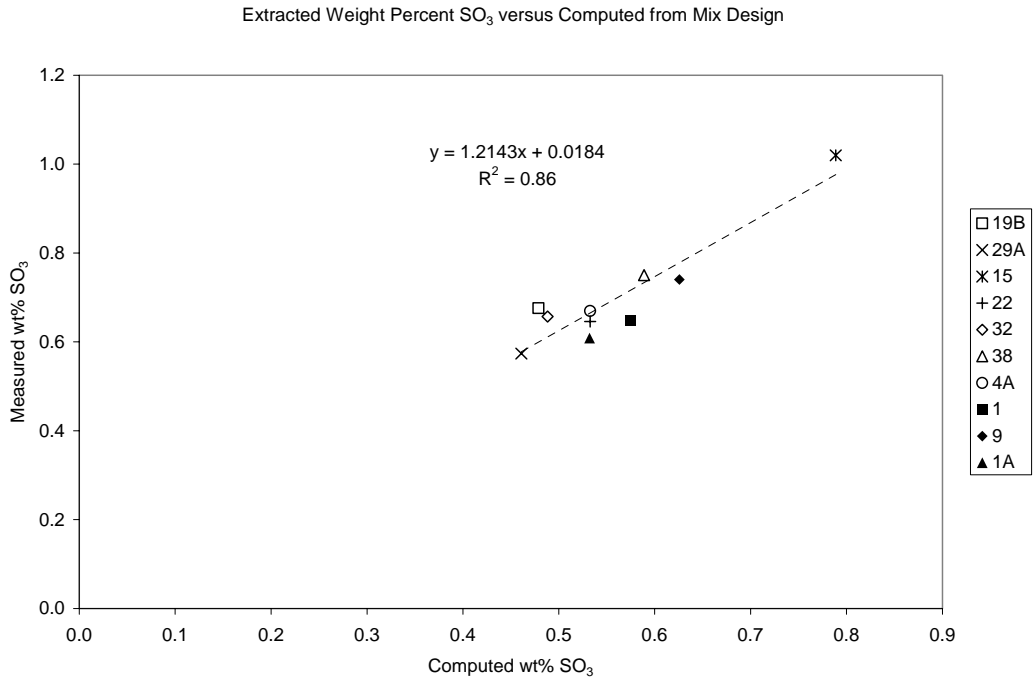


Figure 22. Relationship between measured and computed weight percent SO₃.

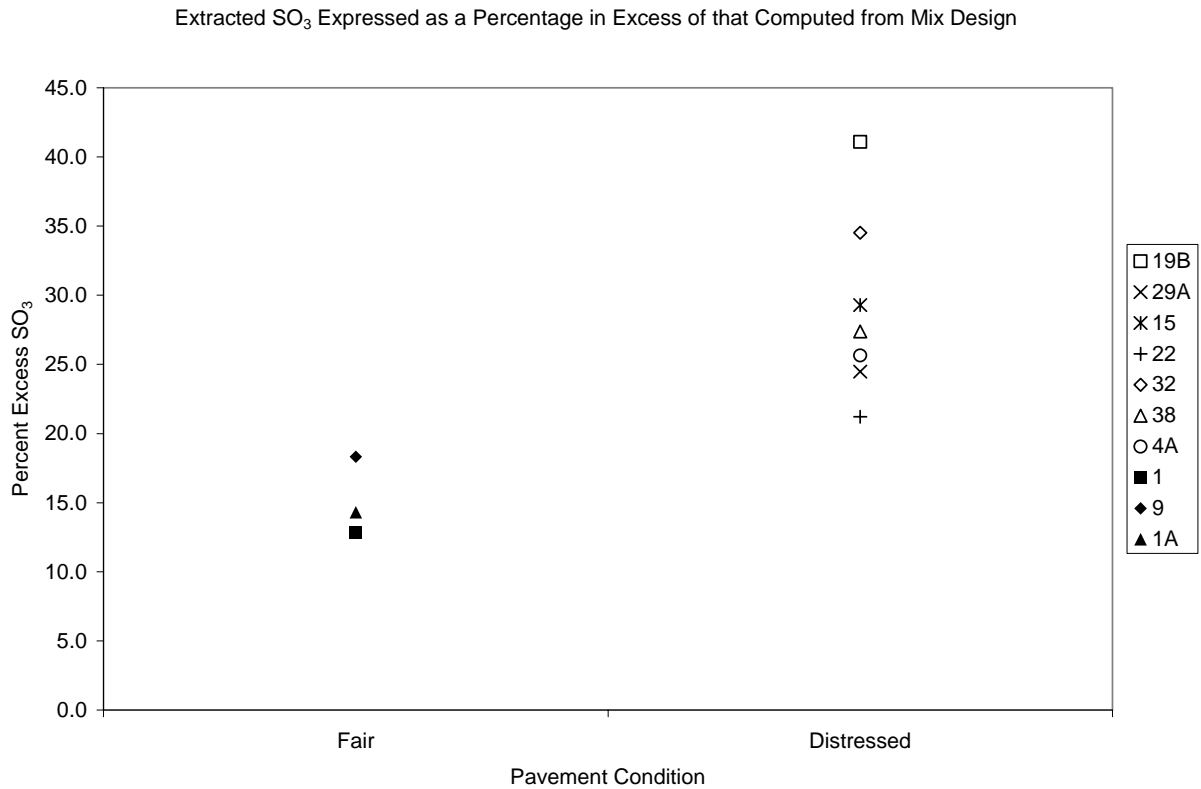


Figure 23. Percent excess SO₃ versus pavement condition.

The sulfate analysis indicates that the concentration of SO₃ in all of the pavements sampled is in excess of that computed. Potential sources of the “excess” sulfate include the likelihood of some error in the assumptions regarding the sulfate levels in the cement and fly ash, although the values selected were selected at the high end of the common range. It is also possible that sulfates in the mix water also added to the total, but it is not likely that this was a significant factor. It is also possible that sulfates may have migrated into the concrete after placement, either through contaminated ground water (very unlikely in these locations) or through deicing salts contaminated with sulfates such as gypsum. Another potential source of excess internal sulfates is the aggregate, slag being the most likely potential contributor. The “excess” sulfates might also be an artifact of the test procedure itself. For these reasons, the data presented focuses more on the percent SO₃ in excess of the predicted amount instead of the absolute values measured.

The effect of the excess sulfates on concrete durability cannot be easily predicted. In the worst case, excess sulfates will react with the hydrated cement paste resulting in sulfate attack. But it is almost impossible to assess the potential for this occurrence for these mixtures because other factors including cement chemistry, the water-to-cement ratio, and concrete permeability will impact the sulfate resistance of the concrete. Further, the presence of admixtures/additives also complicates the situation, particularly the use of the Class C fly ash, which is known to have quite variable effects on the sulfate resistance of concrete¹, at times improving it but on other occasions having a negative impact. Due to all these uncertainties, it is impossible to say at what concentration the excess sulfates might result in sulfate attack.

But it is telling that a statistically significant relationship exists between the excess sulfates and the condition of the pavements. Pavements classified as being distressed have higher percent excess sulfates than those classified as being in fair condition. This is an indication that the excess sulfates may be related to the observed distress.

Discussion

The answer to the question of why US-23N (CS 25031-30798A) is deteriorating prematurely is unclear. It is known that distress was observed on these sections, particularly the cross-over lanes constructed with a high cement content concrete (9 sack mixtures), at a very early age, initially indicating that plastic shrinkage or drying shrinkage cracking might be to blame. There is also evidence, based on discussions with MDOT engineers, that the slag coarse aggregate stockpile was not kept moist during construction, resulting in cracking of the pavement surface. Although this occurrence may have contributed to the onset of the distress by “opening” up the concrete surface, making it more permeable to water and deicers, it alone cannot be blamed for the observed distress at this time.

The deterioration has continued to progress over time, and in the most serious case has required removal and replacement of the highly deteriorated cross-over lanes after only nine years of service. The progression has not only appeared as cracking, but includes staining, spalling, and

¹ Depuy, G.W. (1994). “Chemical Resistance of Concrete.” *Concrete and Concrete Making Materials*. STP 169C. American Society for Testing and Materials. Philadelphia, PA.

what can best be described as complete disintegration of the hydrated cement paste matrix. Microscopically, it is evident that significant infilling of the entrained air-void system has occurred and that in the deteriorated pavement sections, alkali-silica reactivity is causing fracturing of chert fine aggregate particles and subsequent microcracking of the paste. There are currently two hypotheses that are being considered to explain the observed deterioration. The first is that ASR is primarily responsible and the second is that the dissolution of the calcium sulfide found in the slag coarse aggregate is causing a type of internal sulfate attack from excess sulfates. Further, it is possible that both mechanisms are in conjunction with one another, or in combination with as yet unknown factors, such as the occurrence of the initial cracking. Each of these hypotheses is discussed below.

Alkali-Silica Reactivity

The first hypothesis is that ASR is the primary mechanism responsible for the observed deterioration. It is clear from the petrographic analysis that chert particles contained in the fine aggregate are reactive. Further, without exception, in pavements that are showing visible signs of materials-related distress (map cracking, staining, spalling, and deterioration), these fine aggregates are showing deleterious reactions in which the particles are fracturing and alkali-silica reaction product is being produced, filling cracks and nearby air voids. In contrast, in cores obtained from the three “fair” performing sections, few if any such deleterious reactions were observed.

Also supporting the ASR hypothesis is that the total alkali contents for the distressed sections of US-23N were in excess of that recommended for complete protection from ASR. Two of the cores (cores 38 and 22) were even in excess of the limit for mild ASR protection (maximum of $3.0 \text{ kg/m}^3 \text{ Na}_2\text{O equivalent}$)². Two of the distressed sections with lower total alkali content were older than the 1992 sections, and thus the reactions would have had longer to manifest themselves. In contrast, cores from the three fair performing sections all had total alkalis well below the recommended limits set for strong protection.

²Fournier, B., M. Bérubé, and C. A. Rogers (1999). *Proposed Guidelines for the Prevention of Alkali-Silica Reaction in New Concrete Structures*. *Journal of the Transportation Research Board*. No. 1668. Transportation Research Board. Washington, D.C.

But some problems exist with the ability of the ASR theory to completely explain all of the observations. The first is that the observed pavement deterioration is not completely consistent with that solely caused by ASR. Pavements affected by ASR will typically manifest map cracking with exudate, spalling, and evidence of expansion. The US-23N sections show some signs of map cracking (Figures 2 and 4), but little sign of exudates. Further, the observations of the complete deterioration of the hydrated cement paste, as shown in Figures 1 and 3, is inconsistent with deterioration caused by ASR. Another problem with the ASR theory is that the cracking became apparent within a few years of construction. This is an extremely short time frame for ASR, since it is commonly thought to take at least 5 years to become manifest, especially considering that the alkali contents were not extreme for most of the sections.

Another observation that does not support ASR as the exclusive distress mechanism is that the most severe deterioration was observed in the section from which core 15 (CS 25031-30798A) was obtained, yet this section did not have an excessively high total alkali content compared to some other sections, being at $2.1 \text{ kg/m}^3 \text{ Na}_2\text{O}$ equivalent. What is unique about this section was the use of a very high cement content at 502 kg/m^3 (9 sacks) and no fly ash. Based solely on the amount of total alkalis available, it seems likely that this section would have suffered less deterioration than that from which core 38 (CS 25031-30798A) was obtained (which had a total alkalinity of $4.3 \text{ kg/m}^3 \text{ Na}_2\text{O}$ equivalent), but the opposite is true.

It is also known from other work conducted at Michigan Tech that the reactivity problem with the chert particles in the fine aggregate seems to be most closely associated with concrete containing slag as a coarse aggregate. Further work needs to be done regarding this observation, as there seems to be some, as yet undefined, interaction between deleterious ASR and the presence of slag coarse aggregate.

Dissolution of Calcium Sulfide

Work conducted by Michigan Tech in the past has demonstrated through thermodynamic calculations and visual observations that calcium sulfide inclusions present in blast furnace slag

can be highly soluble in the highly alkali environment present in the concrete pore solution.³⁴ This dissolution can result in the secondary formation of ettringite and gypsum in available void space within the concrete. Ettringite filling the air-void system can potentially compromise its ability to protect the paste against freeze-thaw damage.⁵ Of greater concern would be sulfate ions in solution, which could lead to direct sulfate attack of the hydrated cement paste. Evidence supporting this potential distress mechanism is the significant infilling of the air-void system with sulfate-bearing minerals that has been observed in all of the cores that were evaluated. Such infilling is a common feature of in-service concrete, particularly that which has deteriorated. But the infilling in the cores evaluated in this case study is excessive, even in concrete from pavements in “fair” condition. From the US-23N project, the two most severely deteriorated sections (cores 15 and 22 [both from CS 25031-30798A]) have existing spacing factors that would be classified as deficient with regards to freeze-thaw protection, even though the original spacing factors were adequate (see Figure 5). Interestingly, the other two sections having deficient air-void system both had deficient systems as constructed (cores 19b [CS 50011] and 1 [CS 25031-31018A]). Core 1 was obtained from a pavement considered to be in “fair” condition.

As was discussed, the percent of sulfate in excess of that calculated was significantly higher in the distressed pavement sections than in the pavements considered to be in fair condition. Core 15 (CS 25031-30798A), from the most deteriorated section, had the highest calculated and extracted sulfate content, with a percent excess sulfate of approximately 30 percent. The highest percentage of excess sulfate was measured in core 19b (CS 50011), which is from another highly distressed section. In contrast, the three cores (1, 1a, and 9) obtained from pavements in fair condition had significantly lower percentages of excess sulfate. There are too few data points and too many assumptions/factors to make definitive conclusions based on this analysis, but a trend does seem to be emerging that suggests that excess sulfates are contributing to the observed distress.

³ Peterson, K.W., D. Hammerling, L.L. Sutter, T. J. Van Dam, and G.R. Dewey, “Oldhamite: Not Just in Meteorites,” Proceedings of the 21st International Conference on Cement Microscopy, Las Vegas, NV, April 25-29, 1999.

⁴ Hammerling, D., K.R. Peterson, L.L. Sutter, T. J. Van Dam, and G.R. Dewey, “Ettringite: Not Just in Concrete.” Proceedings of the 22nd International Conference on Cement Microscopy, Montreal, Canada. April 30 to May 4, 2000.

⁵ Note that this result is hotly debated in the concrete literature and it is unclear whether air voids could fill sufficiently with secondary ettringite to prevent them from protecting against freeze-thaw damage.

As discussed, the sources of excess sulfate are most likely from other concrete constituents, such as the mixing water and aggregate. For the concrete under investigation, it is quite possibly the result of the dissolution of calcium sulfide and the formation of sulfate-bearing minerals. The solubility of calcium sulfide is directly related to the alkalinity of the pore solution, with higher pH values resulting in increased solubility⁶. Thus, higher alkalinity not only results in higher ASR potential, but would also increase the solubility of calcium sulfide. This is an important interaction and one that should be a focal point for future investigations into the deterioration of concrete containing slag coarse aggregate.

Other Factors

In addition to the two hypotheses described previously, other factors may have contributed to the deterioration either by acting in conjunction with the mechanisms cited or wholly on their own. A major unknown is the conditions present during construction. This relates to the construction process itself (e.g. materials handling, mixing, transporting, placing, and curing of concrete) as well as the ambient conditions that may have occurred during placement (e.g. temperature). It is well known that such conditions can have a significant impact on concrete durability either directly or indirectly. For example, high curing temperatures can lead to the formation of undesirable hydration products and/or desiccation of the surface resulting in cracking. Other factors resulting in an increase in permeability of the concrete will negatively impact its durability simply by allowing moisture and deicers more ready access. This is true for ASR and sulfate attack, both of which require water to facilitate ion transfer and for the transmission of expansive forces that fracture the concrete. Permeability can be negatively affected by many factors including material selection, mix proportions, mixing, placement, and curing. One question that needs to be resolved is whether the permeability of concrete using slag coarse aggregate differs significantly from that of concrete made with natural aggregate.

⁶ Hammerling, D., K.R. Peterson, L.L. Sutter, T. J. Van Dam, and G.R. Dewey, "Ettringite: Not Just in Concrete." Proceedings of the 22nd International Conference on Cement Microscopy, Montreal, Canada. April 30 to May 4, 2000.

Conclusions

Based on the results of this study, the following conclusions can be drawn:

- The results of the air-void system analysis found that most of the concrete originally had an air-void system that was adequate to protect the paste against freeze-thaw damage. Since construction, the air voids have been filling with secondary sulfate mineral deposits, which in some cases might be compromising the efficiency of the air-void system. This was most pronounced in the more seriously deteriorated pavement sections, but even one of the “fair” sections had a deficient air-void system.
- Petrographic evaluation of thin sections demonstrated conclusively that the chert particles in the fine aggregate are undergoing a deleterious alkali-silica reaction in all of the pavement sections classified as distressed. This reaction is characterized by fracturing of the aggregate particles, related fracturing of the surrounding paste, and the production of alkali-silica reaction product observed in cracks and voids. In contrast, examination of thin sections made from pavement sections classified as “fair” did not show similar deleterious deterioration. Although the chert particles were stained yellow by the indicator, little or no aggregate fracturing or reaction product formation was observed.
- The available total alkalis extracted from the various cores showed that in all but one case, the total alkalis measured from cores obtained from distressed pavements were in excess of the recommended limit for strong ASR protection. The two cores having the highest alkali content contained a Class C fly ash. In contrast, all of the cores obtained from fair performing pavements had total alkali contents lower than the limit for strong protection. Two of these sections were constructed with a Class F fly ash.
- The sulfate extraction tests performed indicated that the excess sulfate was significantly higher in cores obtained from distressed sections than that from pavements in fair condition. A source for the excess sulfate could not be unequivocally found, but it is likely that the dissolution of calcium sulfide in the slag coarse aggregate is contributing. The excess sulfate could contribute to the formation of sulfate-bearing minerals (e.g. ettringite) in the available air-void space, potentially compromising its ability to protect the paste against freeze-thaw damage. Further, excess sulfate may be leading to internal sulfate attack of the hydrated cement paste. This dissolution process is directly dependent upon the alkalinity of the pore

solution. Thus there is an interaction between the potential for ASR and dissolution of calcium sulfide.

- In reviewing all available data, there is no definitive single cause that can be forwarded at this time regarding the deterioration observed on US-23N. Two hypotheses have emerged that can at least partially explain the deterioration, and it is possible that the two may be acting together to contribute to the observed deterioration. The first hypothesis focuses on the alkali-silica reactivity of the chert particles in the fine aggregate, which is aggravated by the total alkalinity in the concrete and Class C fly ash. The presence of the Class F fly ash appears to offer a mitigating effect. The second hypothesis focuses on the dissolution of the calcium sulfide and the formation of sulfate-bearing minerals, which results in a type of internal sulfate attack. Construction factors may also play a role, particularly with relation to rate of distress formation and severity.

Appendix A

**Coring and Mixture Design Information as Provided by MDOT for US-23 N and US-23S
Projects**

**Coring on US-23 Just South of Flint
May 30, 2001**

Mix #1 and #2 were from a concrete job done one year after (1993) the job of interest. This section of pavement is in very good condition.

Mix #1: 35P with some fly ash, in the right lane near the on-ramp from the Rest Area (Cores 1-7).

Mix #2: 35HE in the shoulder adjacent to area with Mix #1 (Cores 8-14).

Mixes #3 through #6 are all on the pavement that was built in 1992. This pavement is in varying states of distress. The distress is primarily a crumbling at the joints.

Mix #3: 9 sack fast-set. Primarily used in short sections for crossovers. These sections are in very poor condition (Cores 15-21).

Mix #4: 35P with some fly ash. The area where the cores were taken had some deterioration at the joints, however the cores for MRD analysis were taken at a joint in relatively good condition (Cores 22-28).

Mix #5: 35P without fly ash. This concrete is in pretty good condition with a minimal amount of deterioration (Cores 29-35).

Mix #6: 35P with more fly ash than mix #4. The concrete in this area is in good condition (Cores 36-42).

There are a number of longitudinal cracks within a foot of the centerline joint throughout the entire job. They are prevalent in any one mix design.

Mix design information for all mixes except #3 are attached. Also attached are mill certs for the fly ash used on the 1992 job.
